Soil Quality Determination in Precision Agriculture and Bitumen Residue Determination in Oil Sand Tailings by Fourier Transform Infrared Spectroscopy Coupled with Chemometrics

By

Qianjun Gan

A thesis submitted to the Faculty of Graduate Studies and Research in partial fulfillment of the requirements of the degree of Doctor of Philosophy

Department of Food Science & Agricultural Chemistry

McGill University

Montreal, Canada

December 2016

This thesis is dedicated to my mum, dad, husband and those supporting me with love

ABSTRACT

The need for rapid and inexpensive techniques for soil quality determination has led to the investigation of modern technologies. Infrared spectroscopy in the near-infrared region has been traditionally used, while the mid-infrared region (4000 – 400 cm^{-1}) has been less studied. In this research, the feasibility of employing attenuated total reflectance-Fourier transform mid-infrared (ATR-FTIR) spectroscopy in soil quality determination was studied. The soil quality of 278 soil samples from four Canadian provinces was evaluated by measurement of 10 selected soil properties: total carbon (TC), total nitrogen (TN), carbon-to-nitrogen ratio (C/N), ammonium (NH_4^+), nitrate (NO_3^-), sand, silt, clay, N uptake, and yield. Partial least-squares regression (PLSR) was used to build calibration models for the prediction of these properties from ATR-FTIR spectra of soils. Based on evaluation of the coefficient of determination (r^2) and the residual; predictive deviation (RPD), it was found that the models for TC, TN, C/N, sand, silt, and clay showed very reliable performance ($r^2 > 0.90$, RPD > 2.00). Similar results were found when the same set of samples were analyzed using diffuse reflectance infrared Fourier transform near-infrared (DRIFT-NIR) spectroscopy. Comparison of the prediction results obtained by ATR- FTIR and DRIFT-NIR spectroscopy demonstrated that the ATR-FTIR models showed better prediction accuracy than the DRIFT-NIR models, with an RPD increment between 12% and 36%. This result indicates that ATR-FTIR spectroscopy coupled with PLSR has the potential to model and predict certain important soil properties and therefore may assist in achieving large-scale precision farming.

In the second part of the research, the target of study moved from agricultural soils to bitumen-contaminated tailing soils, where the content and quality of bitumen residues in a tailings remediation process were determined by FTIR spectroscopy. The application of ATR-FTIR and DRIFT-NIR spectroscopy as rapid tools for determination of bitumen residues in tailings and remediated tailings was investigated. In this work, bitumen residues were directly determined in neat samples without any chemical separations or extractions. ATR-FTIR spectroscopy coupled with PLSR yielded the best calibration, with a r^2 of 0.99 and a 1.76 wt% RMSEC over the bitumen range between 0.70 and 40.70 wt%. These methods were reproducible with an average 0.91 wt% difference among triplicate analyses. The classification of unremediated and

remediated tailing soils by principal component analysis (PCA) of their ATR-FTIR spectra was investigated. Soils were successfully classified according to their level of bitumen content, but classification based on discrimination between unremediated and remediated soils was not successful. This result implied the lack of a direct relationship between bitumen content and the remediation process, which was attributed to the variable bitumen content of the feedstocks and the use of an un-optimized remediation process. Therefore, the on-line FTIR-PCA classification as well as the FTIR-PLS quantification is necessary for feedstock categorization based on bitumen level in order to optimize the remediation process and for subsequent evaluation of the remediation process to ensure the remediation goal has been met. In an extension of this work, the use of the green solvent 2-methyltetrahydrofuran (2-MeTHF) for extraction of bitumen from tailing soils was evaluated. Based on gravimetric determination of the bitumen recovery yield, it was found that 89 wt% of the total bitumen was recovered by a room-temperature single-stage 2-MeTHF extraction, which was 9% and 14% higher than the recovery obtained with the traditionally used organic solvents toluene and dichloromethane (DCM) under the same conditions. The quality of the bitumen extracted by the three solvents was analyzed by FTIR spectroscopy, which indicated that less migration of clay minerals into the bitumen product occurred during extraction with 2-MeTHF. However, under the elevated-temperature conditions of Soxhlet extraction, protonation, ring-opening and polymerization reactions of 2-MeTHF were postulated to form oil-like products, which were detected in the FTIR spectrum of the extracted bitumen as well as by atmospheric-pressure chemical ionization mass spectroscopy (APCI-MS). These results indicate that 2-MeTHF has potential to serve as a bitumen extraction solvent, providing a higher recovery yield and better product quality than toluene and DCM. Nevertheless, high-temperature conditions should be avoided in the extraction and solvent recovery processes to prevent polymerization reactions.

RÉSUMÉ

La nMcessitéessitd be avoided in the extraction and pour la détermination de la qualittides sols a excité xcitétude des technologies modernes. La spectroscopie infrarouge dans le proche infrarouge a été beaucoup utilisée, tandis que la spectroscopie de l'infrarouge moyen (4000-400 cm^{-1}) a été moins étudiée. Dans cette étude, on a étudié la faisabilité de l'utilisation de la spectroscopie moyen infrarouge à transformée de Fourier à réflexion totale atténuée (ATR-FTIR) dans la détermination de la qualité du sol. La qualité du sol de 278 échantillons en provenant des quatre provinces canadiennes a été évaluée par mesure de 10 propriétés du sol sélectionnées: Le carbone total (TC), l'azote total (TN), le rapport carbone-azote (C/N), l'ammonium (NH_4^+), le nitrate (NO_3^-), le sable, le limon, l'argile, l'absorption de N et le rendement. La régression des moindres carrés partielle (PLSR) a été utilisée pour construire des modèles d'étalonnage pour la prédiction de ces propriétés à partir des spectres ATR-FTIR des sols. Sur la base de l'évaluation du coefficient de détermination (r^2) et de l'écart prédictif résiduel (RPD), on a constaté que les modèles pour TC, TN, C/N, sable, limon et argile présentaient des performances très fiables ($r^2 >$ 0,90, RPD > 2,00). Des résultats similaires ont été trouvés lorsque le même ensemble d'échantillons a été analysé en utilisant la spectroscopie de réflexion diffuse dans le proche infrarouge (DRIFT-NIR). La comparaison des résultats de prédiction obtenus par spectroscopie ATR-FTIR et DRIFT-NIR a démontré que les modèles ATR-FTIR ont montré une meilleure précision de prédiction que les modèles DRIFT-NIR, avec un incrément RPD entre 12% et 36%. Ce résultat indique que la spectroscopie ATR-FTIR combine avec PLSR a le potentiel de modéliser et de prédire certaines propriétés importantes du sol et peut donc aider à réaliser une agriculture de précision à grande échelle.

Dans la deuxième partie de la recherche, la cible d'étude est passée des sols agricoles aux sols de résidus contaminés par le bitume, où la teneur et la qualité des résidus bitumineux dans un processus d'assainissement des résidus ont été déterminées par FTIR spectroscopie . L'application de la spectroscopie ATR-FTIR et DRIFT-NIR comme outils rapides pour la détermination des résidus bitumineux dans les résidus et les résidus traités a été étudiée. Dans cette étude, les résidus bitumineux ont été déterminés directement dans des échantillons purs sans aucune séparation ou extraction chimique. La spectroscopie ATR-FTIR combine avec PLSR

a donné le meilleur étalonnage, avec un r^2 de 0,99 et un RMSEC de 1,76% en poids pour une gamme de bitume entre 0,70 et 40,70 %m. Ces méthodes étaient reproductibles avec une différence moyenne de 0,91%m parmi les analyses en triple. On a étudié la classification des sols de résidus non réadaptés et traités par l'analyse en composantes principales (PCA) de leurs spectres ATR-FTIR. Les sols ont été classés avec succès en fonction de leur teneur en bitume, mais la classification fondée sur la discrimination entre les sols non remis en état et les sols remis en état n'a pas été couronnée de succès. Ce résultat implique l'absence d'une relation directe entre la teneur en bitume et le processus d'assainissement, ce qui a été attribué à la teneur variable en bitume des charges d'alimentation et à l'utilisation d'un processus d'assainissement non optimisé. Par conséquent, la classification FTIR-PCA en ligne ainsi que la quantification FTIR-PLS sont nécessaires pour la catégorisation des matières premières basée sur le bitume afin d'optimiser le processus d'assainissement et d'évaluer ultérieurement le processus d'assainissement pour s'assurer que l'objectif d'assainissement a été atteint. Dans l'extension de ce travail, on a évalué l'utilisation du solvant vert 2-méthyltétrahydrofurane (2-MeTHF) pour l'extraction de bitume dans les sols de résidus. Sur la base de la détermination gravimétrique du rendement de récupération du bitume, on a constaté que 89%m du bitume total ont été récupérés par une extraction à 2-MeTHF à une étape à température ambiante, qui était de 9% et 14% supérieure à la récupération obtenue avec les solvants organiques traditionnellement utilisés comme toluène et dichlorométhane (DCM) dans les mêmes conditions. La qualité du bitume extrait par les trois solvants a été analysée par FTIR spectroscopie, ce qui a indiqué qu'une moindre migration de minéraux argileux dans le bitume produit s'est produite lors de l'extraction avec du 2-MeTHF. Cependant, dans les conditions de température élevée d'extraction de Soxhlet, les réactions de protonation, d'ouverture de cycle et de polymérisation du 2-MeTHF ont été postulées pour former des produits similaires à l'huile, qui ont été détectés dans le spectre FTIR du bitume extrait ainsi que par spectroscopie de masse à ionisation chimique à pression atmosphérique (APCI-MS). Ces résultats indiquent que le 2-MeTHF a le potentiel d'utiliser comme solvant d'extraction de bitume, fournissant un rendement de récupération plus élevé et une meilleure qualité du produit que le toluène et le DCM. Néanmoins, les conditions de température élevée doivent être évitées dans les procédés d'extraction et de récupération du solvant pour empêcher les réactions de polymérisation.

CONTRIBUTIONS TO KNOWLEDGE

1. Demonstrated the utility of the attenuated total reflectance (ATR) mode of spectral acquisition as a means of monitoring soil quality by Fourier transform infrared (FTIR) spectroscopy.

2. Evaluated the utility of a calibration approach based on the use of ATR-FTIR and DRIFT-NIR soil spectra as calibration set and partial-least-squares regression (PLS) for the development of FTIR and NIR methods for the prediction of 10 selected soil properties, namely, total carbon (TC), total nitrogen (TN), carbon-to-nitrogen ratio (C/N), ammonium (NH_4^+), nitrate (NO_3^-), sand, silt, clay, N-uptake, and yield.

3. Provided experimental evidence that both ATR-FTIR spectroscopy and DRIFT-NIR spectroscopy successfully monitor certain major soil properties, such as TC, TN, C/N, sand, silt, and clay. Based on the model prediction performances, ATR-FTIR spectroscopy was proved to better model soil quality than DRIFT-NIR spectroscopy.

4. Developed a method for the direct determination of bitumen residues in Alberta oil sands tailings soils without any extraction process by ATR-FTIR spectroscopy coupled with PLS.

5. Established a method using ATR-FTIR spectroscopy in conjunction with cluster analysis (CA) and principal component analysis (PCA) for the categorization of tailings soils based on bitumen level, which is beneficial in optimization of tailings remediation processes and in verifying that the remediation goal is met.

6. Provided experimental evidence that the green solvent 2-methyltetrahydrofuran (2-MeTHF) is a potential alternative to the traditionally used organic solvents in bitumen solvent-extraction and provides higher extraction efficiency and better quality extracts than toluene and dichloromethane.

7. Determined the differences between the soluble, less-soluble, and insoluble fractions of bitumen on a structural basis and achieved the quantification of each fraction by using ATR-FTIR spectroscopy.

8. Provided experimental evidence that 2-MeTHF is reactive when heated in the presence of Lewis acids, forming oil-like by-products that cannot be removed from the Soxhlet-extracted bitumen extracts.

TABLE OF CONTENT

LIST OF FIGURES

LIST OF ABBREVIATIONS

APCI-MS	Atmospheric-pressure chemical ionization mass spectroscopy
ATR	Attenuated total reflectance
CA	Cluster analysis
CEC	Cation exchange capacity
C/N	Ratio of carbon to nitrogen
CV	Coefficient of variation
DCM	Dichloromethane
DRIFT	Diffuse reflectance infrared Fourier transform
ERCB	Energy Resources Conservation Board
F_c	Centrifugal force
FTIR	Fourier transform infrared
HPLC	High-performance liquid chromatography
HWEP	Hot water extraction process
IR	Infrared
LVs	Latent variables
2-Me-SEB	2-Methyltetrahydrofuran Soxhlet-extracted bitumen
2-MeTHF	2-Methyltetrahydrofuran
MFT	Mature fine tailings
MIR	Mid-infrared
MSC	Multiplicative signal correction
NIR	Near-infrared
PA	Precision agriculture
PAHs	Polycyclic aromatic hydrocarbons
PC	Principal component

PCA	Principal component analysis
PLS	Partial least squares
PLSR	Partial-least-squares regression
PRESS	Predicted residual error sum of squares
R^2	Correlation coefficient
RHS	Re-usable hydrocarbon sorbent
RMSE	Root mean square error
RMSEC	Root mean square error of calibration
RMSECV	Root mean square error of cross-validation
RPD	Ratio of performance to deviation
RPIQ	Ratio of performance to interquartile range
SARA	Saturates, aromatics, resins, and asphaltenes
SD	Standard deviation
SNV	Standard normal variate
SOM	Soil organic matter
SSM	Site-specific management
TC	Total carbon
THF	Tetrahydrofuran
TMF	Tailings management framework for mineable Athabasca oil sands
TN	Total nitrogen
T-SEB	Toluene Soxhlet-extracted bitumen
USDA	United States Department of Agriculture
UV	Ultraviolet
VPA	Variable rate application

Soil is a vital component of the natural environment that plays an important role in agriculture, the environment, nature protection, landscape architecture, and urban planning (Blum 1993). It is difficult to rate the importance of these roles, since all are vital to our well-being to some extent. However, its function of supporting agriculture and food production is fundamental for the preservation and advancement of human life (FAO and ITPS 2015).

1.1. Soil Quality in Canadian Agriculture

Agriculture is one of the most important activities of human society as food produced from agriculture sustains life. Soil is critical to successful agriculture, since it is the original source of the nutrients and supports the growth of the crops. Therefore, the quality of soil determines the quality and the quantity of the crops. Consequently, soil quality has become the major focus in farming management practices in order to produce the best and highest yield.

However, loss of soil quality and soil degradation phenomena in Canada have been ongoing since the turn of last century. The main causes are erosion by wind and water, salinity, acidity, and improper agricultural management practices (Forge 1998). The improper farming management includes the use of fertilizers which are applied to compensate for the loss of quality but lead to poorer soil quality due to the excessive and homogenous application. Owing to the lack of initial nutrient information prior to fertilizer spraying activities, it is difficult for the farmers to apply the proper amount. In addition, the nutrient levels in soils constantly change over time, but these changes cannot be taken into account by the farmers due to the time-consuming nature of traditional soil analysis, so that the amount of fertilizer sprayed does not match the current need. Furthermore, the homogeneous application over the whole field leads to sub-optimal production due to the spatial variability of many factors within the field (Schueller 1992). Therefore, soil quality and the nutrient input should be better monitored and managed with a new strategy, which can provide detailed, accurate and repeatable information describing the levels of nutrients and their variabilities across the field in a fast and economic manner.

Precision agriculture (PA) is an innovative farm management strategy which was initiated in the early 1980s in the United States and is being rapidly adopted in many developed countries, such as the US, Germany, Canada, Australia, and the UK, in recent decades. PA focuses on effective resource utilization through the management of spatial and temporal variability of the soil. It is defined as the application of information and technologies to manage spatial and temporal variability associated with agricultural production for the purpose of improving crop performance and environmental quality (Pierce and Nowak 1999). It allows farmers to better manage the field, reduce costs, improve yield quantity and quality, and reduce environmental impacts (Reichardt and Jürgens 2009).

PA is information-intensive, as a lot of data covering the variabilities across the field is required to generate a reliable map, according to which treatment of the soil is tailored to each spot within the field. Therefore, a technique that can acquire large amounts of data in a fast, economical, and reproducible manner is in demand. Fourier transform infrared spectroscopy (FTIR) is a rapid, nondestructive, and cost-effective technique that can capture information on the chemical and physical characteristics of soils in seconds owing to the absorption of infrared light by a wide range of soil components. The information captured by FTIR spectroscopy can be used to develop calibration models, which can subsequently be used to monitor the initial nutrient level across a field, design the fertilizer spraying, and predict the crop yield.

1.2. Soil Contamination in the Canadian Environment

Soil contamination is caused by the presence of man-made chemicals or other alterations in the natural soil environment. The exposure of the environment to contaminated soil can cause health risks by direct contact or from secondary contamination of water supplies. In the Canadian province of Alberta, large amounts of bitumen-contaminated soils are produced by oil sands mining activities. As of 2015, over 895 km^2 of land had been disturbed due to oil sands mining (Natural Resources Canada 2015). The disturbed land is required by Alberta's *Directive 074* to be reclaimed by filling with the mined-out soils, which are contaminated by bitumen residues (Alberta Oil Sands Industry 2009).

The mined-out soils are produced and stored in tailing ponds, which contain approximately 1.8% bitumen residues, 27.4% soil minerals and 70.8% wastewater (Energy Resources Conservation Board 2011). After removal of the water, the bitumen residues are enriched in the soils to a level of about 6.16%, as the bitumen is adsorbed on the soil surface or is trapped within the pores of the soil, and therefore cannot be removed with the water. The bitumen-concentrated soils pose environmental concerns and threaten wildlife if they are released back to the environment without a proper remediation process. According to the data provided by Environment Canada's National Pollutant Release Inventory (NPRI), between 2006 and 2009, pollution by polycyclic aromatic hydrocarbons (PAHs) on site increased by 15.5% (Alberta Oil Sands Industry 2009).

Considering the risks to the environment associated with the bitumen-contaminated tailing soils, as well the more and more severe land disruption and larger production of contaminated tailing soils due to the expanding mining operations, sufficient recovery of the tailing soils is necessary. As of 2011, there were about 130 approved primary recovery projects (Energy Resources Conservation Board 2011). Nevertheless, the performance of the recovery cannot be guaranteed without a reliable monitoring technology. With the aid of such a monitoring technology, the recovery of the soil can be evaluated by the determination of the bitumen residue content. In addition, a technology that is amenable to on-line monitoring is desirable, as real-time feedback benefits decision making and on-line assessment.

FTIR spectroscopy is a fast and reliable technology that is used in a standard method for bitumen content determination (US Environmental Protection Agency 2007). However, in this standard method, solvent extraction is required prior to FTIR analysis, which has disadvantages of solvent and labor cost, is time-consuming, and cannot meet the need for on-line analysis (Schwartz, Ben-Dor *et al*. 2012). Therefore, there is a need for an FTIR method that can determine bitumen residues directly in the soil matrix.

1.3. Objectives of the Research
The present research aimed at exploring the application of FTIR spectroscopy in conjunction with partial-least-squares regression (PLSR) for the assessment of soil quality with soils

collected from across Canada and for the quantification of bituminous contamination in Alberta oil sands tailing soils. The specific objectives of this research were as follows:

(1) To establish an FTIR spectral library of Canada-wide agricultural soils containing both mid-infrared (MIR) and near-infrared (NIR) spectra acquired using the attenuated total reflectance (ATR) and the diffuse reflectance infrared Fourier transform (DRIFT) technique, respectively.

(2) To develop ATR-FTIR PLSR calibration models for the assessment of soil quality through the determination of 10 selected soil properties: total carbon (TC), total nitrogen (TN), carbon-to-nitrogen ratio (C/N), ammonium (NH_4^+), nitrate (NO_3^-), sand, silt, clay, N-uptake, and yield.

(3) To develop DRIFT-NIR PLSR models for the assessment of soil quality through the determination of 10 selected soil properties: total carbon (TC), total nitrogen (TN), carbon-to-nitrogen ratio (C/N), ammonium (NH_4^+), nitrate (NO_3^-), sand, silt, clay, N-uptake, and yield.

(4) To compare the performances of ATR-FTIR and DRIFT-NIR spectroscopy for the assessment of soil quality and for use in support of precision agriculture.

(5) To establish an ATR-FTIR PLSR calibration model for the determination of bitumen residues in Alberta tailing soils.

(6) To investigate the bitumen recovery performance of the green solvent 2-methyltetrahydrofuran (2-MeTHF) by using ATR-FTIR and DRIFT-NIR spectroscopy.

The thesis consists of seven chapters. Chapter 2 is a review of the literature related to topics and concepts used to undertake the research work. Chapter 3 describes the development and the evaluation of ATR-FTIR PLSR calibration models for 10 selected soil properties related to soil quality. Chapter 4 reports the development and evaluation of DRIFT-NIR PLSR calibration models for the same soil properties and compares the performances of the ATR-FTIR and DRIFT-NIR calibration models. Chapter 5 concerns the direct quantification of bitumen residues in Alberta tailing soils through the development of an ATR-FTIR PLSR calibration model as well as the categorization of the tailing soils based on their bitumen content by using ATR-FTIR spectroscopy coupled with principal component analysis (PCA). Finally, the evaluation the

bitumen recovery performance of the green solvent 2-MeTHF by ATR-FTIR spectroscopy and the understanding of the structural differences among different bitumen fractions, which affect their solubility in the solvent and therefore affect the solvent extraction performance, are presented in Chapter 6. An overall conclusion made in this research is provided in Chapter 7.

2.1. Introduction

Soil quality determines the quality and quantity of crop yield. Soil quality assessment is routine in farm management and many conventional soil analytical techniques with a wet-chemical extraction process are used. Historically, our understanding of soil and the assessment of its quality has been gained through this type of analysis. However, this approach has two main disadvantages, soil integrity damage and low efficiency. With regard to soil integrity damage, the extraction process disrupts soil's complex structure and multi-component interactions, making the analysis result more difficult to interpret. Moreover, the extraction requires large amounts of solvents, labor, and time, making the efficiency low (Rossel, Walvoort *et al.* 2006). These disadvantages of the conventional techniques became more problematic in the 1990s, when precision agriculture was introduced.

Precision agriculture aims at optimizing farm management to achieve targeted crop yield while reducing the excess application of fertilizers. It requires precise measurement and control of the nutrients in soil (Mintert, Widmar *et al.* 2016). In order to precisely tailor the use of fertilizers, soils across the field should be characterized. Therefore, precision agriculture requires a soil analytical technique that can deal with large amounts of samples in a low-cost and efficient way. (Terra, Demattê *et al.* 2015). The disadvantages of the conventional techniques make them unsuitable for use in precision agriculture. Consequently, other analytical techniques need to be developed, such as infrared spectroscopy, which can better characterize the soil as a complete system and can analyze large numbers of soil samples economically and efficiently.

Precision agriculture aims at environmental sustainability, which is a shared goal with the Alberta oil sands industry. Tailings produced from Alberta oil sands mining receive much concern due to their negative environmental impact and their vast and increasing accumulation. Much attention has been paid in searching new techniques which are of benefit in tailings

volume reduction, mature fine tailings reduction, tailings water reclamation, tailing soil reclamation, and bitumen residue reclamation (Alberta Oil Sands Industry 2009).

2.2. Precision Agriculture

2.2.1. Definition

Precision agriculture (PA) is a concept initiated for site-specific crop management based on observing, measuring, and responding to the variability in soils or in crops, in order to optimize the profitability of the production and the sustainability by reducing the environmental impact (Zarco-Tejada, Hubbard *et al.* 2014). The first definition of PA came from the US House of Representatives (1997), which defined PA as "*an integrated information- and production-based farming system that is designed to increase long term, site-specific and whole farm production efficiency, productivity and profitability while minimizing unintended impacts on wildlife and the environment*" (Whelan and Taylor 2013).

Site-Specific Crop Management (SSM), another commonly used term, which narrows PA's philosophy down to its implementation in cropping systems, is defined by (Whelan and McBratney 2000) as "*a form of PA whereby decisions on resource application and agronomic practices are improved to better match soil and crop requirements as they vary in the field*". Many complex definitions of PA exist, but all of them can be summarized into one simple description, which is "*apply the right treatment in the right place at the right time*" (Gebbers and Adamchuk 2010).

2.2.2. Benefits

The PA concept has been considered worldwide for most common crops, such as rice, cotton, and potato. It has seen adoption in most U.S. states and Canadian provinces, most countries of Western Europe, Australia and New Zealand and some Asian countries, such as Japan, Malaysia, and some regions of China (Robert 2002). As the main function of PA, a better decision making can provide a wide range of benefits. (Griffin, Lambert *et al.* 2005) reported an average of 68% profit increase due to PA based on 234 studies between 1988 and 2005. In addition to the increased profitability, PA can bring additional benefits due to better management practices and

the application of information technologies. It is able to increase crop quality, improve sustainability, minimize environmental impact and risk, and enhance food safety associated with product traceability (Robert 2002; Gebbers and Adamchuk 2010).

2.2.3. Applications

PA was initiated in the mid-1980s to improve the application of fertilizers with varying rates and blends as needed within fields to prevent over- or under-application by using Variable Rate Application (VPA) methods (Robert 2002). However, PA is more than the management of soil variability; it is an information technology that can be used in all areas of agriculture. Presently, PA has been adapted to a variety of practices. For example, PA has been able to reduce machinery to avoid unnecessary crop damage and soil compaction and to reduce input costs while increasing crop yield (Bowman 2008). In addition, in the case of fruit and vegetable farming, PA allows a better product grading as well monitoring of quality and safety based on the use of automated systems to record parameters related to product quality (Njoroge, Ninomiya *et al*. 2002). The tracking information on chemical spraying and the use of fertilizers is beneficial to the risk management and to the food traceability (Zarco-Tejada, Hubbard *et al*. 2014). The benefits of PA related to profitability, risk, and environmental effects, which are key concerns in the late 20th century, resulted in a research boost in the late 1990s (Fig. 2-1).
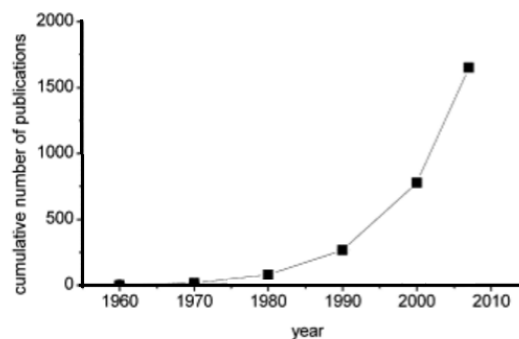
Fig. 2-1. Cumulative number of journal publications referring to precision agriculture from 1960 to 2006 using exact search phrase "precision" and "agriculture"

2.3. Soil Quality

PA technologies are being developed to optimize farm profitability while minimizing the environmental impact by adjusting the production inputs, such as fertilizers and herbicides, based on the specific needs within the field. Among all the applications of PA, one of the first and the most important is the management of soil quality (Thomasson, Sui *et al*. 2001). Proper understanding of soil quality is necessary to achieve precision farming, since only after an accurate measurement of soil quality can the production inputs be optimized based on the information obtained within the field (Kim, Sudduth *et al*. 2009).

2.3.1. Definition

Soil quality is a commonly used concept in soil science. It is a function of soil properties, such as soil nutrients, moisture, minerals, organic matter and so on. The concept of soil quality or soil quality was defined by some researchers as "*the soil's capacity or fitness to support crop growth without resulting in soil degradation or otherwise harming the environment*" (Acton and Gregorich 1995). For a simpler definition, "quality" implies the concept of "fit for purpose" (Dexter 2004). Soil quality is the total concept of soil physical, chemical and biological quality, and each of them is correlated and interdependent (Dexter 2004). Soil quality is very comprehensive and therefore cannot be measured directly but it can be evaluated on the basis of some other soil properties, such as soil nutrients, moisture, minerals, organic matter and so on (Bautista-Cruz, Carrillo-González *et al*. 2007).

2.3.2. Soil Properties

2.3.2.1. Soil Organic Matter (SOM)

SOM is a group of complex organic compounds which come from the remains of dead organisms, such as plants and animals, and also their waste products released to the environment. These compounds are generated by the decomposition of carbohydrates, proteins, lipids, lignins, and cellulose by series of specific reactions (Brady and Weil 1996). Generally, organic matter contains 45 – 55% carbon, 35 – 45% oxygen, 3 – 5% hydrogen, and 1 – 6% nitrogen, by weight (Cabaniss, Madey *et al*. 2005).

In dried soil, SOM only comprises a small portion by weight, between 1 and 6% (Hesse 1971), but its influences on soil physical, chemical, and biological properties extend far out of proportion to the small quantities present. For example, SOM provides much of the cation exchange and water-holding capacities of surface soils; it contains large amount of nutrients required for plant growth and certain organic compounds found to have direct growth-stimulation effect on plants (Brady and Weil 1996).

2.3.2.1.1. Total Carbon (TC)

The concepts of SOM and TC easily cause confusion, since all organic substances contain carbon. However, SOM and TC are not identical and it is improper to use SOM to describe TC. SOM includes all the elements that are components of organic compounds, such as carbon, oxygen, hydrogen, and nitrogen whereas TC is the sum of three carbon forms, organic, elemental, and inorganic. Elemental carbon includes coal, graphite and so on; inorganic carbon usually refers to carbonates, hydrogen carbonate, and carbon dioxide (Hesse 1971).

Compared to SOM, TC is easier to measure directly. Therefore, TC is commonly measured and is converted to SOM by multiplying it by the conversion factor of 1.72, which assumes that SOM contains 58% carbon by weight. However, according to soil type, the percentage of carbon in SOM varies and therefore the conversion factor can be as high as 2.5, such as in the case of sub-soils (Page 1982).

2.3.2.1.2. Total Nitrogen (TN)

Nitrogen limits plant growth more than any other element (Hesse 1971). Plants can utilize CO_2 and H_2O to produce carbohydrates via photosynthesis, but they cannot produce other essential constituents, such as proteins, nucleic acids, enzymes, and energy transfer materials such as chlorophyll, ADP and ATP (adenosine di- and triphosphate), without available nitrogen. Although nitrogen is rich in the atmosphere, which contains 78% nitrogen, it cannot become the nitrogen source of plants until it is chemically combined with hydrogen, oxygen, or carbon. This process is called nitrogen fixation and is usually accomplished in nature by certain microorganisms and lightning. However, the fixed nitrogen amount is far from enough for plant

growth. In addition, the natural nitrogen content in soil is low, normally ranging from 0.02 to 0.5% (Hesse 1971), and cannot meet the demands of plant growth requirement (Troeh and Thompson 2005).

In most soils, nitrogen sources are in organic forms, coming from protein and other complex molecules, such as humic compounds (Hesse 1971). Many of them are in amine form ($-NH_2$) and cannot be used by plants directly. They must be at least partially ionized to become available for plant uptake. "Ammonification" first happens, where the amine group is gradually decomposed by microbes and then absorbs the third hydrogen atom when the carbon-to-nitrogen bond breaks, ammonia (NH_3) or ammonium cation (NH_4^+) is released. Ammonia can be absorbed as a nitrogen source by certain plants but the types of nitrogen most efficiently utilized are nitrite (NO_2^-) and nitrate (NO_3^-). This is because the availability of the ammonium cation is lower due to the cation-exchange site adsorption, while nitrate ions usually freely exist in the soil solution. After ammonification, ammonia is further oxidized to nitrite and then nitrate. This step is called nitrification. Ammonification and nitrification can be called mineralization, where the organic form of nitrogen ($-NH_2$) is converted to inorganic mineral forms (NH_4^+ and NO_3^-). Nitrite (NO_2^-) is rarely retained in soil, since it is immediately oxidized to NO_3^-, which is the end product of these series of reactions, and it is the form of nitrogen optimally utilized by plants (Troeh and Thompson 2005).

2.3.2.1.3. Ratio of Carbon to Nitrogen (C/N ratio)

Not only are carbon and nitrogen key elements of organic matter, but also their relative proportions are important. The C content of dry organic matter is about 44 – 45%, while the N percentage is much lower and varies widely from 1 to 6%. The C/N ratio varies widely between 8/1 and 600/1 in soils, plants, and microbes. C/N ratio is very important to soil quality management. It helps to determine the amount of plant-available nitrogen, the rate of organic decay, and the level of total organic matter (Brady and Weil 1996).

In nature, microbes play an important role in decomposition of organic residues, which become the nutrient sources for crops. C/N ratio determines how well the decomposition is performed and therefore indicates the level of the available mineralized nitrogen in soil. Organic

decomposition is the way that microbes consume nutrients to build up their cells. On average, microbes need 8 parts of C for every part of N to build their cells. Furthermore, microbes can only incorporate 1/3 of total C and respire the rest as carbon dioxide (CO_2) when decomposing the C from the organics. Therefore, the C/N ratio of the organics that satisfies the microbes most is 24/1. However, C/N ratios vary widely from 18/1 for alfalfa hay to 600/1 for sawdust. Those organic residues with C/N ratio exceeding 30/1 cannot provide enough N to the microbes, which will then compete with the crops for the N from the soil solution, causing the crop yield to decrease (Brady and Weil 1996).

Therefore, C/N ratio is able to indicate the soil's nutrient level in terms of plant-available N. If the C/N ratio is lower than 30/1, soils are rich in mineralized N which comes from the decomposition of organic residues. On the other hand, if the C/N ratio is higher than 30/1, soils are short of plant-available N, as microbes consume extra N resources apart from the organic residues (Troeh and Thompson 2005).

In addition to plant-available N, C/N ratio can also indicate soil quality. Commonly, the C/N ratio in soil ranges from 8/1 to 15/1. If the ratio is higher than 30/1, the soils are probably under acidic and highly leached conditions. Therefore, proper soil management practices are required, such as changing the soil's pH by addition of lime to make it more suitable for farming. Furthermore, the C/N ratio can be used as a parameter when selecting a fertilizer. The proper fertilizer can regulate the C/N ratio of soil to make the nutrients more balanced for the crops. The selected fertilizer must provide sufficient N; otherwise, the crops will suffer from N deficiency or oversupply, leading to weak crops, low-quality crops or disease-susceptible crops (Brady and Weil 1996).

2.3.2.2. Minerals

About half of soil is composed of minerals (45%) and these minerals can be classified as sand, silt, and clay according to their particle size. The relative proportions of these three minerals determine soil texture, which has association with soil quality. For example, (Sorensen 1981) and (Ladd, Amato *et al*. 1985) found that organic residues decompose more rapidly in sandy soils than in clay soils. Soil texture has profound effects on the behavior of soils, such as water

holding capacity, nutrient retention and supply, nutrient leaching, and oxygen supply (Cass, Hansen *et al*. 2002).

2.3.2.2.1. Sand, Silt, and Clay

Excluding the large solids (stones and gravel), soil particles range in size from 2.0 mm to smaller than 0.0002 mm (0.2 μm) in diameter. According to the particle size, the mineral constituents of soils can be classified into three categories: sand, silt and clay. Sand particles (2.0 to 0.05 mm) are large enough to be seen by the naked eye. When rubbed between fingers, sand feels gritty and not sticky, since sand particles do not adhere to one another. Silt particles (0.05 to 0.002 mm) are too small to feel individually, so it feels smooth but not sticky. Unlike sand, silt cannot be seen without a microscope. Clay particles are the smallest (<0.002 mm) and adhere together to form a sticky mass when wet. Clay particles have colloidal properties when the particle size is less than 0.001 mm and can only be seen under an electron microscope (Brady and Weil 1996). Such extremely small size provides clay with a tremendous amount of surface area per unit mass. Since the surfaces of clay exhibit electromagnetic charges that attract positive and negative ions as well as water, most of the soil physical and chemical activities occur in this fraction. Some general properties of these three soil particles are summarized in Table 2-1.

Table 2-1. General properties of sand, silt, and clay

Property	Sand	Silt	Clay
Range of particle diameters (mm)	2.0 – 0.05	0.05 – 0.002	< 0.002
Attraction of particles for each other	Low	Medium	High
Attraction of particles for water	Low	Medium	High
Ability to hold chemicals and nutrients	Low	Medium	High

2.3.2.2.2. Colloidal Properties of Clay

Clay has colloidal properties. It is the seat of soil chemical and physical activity. When particle size is down to 1 μm (0.001 mm) in diameter, it is considered to behave as a colloid. Clay is also a highly reactive material due to the electrically charged surfaces. The extremely small size provides an enormous amount of active surface per unit mass.

The main colloidal properties of soil are ion and water adsorption properties. Due to the chemical structure of clay, it normally carries negative charges and therefore mainly attracts cations, such as Al^{3+}, Ca^{2+}, Mg^{2+}, K^+, H^+, and Na^+. This property plays a main role in cation exchange in soil solution, which is important to nutrient cycling. In addition, the colloidal particles attract the oppositely charged end of the water molecules and hold the water in the soil (Brady and Weil 1996).

2.3.3. Determination of Soil Quality

Monitoring soil quality receives much interest due to the increasing emphasis on precision farming, productive farming and sustainable farming. Therefore, certain soil properties that can be soil quality indicators need to be monitored to help the evaluation of the soil quality.

2.3.3.1. Laboratory Methods

Historically, conventional soil chemical and physical laboratory analyses have been used to understand soil, assess its quality and function, and correlate soil's physical and chemical properties with individual soil components (Rossel, Walvoort *et al*. 2006). In the routine laboratory analysis, a soil solution instead of soil itself is commonly analyzed. To obtain soil solution samples, a series of procedures are required, such as sample extraction, targeted component isolation, and targeted component concentration (Ure 1996). For example, cation exchangeable capacity (CEC), which is an important indicator of soil quality and nutrient retention capacity, is measured by atomic absorption spectroscopy after $BaCl_2$ exchange reaction.

Some laboratory analysis methods take a relatively long time to measure each soil property. For example, for the study of soil texture, as measured by the Bouyoucos hydrometer, a uniform soil suspension is obtained by 15 min of mixing, and then the buoyant force on a hydrometer is determined directly by the density of the soil suspension at 40 seconds and 7 hours after mixing stops and sitting starts. Each sample measurement takes about 8 hours to complete (Pansu and Gautheyrou 2007). Some laboratory methods for analysis of soil attributes are summarized in Table 2-2.

Since these conventional methods are destructive, the sample cannot be reused for other measurements after one analysis. Consequently, the number of required subsamples and their consistency, as well their representativeness of the bulk sample, need to be paid attention to by the analyst. However, the introduction of precision agriculture requires a more efficient, precise, economic, and simultaneous analysis method, and accordingly the traditional laboratory methods are no longer the best-suited methods for soil quality assessment (Janik, Merry *et al*. 1998).

Table 2-2. Recommended laboratory methods for analysis of selected soil attributes (Hesse 1971)

Attribute	Methods	Reagents
TC	Dry combustion	Copper oxide
TN	Kjeldahl digestion	Sulfuric acid, sodium hydroxide, boric acid-indicator, hydrochloric acid, catalyst mixture
NH_4^+	Extraction and distillation	Potassium chloride, magnesium oxide, boric acid indicator, hydrochloric acid
NO_3^-	Extraction and distillation	Potassium chloride, magnesium oxide, boric acid indicator, hydrochloric acid

2.3.3.2. Fourier Transform Infrared (FTIR) Spectroscopy

In precision agriculture, accurate site-specific data on the whole field are required, which requires that larger numbers of samples covering the variety and heterogeneity within the field

should be characterized (Bramley and Janik 2005). In addition, crop yield mapping can be achieved since a close relationship between certain soil properties, such as electrical conductivity, and crop yield has been found (Lund, Colin *et al*. 1999; Corwin and Lesch 2003). Furthermore, some specific properties, such as soil nitrate, require a rapid measurement due to their easily leaching and denitrification nature (Kim, Sudduth *et al*. 2009). Consequently, PA requires a fast, economic, and accurate method which can handle large numbers of samples within the acceptable time frame. In recent years, many instruments have been invented based on direct contact technology (Sudduth, Hummel *et al*. 1997), such as FTIR and near-infrared (NIR) spectroscopy, which can determine soil properties in a rapid and non-destructive way (Kim, Sudduth *et al*. 2009). The research on the determination of selected soil properties by using direct spectroscopic measurements on soil that has been published in the last 10 years is summarized in Table 2-3.

Table 2-3. Publications of quantitative predictions of various soil attributes using PLS statistical technique and spectral response in near-infrared (NIR) or visible/near-infrared (Vis/NIR) and mid-infrared (MIR) regions

Attributes	Spectral range	Range	$n_{cali}|n_{vali}$ [a]	r_c^{2} [b]	$RMSE_{CV}$ [c]	RPD [d]	Authors
	DRIFT-MIR	0.98-104	177|60	0.95	3.4	NA	(McCarty, Reeves *et al*. 2002)
Total C (g kg⁻¹)	DRIFT-MIR	0.6-127.4	293|127	0.98	2.4	2.1	(Minasny, Tranter *et al*. 2009)
	DRIFT-NIR	0.98-104	177|60	0.86	5.4	NA	(McCarty, Reeves *et al*. 2002)
	DRIFT-NIR	5-122	228|71	0.85	17	2.6	(Rajendram and Devey 2011)

Table 2-3. cont.

Attributes	Spectral range	Range	$n_{cali}|n_{vali}$ [a]	r_c^2 [b]	RMSE$_{CV}$ [c]	RPD [d]	Authors
Total N (g kg^{-1})	DRIFT-MIR	0.07-4.5	252|90	0.94	0.2	2.0	(Minasny, Tranter *et al.* 2009)
	DRIFT-MIR	0.64-3.6	42|18	0.77	0.3	2.1	(Vohland, Ludwig *et al.* 2014)
	NIR	0.1 – 16.2	228|101	0.84	1.1	2.5	(Rajendram and Devey 2011)
	NIR	0.64-3.6	42|18	0.37	0.49	1.22	(Vohland, Ludwig *et al.* 2014)
Nitrate-N (mg kg^{-1})	DRIFT-NIR	0-115	817|363	0.72	3.63	0.9	(Minasny, Tranter *et al.* 2009)
Sand (g kg^{-1})	ATR-FTIR	150-880	180|90	0.90	78	3.14	(Ge, Thomasson *et al.* 2014)
	DRIFT-NIR	0-910	881|371	0.87	21.42	NA	(Terra, Demattê *et al.* 2015)
	DRIFT-NIR	30 - 990	518|215	0.94	64.7	2.3	(Minasny, Tranter *et al.* 2009)
	Vis-NIR	0-910	881|371	0.85	22.16	NA	(Terra, Demattê *et al.* 2015)
Clay (g kg^{-1})	ATR-FTIR	20-500	180|90	0.94	37	3.38	(Ge, Thomasson *et al.* 2014)
	DRIFT-NIR	0-930	881|371	0.88	84.48	NA	(Terra, Demattê *et al.* 2015)
	DRIFT-NIR	6-890	518|217	0.90	52.7	2.6	(Minasny, Tranter *et al.* 2009)

[a] n_{cali} – number of calibration samples; n_{vali} – number of validation samples

[b] r_c^2 – coefficient of determination in calibration

[c] RMSE$_{CV}$ – root-mean-square error in cross-validation

[d] RPD – ratio of performance to deviation, RPD > 2, "excellent"

2.3.3.2.1. Near Infrared (NIR) Spectroscopy

NIR spectroscopy was first introduced into soil science in the 1960s (Bowers and Hanks 1965). Nowadays, NIR spectroscopy has been successfully applied in many areas of soil science, such as soil biochemistry, biology, chemistry and physics. Its ability to simultaneously characterize and quantify various soil attributes using a single spectrum per soil sample makes this technique attractive for soil analysis (Rossel, Walvoort *et al*. 2006). Due to this feature, NIR spectroscopy is estimated to save at least 80% of the laboratory cost associated with conventional reference methods (Foley, McIlwee *et al*. 1998). Specifically, by using NIR spectroscopy, the expected reduction of analytical cost is estimated to be about 63% in Canada (Nduwamungu, Ziadi *et al*. 2009).

2.3.3.2.1.1. Theory

The molecular bonds of an organic material continually vibrate at specific frequencies that are characteristic of the bond or the functional group. When an organic material is irradiated by an incident beam of light, the frequencies of the incident light that match the frequencies of the vibrations of its bonds are absorbed whereas other frequencies are reflected or transmitted (Foley, McIlwee *et al*. 1998). Therefore, the spectrum of light reflected by or transmitted through the sample contains detailed information about the chemical composition of that sample (Shenk and Westerhaus 1991).

Near-infrared radiation, with wavelengths between 750 and 2500 nm, is absorbed mainly by C – H, N – H, and O – H bonds, which are the primary components of organic compounds (Osborne, Fearn *et al*. 1993). However, the bands in an NIR spectrum are not sharp or distinct because they correspond to overtones and combinations of fundamental absorptions in the mid-infrared region. In addition, light scattering is another factor giving rise to the lack of distinct bands. Consequently, it is difficult to directly correlate sample attributes to the peaks and therefore, a multivariate statistical model needs to be developed to describe the relationship between NIR spectral absorbance and the components of interest (Foley, McIlwee *et al*. 1998).

2.3.3.2.1.2. Applications and Limitations

NIR spectroscopy has been widely used for determination of soil properties. There are several advantages associated with the use of NIR spectroscopy by comparison with mid-IR spectroscopy. Firstly, the optics are less expensive. In addition, in situ and on-site applications are possible. Moreover, minimum sample preparation is needed. Although the NIR absorption bands due to overtones and combinations are weak and overlapping, the rapid advancement of computational and multivariate modelling capabilities makes it efficient to extract relevant information from NIR spectra (Ge, Thomasson *et al*. 2014). Another point that has been discussed regarding the reliability of NIR soil analysis is that NIR spectroscopy is insensitive to quartz, a major component of most soils. However, NIR spectroscopy is well supported commercially, is well suited to field portability and remote sensing, and can deal with larger bulk soil samples. Therefore, NIR spectroscopy is still widely studied and applied in soil analysis.

2.3.3.2.2. Mid Infrared (MIR) Spectroscopy

The use of MIR spectroscopy for soil analysis has been continuously increasing. MIR spectroscopy in most of the early work focused on soil classification and qualification by relating spectral bands to soil chemical groups including organic matter (Baes and Bloom 1989; Niemeyer, Chen *et al*. 1992; Janik, Skjemstad *et al*. 1995) and soil minerals (Nguyen, Janik *et al*. 1991). Later, when Fourier transform instruments became widely available, diffuse reflectance infrared Fourier transform spectroscopy (DRIFTS) was used for quantitative analysis of many soil properties including sand, clay, water potential, total nitrogen content, carbon content, cation exchange capacity (CEC) and pH (Janik, Merry *et al*. 1998; Rossel, Walvoort *et al*. 2006). More recently, different fractions of carbon were quantified using MIR spectroscopy (McCarty, Reeves *et al*. 2002; Bellon-Maurel and McBratney 2011).

2.3.3.2.2.1. Theory

As described previously, infrared spectroscopy is based on the vibrations of covalent bonds of a molecule. In the MIR region, fundamental vibrations occur where molecules transit from the vibrational ground state to the first excited vibrational state. The energy absorbed by part of the

molecule corresponds to the frequency of the vibration and is observed as a peak in an IR absorption spectrum. In contrast to the bands in NIR spectra, the bands due to fundamental absorptions observed in MIR spectra are intense and distinct (Du, Ma *et al*. 2015). Broadly, MIR spectroscopy can be classified as transmission and reflectance (internal and external) spectroscopy.

2.3.3.2.2.2. Applications and Limitations

The main advantage of MIR spectroscopy is that the fundamental vibrational bands are strong and can be distinctively associated with certain bonds or functional groups. This also becomes a limitation of MIR spectroscopy, where the absorption bands are usually so strong, causing band distortion (Ge, Thomasson *et al*. 2014). To address this problem, in the early research, sample dilution with potassium bromide (KBr) was used. However, the sample preparation is time-consuming and the KBr dilution may cause interference due to ion exchange between the samples and the KBr matrix. Consequently, its application is limited in many cases, especially in soil analysis where large numbers of samples need to be analyzed.

DRIFTS allowing for soil analysis without sample dilution emerged in the early 1990s, but its application was restricted to qualitative analysis (Nguyen, Janik *et al*. 1991). It is commonly used with non-mirror or rough surfaces where the radiation is absorbed, refracted, reflected and scattered in the bulk material. Due to the surface reflections, DRIFT spectra are nonlinear even after the linearizing transforms such as log-transform into absorbance or Kubelka-Munk transform using a scaling factor (Kattner, Lilek *et al*. 2011). This problem is partly addressed by applying multivariate analysis which can effectively correct this nonlinearity problem and yield satisfactory results, which was proved by researchers who successfully used DRIFT coupled with multivariate analysis to quantify various soil properties (Janik and Skjemstad 1995).

Attenuate total reflectance (ATR) as spectroscopic sampling technique that has been widely applied in many fields including food, agriculture, and environmental science (Oliveira, Montalvão *et al*. 2006). The great advantage of ATR is that it requires minimum sample preparation. It enables samples to be examined directly in the solid or liquid state. The applications of ATR-FTIR spectroscopy in soil analysis mainly focus on soil identification and

nitrate determination, which was first reported in 2001 (Kemsley, Tapp *et al.* 2001). Lately, ATR-FTIR spectroscopy in soil analysis was further developed but still was primarily applied for nitrate determination (Shaviv, Kenny *et al.* 2003; Linker, Shmulevich *et al.* 2005; Jahn, Linker *et al.* 2006). ATR-FTIR spectroscopy has not received much attention in soil analysis and only a few publications report on the use of ATR-FTIR spectroscopy to determine other soil components (Ge, Thomasson *et al.* 2014).

2.3.3.3. Multivariate Analysis

In both NIR and MIR soil spectra, peaks overlap and cannot be directly assigned to a specific soil component. Furthermore, some soil properties are collinear. Therefore, using simple correlation to set up a relationship between the selected infrared peak intensities and the soil attributes is inappropriate. Pioneering work demonstrated that simple, univariate methods of analysis can be replaced by much more effective multivariate methods, such as principal components analysis (PCA) and partial least-squares (PLS) analysis (Haaland and Thomas 1988; Janik and Skjemstad 1995).

2.3.3.3.1. PCA

PCA is a data compression process which reduces a complex multidimensional dataset (e.g. spectra) into a smaller number of principal components (PCs) which reflect the underlying structure and still contain most of the information in the original dataset. Each PC describes part of the variation within the dataset in decreasing order; the first PC describes the most variation in the dataset and each succeeding component accounts for as much of the remaining variation as possible. Because the PCs are orthogonal to one another, they can be interpreted independently. By plotting the PCs in a two-dimensional data space, interrelationships between samples and variables can be examined (Yang and Mouazen 2012).

2.3.3.3.2. PLSR

PLSR is a regression extension of PCA, which connects the information in x and y variables to each other. PLSR is a bilinear regression modeling method where the original x variables are

projected onto a much smaller number of PLS components, which are commonly referred to as "latent variables" or "factors". These factors are calculated according to the same mathematical procedures as PCs, but the data in the Y-matrix are also incorporated in the calculation. The regression establishes the relationship between the X-matrix (e.g. soil spectra) and the Y-matrix (e.g. reference data), with the aim being to predict the y variables by using the most relevant factors (Nieuwoudt, Prior *et al*. 2004).

2.4. Alberta Oil Sands

2.4.1. Definition

Canada has the third-largest oil reserves in the world, after Saudi Arabia and Venezuela. According to the latest governmental report (Alberta Oil Sands Industry 2016), it is estimated that the total oil reserves of Canada is about 1.8 trillion barrels. The oil resources in Canada are called "oil sands" because the oil is very viscous and is bound to the soil minerals surrounded by a thin layer of water (Fig. 2-2). Oil sand is basically a mixture of bitumen, minerals, and water. The bitumen content is variable, averaging 12 wt% of the deposit, but ranging from zero to 18 wt%. Water typically constitutes 3% to 6% of the mixture, increasing as bitumen content decreases. The mineral content, predominantly quartz, is relatively constant, ranging from 84% to 86 %. For a typical sand grain of 100 μm diameter, the water film thickness is believed to be on the order of 2 μm, and the bitumen film thickness is 5-6 μm (Friesen 1996).

Fig. 2-2. Composition of oil sands

2.4.2. Tailings

2.4.2.1. Formation

Oil companies have been extracting bitumen from Alberta's oil sands for four decades using a process which leaves behind large amounts of toxic sludge, namely, "tailings". The toxic sludge is stored and accumulated to form lakes, which are called tailing ponds (Rezac 2010).

The extraction process was designed based on the unique properties of oil sands, where the coarse sands are hydrophilic and are attached to the water film, while the bitumen is hydrophobic and repels wetted surfaces. Consequently, a special technique, "Hot Water Extraction Process (HWEP)", which was patented in 1929, has been commercially used to extract bitumen since 1967. The process mixes hot water heated to between 35 and 80 ℃ with crushed ore and additional sodium hydroxide to separate the ore into its constituent parts (Rezac 2010). Bitumen, which has similar density to water, floats to the top as froth via attachment to the injected air bubbles and is later skimmed off to achieve the recovery. The "tailings", which are the by-product from the extraction process, are sent to and stored in ponds constructed near the mining site (Clark and Pasternack 1932).

2.4.2.2. Composition

Tailings are composed mostly of water (70.8%), soil minerals (27.4%), and a small amount of bitumen residues, which is about 1.8% (Kessick 1977). When deposited in a tailing pond, the sand settles out quickly to form dykes and beaches. However, in the case of the fine materials, such as clays, their destiny in the tailing pond varies. Depending on the makeup of the tailings stream and the method of deposition, only 1/3 to 1/2 of the fine materials are retained in the tailings sand deposits. The majority of the fines separates during tailings sand deposition and becomes suspended in the water to form mature fine tailings (MFT). It is reported that about 33% of the solids content in fluid tailings is almost all fines (Scott and Ozum 2010).

2.4.2.3. Concerns

The HWEP technique and the accompanying tailings give rise to many concerns due to their environmental impact. Some of these concerns are related to the huge water consumption and

contamination. To produce one barrel of bitumen, seven to nine barrels of water are required. Although only 1/3 of the water is fresh water from the Athabasca River and most of the water is recycled from the tailing ponds, large amounts of non-recycled tailing waters are still generated, resulting from the large daily bitumen production, which reaches 1.7 million barrels per day and is projected to more than double to 3.7 million barrels per day by 2019. Currently, Alberta's inventory of tailing ponds is about 720 million cm^3, which cover an area of about 130 km^2 (Steward and Williams 2013). Various types of compounds are found in the tailing waters such as naphthenic acids, polycyclic aromatic hydrocarbons (PAHs), BTEX compounds (benzene, toluene, ethylbenzene and xylene), metals, salts and residual bitumen, which are believed to be toxic to aquatic organisms (Strosher and Peake 1978; Rezac 2010). Another concern is the disrupted mining area and the bitumen-contaminated tailing soils. It was reported that as of 2015, over 895 km^2 of land had been disturbed by oil sands mining activities (Natural Resources Canada 2015).

2.4.2.4. Regulations

These hazards of oil sands tailings were documented as early as 1973, but they did not receive much attention and did not become a high priority for government, industry, academia, and the news media until 2000. In 2008, tailings became the focus of intense discussion after the "1,600 ducks died" issue occurred in Syncrude tailings (Steward and Williams 2013). In 2009, Directive 074 was announced by Alberta's Energy Resources Conservation Board (ERCB) to set tailings performance criteria and to ensure the environmentally sustainable development of Alberta's oil sands (Alberta Oil Sands Industry 2009). It requires the amount of fluid tailings to be reduced; the size of the storage ponds to be minimized and eventually eliminated; and the fine tailings to be converted to reclaimable landscapes (Alberta Energy Regulator 2009). In March 2015, Directive 074 was suspended since new requirements for tailings management, the Tailings Management Framework for Mineable Athabasca Oil Sands (TMF), was released by the Government of Alberta. In addition to the requirements addressed in Directive 074, the TMF emphasizes the requirement of performance-monitoring to keep industry on track (Alberta Energy Regulator 2015).

2.4.2.5. Remediation

Currently, there are 33 approved oil sands exploitation projects; and there are about 130 primary recovery projects (Energy Resources Conservation Board 2011). They are all directed toward minimizing the release of contaminants to the surrounding environment, as well turning tailings into reclaimable dry and wet landscapes (Rezac 2010). Farkish and Fall (2013) proposed a new technique to remove sufficient amounts of water from MFT by using a super-absorbent polymer (SAP), which is a remarkable class of hydrophilic gels capable of absorbing and retaining large volumes of water or any other fluids (Rosa and Casquilho 2012). Their results showed that the solids content of MFT dewatered by a SAP can reach values up to 80% by weight, and the undrained shear strength can reach values between 2 and 10 kPa, depending on the amount of SAP used. Afshar, Mirmontazeri *et al.* (2014) proposed using naphthenic acids as a surfactant to remediate the oil residues trapped in tailing soils. Naphthenic acids dislodge residual oil by reducing the capillary forces that retain the oil in the void spaces, thereby lowering the oil-water interfacial tension (IFT) and reducing the contact angle at the oil-water interface. Other commercial methods have also been adopted, such as adding gypsum as a coagulant to change the chemical properties of the suspended fine clay particles, thus enabling the fines to bind to heavier sand particles to form consolidated tailings (Syncrude Canada Ltd. 2008); mixing MFT with a polymer flocculent (anionic polyacrylamide) and depositing the mixture onto beach areas in thin layers to evaporate the water (Suncor Energy Inc. 2010); and centrifugation to obtain dry tailings (Suncor Energy Inc. 2009).

2.5. Bitumen

2.5.1. Definitions

Bitumen, also known as asphalt, is a glossy black, very sticky and viscoelastic liquid at room temperature and is the residue fraction obtained by fractional distillation of crude oil. Among all the fractions distilled from crude oil, such as fuels, lubricating oils, and waxes, bitumen is the heaviest fraction and the one with the highest boiling point. At room temperature, it is even more viscous than molasses, and it is denser than water. Therefore, bitumen does not flow freely.

According to the current European specifications, bitumen is now defined as a "*virtually involatile, adhesive and waterproofing material derived from crude petroleum, or present in natural asphalt, which is completely or nearly completely soluble in toluene, and very viscous or nearly solid at ambient temperatures*" (European Committee for Standardization 2000). Another still widely used term, "tar", generates somewhat confusing nomenclature. The properties of tar are similar to those of bitumen, but tar, as a by-product of coke production, is extracted from coal rather than from crude oil. However, for economic reasons, such as the decline of the coal industry and the rise of the petroleum industry in the 1950s, the use of tar has almost disappeared (Lesueur 2009).

2.5.2. Physical and Chemical Properties

The density of bitumen at room temperature is typically between 1.01 and 1.04 g/cm^3. The chemical properties of bitumen are very complex; as there are many different chemicals presenting in it. Bitumen mainly consists of carbon and hydrogen atoms (Table 2-4). Therefore, the main component of bitumen is hydrocarbons, whose content is greater than 90 wt%.

Table 2-4. Elemental analysis of bitumen from oil sands

	C	H	C+H	H/C	S	O	N
Wt %	83.9	10.0	93.9	1.43	5.5	0.6	0.5

Bitumen can be separated into four components (saturates, aromatics, resins, and asphaltenes, SARA) based on solubility in *n*-heptane and toluene. Bitumen can be firstly separated into two main components, asphaltenes and maltenes, by using *n*-heptane, where the former component is insoluble in *n*-heptane and the latter component is soluble in *n*-heptane. The maltene fraction can be further separated into saturates, aromatics, and resins by using *n*-heptane, toluene and pyridine. The chemical properties of bitumen and each fraction are presented in Table 2-5 (Ali, Bukhari *et al*. 1989; Peramanu, Pruden *et al*. 1999; Rudzinski, Aminabhavi *et al*. 2000).

Table 2-5. Chemical properties of bitumen and SARA fractions

	Bitumen	Saturates	Aromatics	Resins	Asphaltenes
Percentage of total bitumen	100	5 – 15	30 – 45	30 – 45	5 – 20
H/C	1.5	1.9	1.5	1.4	1.1
Average molecular weight	557	381	408	947	2005

According to the elemental analysis, the asphaltene fraction has the lowest H/C ratio and contains the highest content of heteroatoms (including 8% sulfur). According to the hydrogen distribution obtained from ^{1}H NMR analysis, the asphaltene fraction contains more fused aromatic rings and is highly branched. On the other hand, the saturate fraction has the highest H/C ratio and is composed mostly of aliphatic chains. Aromatics constitute one of the two most abundant fractions in bitumen, with the second highest H/C ratio. It is composed of aromatic rings with a few aliphatic side chains. Resins are the other most abundant fraction in bitumen with a similar H/C ratio to aromatics. Therefore, they are of similar polarity. Nevertheless, resins have more heteroatoms than aromatics, making them a bit more polar than aromatics (Spiecker, Gawrys *et al*. 2003).

2.5.3. Bitumen Determination

2.5.3.1. Solvent Extraction

Solvent extraction coupled with FTIR spectroscopy for bitumen quantification was once a commonly used method for assessing total petroleum hydrocarbons in soil (US Environmental Protection Agency 2007; Schwartz, Ben-Dor *et al*. 2012). The commonly used solvent was 1,1,2-trichloro-1,2,2-trifluoroethane (Freon 113), which was banned in 2007 due to its negative impact on ozone (US Environmental Protection Agency 2007). Other methods of bitumen quantification were proposed by other agencies, such as using gas chromatography (ISO 16703:2004), using liquid chromatography (ISO 13877:1998), or using gravimetric method (ASTM D 5765-95) instead of FTIR quantification. These methods still have the limitation of requiring a sample

extraction step, where it is indicated that the repeatability (intra-laboratory) and the reproducibility (inter-laboratory) of solvent extraction are low, with an average variation of the results of 20% (intra-laboratory) and 103% (inter-laboratory). This variability results from the solvent extraction efficiency and differences in the properties of the samples (Schwartz, Ben-Dor *et al*. 2012). In addition, solvent extraction also poses other disadvantages, such as organic solvent consumption, long processing time, and labor requirements.

2.5.3.1.1. Green Solvents

In bitumen extraction, solvents are used in large quantities. In particular, organic solvents such as toluene, dichloromethane, and tetrahydrofuran (THF) have been reported in the bitumen extraction (Yoon, Bhatt *et al*. 2009; Schwartz, Ben-Dor *et al*. 2012). These solvents have large impacts on the environment, cost, safety and health issues. The concept of green solvents has emerged, which aims to minimize the environmental impact. There are four main features of green solvents. Firstly, they have better environmental, health and safety properties, such as increased biodegradability or reduced ozone depletion potential. Secondly, they are bio-solvent, produced from renewable resources such as ligno-cellulosic materials instead of fossil resources (Capello, Fischer *et al*. 2007). In addition, they can be supercritical fluids that are environmentally harmless. As well, they can be ionic liquids that have low vapor pressure and thus less emission into the air (Lévêque and Cravotto 2006; Scammells, Scott *et al*. 2005). Using ionic liquids as replacements for organic solvents for bitumen recovery has been reported by several researchers (Painter, Williams *et al*. 2009; Li, Sun *et al*. 2011; Pulati, Lupinsky *et al*. 2015). They reported that the bitumen recovery by ionic solvents can be up to 95% at room temperature. In addition, much less clay fines were present in the recovered bitumen than when using organic solvent extraction.

2-Methyltetrahydrofuran (2-MeTHF) is considered a green solvent and a good substitute for THF and dichloromethane. 2-MeTHF can be produced from renewable resources by using substrates such as furfural or levulinic acid (Huber, Iborra *et al*. 2006). In addition, 2-MeTHF can be degraded by sunlight and air, presumably via oxidation and ring-opening (Pace, Hoyos *et al*. 2012). Furthermore, its miscibility in water is limited (14g/100g), which make it easy to recover

from water. As well, it has a low heat of vaporization, resulting in less solvent loss and less energy requirement during distillation.

2.5.3.2. Direct Determination by FTIR Spectroscopy

Long, Dabros *et al.* (2004) successfully determined the asphaltene content in bitumen from oil sands froth using NIR spectroscopy and partial least-squares regression (PLS). The predictions were accurate, where the standard errors of calibration were 0.2 wt% for 0 to 20 wt% asphaltene in bitumen and 1.1 wt% for 20 to 100 wt% asphaltene in bitumen. Aske, Kallevik *et al.* (2001) reported a successful direct determination of four components (saturates, aromatics, resins, and asphaltenes) in crude bitumen using both MIR and NIR spectroscopies coupled with PLS chemometrics. The prediction uncertainties by MIR spectroscopy were found to be 2.5, 2.2, 1.4, and 1.3 wt% for these four components respectively were even lower than the uncertainties obtained from high-performance liquid chromatography (HPLC) with ultraviolet (UV) detection. Yuan, Chu *et al.* (2006) also reported their achievement in determination of physical and chemical parameters of bitumen residues, such as saturates, aromatics, resins, asphaltenes, density, and viscosity, using ATR-FTIR spectroscopy coupled with PLS. They reported an accurate and consistent calibration model which can determine multiple properties from a single spectrum. Yoon, Son *et al.* (2009) proposed a simple prediction method of bitumen content in oil sands without solvent extraction. They established a quantification equation using FT-MIR spectroscopy and linear least-squares fitting by correlating the bitumen IR signal to the bitumen content spiked into the clean sand. They reported an accurate bitumen prediction (10.5 wt%) using the equation, which was similar to the result obtained by solvent extraction (9.1 wt%).

CHAPTER 3

CONNECTING STATEMENT

Although soil quality modeling by FTIR spectroscopy has already been studied by other researchers, only a few properties related to soil quality have been modeled by using ATR-FTIR spectroscopy. Chapter 3 covers the development of ATR-FTIR calibrations by the PLSR technique to model 10 soil properties, which are closely related to soil quality, using a set of 278 soil samples from four Canadian provinces. In addition, the correlation between the physical and chemical properties of the soils as well as between these properties and the MIR spectral information is studied.

SOIL QUALITY DETERMINATION BY ATR-FTIR SPECTROSCOPY BASED ON MODELING OF SELECTED PROPERTIES OF SOIL USING PRINCIPAL COMPONENT ANALYSIS AND PARTIAL-LEAST-SQUARES REGRESSION

Abstract

The need for rapid and inexpensive techniques for soil quality determination has led to the investigation of modern technologies. Infrared spectroscopy in the near-infrared (NIR) region has been traditionally used, but the mid-infrared (MIR) region (400 – 4000 cm^{-1}) is less studied. However, due to the specificity of the absorption bands in the mid-infrared region, the adoption of MIR spectroscopy for soil quality determination has been increasingly investigated. In this study, the feasibility of employing attenuated total reflectance mid-infrared (ATR-FTIR) spectroscopy in soil quality determination was evaluated by examining 10 selected soil properties: total carbon (TC), total nitrogen (TN), carbon-to-nitrogen ratio (C/N), ammonium (NH_4^+), nitrate (NO_3^-), sand, silt, clay, N uptake, and yield. A total of 278 soil samples from four Canadian provinces were collected to built the partial-least-squares regression calibration models. By using r^2 and residual predictive deviation (RPD) values for the evaluation of model predictive performance, it was found that the models for TC, TN, C/N, sand, silt, and clay showed very reliable performance ($r^2 > 0.90$, RPD > 2.00), while the models for NH_4^+, NO_3^-, N uptake, and yield showed less reliable performance. This result indicates that ATR-FTIR spectroscopy coupled with PLSR has the potential to model and predict certain important soil properties and therefore can help in achieving large-scale precision farming.

Keywords   soil quality   precision farming   ATR-FTIR   PLSR

3.1. Introduction

Soil is the essential resource of earth, providing a medium for the growth of plants, animals, and microbes. Furthermore, soil quality or quality determines the growth of these living things and it is closely related to the production of food. Therefore, soil quality assessment is a routine task in soil management and crop production. Dating back a century, soil chemists have developed a range

of methodologies for soil quality assessment, but they have highly relied on wet-chemical methods via soil extraction (Janik, Merry *et al.* 1998). Although these methods play a vital role in soil analysis, they are relatively slow and labor-intensive, consume large amounts of chemicals, and are expensive, constraining their usage. These drawbacks have become especially marked in recent decades with the introduction of prescription farming, which requires a fast, accurate, and low-cost methodology to monitor soil quality on the field and farm scale.

Working with the solid soil matrix directly as the experimental sample can overcome the problems associated with the tedious soil extraction procedure required by wet chemistry methods. This makes infrared spectroscopy an interesting alternative as a soil analysis technique. It is a non-destructive technique and does not require any chemical solvents or extensive sample preparation. It is rapid and less expensive than wet-chemical methods and therefore is more efficient when a large number of samples need to be tested. An additional merit of infrared spectroscopy is that all the attributes that can be determined by this technique are captured in a single measurement.

Papers on soil analysis using infrared spectroscopy have been published since the 1970s and the number of papers published has increased since the 1990s, with an even more rapid increase in the last 10 years (Du, Ma *et al.* 2015). Near-infrared (NIR) spectroscopy was first studied and applied for the determination of organic matter, moisture, and texture (Bowers and Hanks 1965). Later, many researchers reported the success application of NIR spectroscopy to measure many soil properties. For instance, McCarty *et al.* (2002) reported a calibration for TC with an r^2 of 0.86, Xie *et al.* (2011) reported an r^2 of 0.97 for TN and an r^2 of 0.94 for C/N, and Cozzolino and Moron (2003) reported r^2 values of 0.90 for clay, 0.84 for silt, and 0.80 for sand. However, in the 1990s, interest in soil analysis by infrared spectroscopy gradually moved to mid-infrared spectroscopy (MIR), mainly focusing on diffuse-reflectance mid-infrared spectroscopy (DRIFT-MIR). Due to their origin in fundamental vibrations, signals in the MIR spectral region are more intense and distinct than the signals in the NIR spectral region, where combinations and overtones of the fundamental vibrations occur. Furthermore, one of the main components in soil, sand, is NIR inactive but has strong MIR absorption, making MIR spectroscopy a promising alternative for soil analysis. In the last few decades, many publications on applications of DRIFT-MIR spectroscopy in soil analysis provided convincing evidence of the potential utility of this technique in soil

analysis. For example, the DRIFT-MIR calibrations reported by Minasny *et al.* (2009) had r^2 values of 0.98 for TC, 0.94 for TN, 0.94 for sand, and 0.90 for clay.

Attenuated total reflectance mid-infrared (ATR-FTIR) spectroscopy emerged later and its application to soil analysis has not been widely reported. It is a simple technique that requires minimal sample preparation and can be readily employed with solid, liquid, and gaseous samples. The application of ATR-FTIR spectroscopy in soil analysis has mainly been focused on nitrate quantification in wet soil or soil paste (Shaviv, Kenny *et al*. 2003; Linker, Kenny *et al*. 2004; Linker, Shmulevich *et al*. 2005), soil characterization (Linker, Weiner *et al*. 2006), and organic carbon speciation (Solomon, Lehmann *et al*. 2005). In the last few years, only a few papers were published on ATR-FTIR quantification of various soil properties, as summarized in Table 3-1.

In order to fill the gap and be able to provide evidence when choosing the best suited infrared spectroscopic technique for soil analysis, the present study focused on soil quality determination by using ATR-FTIR spectroscopy coupled with PLSR. Soil quality is a concept defined as the ability of soil to support plant growth in a sustainable way (Acton and Gregorich 1995). It is a function of soil properties including soil nutrients, moisture, mineral, and organic matter (Desbiez, Matthews *et al*. 2004). Therefore, soil quality is very comprehensive and cannot be measured directly but can be evaluated on the basis of other properties (Bautista-Cruz, Carrillo-González *et al*. 2007). In this study, a total of ten properties closely related to soil quality were chosen to be quantified. Among the properties, eight of them relate to soil nutrients and soil texture, including total carbon (TC), total nitrogen (TN), carbon-to-nitrogen ratio (C/N), ammonium (NH_4^+), nitrate (NO_3^-), sand, silt, and clay. The other two properties, N uptake and yield, are two parameters directly indicating plant nutrient condition and soil productivity. This study will be the first study to model these 10 properties in soils from across Canada by using ATR-FTIR spectroscopy with PLSR chemometrics.

Table 3-1. Literature published in past 10 years on soil analysis using ATR-FTIR spectroscopy

Attributes	Range	$n_c|n_v$ [a]	r_c^2 [b]	$RMSE_{cv}$ [c]	RPD [d]	LVs [e]	Authors
Total C (g/kg)	9.5-34.1	122|0	0.89	NA	3.02	6	(Yang and Mouazen 2012)
Organic C (g/kg)	5-58	180|90	0.80	5.1	2.26	11 (PLS)	(Ge, Thomasson *et al*. 2014)
	8.5-30.2	122|0	0.89	NA	3.10	6	(Yang and Mouazen 2012)
Inorganic C (g/kg)	0-95	189|90	0.92	6.6	3.52	6	(Ge, Thomasson *et al*. 2014)
	0-6.4	122|0	0.72	NA	1.93	5	(Yang and Mouazen 2012)
Total N (g/kg)	0.9-3.1	122|0	0.92	NA	3.75	6	(Yang and Mouazen 2012)
Nitrate (mg/kg)	0-1000	NA	0.99	24	NA	Peak integration	(Jahn, Linker *et al*. 2006)
Sand (g kg^{-1})	150-880	180|90	0.90	78	3.14	6 (PLS)	(Ge, Thomasson *et al*. 2014)
Clay (g kg^{-1})	20-500	180|90	0.94	37	3.38	6 (PLS)	(Ge, Thomasson *et al*. 2014)

[a] n_c – number of calibration samples; n_v – number of validation samples

[b] r_c^2 – coefficient of determination in calibration

[c] $RMSE_{CV}$ – root-mean-square error in cross-validation

[d] RPD – ratio of performance to deviation, RPD > 2, "excellent"

[e] LVs – number of latent variables

3.2. Materials and Methods

3.2.1. Samples

3.2.1.1. Description of Agricultural Sites

The soil samples ($n = 278$) were originally collected from the top 0-15 cm of the soil layer from experimental sites in four Canadian provinces (British Columbia, Ontario, Quebec and New Brunswick). Among these samples, 76% ($n = 210$) were collected from Quebec between 2007 and 2009. A total of 30 sites, 32 sites and 15 sites in 2007, 2008, and 2009 were sampled in 3 or 4 replicates and the sampling sites each year were different. Corn was grown at these sites with phosphorus and potassium fertilizers being applied before planting at rates of 50 kg P and 75 kg K ha^{-1} as triple superphosphate and potassium chloride. The corn hybrids varied across the three years and sites according to local recommendations. Weed was controlled by using glyphosate as herbicide at 1.75 L ha^{-1} (Nyiraneza, N'Dayegamiye *et al*. 2010).

The other soil samples ($n = 68$) were collected from 2000 to 2007 from sites in 4 or 5 replicates in four Canadian provinces: one site in British Columbia (Agassiz, 49°10' N, 124°15' W), one site in Ontario (Woodslee, 42°13' N, 107°43' W), five sites in Quebec (L'Acadie, 45°17' N, 73°20' W; St-Catherine, 46°49' N, 71°39' W; St-Basile, 46°48' N, 71°46' W; St-Louis, 45°51' N, 73°00' W; and Harlaka, 46°47' N, 71°08' W), and two sites in New Brunswick (Sussex, 45°43' N, 65°32, W and Keswick-Ridge, 45°52' N, 66°31' W). All the sites were for corn production with starter nitrogen fertilizer up to 50 kg N ha^{-1}, except the sites in British Columbia and Ontario where no nitrogen fertilizer was applied. Phosphorus and potassium fertilizers were applied according to local recommendations. Conventional tillage was practiced at all sites and weed control followed local recommendations (St Luce, Ziadi *et al*. 2012).

All soil samples were collected in spring before fertilizer application, air-dried, and ground to pass a 0.25-mm sieve. A small amount of soil was used for chemical analysis, whereas the majority of the sample was kept for spectroscopic measurement. All the samples were stored in sealed containers in a dark environment to minimize sample degradation.

3.2.1.2. Soil Textures

The 278 soil samples used in this study had various proportions of sand, silt, and clay and therefore belonged to nine soil textures: clay, silt clay, clay loam, sandy clay loam, silty clay loam, loam, sandy loam, silt loam, and loamy sand (Figure 3-1 & Table 3-2), according to the United States Department of Agriculture (USDA) triangular diagram of soil texture classifications.

According to the clay content in the soil, the soil samples were further divided into a fine-texture subset ($\geq$ 350 g clay kg^{-1} soil, n = 100) and a coarse-texture subset (< 350 g clay kg^{-1} soil, n = 178).
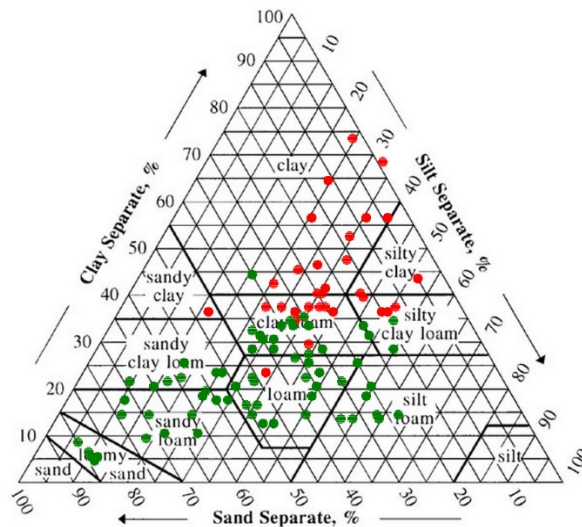
Fig. 3-1. Soil texture of 278 soil samples according to USDA triangular diagram
(red: fine-texture subgroup; green: coarse-texture subgroup)

Table 3-2. Description of the sites in the four targeted provinces

Year	Province [a]	Sand % [b]	Silt % [b]	Clay % [b]	Soil type [c]
2007		34.1	34.1	31.8	Clay loam
2008	QC	36.2	29.9	33.9	Clay loam
2009		32.0	33.5	34.5	Clay loam
	BC	27.1	58.8	14.1	Silt loam
	ON	30.4	33.4	36.2	Clay loam
2000 – 2007	QC	47.2	30.2	22.6	loam
	NB	39.4	46.7	13.9	loam

[a] QC – Quebec; BC – British Columbia; ON – Ontario; NB – New Brunswick.

[b] Average value of the soils from the same provinces or from the same sampling year.

[c] According to USDA triangular diagram relating particle size distribution to soil texture.

3.2.2. Reference Methods

Particle size analysis was performed by the pipette method after the destruction of organic matter with hydrogen peroxide (H_2O_2) and dispersion with sodium polymetaphosphate (Gee, Bauder *et al*. 1986; Nyiraneza, N'Dayegamiye *et al*. 2010).

Total carbon (TC) and total nitrogen (TN) were determined by dry combustion using a CNS-1000 (Leco Corp., St. Joseph, MI) following the protocol from the supplier (St Luce, Ziadi *et al*. 2012).

Nitrate (NO_3^-) concentration was determined with nitrate-test strips (EM Quant cat. no. 10020-1, EMD chemicals, Gibbstown, NJ) and a hand-held reflectometer (Nitrachek 404, QuoMed Ltd, West Sussex, England) following the protocol from the supplier (Nyiraneza, N'Dayegamiye *et al*. 2010).

Ammonium (NH_4^+) concentration was measured colorimetrically at 660 nm (Lachat QuikChem 8500 Flow Injection Analyzer).

Corn nitrogen uptake (N uptake) was calculated for the whole plant (plant tissue and grain) as the product of the TN concentration and dry matter yield. About 800 g of plant tissue or grain were taken and dried at 65 °C to a constant mass to determine dry matter and TN content (Nyiraneza, N'Dayegamiye *et al*. 2010).

Corn grain yields were determined by harvesting the two center rows from each plot. Each plot was 10- to 12-meter long and 3-meter wide, containing 4 rows of corn with 0.75-meter row spacing (Nyiraneza, N'Dayegamiye *et al*. 2010).

3.2.2.1. Normalization of Data Distribution

The normality of the distribution of the reference data was tested by using the Kolmogorov-Smirnov normality test at 95% confidence level. The "skewness" value from each variable's normality test was used to determine the normality of the data distribution; this value measures the asymmetry of the probability distribution of a random variable about its mean. Skewness can be positive, negative, and zero. When it is positive, the data is left-skewed, meaning that the mass of the distribution is concentrated on the right causing the "tail" on the left side of the probability density function to be longer. Conversely, negative skewness means the mass of the distribution is concentrated on the left and the data is right-skewed. When skewness is equal to 0, the dataset is normal distributed. Therefore, the closer the absolute value of skewness to 0, the closer the distribution of the dataset is to a normal distribution.

Logarithmic transformation (log_{10}) was used in this study to normalize data to obtain a normal distribution. The skewness values of the raw dataset and the log_{10} transformed dataset were compared. A box-and-whisker plot was used to study the distribution, and the data falling below the 1st quartile (Q_1, median of the lower half of the data set) or above the 3rd quartile (Q_3, the median of the higher half of the data set) were considered as outliers and removed from the reference data. Both the raw reference dataset and the log_{10} transformed reference dataset were used to build the calibration models and the performances of the models were compared to study whether the normality of the reference dataset affects the model performance.

3.2.3. Spectroscopic Method

3.2.3.1. Principle of ATR-FTIR Spectroscopy

ATR-FITR spectroscopy operates by measuring the changes of an internally reflected infrared beam when contacting a sample (Figure 3-2). The infrared beam entering a crystal with high refractive index (e.g., diamond or ZnSe) at the critical angle will undergo total internal reflection. The internal reflectance creates an evanescent wave that extends beyond the surface of the crystal into the sample placed on the crystal. The evanescent wave only extends a few microns (0.5 – 5 μm) beyond the crystal surface, and therefore a good contact between the sample and crystal surface is required. The sample selectively absorbs the evanescent wave, causing attenuation of the evanescent wave. The resultant evanescent wave is passed back to the infrared beam, which exits at the other end of the crystal and is passed to the detector in the IR spectrometer. The IR beam is then measured and plotted as a function of wavenumber to generate the absorption spectrum characteristics of the sample (Du, Ma *et al*. 2015).
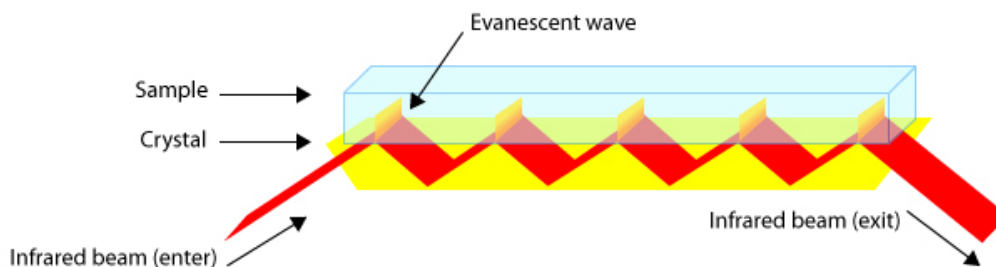
Fig. 3- 2. Schematic drawing of a multiple-reflection ATR device

(www.chromacademy.com)

3.2.3.2. ATR-MIR Spectral Acquisition

ATR-FTIR spectra were collected by an ALPHA Fourier transform infrared (FTIR) spectrometer equipped with a ZnSe ATR crystal sampling accessory (Bruker Optics, Billerica, MA, USA). The spectral range collected was $4000 – 400$ cm^{-1} with 2 cm^{-1} resolution, and 128 scans were co-added. Spectra were scanned directly into a computer using OPUS software (Bruker) and were saved in .spc format. An initial background spectrum was run to test the spectrometer

performance and as a reference for calculating the sample spectra in absorbance units. Each spectral acquisition (128 scans) took about 1 minute per sample.

3.2.4. Spectral Processing and Development of Calibration Models

3.2.4.1. Principal Component Analysis (PCA)

PCA is a data compression process that reduces complex multidimensional data (e.g. spectra) into a smaller number of principal components (PCs) which reflect the underlying structure and still contain most of the information in the original dataset. Each PC describes part of the variation among the dataset in decreasing order; the first PC describes the most variation in the dataset and each succeeding component accounts for as much of the remaining variation as possible. Because each PC is orthogonal to all the others, PCs can be interpreted independently. By plotting the PCs in two dimensions, interrelationships between samples and variables can be examined (Yang and Mouazen 2012).

The complete dataset, defined by the variables in the columns (in this study, 1800 wavenumbers) and the samples in the rows (in this study, 278 soil samples), can be viewed as the original data matrix, defined by $X(n,m)$ (in this study, $X(278,1800)$). PCA models the maximum directions of variation in the original data matrix by projecting the objects (in this study, the FTIR spectra) as a swarm of points in a new plane defined by PCs. The first PC represents the dimension or direction where the most variability occurs in the original dataset, and the second PC represent the orthogonal dimension where the second most variability occurs in the remaining dataset. The new co-ordinate value of the observations (278) projected onto each of the new co-ordinate lines (PC-lines, k) is known as a *score*. The scores of all the observations form a matrix $T(n,k)$, as in this study, $T(278,k)$. The correlation between PCs and the original variables is called *loadings*, which indicate the amount of variation in the original variables (1800 wavenumber) explained by each PC. The loadings of all the PCs form a matrix $P(m,k)$, as in this study, $P(1800,k)$. The PCA algorithm describing the data matrix decomposition is presented as:

$$X(278,1800) = T(278,k)P(1800,k)^{\mathrm{T}} + E(278,1800) \ \ldots\ldots\ldots\ldots\ldots\ldots\ldots\ldots\ldots\ldots\ldots.(3\text{-}1)$$

where, X is the independent variable matrix, T is the scores matrix, P is the loadings matrix, E is the error matrix, 278 is the number of observations, 1800 is the number of variables, and k is the number of PCs used ((Nieuwoudt, Prior *et al*. 2004; Eriksson, Byrne *et al*. 2013).

3.2.4.2. Partial Least Squares Regression (PLSR) Analysis

PLSR is a regression extension of PCA, which connects the information in x and y variables to each other. PLSR is a bilinear regression modeling method where the original x variables are projected onto a much smaller number of PLS components, which are commonly referred to as "latent variables" or "factors". These factors are calculated according to the same mathematical procedures as PCs, but the data in the Y-matrix are also incorporated in the calculation. The regression establishes the relationship between the X-matrix (in this study, soil spectra) and the Y-matrix (in this study, the reference data for a given soil property), with the aim of predicting the y variables by using the most relevant factors (Nieuwoudt, Prior *et al*. 2004).

In an analogous but different manner to PCA, both the $X(n,m)$ matrix (in this study, $X(278,1800)$) and the $Y(n,l)$ matrix (in this study, the column vector Y(278,1) as each property was modeled individually) are projected as a swarm of points in a new plane, and the corresponding scores matrices $T(n,l)$ of the X-matrix and $U(n,l)$ of the Y-matrix and the loadings matrices $P(m,l)$ of the X-matrix and $Q(p,l)$ of the Y-matrix are obtained. The PLS algorithm is presented as:

$$X(278,1800) = T(278,l)P(1800,l)^{\mathrm{T}} + E(278,1800) \ldots\ldots\ldots\ldots\ldots\ldots\ldots\ldots\ldots \text{ (3-2)}$$

$$Y(278,1) = U(278,l)Q(1,l)^{\mathrm{T}} + F(278,1) \ldots\ldots\ldots\ldots\ldots\ldots\ldots\ldots\ldots\ldots \text{ (3-3)}$$

where X is the independent variable matrix, T is the scores matrix of X , P is the loadings matrix of X, E is the error matrix of X, Y is the dependent variable matrix, U is the scores matrix of Y, Q is the loading matrix of Y, F is the error matrix of Y, 278 is the number of observations, 1800 is the number of variables, the number "1" indicates that a single property is modeled by the PLS calibration, and l is the number of latent factors used. In the PLS algorithm of PLS, covariance

between the scores matrixes *T* and *U* is maximized. Thus, the information contained in the Y-matrix (usually, concentration data) is employed in the decomposition of the *X*-matrix, which is not the case in PCA. Therefore, most of the variation in the Y-matrix is explained by the first few latent factors, where the first PLS factor explains the variation in the *X*-matrix that provides the highest correlation with the *Y*-matrix and hence provides an estimate of a "pure component spectrum."

3.2.4.3. Spectral Pre-processing and Model Calibration

Before the absorbance spectra were employed to develop calibration models for the prediction of soil properties, they were subjected to various spectral pre-processing algorithms to reduce or eliminate noise and baseline tilts and offset in the raw spectra. Commonly used spectral pre-processing algorithms were investigated in this research including Savizky-Golay smoothing, standard normal variate (SNV), multiplicative scatter correction (MSC), 1st and 2nd derivative, and spectral normalization. The performance of the spectral pre-processing algorithms cannot be assessed until the resulting spectra have been used to develop calibration models. In the Results section of this chapter, only the pre-processing algorithms that resulted in the calibration models with the best performance are reported.

PCA analysis was conducted using the UnscramblerX10.3® software package (CAMO, Oslo, Norway). Spectral pre-processing and PLSR were conducted using the TQ Analyst™ software package (Professional Edition 7.2.0.161, Thermo Fisher Scientific, USA). The PLSR algorithm was used to decompose the raw or pre-processed spectra into a maximum of 10 factors. In order to obtain the optimized calibration model for each soil property according to their unique spectral information, the model for each property was built separately. All PLSR models were validated with a full cross-validation approach (leave-one-out) where each spectrum was in turn excluded from the calibration set and was predicted from the model calibrated on the remaining spectra. The optimal number of factors was determined by minimizing the predicted residual error sum of squares (PRESS) in the cross-validation.

3.2.4.4. Model Assessment

To evaluate the overall performance of a model, the distance between the predicted and reference results is central from a statistical perspective (Hastie, Tibshirani *et al.* 2001). These distances are related to the concept of "goodness-of-fit" of a model. A good model should have small distances between predicted and reference results (Steyerberg 2009).

The parameters commonly used to evaluate the goodness-of-fit of a model are the coefficient of determination (r^2), root mean square error (RMSE), and residual predictive deviation, also referred to as ratio of performance to deviation (RPD). The value of r^2 represents the degree of correlation between two sets of data. It is widely used by many researchers but it is strongly related to the range of values spanned by the sample set, where r^2 increases as the range of values increases (Daviesa and Fearnb 2006). The accuracy of a model is given by the RMSE, which is a measure of the differences between the predicted and reference values for a set of samples. The RMSE obtained for a validation set determines the limits of the confidence interval in which a future prediction is to be found for a new sample (Draper, Smith et al. 1966):

$$ RMSE = \sqrt{\frac{\sum_N (X_i - Y_i)^2}{N}} \quad \text{.. (3-4)} $$

where, X_i is the predicted value of the ith sample, Y_i is the reference value of the ith sample, and N is the number of samples. RMSE includes contributions from several sources, such as the errors from modeling and errors in the reference measurements. It is also sensitive to the range of values spanned by the sample set, where RMSE increases as the range of values increases (Daviesa and Fearnb 2006).

In order to standardize the value of RMSE, with respect to the natural dispersion of the samples, RPD has been proposed. It is the ratio of the standard deviation of the reference values to the RMSE of the calibration set obtained by cross-validation:

$$ RPD = \frac{SD}{RMSE} \quad \text{... (3-5)} $$

It was first used in soil science in 1993 (Sudduth and Hummel 1993) and later it was commonly used as a threshold to gauge the performance of the prediction (Chang and Laird 2002; Yang and Mouazen 2012). The RPD value still depends on the range and distribution of the population, and the relevance of this parameter is highly questionable (Bellon-Maurel, Fernandez-Ahumada *et al.* 2010). However, it is widely adopted by many researchers, and hence in this study it is included in our model performance evaluation. A larger value of RPD indicates better performance of the model but currently, there is no critical level of RPD for infrared analysis in soil science. Three categories based on RPD in the ranges >2.0, 1.4 – 2.0, and <1.4 were used to indicate decreasing reliability of predicting (Chang, Laird *et al.* 2001). Other researchers reported the similar results of suitable limits for RPD (Dunn, Batten *et al.* 2002; Pirie, *Singh et al.* 2005).

In this study, the values of r^2, RMSE, and RPD obtained from cross-validation of calibration models were assessed to determine the performance of the calibration models. The reliability of the models was categorized based on the following criteria: very reliable (VR) models with r^2 >0.9 and RPD >2.0; reliable (R) models with $0.75 \leq r^2 \leq 0.9$ and $1.4 \leq$ RPD ≤ 2.0; less reliable (LR) models with r^2 <0.75 and RPD <1.4.

3.3. Results

3.3.1. Statistical Description of Reference Values

Means and distributions of the reference values of the 10 soil properties selected in this study (total carbon (TC), total nitrogen (TN), carbon-to-nitrogen ratio (C/N), ammonium (NH_4^+), nitrate (NO_3^-), sand, silt, clay, N uptake, and yield) for the whole sample set ($n=278$ and the fine-texture ($n=100$), and coarse-texture subsets ($n=178$) are summarized in Table 3-3, 3-4, and 3-5. The concentration ranges of TC, TN, and C/N are in accordance with those studied by other researchers (Yang and Mouazen 2012). The coefficient of variation (c.v.) and the differences between the mean and the median value of NH_4^+, NO_3^-, and N uptake in the three sample sets are large, leading to large skewness of the distributions of these three properties.

The skewness values of the original and the log_{10} transformed datasets are summarized in Table 3-6. Log_{10} transformation performed well for the properties TC, NH_4^+, and N uptake in all three

sample sets, causing a more symmetric distribution with a much smaller skewness value. After logarithmic transformation, the skewness values for the whole set were reduced from 0.88 to -0.01 for TC, from 3.47 to 0.9 for NH_4^+, and from 1.89 to 0.33 for N uptake. In the case of the other properties, log_{10} transformation did not significantly improve the normality of the distribution, except for the distribution of TN and yield in the fine-texture subset, with a reduction in skewness from 0.55 to -0.16 for TN from 1.45 to -0.27 for yield. However, in the case of the properties sand, silt, and clay, log_{10} transformation decreased the symmetry of the distribution.

The box-and-whisker plots of the whole dataset for the property NH_4^+ obtained for the original and the log_{10} transformed data are shown in Figure 3-3. The histogram displays the distribution of all the data points while the box-and-whisker plot graphically depicts how the data points cluster through the quartiles and identifies possible outliers. The box includes the data points within the 1st and 3rd quartile range, and the diamond in the box represents the 95% confidence interval for the mean. The lines (whiskers) extend vertically from the boxes to the outermost data point that falls within the distances computed as:

$$1^{st} \text{ quartile} - 1.5 \times \text{interquartile range} \dots\dots\dots\dots\dots\dots\dots\dots\dots\dots\dots\dots \text{(3-6)}$$

$$3^{rd} \text{ quartile} + 1.5 \times \text{interquartile range} \dots\dots\dots\dots\dots\dots\dots\dots\dots\dots\dots\dots \text{(3-7)}$$

where the interquartile range is the difference between the 1st and 3rd quartiles. The data points that do not fall within the computed ranges are shown as dots and are the potential outliers. The red bracket outside of the box shows the densest 50% of the data points. The distribution of the original data points for the property NH_4^+ was highly right-skewed with a long right tail. The mass of the distribution was highly concentrated on the right, which was the low concentration side in this study. The interquartile range was narrow with the 1st quartile of 1.10 mg/kg and 3rd quartile of 4.18 mg/kg. Twenty-eight data points with high concentrations were considered as outliers. After log_{10} transformation, the data points were distributed much more symmetrically

and were more evenly spread out instead of being concentred within a narrow range. Most of the data were included within the whiskers region with only 3 potential outliers out of range.

Table 3-3. Statistical description of the reference values of 10 properties of soils in the whole sample set and the fine-texture and coarse-texture subsets

Soil property	Whole sample set				
	Mean	Median	Range	s.d. [a]	c.v. [b]
TC (g/kg)	17.15	16.02	5.41-39.06	5.87	34.20
TN (g/kg)	1.56	1.53	0.47-3.36	0.49	31.53
C/N	11.07	10.96	6.05-18.41	1.78	16.12
NH_4^+ (mg/kg)	4.34	1.80	0.39-49.19	6.75	155.44
NO_3^- (mg/kg)	10.30	8.93	0.09-51.3	7.25	70.36
Sand (g/kg)	370.28	335.50	0.00-860.00	211.83	57.21
Silt (g/kg)	334.23	340.00	60.00-619.40	129.44	38.73
Clay (g/kg)	295.48	280.00	42.00-750.00	149.47	50.59
N uptake (kg N/ha)	42.38	29.88	6.36-198.25	37.00	87.31
Yield (kg/ha)	4534.05	4255.00	820.00-11532.00	1873.79	41.33

[a] Standard deviation; [b] coefficient of variation (= 100s.d./mean)

Table 3-4. Statistical description of the reference values of 10 properties of soils in the fine-texture subset

Soil property	Fine-texture subset				
	Mean	Median	Range	s.d. [a]	c.v. [b]
TC (g/kg)	19.06	18.07	8.51-39.06	5.99	31.45
TN (g/kg)	1.76	1.65	0.84-3.36	0.51	28.74
C/N	10.83	10.83	8.49-13.43	1.03	9.53
NH_4^+ (mg/kg)	4.29	2.04	0.39-29.71	5.97	139.24
NO_3^- (mg/kg)	9.14	7.35	0.09-51.3	7.20	78.76
Sand (g/kg)	187.93	185.00	0.00-480.00	109.61	58.33
Silt (g/kg)	358.70	350.00	160.00-570.00	95.54	26.63
Clay (g/kg)	453.37	409.00	351.00-750.00	104.48	23.05
N uptake (kg N/ha)	37.06	23.88	9.67-141.84	29.62	79.92
Yield (kg/ha)	4777.33	4248.00	941.00-11532.00	1939.79	40.60

[a] Standard deviation; [b] coefficient of variation (= 100s.d./mean)

Table 3-5. Statistical description of the reference values of 10 properties of soils in the coarse-texture subset

Soil property	Coarse-texture subset				
	Mean	Median	Range	s.d. [a]	c.v. [b]
TC (g/kg)	16.08	14.94	5.41-33.86	5.53	34.37
TN (g/kg)	1.45	1.41	0.47-2.73	0.45	31.07
C/N	11.21	11.08	6.05-18.41	2.08	18.57
NH_4^+ (mg/kg)	4.37	1.68	0.43-49.19	7.12	162.83
NO_3^- (mg/kg)	10.96	10.00	0.36-41.64	7.22	65.86
Sand (g/kg)	472.73	446.00	150.00-860.00	184.84	39.10
Silt (g/kg)	320.48	323.5	60.00-619.40	143.48	44.77
Clay (g/kg)	206.79	210.00	42.00-346.00	82.87	40.07
N uptake (kg N/ha)	45.51	33.13	6.36-198.25	40.50	88.99
Yield (kg/ha)	4396.69	4262.00	820.00-9380.00	1827.88	41.57

[a] Standard deviation; [b] coefficient of variation (= 100s.d./mean)

Table 3-6. Skewness values of the original and $\log_{10}$ transformed datasets for the total, fine-texture, and coarse-texture sample sets

Soil property	Total set		Fine-texture subset		Coarse-texture subset	
	Original	Log_{10}	Original	Log_{10}	Original	Log_{10}
TC	0.83	-0.01	0.80	-0.01	0.88	0.05
TN	0.42	-0.44	0.55	-0.16	0.22	-0.50
C/N	0.51	-0.46	-0.17	-0.43	0.36	-0.52
NH_4^+	3.47	0.90	2.89	1.00	3.61	0.91
NO_3^-	1.88	-1.50	3.19	-1.94	1.23	-1.28
Sand	0.50	-2.85	0.29	-2.65	0.44	-0.36
Silt	-0.07	-1.14	0.16	-0.57	0.05	-0.86
Clay	0.63	-0.77	1.17	0.90	-0.09	-1.04
N uptake	1.89	0.33	1.70	0.58	1.81	0.20
Yield	0.83	-0.81	1.45	-0.27	0.42	-0.89
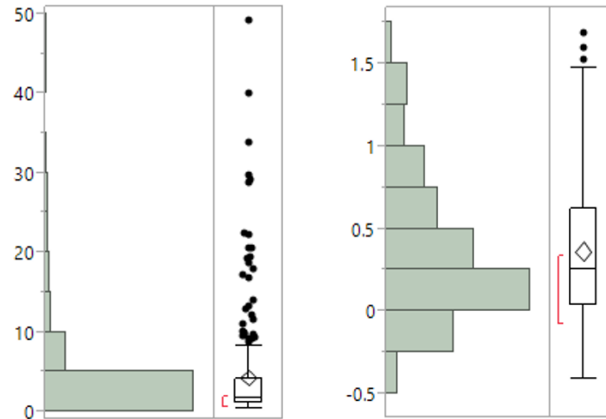
Fig. 3-3. Box-and-whisker plot showing distribution of values for the property NH_4^+ in the total sample set in the original (left, 3.47 skewness) and the $\log_{10}$ transformed (right, 0.90 skewness) data format

3.3.2. ATR-FTIR Spectral Analysis and Model Calibration

3.3.2.1. ATR-FTIR Soil Spectral Analysis

Different MIR absorption bands respond to different chemical components in soils. Figure 3-4 shows the ATR-FTIR spectra of three selected soil samples, denoted as A, B, and C, from two types of soil: clay (A and B) and loamy fine sand (C), with high and low TC content. All the spectra have a similar pattern, where the major absorption peaks occur in the regions 3700 – 2800 cm^{-1} and 1720 – 1300 cm^{-1} and the region below 1200 cm^{-1}. These major absorption peaks are attributed to specific chemical constituents including sand, clay, and organic carbon. The peaks in the region 1720 – 1300 cm^{-1} are overlapping and cannot be assigned to a specific component. In general, the broad band between 1720 and 1500 cm^{-1} may be due to C=O stretching (1725 – 1720 cm^{-1}); aromatic C=C stretching, O-H bending in the lattice of clay, H-O-H bending in water, and N-H bending (1620 – 1600 cm^{-1}); COO$^-$ stretching, C=C stretching, N-H deformation, and C=N stretching (1590 – 1520 cm^{-1}). The weak broad band between 1480 and 1330 cm^{-1} may be due to the C-H bending and O-H deformation (1460 – 1450 cm^{-1}); C-H deformation of methyl and methylene groups, and COO$^-$ asymmetric stretching in the region between 1400 and 1390 cm^{-1} (Yang and Mouazen 2012; Janik, Merry *et al*. 1998). The region below 1200 cm^{-1} is the fingerprint region of soil, where the absorptions are mainly due to clay,

silt and sand. It is difficult to assign the peaks in that region to a specific compound or chemical bond but the soil mineral structure can be reflected. Therefore, the absorption pattern in the fingerprint region is unique to each soil.
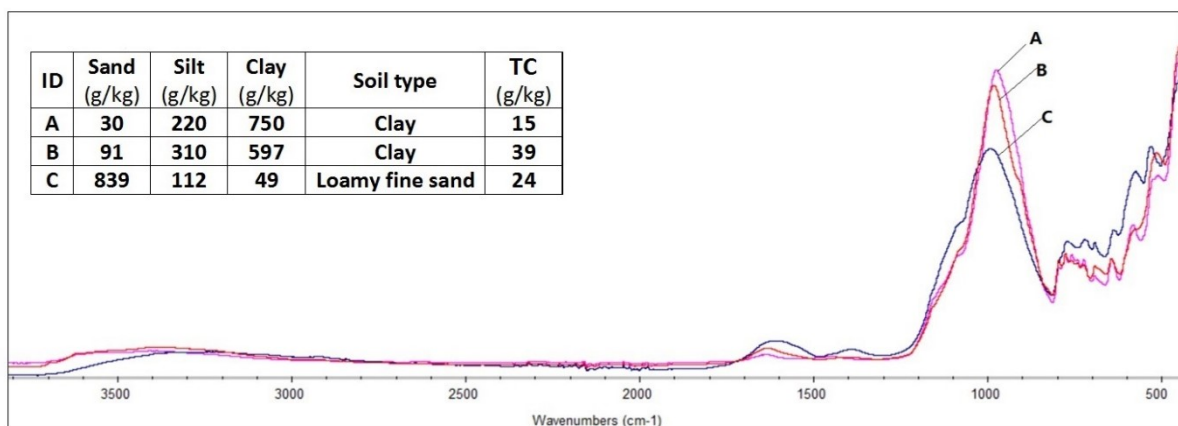
Fig. 3-4. ATR-FTIR spectra $(4000 - 400 \text{ cm}^{-1})$ of soil samples of two soil textures with high and low TC content

Both sample A and B are high in clay content, 75% and 60%, respectively. Clay absorption bands at 3620 and 3550 cm^{-1}, due to the O-H stretching of inner-surface hydroxyl groups, are observed in the spectra of A and B (Fig. 3-5). Sample C is low in clay but is high in sand. Hence, no O-H band is observed in the 3600 cm^{-1} region and also the fingerprint region is very different from those of samples A and B, which have similar clay content. The high sand content in sample C has strong O-Si-O absorption, which appears as a shoulder at 1080 cm^{-1}.

Organic carbon has strong absorption in the MIR region. The absorption due to the C-H stretching vibration of methyl and methylene groups occurs between 2950 and 2850 cm^{-1}. The C-H absorption bands are clearly observed in the spectra of samples B and C, which contains relatively high amounts of TC, 39 and 24 g/kg, respectively. In the case of sample A, in which TC is low, 15 g/kg, the C-H band is not intense enough to be observed by eye.
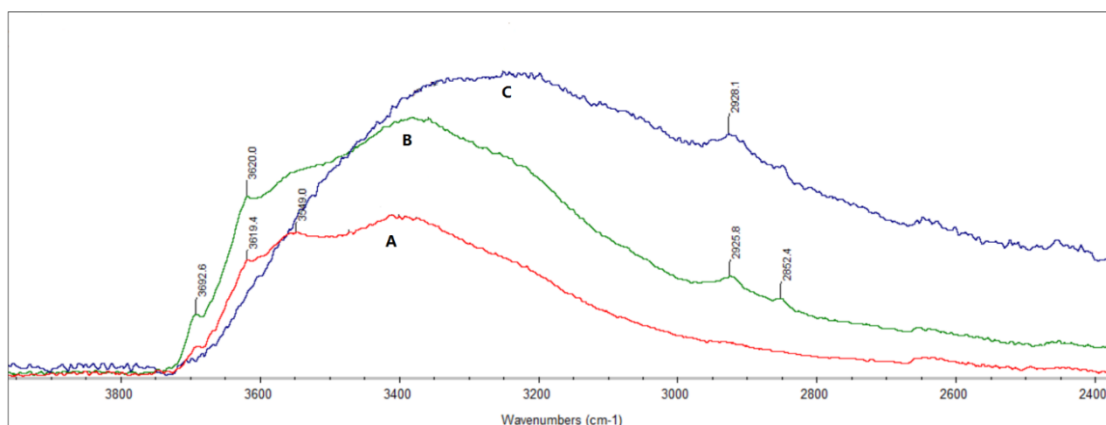
Fig. 3-5. ATR-FTIR spectra (4000 – 2400 cm^{-1}) of soil samples of two soil textures with high and low TC content

3.3.2.2. PCA of ATR-FTIR Spectra

The complete data matrix including all the samples (n=278) and all the wavenumbers (4000 – 400 cm^{-1}) was modeled. The first two PCs accounted for 85% (PC1) and 11% (PC2) of the total variance of the data, cumulatively contributing 96% of the variance (Fig. 3-6), and the rest of the PCs only explain the rest of the variance, which is only 4%. Therefore, only the first two PCs were selected to analyze.
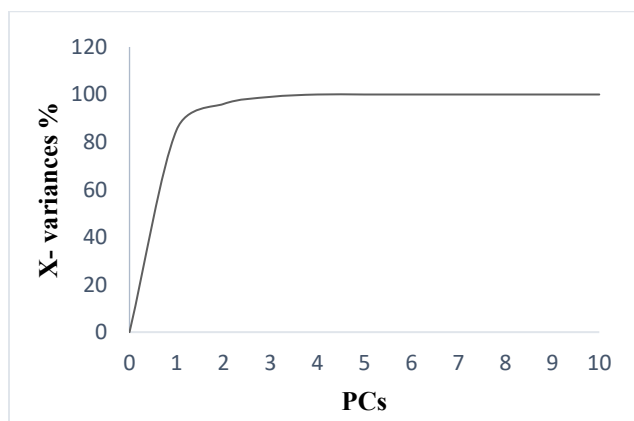
Fig. 3-6. Explained variance of the sample set by 10 PCs

52

Loadings are the correlations between the components (PCs) and the original variables (wavenumbers), and each PC's loadings plot indicates how much of the variations in a variable (wavenumber) is explained by the PC (Fig. 3-7). The higher the loadings value, the more variation is explained. Therefore, by examining the loadings plot, it is clear at which wavenumbers the most variations explained by that PC occur. Figure 3-7 (a) is the loadings plot of PC1, which is similar to the ATR-FTIR spectrum of soil. In the PC1 loadings plot, the loadings values are high in the region below 1200 cm^{-1}, which is the specific absorption region of soil minerals. In addition, there are relative high variations in the regions 3620 – 3550 cm^{-1} and 1700 – 1570 cm^{-1}, which are characteristic of clay minerals and organic matter, respectively. Therefore, PC1 mainly represents the variations of soil minerals and organic matter. Moreover, these correlations between PC1 and these variations are positive, as indicated by the positive loadings values. Figure 3-7 (b) is the loadings plot for PC2, which is also similar to the ATR-FTIR spectrum of soil, but with weak absorption intensity. In the loadings plots, relatively high loadings values are observed in the region below 1200 cm^{-1}, which indicates that the variations of soil minerals are explained by PC2. Overall, the loadings value of PC2 is low compared to the loadings values of PC1. This illustrates that the variations explained by PC2 are small, which is true since this PC accounts for only 11% of the total variance.

Scores plots are another important type of information obtained from PCA, as they show the relationships among samples and the PCs. Thirteen scores plots (PC1 versus PC2) for 13 parameters, including the 10 selected properties (TC, TN, C/N, NH_4^+, NO_3^-, sand, silt, clay, N-uptake and yield) and 3 additional parameters (texture, sampling locations and sampling years), based on PCA of the 278 ATR-FTIR spectra in the full dataset are presented in Fig. 3-8. For the interpretation of the scores plots for the 10 selected properties, the total of 278 samples were separated into two groups according to their reference value for the property, where samples with values smaller than the median were grouped together, as were those with values greater than the median. For the texture parameter, samples were grouped into fine-texture and coarse-texture groups; while for sampling location, samples were grouped based on the sampling provinces and for sampling years, samples were placed in three groups, corresponding to 2007, 2008, and 2009, respectively. In these 13 scores plots, each point represents a sample and those points in the same color are from the same group. In addition, points that are close together indicate that the

samples they represent are similar. Therefore, the similarity among samples is revealed by examination of the distribution of the colored points.
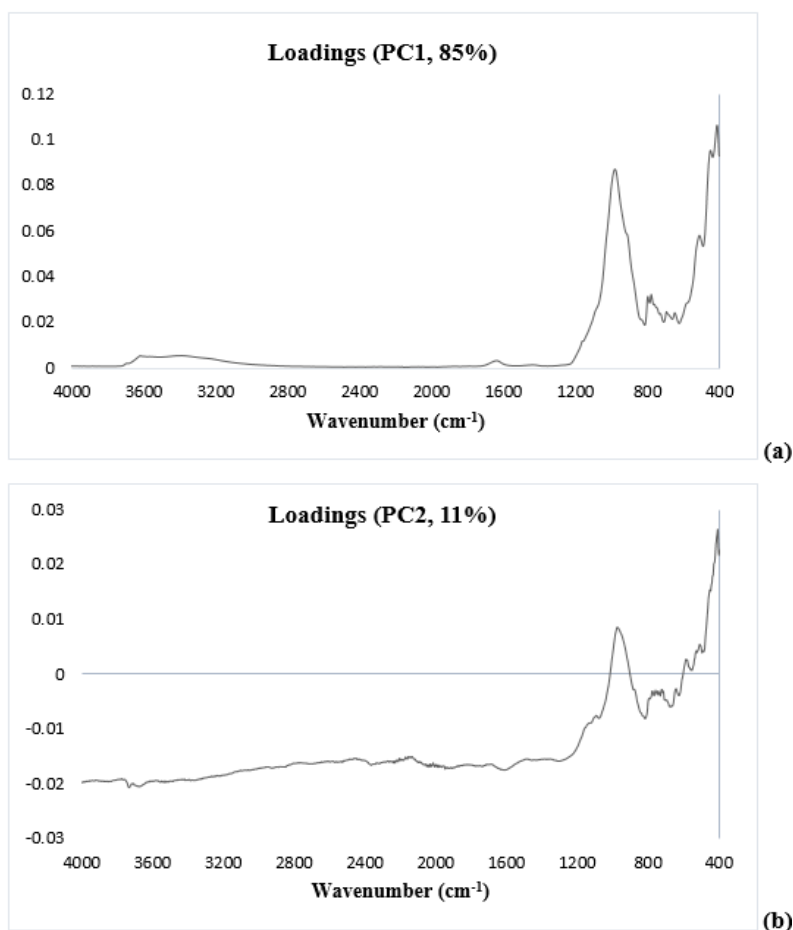
Fig. 3-7. PCA loadings plots: (a) PC1; (b) PC2.

The scores plots show a distinct clustering of the samples in relation to the properties sand, clay, and texture (Fig. 3-8-f; -h; -k). The clustering of these properties is due to the PC1 scores, either negative or positive. However, the points are randomly spread in the PC2 dimension. This indicates that the original values of the properties sand, clay, and texture are overwhelmingly explained by PC1. In the scores plot for clay, samples with high values (greater than the median) are clustered on the positive side of PC1, which suggests that the variation of clay minerals is

positively correlated to PC1. This is proved by the positive loadings values in clay-specific absorption regions in the PC1 loadings plot. In the case of the property sand, the opposite is observed, where samples with high sand content are clustered on the negative side of PC1. This suggests that the correlation between the variation of sand and PC1 is negative, as well as that the correlation between sand and clay is negative. This finding is in agreement with the correlation analysis where a -0.80 correlation coefficient (r^2) is found between sand and clay. Since soil texture is determined by the content of clay and sand, the clustering of samples in the soil texture scores plot is comparable to their clustering in the scores plots for clay and sand, where fine-texture samples with high clay content are grouped on the positive side of PC1, while coarse-texture samples with high sand content are grouped on the negative side of PC1. However, with respect to the other properties examined, no distinct clustering is observed in the scores plots. This might be due to the weak intensity of the signals of these properties are weak and their masking by the relatively strong mineral signals.

There is a moderate clustering on the scores plot for sampling locations (Figure 3-8-l), where the QC cluster is mainly located toward the negative end of PC1; points representing NB are clustered in the center and points representing ON are clustered toward the positive end of PC1. However, there is no significant clustering of BC soils. It is not surprising that the clustering based on sampling location exists, since the sampling location is inherently related to soil texture. On the other hand, no clustering pattern is found in the scores plot for sampling year (Figure 3-8-m).
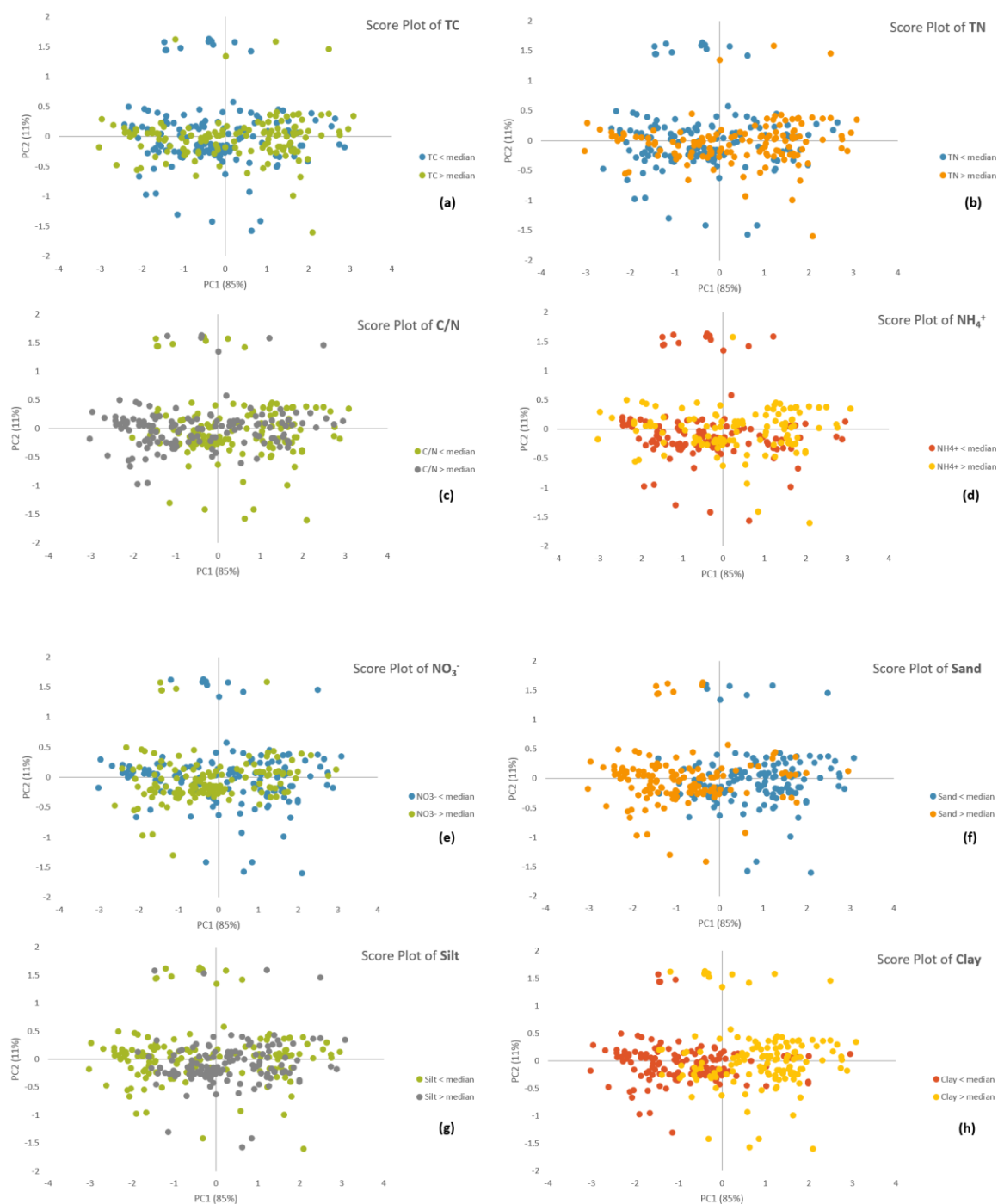
Fig. 3-8. PCA scores plots for selected properties derived from ATR-FTIR spectra ($n = 278$); (a) TC; (b) TN; (c) C/N; (d) NH_4^+; (e) NO_3^-; (f) sand; (g) silt; (h) clay; (i) N-uptake; (j) yield; (k) texture; (l) sampling locations ($n = 87$); (m) sampling years.

Fig. 3-8. Cont.

3.3.2.3. Correlation Analysis

The correlation coefficients among 10 properties of soil and the scores of PC1 and PC2 are summarized in Table 3-5 (original values of the 10 properties) and Table 3-6 ($\log_{10}$ transformed values of the 10 properties). The closer the absolute value of the coefficient to 1.00, the stronger the linear relationship between the two variables; the positive and negative values indicate whether the two are positively or negatively correlated. The analysis (Table 3-5) showed strong relationships between TC and TN, sand and silt, and sand and clay, with correlation coefficients

57

of 0.87, -0.72, and -0.80 respectively. In addition, the results showed a moderate correlation between N uptake and yield, with a 0.63 correlation coefficient. The relationships between TC and TN as well as between N uptake and yield were much stronger in the fine-texture subset, while the relationships among sand, silt, and clay were generally stronger in the coarse-texture subset. However, there were no significant correlations among other properties, except N uptake, NH_4^+, and NO_3^-, which were moderately correlated. The relationships among the properties appear complex, and therefore it is impossible to predict one from another.

The correlations among the properties and the spectra were examined by studying the correlation coefficients between the scores of the first two PCs and the properties, which are summarized in Table 3-7. PC1 had strong correlations with sand, silt, and clay and moderate correlations with TN and C/N. This is in accordance with the loading spectrum of PC1, which showed most variation in the mineral absorption region. A correlation between PC1 and TN existed but it was weak, which may be due to the weak intensity of the signals associated with TN in the ATR-FTIR spectra. It is not surprising that the relationships between PC1 and other properties did not exist, as the concentrations for many of these properties were low and others (yield and N uptake) cannot be directly measured by infrared spectroscopy. However, no relationship was observed between PC1 and TC, which had relatively high concentration values and strong spectral signals. The correlations between PC2 and all the properties were weak due to the low amount of variance explained by PC2.

After using logarithmic data transformation, the correlations between some variables were improved, but some were weakened, as shown in Table 3-8. For example, in the total set, the correlation coefficient of PC1 and silt increased from 0.36 to 0.44, while the correlation coefficient of PC1 and sand decreased from 0.74 to 0.64. The changes of the correlations caused by the $\log_{10}$ data transformation were not considered significant.

Table 3-7. Correlation matrix between 10 properties of soils (original dataset) and the first two PC scores obtained by principal component analysis of the ATR-FTIR spectra of the total sample set, the fine-texture subset, and the coarse-texture subset

	TC	TN	C/N	NH_4^+	NO_3^-	Sand	Silt	Clay	N uptake	Yield
					Total set					
TC	1.00									
TN	**0.87**	1.00								
C/N	0.32	-0.18	1.00							
NH_4^+	0.15	0.34	-0.34	1.00						
NO_3^-	0.00	0.09	-0.20	0.05	1.00					
Sand	-0.14	-0.30	0.29	-0.06	0.06	1.00				
Silt	-0.04	0.11	-0.27	0.14	0.14	**-0.72**	1.00			
Clay	0.23	0.33	-0.19	-0.03	-0.22	**-0.80**	0.15	1.00		
N uptake	-0.02	0.17	-0.36	**0.58**	**0.44**	0.07	0.17	-0.25	1.00	
Yield	0.06	0.13	-0.10	0.13	**0.41**	0.04	-0.03	-0.03	**0.63**	1.00
PC1	0.15	**0.35**	**-0.36**	0.23	-0.15	**-0.74**	0.36	**0.74**	0.02	-0.02
PC2	-0.06	-0.10	0.05	0.01	-0.09	-0.01	-0.06	0.07	-0.07	0.09
					Fine-texture subset					
TC	1.00									
TN	**0.94**	1.00								
C/N	0.38	0.07	1.00							
NH_4^+	0.11	0.31	-0.47	1.00						
NO_3^-	-0.08	-0.10	0.02	-0.20	1.00					
Sand	-0.37	-0.27	-0.32	0.18	0.02	1.00				
Silt	0.17	0.10	0.22	-0.09	0.16	-0.49	1.00			
Clay	0.23	0.19	0.14	-0.10	-0.17	**-0.61**	-0.40	1.00		
N uptake	0.08	0.08	0.10	0.37	0.25	0.00	0.09	-0.08	1.00	
Yield	0.01	0.02	0.04	0.00	0.38	0.02	0.14	-0.16	**0.91**	1.00
PC1	0.11	0.22	-0.28	0.27	-0.30	**-0.31**	-0.20	**0.51**	0.18	0.06
PC2	-0.12	-0.18	0.09	0.05	-0.09	0.07	0.00	-0.07	0.00	0.03

Table 3-7. Cont.

	TC	TN	C/N	NH$_4^+$	NO$_3^-$	Sand	Silt	Clay	N uptake	Yield
					Coarse-texture subset					
TC	1.00									
TN	**0.80**	1.00								
C/N	0.37	-0.24	1.00							
NH$_4^+$	0.18	0.38	-0.32	1.00						
NO$_3^-$	0.10	0.28	-0.29	0.16	1.00					
Sand	0.17	-0.10	0.40	-0.14	-0.04	1.00				
Silt	-0.18	0.06	-0.34	0.20	0.17	**-0.90**	1.00			
Clay	-0.06	0.13	-0.30	-0.03	-0.22	**-0.65**	0.28	1.00		
N uptake	-0.03	0.31	-0.45	0.58	0.52	0.00	0.21	-0.41	1.00	
Yield	0.06	0.16	-0.14	0.13	0.45	0.19	-0.12	-0.22	0.55	1.00
PC1	-0.05	0.24	**-0.40**	0.28	-0.01	**-0.64**	**0.52**	**0.54**	0.11	-0.23
PC2	-0.07	-0.10	0.05	0.00	-0.08	0.05	-0.10	0.07	-0.09	0.12

Table 3-8. Correlation matrix between 10 properties of soils ($\log_{10}$ transformed dataset) and the first two PC scores obtained by principal component analysis of the ATR-FTIR spectra of the total sample set, the fine-texture subset, and the coarse-texture subset

	TC	TN	C/N	NH_4^+	NO_3^-	Sand	Silt	Clay	N uptake	Yield
					Total set					
TC	1.00									
TN	**0.88**	1.00								
C/N	0.27	-0.22	1.00							
NH_4^+	0.19	0.37	-0.38	1.00						
NO_3^-	-0.04	0.00	-0.09	-0.28	1.00					
Sand	-0.25	-0.30	0.29	-0.05	0.03	1.00				
Silt	-0.04	0.13	-0.27	0.17	0.08	-0.45	1.00			
Clay	0.16	0.26	-0.19	-0.10	-0.14	**-0.67**	0.39	1.00		
N uptake	0.07	0.23	-0.31	0.50	0.48	0.10	0.15	-0.29	1.00	
Yield	0.15	0.23	-0.15	0.05	0.52	-0.02	0.00	0.00	**0.66**	1.00
PC1	0.20	**0.37**	**-0.33**	0.28	-0.18	**-0.62**	**0.44**	**0.72**	-0.01	-0.02
PC2	-0.09	-0.13	0.07	-0.03	-0.09	-0.03	-0.02	0.07	-0.06	0.07
					Fine-texture subset					
TC	1.00									
TN	**0.95**	1.00								
C/N	0.36	0.04	1.00							
NH_4^+	0.11	0.29	-0.48	1.00						
NO_3^-	-0.07	-0.16	0.25	-0.51	1.00					
Sand	-0.31	-0.24	-0.27	0.08	-0.10	1.00				
Silt	0.15	0.12	0.14	-0.12	0.14	-0.20	1.00			
Clay	0.24	0.20	0.16	-0.11	-0.03	**-0.63**	-0.37	1.00		
N uptake	0.05	0.04	0.07	0.13	0.25	0.06	0.06	-0.11	1.00	
Yield	0.08	0.08	0.06	-0.09	0.40	-0.02	0.13	-0.19	**0.81**	1.00
PC1	0.14	0.24	-0.29	**0.35**	-0.25	**-0.35**	-0.14	**0.52**	0.14	0.02
PC2	-0.18	-0.22	0.08	0.08	-0.09	-0.02	0.00	-0.07	-0.02	0.03

Table 3-8. Cont.

	TC	TN	C/N	NH$_4^+$	NO$_3^-$	Sand	Silt	Clay	N uptake	Yield
					Coarse-texture subset					
TC	1.00									
TN	**0.84**	1.00								
C/N	0.30	-0.27	1.00							
NH$_4^+$	0.20	0.40	-0.37	1.00						
NO$_3^-$	0.01	0.13	-0.21	-0.17	1.00					
Sand	0.08	-0.12	0.35	-0.11	0.03	1.00				
Silt	-0.17	0.07	-0.41	0.22	0.10	**-0.86**	1.00			
Clay	-0.10	0.05	-0.27	-0.25	-0.12	**-0.63**	0.45	1.00		
N uptake	0.12	0.38	-0.40	0.56	0.57	0.10	0.21	-0.39	1.00	
Yield	0.13	0.26	-0.19	0.07	0.58	0.22	-0.06	-0.13	0.63	1.00
PC1	0.02	0.25	**-0.40**	0.28	-0.10	**-0.62**	**0.54**	**0.53**	0.02	-0.22
PC2	-0.08	-0.13	0.08	-0.09	-0.08	0.07	-0.04	0.05	-0.08	0.88

3.3.2.4. PLSR Calibration Models Based on ATR-FTIR Spectra

Tables 3-9, 3-10, and 3-11 summarize the calibration and cross-validation statistics of the PLSR models developed for the total set and the fine-texture and coarse-texture subsets, with various pre-processing options (baseline correction, standard normal variate, or multiplicative signal correction). The ATR-FTIR spectra in both the original and log$_{10}$ transformed data format were employed to develop calibration models. Several spectral pre-processing methods were used but only the methods resulting in the best calibrations are shown. For the total sample set (Table 3-9), PLSR models produced excellent prediction accuracy for TC, TN, C/N, sand, and clay with R_c^2 (calibration) of 0.86 – 0.94, R_{cv}^2 (cross-validation) of 0.83 – 0.91, and RPD of 1.76 – 2.45. The correlations between the measured and predicted values as well as the predicted residual error sum of squares (PRESS) plots for these five properties are shown in Fig. 3-9. PRESS plots indicate how the predicted residual error sum of squares decreases with the number of latent variables used. The number of latent variables used in each calibration corresponded to the

minimum value in the PRESS plot. To prevent overfitting, the maximum number of latent variables was less than 10 in all cases.

For the properties silt, N uptake, and NH_4^+, PLSR models had moderate prediction accuracy with R_c^2 of 0.80 – 0.83, R_{cv}^2 of 0.64 – 0.77, and RPD of 1.29– 1.55. For the remaining properties, NO_3^- and yield, for which the R_c^2 was below 0.73, R_{cv}^2 was below 0.58, and RPD was below 1.22, where the PLSR model predictions were not considered accurate.

For the fine-texture subset (Table 3-10), similar results to those obtained for the total set were found, where the PLSR models for TC, TN, CN, sand, and clay were considered to have excellent prediction performances, with R_c^2 of 0.84 – 0.96, R_{cv}^2 of 0.73 – 0.92, and RPD of 1.45 – 2.52. The prediction performances for silt, N uptake, NH_4^+ and yield were acceptable, with R_c^2 of 0.76 – 0.89, R_{cv}^2 of 0.51 – 0.76, and RPD of 1.11 – 1.52. However, the prediction of NO_3^-, for which the R_c^2 was below 0.30, R_{cv}^2 was below 0.10, and RPD was below 0.99, was considered unsuccessful.

For the coarse-texture subset (Table 3-11), excellent PLSR prediction performances were found for the properties TC, TN, C/N, sand, and clay, for which the R_c^2 was above 0.85, R_{cv}^2 was above 0.77, and RPD was above 1.54. For the property silt, PLSR also provided excellent modelling performance (R_c^2 0.83, R_{cv}^2 0.73, and RPD 1.44), whereas the silt calibration models for the other two sample sets did not perform as well. In addition, in the case of the properties NO_3^- and yield, for which PLSR models were not successfully built in the case of both the total and fine-texture sample sets, the models obtained with the coarse-texture subset were much improved, with R_c^2, R_{cv}^2, and RPD values of 0.75, 0.65, and 1.31 for NO_3^- and 0.72, 0.58, and 1.22 for yield. Although there was an improvement in the coarse-texture subset, PLSR still cannot quantitatively model these two properties according to the RPD criteria.

The RPD values of the calibration models developed with the total, fine-texture, and coarse-texture sample sets in the original and the log_{10} transformed data format are plotted for the 10 properties in Fig. 3-10. The two horizontal lines divide the plot into three zones, corresponding to RPD above 2.0, RPD between 1.4 and 2.0, and RPD below 1.4. These three zones indicated the reliability of the PLSR model to be very reliable, reliable or less reliable, respectively. According to this criterion, the models of TOC, TN, C/N, NH_4^+, sand, silt, and clay were all

considered reliable. Moreover, the prediction performances of TC, TN, and clay in the fine-texture subset and of sand and silt in the coarse-texture subset were even better, and these models were considered very reliable. However, for the properties NO_3^-, N uptake and yield, their PLSR models were considered less reliable in quantification, but acceptable in classification. Among these three properties, the model for N uptake showed improved prediction accuracy in the coarse-texture subset and the quantification was considered reliable.

Log_{10} transformation, in general, did not effectively improve the models. However, for the properties TN and clay in all the sample sets and NH_4^+ in the coarse-texture subset, log_{10} transformation improved model performances, making the models reliable or even very reliable. However, opposite results were found for the TC and silt models in all the sample sets, as well as the C/N and sand models in the total sample set, where log_{10} transformation significantly reduced the model's reliability.

Table 3-9. Calibration (C) and cross-validation (CV) of PLSR models with original and log_{10} transformed datasets: Total sample set ($n = 278$)

Property	Dataset	Model information		Evaluation parameters				
		Spectral pre-treatment	Calibration regions (cm^{-1})	$R_c^2|R_{cv}^2$	RMSEC	RMSECV	LV$_S$	RPD
TC	Original	Baseline correction [a]	2990 – 2798 1732 – 1350	0.88|0.86	2.61	2.88	8	1.95
	Log$_{10}$	SNV [e]	2982 – 2816 1766 – 1278	0.86|0.83	0.07	0.08	9	1.76
TN	Original	Baseline correction [a]	1903 – 1350	0.88|0.83	0.24	0.30	8	1.78
	Log$_{10}$	Baseline correction [b]	1844 – 1270 860 – 800 *	0.87|0.83	0.07	0.07	10	1.82
C/N	Original	-	2974 – 2827 1740 – 1301	0.92|0.89	0.63	0.73	10	2.19
	Log$_{10}$	-	1849 – 1301	0.88|0.83	0.03	0.04	7	1.81
NH$_4^+$	Original	Baseline correction [c]	3526 – 3013 1852 – 1253 848 – 787 *	0.62|0.55	2.12	2.25	6	1.20
	Log$_{10}$	MSC [f]	3537 – 3183 * 1769 – 1240	0.83|0.74	0.23	0.33	7	1.48
NO$_3^-$	Original	-	1950 – 1275 896 – 784	0.65|0.58	4.14	4.45	10	1.22
	Log$_{10}$	Baseline correction [c]	1605 – 1240 871 – 797	0.40|0.27	0.26	0.28	8	1.03

Table 3-9. Cont.

	Model information			Evaluation parameters				
Property	Dataset	Spectral pre-treatment	Calibration regions (cm^{-1})	$R_c^2\|R_{cv}^2$	RMSEC	RMSECV	LV$_S$	RPD
Sand	Original	MSC [f]	1246 – 417	0.94|0.91	68.60	87.06	8	2.45
	Log$_{10}$	SNV [e]	1246 - 423	0.90|0.87	0.13	0.15	7	2.03
Silt	Original	MSC [f]; Baseline correction [a]	3738 – 3588 1235 – 410 *	0.88|0.73	59.80	87.20	7	1.44
	Log$_{10}$	Baseline correction [d]	3732 – 3593 1228 – 442	0.83|0.77	0.10	0.12	6	1.55
Clay	Original	MSC [f]	3732 – 3521 1253 – 409	0.94|0.88	46.30	69.70	9	2.05
	Log$_{10}$	-	1009 – 405	0.92|0.90	0.09	0.11	8	2.29
N uptake	Original	SNV [e]	3755 – 3468 1264 – 429 *	0.80|0.64	18.80	24.30	8	1.29
	Log$_{10}$	-	3734 – 2519 1252 – 444 *	0.82|0.68	0.18	0.24	9	1.35
Yield	Original	-	831 – 419 *	0.73|0.47	1230	1660	8	1.09
	Log$_{10}$	-	821 – 412	0.65|0.54	0.14	0.16	8	1.18

[a] Piecewise linear correction: minimum in range; [b] average in range; [c] quadratic removed
[d] maximum in range; [e] standard normal variate (SNV); [f] multiplicative signal correction (MSC);
* first derivative

Table 3-10. Calibration (C) and cross-validation (CV) of PLSR models with original and $\log_{10}$ transformed datasets: Fine-texture sample set ($n = 100$)

	Model information			Evaluation parameters				
Property	Dataset	Spectral Pre-treatment	Calibration regions (cm^{-1})	$R_c^2 \mid R_{cv}^2$	RMSEC	RMSECV	LV$_S$	RPD
TC	Original	-	2982 – 2818 1712 – 1350	0.93|0.88	2.07	2.62	6	2.13
	Log$_{10}$	Baseline correction [b]	2984 – 2817 1712 – 1350	0.94|0.86	0.05	0.07	8	1.93
TN	Original	SNV [e]	3407 – 1187	0.93|0.89	0.18	0.22	6	2.23
	Log$_{10}$	MSC [f]	3300 – 1406 920 – 785	0.96|0.92	0.04	0.05	10	2.52
C/N	Original	SNV [e]	3508 – 1240 617 – 567	0.92|0.77	0.40	0.76	5	1.57
	Log$_{10}$	SNV [e]	3507 – 1252	0.95|0.81	0.01	0.02	10	1.72
NH$_4^+$	Original	MSC [f]	3507 – 3010 1803 – 1300 * 802 – 746 * 555 – 440	0.89|0.76	2.54	3.58	8	1.52
	Log$_{10}$	-	1500 – 1400 1124 – 733 * 563 – 440 *	0.83|0.61	0.21	0.32	7	1.23
NO$_3^-$	Original	-	1552 – 1250 1264 – 784 *	0.30|0.10	3.84	4.10	3	0.99
	Log$_{10}$	MSC [f]	1410 – 1340 * 860 – 800 *	0.33|0.14	0.18	0.19	2	1.00

Table 3-10. Cont.

	Model information			Evaluation parameters				
Property	Dataset	Property	Dataset	$R_c^2 \mid R_{cv}^2$	RMSEC	RMSECV	LV_S	RPD
Sand	Original	SNV [e]; Baseline correction [c]	3738 – 3494 * 1227 – 436 *	0.84|0.73	51.50	66.20	4	1.45
	Log₁₀	SNV [e]; Baseline correction [c]	3773 – 3006 1251 – 799	0.92|0.81	0.12	0.20	6	1.70
Silt	Original	SNV [e]	1227 – 818 * 814 – 618 636 – 417 *	0.86|0.70	42.80	61.70	6	1.39
	Log₁₀	SNV [e]	1270 – 429 *	0.83|0.51	0.06	0.10	5	1.11
Clay	Original	MSC [f]	3724 – 3581 1250 – 814 770 – 625	0.88|0.81	47.50	59.80	4	1.70
	Log₁₀	-	3736 – 3521 1252 – 802 769 – 625	0.90|0.86	0.04	0.05	5	1.98
N uptake	Original	SNV [e]	1421 – 1300 * 985 – 779 *	0.76|0.55	15.80	20.60	6	1.18
	Log₁₀	-	1421 – 1241 * 979 – 750 *	0.80|0.65	0.18	0.23	6	1.31
Yield	Original	Baseline correction [d]	3749 – 2498 1450 – 1300 983 – 769	0.70|0.54	1200	1450	7	1.17
	Log₁₀	MSC [f]	1250 – 414	0.81|0.61	0.08	0.12	8	1.22

[a] Piecewise linear correction: minimum in range; [b] average in range; [c] quadratic removed
[d] maximum in range; [e] standard normal variate (SNV); [f] multiplicative signal correction (MSC);
* first derivative

Table 3-11. Calibration (C) and cross-validation (CV) of PLSR models built with original and $\log_{10}$ transformed datasets: Coarse-texture sample set ($n = 178$)

Properties	Dataset	Spectral pre-treatment	Calibration regions (cm^{-1})	R_c^2|R_{cv}^2	RMSEC	RMSECV	LV$_S$	RPD
TC	Original	MSC [f]	2980 – 2823 * 1736 – 1336 *	0.94|0.85	1.89	2.86	7	1.90
	Log$_{10}$	SNV [e]	2989 – 2823 1801 – 1299 *	0.91|0.84	0.06	0.07	6	1.85
TN	Original	SNV [e]	1979 – 1336	0.90|0.80	0.19	0.26	9	1.65
	Log$_{10}$	MSC [f]	3299 – 1405 919 – 784	0.85|0.80	0.08	0.09	8	1.67
C/N	Original	-	3589 – 2820 * 1495 – 1339 *	0.85|0.72	1.03	1.38	4	1.44
	Log$_{10}$	-	3572 – 2790 * 1807 – 1219 *	0.95|0.80	0.02	0.05	7	1.68
NH$_4^+$	Original	MSC [f]	3563 – 3033 * 1551 – 1269	0.76|0.71	1.31	1.43	4	1.42
	Log$_{10}$	Baseline correction [a]	3531 – 3205 * 1556 – 1255	0.87|0.78	0.20	0.26	8	1.57
NO$_3^-$	Original	SNV [e]	1506 – 1198 * 985 – 795 *	0.75|0.65	3.64	4.18	7	1.31
	Log$_{10}$	MSC [f]	1604 – 1251 * 979 – 797 *	0.78|0.61	0.19	0.24	8	1.24

Table 3-11. Cont.

	Model information			Evaluation parameters				
Properties	Dataset	Spectral pre-treatment	Calibration regions (cm^{-1})	$R_c^2|R_{cv}^2$	RMSEC	RMSECV	LV_S	RPD
Sand	Original	MSC [f]; Baseline correction [a]	1210 – 420	0.89|0.86	81.70	92.50	6	1.96
	Log$_{10}$	MSC [f]	1210 – 415	0.89|0.86	0.07	0.08	6	1.96
Silt	Original	MSC [f]	3726 – 3598 1216 – 411	0.89|0.87	63.50	69.60	5	2.04
	Log$_{10}$	MSC [f]	3738 – 3596 1200 – 401	0.86|0.83	0.11	0.12	5	1.80
Clay	Original	Baseline correction [d]	1203 – 416	0.87|0.77	39.90	53.00	7	1.54
	Log$_{10}$	Baseline correction [a]	3741 – 3557 1220 – 411	0.88|0.84	0.10	0.11	8	1.82
N uptake	Original	Baseline correction [b]	1938 – 1228 1240 – 411	0.87|0.79	14.60	18.45	7	1.63
	Log$_{10}$	Baseline correction [c]	3579 – 2801 1891 – 1201 1251 – 405	0.83|0.75	0.19	0.22	8	1.52
Yield	Original	MSC [f]	3572 – 2790 1252 – 411	0.70|0.54	1260	1510	8	1.18
	Log$_{10}$	Baseline correction [a]	3586 – 2790 1873 – 1240 1234 – 411	0.72|0.58	0.14	0.17	8	1.22

[a] Piecewise linear correction: minimum in range; [b] average in range; [c] quadratic removed
[d] maximum in range; [e] standard normal variate (SNV); [f] multiplicative signal correction (MSC);
* first derivative

Fig. 3-9. Calibration (left) and PRESS plots (right) of PLSR calibrations based on the ATR-FTIR spectra of the total sample set for the properties TC (a), TN (b), C/N (c), sand (d), and clay (e)

71
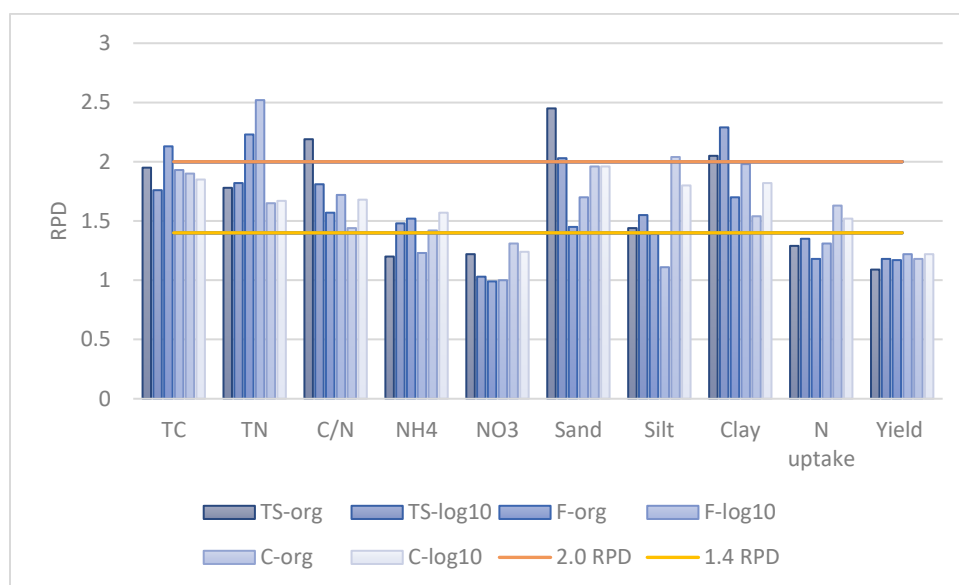
Fig. 3-10. Comparison of RPD values of the models for 10 properties developed with the total sample (TS) set and the fine-texture (F) and coarse-texture (C) subsets in the original and the $\log_{10}$ transformed data format.

3.3.2.5. Statistical Spectral Displaying Correlation between Spectral and Reference Information
Figure 3-11 shows the stacked statistical spectra of the 10 properties generated by correlating the spectral and concentration information of all the samples. These spectra represent the spectral regions that correlate with changes in component concentration. According to the spectral information, the spectra are divided into 4 regions: $2950 - 2850$ cm^{-1} (A), $3620 - 3550$ cm^{-1} (B), $1750 - 1350$ cm^{-1} (C), and < 1200 cm^{-1} (D), which represent the presence of carbon; clay; nitrogen and carbon; and minerals, respectively. The statistical spectra showed a good correlation between the spectral and concentration information of the 278 standards for TC, TN, sand, silt, and clay properties, all of which have primary mid-infrared signals. The statistical spectra for TC and TN showed strong correlation in regions A and C, but weak or zero correlation in regions B and D. This finding is not surprising since regions A and C are the absorption regions for the vibrations involving bonds to carbon and nitrogen. The statistical spectra for TC and TN are similar since there is a high correlation between the levels of TC and TN in the samples, with a
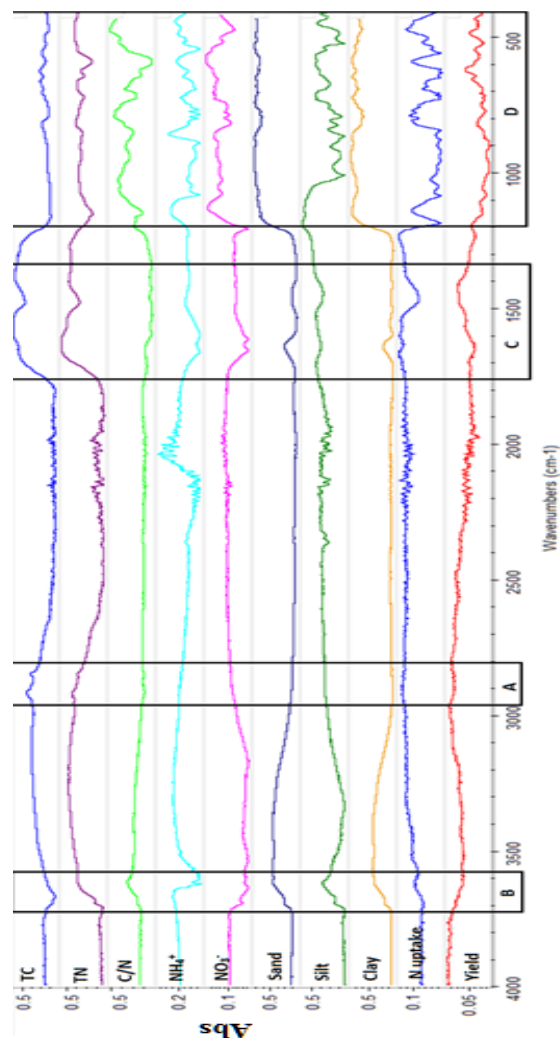
Fig. 3-11. Statistical spectra for 10 properties showing correlation between spectral data and reference values for the total of 278 total samples.

0.94 correlation coefficient. Sand, silt, and clay, on the other hand, showed positive correlation in regions B and D, which are the characteristic and fingerprint regions for soil minerals. In the case of NH_4^+ and NO_3^-, which should exhibit MIR absorptions in the regions $3410 – 3030$ cm^{-1}, $1390 – 1340$ cm^{-1}, and $840 – 730$ cm^{-1} (Miller and Wilkins 1952); there were no significant correlations observed in the statistical spectra, which may be due to their low concentration in the soil samples. For the properties C/N, N uptake, and yield, which do not have a primary MIR signal, no significant correlations between the reference values and spectral signals were observed from the statistical spectra. Moreover, since these properties have no significant

correlations to those with a strong primary MIR signal, their statistical spectra show weak relationships between the spectral information and the reference values (Table 3-7).

3.3.2.6. Pure Component Spectra derived from PLSR Analysis of ATR-FTIR Spectra

Figure 3-12 shows the pure component spectra for the 10 properties, which are extracted from the overlapping spectra of the soil samples by the PLS analysis. Similar to the spectrum of the soil matrix, the pure component spectra are also divided into 4 absorption regions: $2950 - 2850$ cm^{-1} (A), $3620 - 3550$ cm^{-1} (B), $1750 - 1350$ cm^{-1} (C), and < 1200 cm^{-1} (D). In the pure component spectra of TC, TN and C/N, a significant absorption band is observed in region A, which represents the presence of organic carbon. However, in the case of the pure component spectra for the other properties, no bands are observed in region A. This indicates that the bands in region may be considered characteristic of TC. In the pure component spectrum of TN, absorptions were observed in region B, which includes vibrations involving bonds to N. Due to the high correlation between TC and TN, absorption bands specific for organic carbon were also included in the TN pure component spectrum.

The pure component spectra of sand, silt and clay were similar in region B, which is the characteristic region for clay. They all have strong absorption in region D, but the patterns of the absorption are different due to the different mineral structures and compositions.

In the case of NH_4^+ and NO_3^-, their pure component spectra show absorption in region C, but the bands in this region are broad and overlapping, and therefore they cannot characterize NH_4^+ and NO_3^-. Absorptions in regions B and D, which are irrelevant to NH_4^+ and NO_3^-, are also observed. This might be due to the spectral variability caused by variation in the particle size, which is also modeled by PLSR and is mistakenly considered as chemical variability. Therefore, these bands related to minerals are also found in the pure component spectra of TC, TN, and C/N. For N uptake and yield, no significant bands are found in any of the four regions. This might be due to the fact that there are no MIR absorptions directly related to these two properties. Moreover, there are no significant correlations between these two properties and other properties that are directly related to MIR absorptions. The pure component spectra of these two properties are also noisy, which might be due to overfitting of the models.
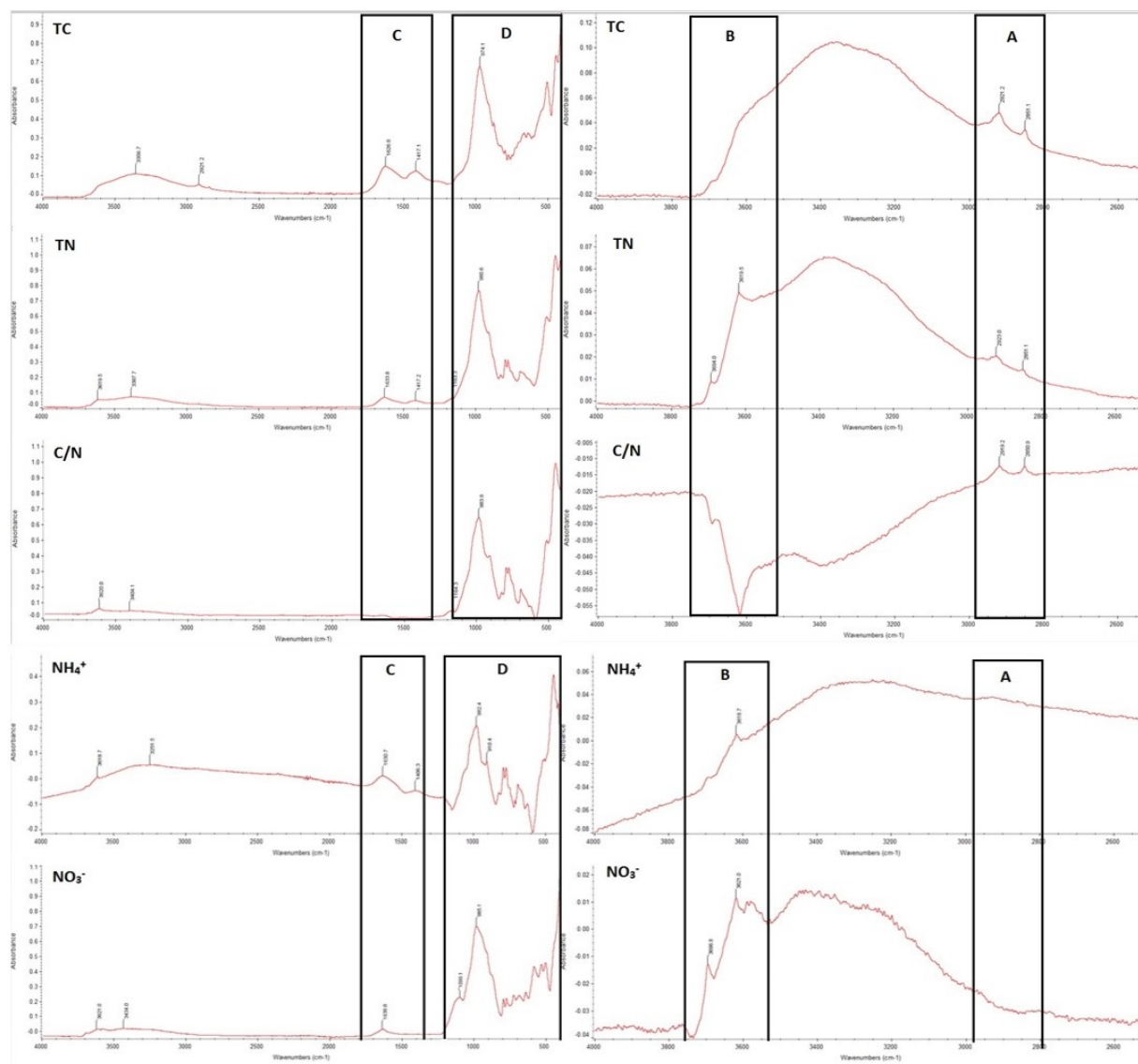
Fig. 3- 12. Pure component spectra for10 soil properties obtained from PLSR modeling of ATR-FTIR spectra against original reference data of the total sample set; left: whole MIR region (4000 – 400 cm^{-1}); right: zoomed-in MIR region (4000 – 2500 cm^{-1}).
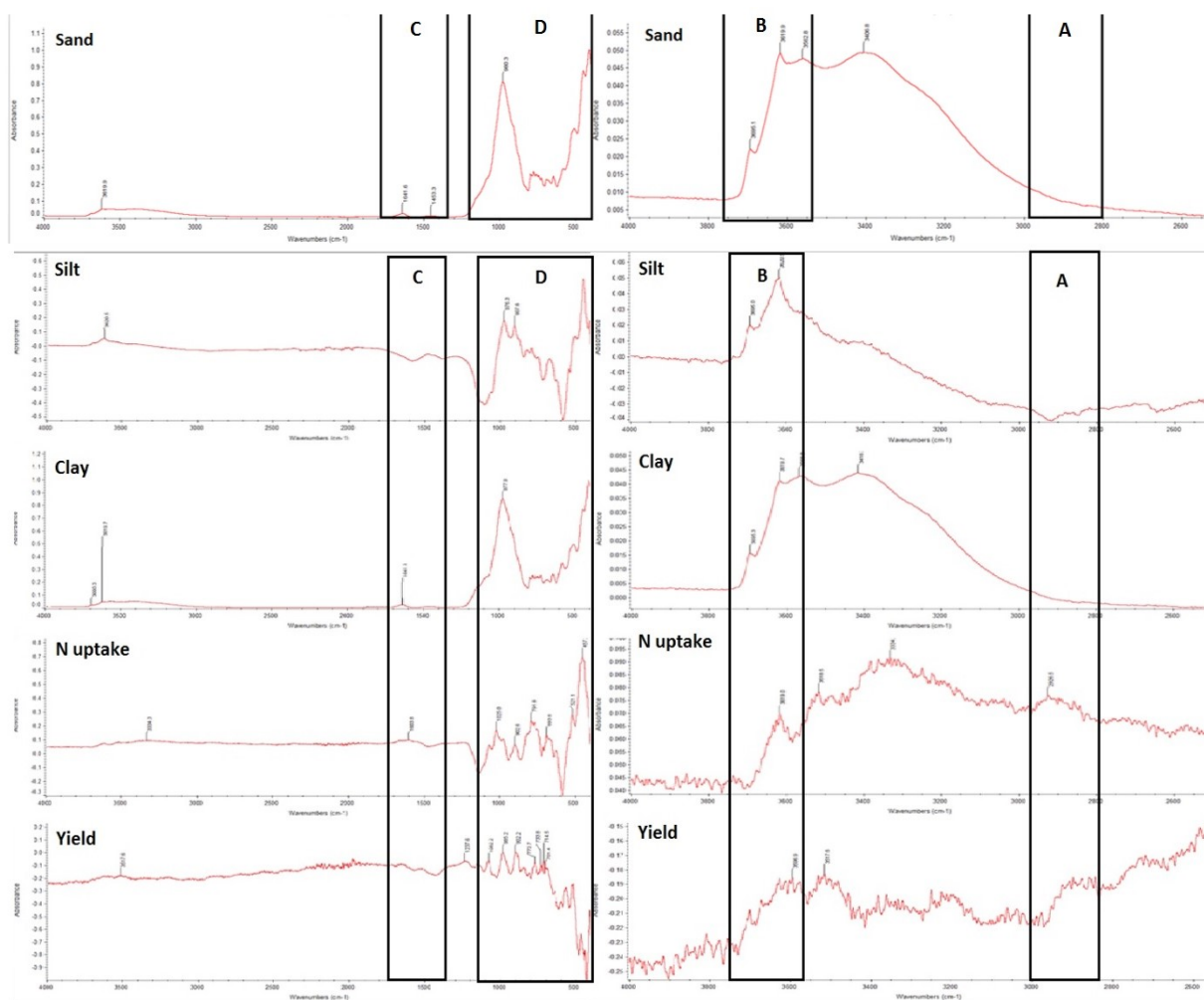
Fig. 3-12. Cont.

3.4. Discussion

3.4.1. Quality of ATR-FTIR-PLSR Models of 10 Soil Properties

How good are the models obtained in this study? According to the assessment criteria, where models with $r^2 \geq 0.90$ and RPD ≥ 2.00 are considered very reliable; models with $0.75 \leq r^2 < 0.90$ and $1.40 \leq$ RPD < 2.00 are reliable; and models with $r^2 < 0.75$, and RPD < 1.40 are less reliable. Models for the properties TC, TN, C/N, sand, silt, and clay are regarded as reliable to very reliable, whereas the models for the properties NH_4^+, NO_3^-, N uptake, and yield are less reliable.

76

It is not surprising that PLSR models well the properties TC, TN, C/N, sand, silt, and clay. Except for C/N, all these properties have assigned MIR absorption signals, with distinct and characteristic bands or regions observed in MIR soil spectra. TC, TN, sand, silt, and clay are the major components in the soil matrix, where the sum of TC and TN makes up around 6% of the total volume of soil; sand, silt, and clay comprise the mineral portion of soil, which accounts for 45% of the total volume. Their high mass in soil provides intense absorptions, leading to a stronger correlation between the spectral signals and reference values. An interesting point raised by some researchers is whether the prediction of TN relies on its high correlation to TC or on independent measurement of vibrations involving bonds to N (Chang and Laird 2002; Martin, Malley et al. 2002; Yang and Mouazen 2012). In our study, the excellent prediction of TN may be due to its high correlation with TC (r^2 0.94), as indicated by the similar pure component spectra of TN and TC (Fig. 3-12). Moreover, the C-H stretching band between 2900 and 2800 cm^{-1} was also observed in the pure component spectrum of TN, but its intensity was not as strong as that observed in the pure component spectrum of TC.

Models of good quality were also published by other researchers. For example, Minasny, Tranter *et al*. (2009) reported r^2 0.98 and RPD 2.1 for TC; r^2 0.94 and RPD 2.0 for TN; r^2 0.94 and RPD 2.3 for sand; r^2 0.90 and RPD 2.6 for clay using the DRIFT-MIR technique to analyze soil samples collected from three repositories in Australia. ATR-FTIR spectroscopy with chemometrics has been less extensively used to model soil properties than DRIFT-MIR spectroscopy. Recently, Ge, Thomasson *et al*. (2014) reported the modeling of 4 properties by ATR-FTIR spectroscopy with PLSR, with r^2 0.80 and RPD 2.26 for organic carbon; r^2 0.92 and RPD 3.52 for inorganic carbon; r^2 0.90 and RPD 3.14 for sand; and r^2 0.94 and RPD 3.38 for clay. By comparing our results to those of other researchers, it is apparent that the performance of the models obtained by ATR-FTIR spectroscopy coupled with PLSR in our work is in accordance with that of others. However, the methods employed by other researchers are diverse. Therefore, when comparing the performance of the models, in addition to model assessment parameters such as r^2 and RPD, we should also carefully examine the models with regard to several considerations. These include the type of technique used (DRIFT-MIR/ATR-FTIR, or/DRIFT-NIR) and the way it is applied (in the laboratory with dried and ground samples or fresh/moist samples, or in the field on extracted cores or top-soils, or on-the-go with sensors

embedded on machines); in addition, the range and diversity of the soils tested in the study (samples from a single field versus large-scale or nationwide study) must be considered; last but not least, an important consideration is the way in which the model was validated by either using samples of the same origin as the calibration samples or by using fully independent validation sets (Bellon-Maurel and McBratney 2011).

In our study, a total of 278 Canada-wide soil samples were modeled in the calibration. The type of soil varied from clay/silty clay to loamy sand according to the soil texture triangular diagram (Figure 3-1). The ranges of the major properties in our samples are in accordance with the reference value (Brady & Weil, 1996), where TC ranges from 5.41 to 39.06 g/kg (reference value 6 – 36 g/kg), TN ranges from 0.47 to 3.36 g/kg (reference value 0.2 – 5 g/kg), and C/N ranges from 6.05 to 18.41 (reference value 8 – 15). For calibration, in order to prevent model overfitting, a total of 10 latent variables (LVs) were considered, while 15 LVs were used in the work of (Ge, Thomasson et al. 2014). The optimal number of factors was selected at the first minimum of the root mean squared error (RMSE) in leave-one-out cross-validation.

For the properties, NH_4^+, NO_3^-, N uptake, and yield, the model performances were considered as less reliable when the models were developed using the total sample set. In the two texture subsets, the prediction reliability for NH_4^+ and N uptake increased and these models were considered reliable. Generally speaking, the prediction performance of these 4 properties is weak, and there are several reasons leading to this result.

One of these reasons is the low concentration of NH_4^+ (4.34 mg/kg ± 6.75 S.D.) and NO_3^- (10. 30 mg/kg ± 7.25 S.D.) in the soils and their weak absorption signals in the ATR-FTIR spectra of soils. The MIR absorption bands of NH_4^+ and NO_3^- occur in the regions $3410 – 3030$ cm^{-1}, $1390 – 1340$ cm^{-1}, and $840 – 730$ cm^{-1} (Miller and Wilkins 1952), but are masked by the stronger bands of minerals and organic matter. Linker, Shmulevich et al. (2005) reported that the absorption band of NO_3^- located around 1370 cm^{-1} might be overshadowed by the large CO_3^{2-} peak found at approximately 1450 cm^{-1}.

Moreover, the NO_3^- content in soil samples changes with time. Unlike NH_4^+, NO_3^- is negatively charged, causing repulsion by soil particles, which mainly have negative charges. As a consequence, NO_3^- does not attach to soil but dissolves in and travels with water (Page 1982).

This may lead to an accuracy problem when measuring NO_3^- content in soil, since it changes with the water travel pathway in soil and with water content. After sampling, NO_3^- content may change with changes in the moisture content of the soil over time during storage. In addition, the ATR-FTIR spectra were obtained from dried and ground samples. Therefore, the content of NO_3^- in the sample employed for the spectroscopic analysis would be different from that of the sample employed for chemical analysis, leading to error in the calibration, which was built based on the correlation between the spectral signals caused by the property measured and the reference values. Rossel, Walvoort *et al*. (2006) reported an r^2 of -0.02 for a NO_3^- calibration using DRIFT-MIR spectroscopy with PLSR developed with 49 dried soil samples from one agricultural field in Australia. Linker, Shmulevich *et al*. (2005) reported a better NO_3^- quantification using ATR-FTIR spectroscopy with Beer's law. However, this work was done with moist saturated soil spiked with up to 1000 mg KNO_3/kg. Although the final result was converted to a dry soil basis, the high concentration range of NO_3^- makes the comparison to our result less meaningful.

In addition, the weak relationship between the reference values of N uptake and yield and soil spectral signals may lead to the poor performance of the models for these properties. In our study, soils for chemical and spectroscopic analysis were sampled before seeding and fertilizer application. However, after soil sampling, routine farming management proceeded, such as the application of fertilizer and herbicide. Therefore, the information from the sampled soil which was used in our study to model yield is very limited, since yield is also determined by many other factors, such as the application of fertilizer, pesticide, and herbicide, as well as farming management and weather. Among these factors, the impact of soil properties on yield is not significant enough to be modeled, which can be proved by the correlation analysis between yield and other properties, with $r^2 < 0.13$ (Table 3-5). On the other hand, N uptake is measured as the total nitrogen from the crop. The nitrogen taken up by the crop comes from the inorganic form of nitrogen, NH_4^+ and NO_3^- in soil. Therefore, a correlation between N uptake and NH_4^+ and NO_3^- was found but the correlation was not strong (r^2 0.58 and 0.44, respectively) since external N sources were applied as fertilizer during cultivation. Since there is no N uptake information directly carried by the spectrum, and the correlation between NH_4^+ and N uptake was weak, N uptake cannot be fully modeled by ATR-FTIR spectroscopy with chemometrics.

3.4.2. Effect of Soil Texture on Model Performance

How does soil texture affect model performance? This question may be addressed by comparing the models obtained with the fine-texture and coarse-texture sample sets. Soil texture is determined by the content of clay. Soils with more than 350 g clay/kg are considered as fine-textured, whereas those with less than 350 g clay/kg are considered as coarse-textured. In the soil matrix, there is a positive correlation between clay and soil organic matter, where both show surface activity and colloidal activities (Brady and Weil 1996). On the other hand, the proportion of sand, silt, and clay determines the size of the soil particles and therefore the light scattering effects when detected by infrared spectroscopy.

For the properties TC, TN, C/N, and clay, the models showed better prediction performances for the fine-texture set than for the coarse-texture set, with increases in the RPD value of 12%, 35%, 8%, and 10%, respectively. It is not surprising to see a better model of clay for the fine-texture set, as the higher content of clay provides a stronger signal in the infrared spectrum and therefore a more significant correlation is established. The positive correlation between soil organic matter and clay content in the soil matrix and the stronger correlation between TC and TN in the fine-texture set (r^2 0.94) than in the coarse-texture set (r^2 0.80) both contribute to the improvement of the prediction performance. This improvement is most notable in the case of TN, and the model for the fine-texture set is considered very reliable.

Conversely, for the properties sand, silt, NH_4^+, NO_3^-, and N uptake, the model performances are better for the coarse-texture set than for the fine-texture set. Similar to the case of clay considered above, sand has a more intense spectral signal in coarse-textured samples, leading to a stronger correlation between spectral signals and sand content. Silt is measured by the subtraction of sand and clay and shows a much higher correlation with sand (r^2 0.90) than with clay (r^2 0.28). Consequently, prediction of silt shows a better accuracy for the coarse-texture subset. In the case of the properties NH_4^+, NO_3^-, and N uptake, although their model performances are regarded as reliable to less reliable, the performances for the coarse-texture subset are relatively better. This is not due to correlation with sand content but rather to the stronger scattering effect caused to the infrared spectra. The scattering effect due to the larger particle size in the coarse-texture set causes the variations in the spectral signal related to the

physical information instead of the chemical information, which are modeled. This is apparent in Figure 3-12, where mineral contributions are integrated into the pure component spectra of NH_4^+, NO_3^-, and N uptake.

For the property yield, the prediction performances were considered less reliable in both soil texture subsets. The effect of texture on the prediction performance is not significant, given that the RPD value is not significantly altered in the texture subsets. As can be seen in Figure 3-12 mainly noise was modeled in the pure component spectrum for this property.

3.4.3. Effect of Data Pre-treatments on Model Performance

How do data pre-treatments affect model performance? Most soil properties such as TOC, TN, and exchangeable cations were non-normally distributed but follow a lognormal-like distribution, which means the data is in a normal distribution after logarithmic transformation (Reimann and Filzmoser 1999, Brejda, Moorman et al. 2000). In our study, by assessing the skewness value from the parametric test, which measures the asymmetry about the mean, 9 out of 10 properties are not normally distributed (with 95% confidence interval) but are positively skewed, where the presence of a few exceptionally large values lengthens the right tail (Figure 3-3). In fact, most soil properties are positively skewed since most of them cannot have negative values, therefore constraining the left tail at zero (Brejda, Moorman *et al*. 2000). Logarithmic transformation with the base of 10 (log_{10}) is one of the commonly used data transformation techniques, especially in soil science, and is suitable to the situation with all positive observations and right skewness. In our study, log_{10} transformation was applied to all the reference values of each soil property. By comparing the skewness value before and after transformation, the skewness of the properties TC, NH_4^+, and NO_3^- was greatly decreased and they were approximately normally distributed after log_{10} transformation. However, in the case of other properties, such as TC, C/N, NO_3^-, clay and yield, log_{10} transformation did not improve the normality. In the case of the properties sand and silt, the normality even decreased (Table 3-6). Therefore, other distribution patterns in addition to log-normal distribution may occur in the case of some properties, and the normality of their distribution may be increased by using other types of transformation techniques. However, in our study, only log_{10} transformation was studied.

There are several reasons for transforming the reference data prior to modeling. Firstly, it can reduce the influence of extreme observations on the model and prevent their domination over other observations. It is undesirable to build a model based on the variation in a property mainly coming from the extreme and odd values. However, one should carefully understand the concept of sample variety when making a calibration, since a robust calibration should cover as much of the variety of the property as possible. Therefore, an extreme value should be carefully treated in order to identify whether it is the true value of the sample or an erroneous value. Secondly, data transformation can reduce the risk of unnecessarily removing samples as potential outliers because they fall outside the whisker region. The number of potential outliers is greatly reduced via data compression and the deviation from the mean decreases after $\log_{10}$ transformation. In our study, as shown in Figure 3-3, only 3 of the $\log_{10}$ transformed NH_4^+ reference values were considered as potential outliers instead of 26 before $\log_{10}$ transformation. Other benefits of data transformation include stabilizing the variance of the residuals, making the distribution of the residuals more normal, making data spread more equally, and making the dataset easier to handle owing to the much smaller scale (Eriksson, Byrne $et\ al.$ 2013).

In our study, both the original and $\log_{10}$ transformed reference data were used to build the calibrations for each property to study the effect of data transformation on calibration performance, which was evaluated by the RPD value (Table 3-12). Among the 10 properties, the models for TN, NH_4^+, silt, N uptake, and yield showed better RPD values when using the $\log_{10}$ transformed data instead of the original data. However, the increase in RPD was only $5-8\%$ except in the case of the model for NH_4^+, with a 23% increase in RPD, thereby promoting the model reliability from less reliable to reliable.

Reducing skewness and normalizing the distribution of the dataset is one of the main functions of $\log_{10}$ normalization. However, there is a lack of information about the relationship between the skewness value of the dataset and the RPD value. In our results, most of the model performances do not show a trend with the data normality, with the exception of the models for NH_4^+, where $\log_{10}$ transformation resulted in 23% increase in RPD and 74% reduction in skewness, and sand, where $\log_{10}$ transformation resulted in 21% decrease in RPD and 82% increase. Among all the properties examined in this study, these two represent the most extreme

skewness changes after $\log_{10}$ transformation, where the NH_4^+ dataset was almost normalized but the normality of the sand dataset decreased and the distribution became highly left-skewed. These results may suggest that the contribution of data normality to calibration performance exists but only becomes significant when the normality is significantly changed. In addition to data normality, the decrease of residual variances and the pulling in of some extreme values otherwise considered as potential outliers may also have more or less impact on the calibration performance.

Table 3-12. Comparison of skewness and RPD value of calibrations built with original or log10 transformed reference dataset

Properties	Original		Log_{10} transformed		
	Skewness	RPD	Skewness	RPD	Improvement [a]
TC	0.83	1.95	-0.01	1.76	
TN	0.42	1.78	-0.44	1.82	*
C/N	0.51	2.19	-0.46	1.81	
NH_4^+	3.47	1.2	0.9	1.48	*
NO_3^-	1.88	1.22	-1.5	1.03	
Sand	0.5	2.45	-2.85	2.03	
Silt	-0.07	1.44	-1.14	1.55	*
Clay	0.63	2.05	-0.77	2.29	
N uptake	1.89	1.29	0.33	1.35	*
Yield	0.83	1.09	-0.81	1.18	*

[a] Models with higher RPD (better performance) following $\log_{10}$ transformation.

3.5. Conclusion

ATR-FTIR spectroscopy coupled with PCA and PLSR was applied for soil classification and prediction of 10 properties closely related to soil quality, including TC, TN, C/N, NH_4^+, NO_3^-, sand, silt, clay, N uptake, and yield. Results of PCA indicated that the information captured in ATR-FTIR spectra was adequate to discriminate among soil textures based on the strong IR absorption of minerals. A total of 278 soils collected from four Canadian provinces were successfully clustered into fine-texture and coarse-texture groups by PCA of their ATR-FTIR spectra.

Calibration models for the 10 properties examined were built using PLSR. Six out of the 10 models, including those for TC, TN, C/N, sand, silt, and clay, were considered reliable to very reliable on the basis of evaluation criteria widely adopted by other researchers. However, for other properties, such as NH_4^+, NO_3^-, N uptake, and yield, the calibrations were less reliable and therefore ATR-FTIR spectroscopy is not recommended to be used in quantification of these properties but is suitable for their qualitative analysis. Results also indicated that soil texture and data transformation had a certain impact on model prediction performance, but the magnitude of the impact is strongly related to the nature of the property and the degree of normality of the dataset.

By comparing the results obtained in this study with those published by other researchers, we suggest that ATR-FTIR spectroscopy, coupled with proper spectral pre-processing and data transformation, has the potential for successful prediction of soil TC, TN, C/N, sand, silt, and clay.

CHAPTER 4

CONNECTING STATEMENT

The development of calibration models for 10 soil properties based on ATR-FTIR spectra was presented in Chapter 3. Among the 10 properties, the properties TC, TN, C/N, sand, silt, and clay were successfully modeled by ATR-FTIR spectroscopy, while the properties NH_4^+, NO_3^-, N uptake, and yield could not be modeled with acceptable accuracy. In order to investigate whether the modeling of these properties can be accomplished based on spectral features in the near-infrared region, DRIFT-NIR spectroscopy was used to model these properties, as described in Chapter 4. Furthermore, the suitability of ATR-FTIR and DRIFT-NIR spectroscopy in soil quality modeling is compared in terms of accuracy, feasibility, and cost.

SOIL QUALITY DETERMINATION BY MODELING OF SELECTED PROPERTIES OF SOIL USING DRIFT-NIR SPECTROSCOPY COUPLED WITH PCA AND PLSR AND MODEL PREDICTION PERFORMANCE COMPARISON BETWEEN DRIFT-NIR AND ATR-FTIR SPECTROSCOPY

Abstract

Near-infrared (NIR) spectroscopy has been widely adopted in precision agriculture to determine some properties of interest, such as SOM and clay minerals. However, several minor components and comprehensive properties have rarely been modeled by NIR spectroscopy. In our study, we use DRIFT-NIR spectroscopy with PCA and PLSR to characterize 278 soil samples from four Canadian provinces and quantify 10 selected soil properties, including chemical properties, such as TC, TN, C/N as well as the minor components, NH_4^+ and NO_3^-; physical properties, such as sand, silt, and clay; and the comprehensive properties N-uptake and yield. Our results show successful classification of the soils into fine-texture and coarse-texture groups by using PCA. In addition, the properties TC, TN, C/N, sand, and clay are successfully modeled by PLSR based on the correlation coefficient (r^2), the ratio of performance to predictive deviation (RPD), and the ratio of performance to interquartile range (RPIQ), where models for TC and TN are considered very reliable with RPD $\geq$ 2.0 and RPIQ $\geq$ 2.5, while models for C/N, sand, and clay are considered reliable with RPD $\geq$ 1.40 and RPIQ $\geq$ 2.0. However, in the case of the properties NH_4^+, NO_3^-, silt, N-uptake, and yield, calibrations were not successfully built, with both RPD and RPIQ values below 1.4. Comparison of the performance of these DRIFT-NIR calibration models with those developed using the ATR-FTIR spectra of the same sample set indicates that the ATR-FTIR calibration models have better prediction accuracy than the DRIFT-NIR models, especially in the case of SOM and mineral properties, with RPIQ increments between 12% and 36%. However, considering the higher cost and more sample preparation required by ATR-FTIR spectroscopy, DRIFT-NIR spectroscopy is suitable for use in precision agriculture, especially for in-field applications, where cost and efficiency are important.

Key words soil quality precision agriculture DRIFT-NIR PCA PLSR

4.1. Introduction

Soil quality determines the quality and quantity of crop yield. Soil quality assessment has been routine practice in farm management and many conventional soil analytical techniques involving a wet chemical extraction process are used. Historically, our understanding of soil and the assessment of its quality has been gained through this type of analysis. However, these techniques have two main disadvantages, soil integrity damage and low efficiency. The first of these refers to the disruption of the soil's complexity and multi-component interactions during the extraction process, making the analytical results more difficult to interpret. Moreover, the extraction requires large amounts of solvents, labor, and time, making the efficiency low (Rossel, Walvoort *et al*. 2006). These disadvantages of the conventional techniques became more problematic in the 1990s, when precision agriculture was introduced.

Precision agriculture aims at optimizing farm management to achieve targeted crop yield while reducing the application of excess fertilizers. It requires precise detection and control of the nutrients in soil (Mintert, Widmar *et al*. 2016). Therefore, to precisely tailor the usage of nutrients and fertilizers, soils from multiple sampling sites within the field should be characterized. Hence, precision agriculture requires a soil analytical technique that is capable of handling large numbers of samples in a low-cost and efficient way (Terra, Demattê *et al*. 2015). In this context, the disadvantages of the conventional techniques make them unsuitable for use in precision agriculture. Consequently, we need to further develop an analytical technique, such as infrared spectroscopy, that allows a better understanding of the soil as a complete system and can be used to characterize large numbers of soil samples economically and efficiently.

Although near-infrared (NIR) spectroscopy for soil analysis was first introduced in the 1970s (Bowers and Hanks 1965), the study of this approach boomed starting in 2000 (Rossel, Walvoort *et al*. 2006). Numerous investigations have been carried out with NIR spectroscopy to characterize many properties of soil, such as total carbon, organic carbon, inorganic carbon, total nitrogen, and soil minerals. McCarty, Reeves *et al*. (2002) and St Luce, Ziadi *et al*. (2012) successfully measured two important soil properties, total carbon (TC) and total nitrogen (TN), by using NIR spectroscopy, with coefficients of determination (r^2) of 0.86 and 0.89, respectively, which represent high accuracy of TC and TN determination. Since soil organic matter (SOM)

and clay minerals have proved to be successfully modeled by NIR spectroscopy, and in addition they are the most important properties determining soil quality, many researchers have worked on these major components. However, other minor components, such as mineralized nitrogen, namely, NH_4^+ and NO_3^-, which are the nutrients directly available for crop uptake, are rarely studied and modeled using NIR spectroscopy. In addition, some comprehensive properties, such as N-uptake and yield, are more straightforward to interpret as they indicate the production of the farm and the quantity of N-nutrients the crops need. However, these comprehensive properties lack a basis in chemical, physical, or biological information that can be directly measured. Moreover, the relationship between these comprehensive properties and other chemical, physical, and biological properties is unclear, making the evaluation of these comprehensive properties difficult.

In this chapter, our goal is to establish calibration models for 10 selected soil properties using DRIFT-NIR spectroscopy coupled with PLSR chemometrics. The selected soil properties include chemical properties, such as TC, TN, carbon-to-nitrogen ratio (C/N), ammonium (NH_4^+), and nitrate (NO_3^-); physical properties, such as particle size, including sand, silt, and clay; as well as comprehensive properties, such as N-uptake and yield. The reliability of the models will be assessed by using the commonly adopted evaluation criteria of RPD and RPIQ. In addition, since the absorption bands in NIR spectra are generally weak and overlapping, and some soil components are even NIR-inactive, the underlying basis behind the calibration against NIR information is usually unclear, making the explanation of the NIR quantification models difficult. Therefore, to better understand the PLSR calibration using NIR soil spectra, the relationship between soil properties and the absorption signals from NIR spectra is studied. In addition, the pure component spectrum of each model extracted by PLSR is analyzed to understand which regions of the NIR spectra are most related to the soil property. Furthermore, the models built by using DRIFT-NIR spectral information are compared to those built by using ATR-FTIR spectral information in terms of prediction accuracy, cost, and sample preparation requirements, in order to provide the evidence to the farmers who are interested in precision farming and want to select a suitable technique to do so.

4.2. Materials and Methods

4.2.1. Description of the Samples

The soil samples used for NIR spectral acquisition were identical to those used for ATR-FTIR spectral acquisition, described in Chapter 3. After drying and grinding, approximately 10 g of soil representing each sampling plot was taken for both NIR and ATR-FTIR spectroscopic analysis.

A total of 278 soil samples were studied, which were further separated into two texture subsets according to the clay content, namely, a fine-texture subset ($\geq$ 350g clay kg^{-1} soil, $n = 100$) and a coarse-texture subset ($<$ 350 g clay kg^{-1} soil, $n = 178$). The detailed statistical description of the reference values for the 278 soil samples is presented in Chapter 3, Table 3-3, 3-4, and 3-5.

4.2.2. Spectroscopic Method

4.2.2.1. Principle of DRIFT-NIR Spectroscopy

Near-infrared radiation, with wavelengths between 750 and 2500 nm, is absorbed mainly by C – H. N – H, and O – H bonds, which are the primary components of organic compounds (Osborne, Fearn et al. 1993). However, the bands in an NIR spectrum are not sharp or distinct because they correspond to overtones and combinations of the fundamental absorptions observed in the mid-infrared region. In addition, light scattering is another factor giving rise to the lack of well-defined bands in NIR spectra. Consequently, it is difficult to directly correlate sample attributes to specific peaks.

Diffuse reflectance occurs when light impinges on a rough surface of a material, where it is partially reflected, absorbed and transmitted. The light passing into the material may also be absorbed or reflected. Therefore, the radiation that is reflected from the material is composed of surface-reflected and bulk re-emitted radiation, which is summed as the diffuse reflectance of the sample (Yang and Mouazen 2012). DRIFT-NIR analysis is conducted by directing NIR light onto the soil and the reflected light is collected by the IR detector. According to the Beer-Lambert law, absorbance is linearly related to the analyte concentration. Therefore, the reflectance signal is converted to absorbance using the equation

$$A = Log \frac{1}{R} \dots\dots\dots\dots\dots\dots\dots\dots\dots\dots\dots\dots\dots\dots\dots\dots\dots\dots \text{(4-1)}$$

where A is absorbance and R is the reflectance signal.

4.2.2.2. DRIFT-NIR Spectral Acquisition

DRIFT-NIR spectra were collected by a TANGO Fourier transform infrared (FTIR) spectrometer (Bruker Optics, Billerica, MA, USA). Approximate 5 g of soil sample contained in a clean glass vial was placed into a measurement window with 10 mm diameter. All spectra were recorded in diffuse reflectance mode over the wavenumber range of $4000 – 12,500$ cm^{-1} ($2500 – 800$ nm) with 4 cm^{-1} resolution by co-addition of 128 scans (spectral acquisition time of about 1 minute). These spectra were transformed into absorbance spectra by computing $log(1/R)$, as absorbance is directly proportional to the concentration of the absorber according to the Beer-Lambert law. The absorbance spectra were generated using OPUS spectroscopic software (Bruker) and were further saved in SPC format.

Each soil sample was scanned in duplicate and the duplicate spectra were later averaged to produce a single spectrum per sample. Before sample spectral acquisition, an initial blank spectrum was recorded to test the spectrometer performance and as a reference for calculating the sample spectra in absorbance units.

4.2.3. Spectral Processing and Development of Calibration Models

4.2.3.1. PCA

PCA is a data compression process, which reduces a data matrix into a smaller number of principal components (PCs), which reflect the underlying structure of the original dataset. A more detailed description of PCA is provided in Chapter 3, Section 3.2.4.1. In the present study, PCA was applied to extract the information containing the most variations from the spectra. By plotting the PCs in two dimensions, interrelationships between the samples and variables can be examined.

4.2.3.2. PLSR

PLSR is an extension of PCA, where PLSR shows the correlations between the property values and the spectral features. The advantage of PLSR over PCA is that both the spectral (X-matrix) variation and the property (Y-matrix) variation are extracted to provide the highest correlation in the regression calculation. A more detailed description of PLSR is provided in Chapter 3, Section 3.2.4.2. In the present study, PLSR was applied to establish quantitative calibration models for 10 selected soil properties using the total set of soil spectra as well as the fine-texture and coarse-texture subsets.

4.2.3.3. Spectral Pre-processing and Development of Calibration Models

Spectral pre-processing aims to eliminate or minimize variability unrelated to the property of interest. For example, solid powdered samples vary greatly in particle size distribution, sample packing density, and sample morphology, leading to light scattering effects, which are particularly severe in NIR spectroscopy. The light scattering appears as baseline shifts, tilt or curvature, which are unrelated to the chemical response and may mask the subtle chemically induced variation in the spectra. Thus, in order to model the chemical response more effectively, it is critical to apply appropriate pretreatment to minimize such physical effects on the spectra.

The most commonly used spectral pre-processing methods in NIR spectroscopy are derivatives, de-trending baseline correction, Standard Normal Variate (SNV), and Multiplicative Scatter Correction (MSC). In this study, a Savitzky-Golay filter with 7 data points and a 2nd-degree polynomial in combination with multipoint baseline correction and 1st derivative were used to minimize unwanted variations while maintaining the signals of interest.

PCA was conducted using UnscramblerX10.3® (CAMO, Oslo, Norway). Spectral pre-processing and PLSR calibration were conducted using TQ Analyst™ (Professional Edition 7.2.0.161, Thermo Fisher Scientific, USA). The PLSR algorithm was used to decompose the raw or pre-processed spectra into a maximum of 10 factors. In order to obtain the optimized calibration model for each soil property, an individual model was developed for each property. All PLSR models were validated using a full cross-validation approach (leave-one-out) where each spectrum was in turn excluded from the calibration sample set and was predicted by the

model calibrated with the remaining spectra. The optimal number of factors was determined by minimizing the predicted residual error sum of squares (PRESS) in cross-validation.

4.2.3.4. Model Assessment

In addition to the parameters mentioned in Chapter 3, another widely proposed evaluation parameter was adopted to estimate the usefulness of the model predictions, namely, the ratio of performance to interquartile range (RPIQ). It is determined as the ratio of the interquartile range of the reference values to the error of prediction in cross-validation:

$$RPIQ = \frac{Interquartile\ Range}{RMSE} \quad\ldots\ldots\ldots\ldots\ldots\ldots\ldots\ldots\ldots\ldots\ldots\ldots\ldots\ldots\ldots\ldots\ldots\ldots\ldots\ldots (4\text{-}2)$$

In contrast to RPD, RPIQ accounts for the spread of a population in a dataset with a skewed distribution by using the interquartile range instead of the standard deviation. The RPIQ statistic was proposed by Bellon-Maurel, Fernandez-Ahumada *et al.* (2010), and it is better suited to data that does not fit a normal distribution, for which high skewness of the dataset is found.

In our study, models are divided into performance categories in a manner similar to that employed by other researchers (Chang, Laird *et al.* 2001; Veum, Sudduth *et al.* 2015; Ji, Li *et al.* 2016) using the statistics r^2, RPD, and RPIQ. Models in the first category are considered very reliable ($r^2 \geq 0.75$, RPD ≥ 2.00, and RPIQ ≥ 2.50), while those in the second category are considered reliable ($r^2 \geq 0.63$, RPD ≥ 1.40, and RPIQ ≥ 2.00), and those in the third category are considered less reliable ($r^2 < 0.63$, RPD < 1.40, and RPIQ < 2.00).

4.3. Results

4.3.1. Statistical Description of Reference Values

A total of 278 soil samples were used in the NIR spectroscopic study. The statistical information for these samples is presented in Table 4-1. According to the clay content, the set of samples is divided into fine-texture and coarse-texture groups, and the statistical information for these two

subgroups is also presented in Table 4-1. Most of the soil properties do not follow a normal distribution, as can be evaluated by the skewness value. All the properties in our study are skewed to a certain extent, with most of them being right-skewed, which means that the mass of the distribution is concentrated in the small values. In particular, the distribution of NH_4^+ and N-uptake are highly skewed. However, in the case of the property C/N in all the sets, sand in the fine-texture set, and clay in the coarse-texture set, the distribution is left-skewed with a negative skewness, where the population is concentrated more in the higher values.

Table 4-1. Statistical description of the reference values of 10 properties of soils in the whole set of samples and the fine-texture and coarse-texture subsets

Soil properties	Total set				
	Mean	Range	Skewness	SD [a]	IQ [b]
TC (g/kg)	17.15	5.41-39.06	0.75	5.87	8.33
TN (g/kg)	1.56	0.47-3.36	0.47	0.49	0.69
C/N	11.07	6.05-18.41	-0.29	1.78	1.70
NH_4^+ (mg/kg)	4.34	0.39-49.19	2.74	6.75	2.56
NO_3^- (mg/kg)	10.30	0.09-51.3	0.51	7.25	7.44
Sand (g/kg)	370	0-860	0.47	212	290
Silt (g/kg)	334	60-619	-0.11	129	180
Clay (g/kg)	296	42-750	0.64	150	191
N-uptake (kg N/ha)	42.38	6.36-198.25	1.96	37	31.28
Yield (kg/ha)	4534	820-11532	0.47	1874	2026

Table 4-1. Cont.

Soil properties	Fine-texture set				
	Mean	Range	Skewness	SD [a]	IQ [b]
TC (g/kg)	19.06	8.51-39.06	0.87	5.99	7.97
TN (g/kg)	1.76	0.84-3.36	0.63	0.51	0.73
C/N	10.83	8.49-13.43	-0.44	1.03	1.37
NH_4^+ (mg/kg)	4.29	0.39-29.71	1.39	5.97	2.79
NO_3^- (mg/kg)	9.14	0.09-51.3	0.48	7.20	5.40
Sand (g/kg)	188	0-480	-0.11	110	169
Silt (g/kg)	359	160-570	0.38	96	115
Clay (g/kg)	453	351-750	1.28	105	170
N-uptake (kg N/ha)	37.06	9.67-141.84	1.71	29.62	27.31
Yield (kg/ha)	4777	941-11532	1.66	1940	1839

Soil properties	Coarse-texture set				
	Mean	Range	Skewness	SD [a]	IQ [b]
TC (g/kg)	16.08	5.41-33.86	0.79	5.53	7.48
TN (g/kg)	1.45	0.47-2.73	0.26	0.45	0.69
C/N	11.21	6.05-18.41	-0.32	2.08	1.97
NH_4^+ (mg/kg)	4.37	0.43-49.19	2.96	7.12	2.40
NO_3^- (mg/kg)	10.96	0.36-41.64	0.40	7.22	8.84
Sand (g/kg)	473	150-860	0.41	185	284
Silt (g/kg)	320	60-619	0.11	144	223
Clay (g/kg)	207	42-346	-0.17	83	131
N-uptake (kg N/ha)	45.51	6.36-198.25	1.92	40.50	33.80
Yield (kg/ha)	4397	820-9380	0.37	1828	2125

[a] Standard deviation; [b] interquartile range

4.3.2. DRIFT-NIR Spectral Analysis and Development of Calibration Models

4.3.2.1. DRIFT-NIR Soil Spectral Analysis

Absorptions in the NIR region are due to the combinations and overtones of the fundamental vibrations occurring in the MIR region. The overtones and combinations detected in the NIR

region are of low probability and hence give rise to weak absorption. Generally, the bands in NIR spectra are characterized as broad, overlapping, and weak. As illustrated in Fig. 4-1-a, the NIR spectra of soil only exhibit a few broad features as well as a pronounced baseline tilt with increasing wavenumber.

Due to the broad and superimposed bands, soil NIR spectra contain fewer bands than MIR spectra and the interpretation of these NIR bands is more difficult. Three broad bands were observed in the combination and 1st overtone region of the soil NIR spectra. However, not much information was found in the 2nd overtone region and only noise was observed in the 3rd overtone region (Fig. 4-1-a). Due to the overlapping of the bands, it is impossible to directly associate them with specific functional groups. Nevertheless, these bands carry important information about the organic matter and minerals in soil. As reported in the literature (Madari, Reeves *et al*. 2006; Stenberg, Rossel *et al*. 2010; Xie, Yang *et al*. 2011), bands between 7300 and 6900 cm^{-1} (1370 – 1450 nm) are due to the 1st overtone of the H-O-H bending vibration of free water and water in the lattice of clay minerals, as well as the 1st overtone of aliphatic C-H bending. Bands between 5360 and 4930 cm^{-1} (1865 – 2028 nm) are due to the combinations of O-H stretching and organic matter vibrations such as N-H and C-H stretching. Bands between 4630 and 4410 cm^{-1} (2160 – 2268 nm) are due to phenolic O-H, amine N-H, amide N-H, and aliphatic C-H groups, as well as the mineral lattice (Madari, Reeves *et al*. 2006; Stenberg, Rossel *et al*. 2010; Xie, Yang *et al*. 2011).

The NIR spectrum of soil is strongly influenced by soil texture. The stacked spectra in Fig. 4-1-a show representative raw NIR spectra of three selected samples of different soil types, i.e., fine-texture, clay type (sample A), coarse-texture, sandy clay loam type (sample B), and fine-texture, clay loam type (sample C). Shifts and tilts of the overall baselines are observed, which is due to the scattering effect caused by the different particle size distribution in the three soil samples (Madari, Reeves *et al*. 2006; Yang and Mouazen 2012). The degree of scattering is more pronounced at shorter wavelength (larger wavenumber), therefore, stronger shift is observed in the overtone compared to the combination region. In addition, spectrum B has a higher baseline, which is caused by the stronger scattering effect of larger particles. However, the higher absorption coefficients for the clay fraction dominate over the particle size effect, resulting in

higher absorbance. Therefore, samples A and C, which are high in clay content, exhibit stronger absorbance than sample B, which has the lowest clay content.
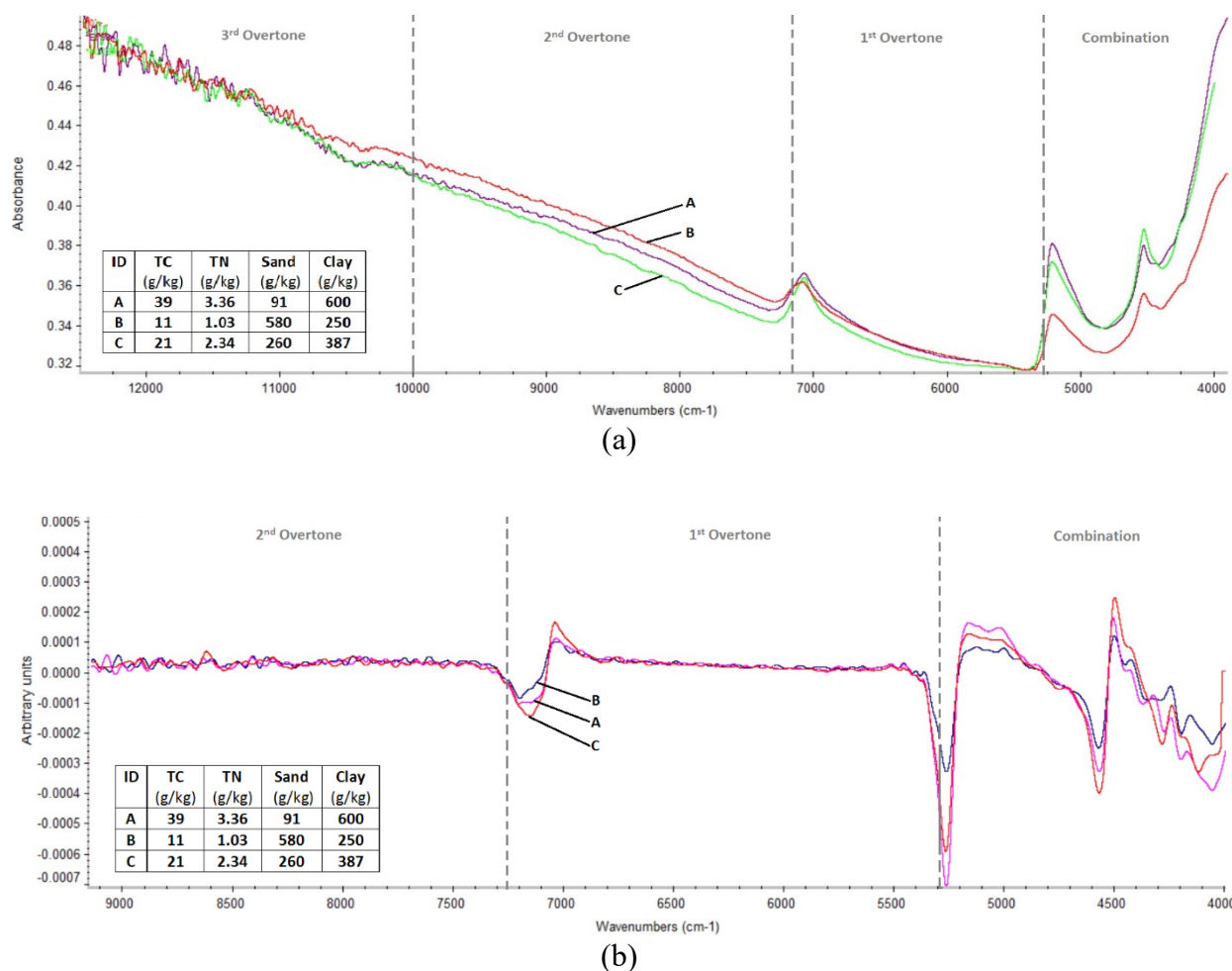
Fig. 4-1. DRIFT-NIR spectra (12,500 – 4000 cm^{-1}) of selected samples of fine and coarse texture with different TC and TN content. (a) Original spectra; (b) magnified 1st derivative spectra

In order to minimize the undesirable scattering effect, soil spectra were converted to their 1st derivatives (Fig. 4-1-b). Derivative spectral pre-treatment is mainly used to eliminate baseline drift between samples and resolve overlapping peaks. However, it can also increase noise. Compared to the raw spectra, the 1st derivative spectra exhibit increased noise in the 2nd and 3rd overtone regions.

In addition to soil type variations, the three selected samples in Fig. 4-1 have different TC and TN contents: sample A contains the highest amount of TC and TN, followed by sample C and then sample B. The difference in band absorbance due to variations in TC and TN content is more clearly revealed after resolving the overlapping peaks via the 1st derivative (Fig. 4-1-b).; bands between 5370 and 5200 cm^{-1} (1862 – 1923 nm) and between 4730 and 4530 cm^{-1} (2114 – 2208 nm), which are related to organic matter C-H and N-H functional groups, have highest absorbance in spectrum A, followed by spectra C and B. In addition, the band between 7370 and 7070 cm^{-1} (1357 – 1414 nm) is due to the O-H bond of clay; hence, the intensity of this band is highest in spectra C and A.

4.3.2.2. PCA of DRIFT-NIR Spectra

The complete data matrix including all samples and all the wavenumbers (12,500 – 4000 cm^{-1}) was modeled by PCA. The first two PCs explained 99% of the total variance of the data set, with PC1 and PC2 accounting for 92% and 7%, respectively (Fig. 4-2). The rest of the PCs explain only 1% of the variance. Therefore, the first two PCs were selected for later analysis.
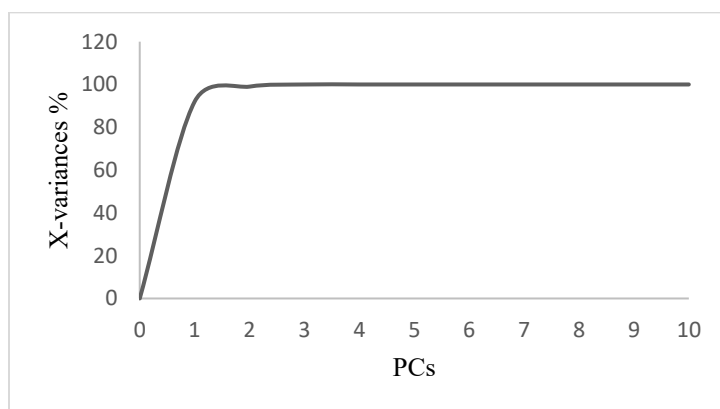
Fig. 4-2. Explained variance of the sample set by 10 PCs

Loadings are the correlations between the PCs and the original variables. The loadings plots for PC1 and PC2 presented in Fig. 4-3 indicate how much of the variation in a variable (wavenumber) is explained by each component. The higher the loadings value for the variable, the more variation of that variable is explained by the PC. In addition, loadings can be negative or positive, which indicates whether the PCs and variables are negatively or positively correlated. Figure 4-3-a is the loadings plot for PC1, which resembles an inverted NIR spectrum of soil. The loadings values are high at wavenumbers in the regions between 7280 and 6862 cm^{-1} (1373 – 1457 nm), 5358 and 4902 cm^{-1} (1866 – 2040 nm), and 4655 and 4408 cm^{-1} (2148 – 2268 nm). These NIR regions contain the bands characteristic of clay minerals and organic matter. Therefore, PC1 mainly accounts for the variations of clay minerals and organic matter within the set of 278 soil samples. Nevertheless, the negative values of the loadings indicate that the correlations between PC1 and the variations of clay minerals and organic matter are negative.
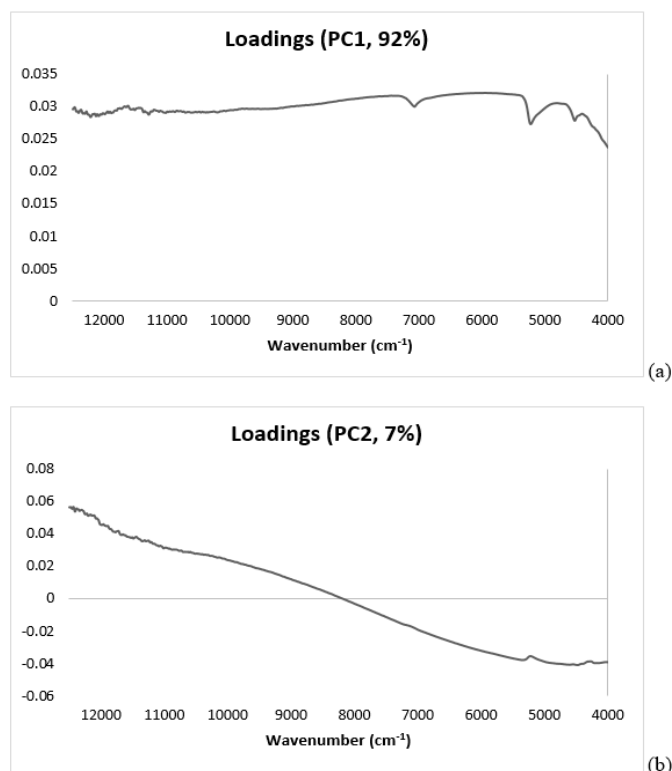
Fig. 4-3. PCA loadings plots: (a) PC1; (b) PC2

Figure 4-3-b is the loadings plot for PC2, which resembles the tilted baseline in soil NIR spectra. Moreover, there is a small bump in the region between 5296 and 5049 cm^{-1} (1888 – 1980 nm), which is characteristic to clay minerals. PC2 explains 7% of the total variance of the dataset, where the explained variation is mainly from the baseline tilt. As well, a small part of the variation of clay minerals is also explained by PC2.

Scores are the values of the original data for each sample projected onto the new coordinate system formed by the PCs. By plotting the scores value between two PCs, the relations among samples and the PCs can be revealed. Eleven scores plots (PC1 versus PC2) generated from PCA of the 278 DRIFT-NIR spectra are presented in Fig. 4-4. In each scores plot, a specific property of the samples is examined. These 11 properties are TC, TN, C/N, NH_4^+, NO_3^-, sand, silt, clay, N-uptake, yield, and texture. For the interpretation of the scores plots for each of the first 10 properties, the samples were separated into two groups according to the property's reference values, where the samples with values below the median are grouped together, as are those with values above the median. For the property of soil texture, the samples were separated into fine-texture and coarse-texture sets. In the scores plots, each point represents a sample; and points in the same color represent samples from the same group. In addition, points that are close together indicate that the samples they represent are similar. Therefore, by examining the distribution of the colored points, the relationships among samples and PCs are revealed.

The scores plots show a distinct clustering of the samples related to the properties silt, clay, and texture (Fig. 4-4-g; -h; -k). The two clusters observed for each of these properties are located at the two extremes of PC1, while the points are randomly spread in the PC2 dimension. This indicates that the original values of the properties silt, clay, and texture are overwhelmingly explained by PC1. Samples high in clay content have negative scores in PC1 (Fig. 4-4-h), which is explained by the negative loadings for clay signals in PC1. Fine texture is related to high clay content, and therefore points representing fine texture are clustered at the left extreme of PC1, where the scores values are negative (Fig. 4-4-k). However, samples with high silt content are clustered in the region where the scores of PC1 are positive (Fig. 4-4-g). This indicates that silt is positively correlated to PC1. However, in the case of the other properties, no distinct clustering is observed in the scores plots. This might due to masking of the signals of these properties by

the relatively strong mineral signals. Sand is the biggest component in soil, but no cluster is found in its scores plot. This is because sand is NIR-inactive and thus no information on sand can be captured in NIR spectra.
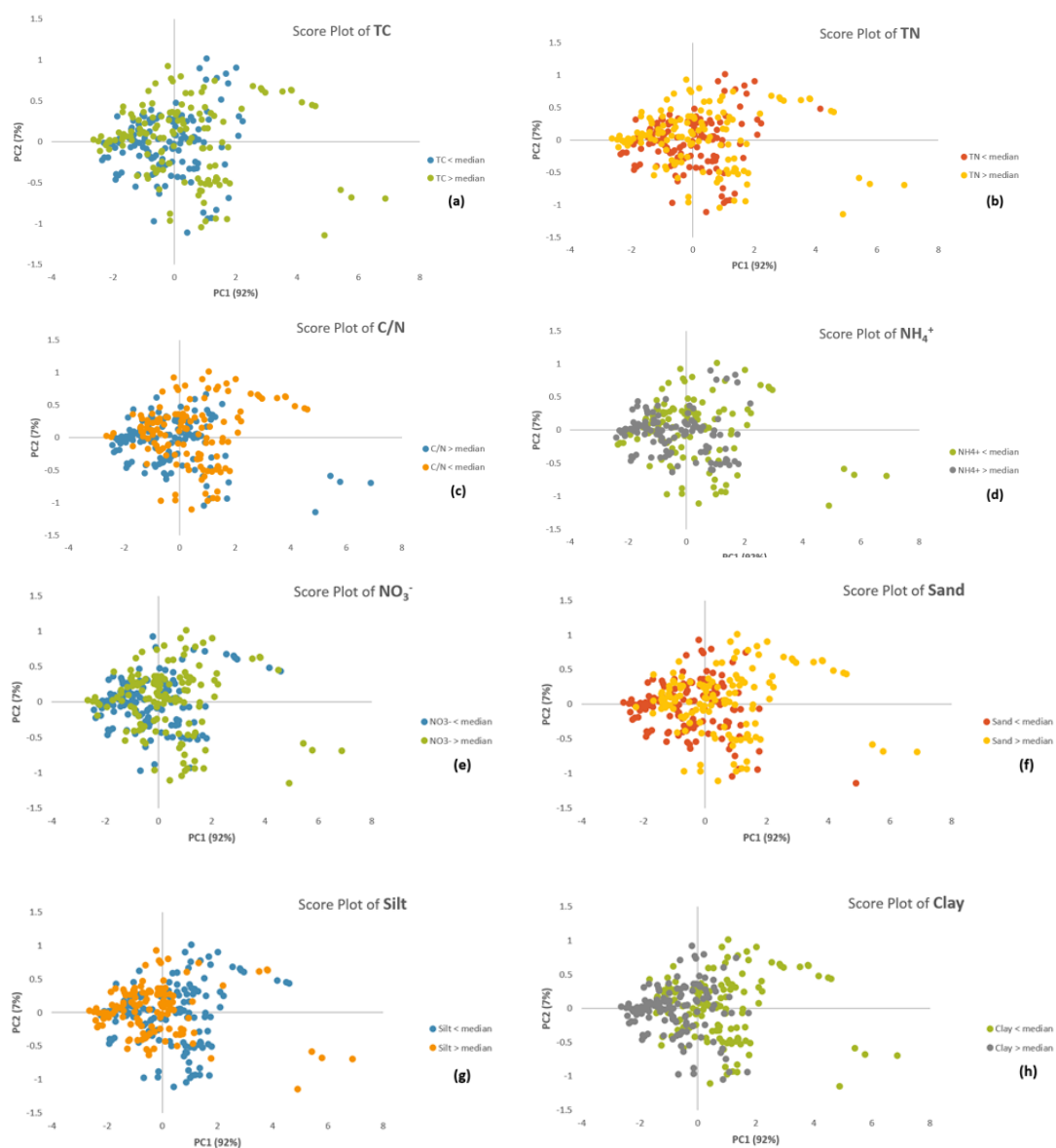
Fig. 4- 4. PCA scores plots for selected properties derived from DRIFT-NIR spectra of 278 soil samples: (a) TC; (b) TN; (c) C/N; (d) NH_4^+; (e) NO_3^-; (f) sand; (g) silt; (h) clay; (i) N-uptake; (j) yield; (k) texture
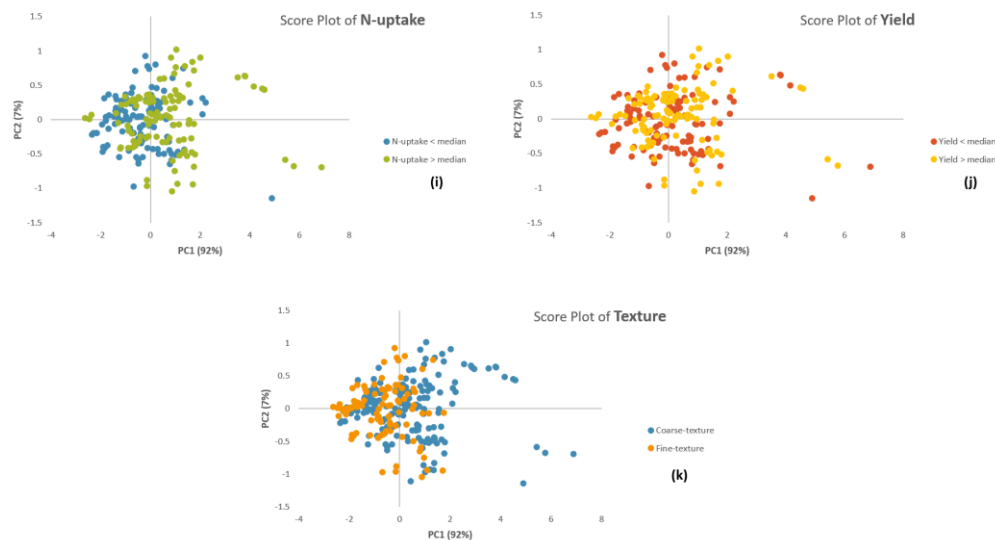
Fig. 4-4. Cont.

4.3.2.3. Correlation Analysis

The correlation coefficients among 10 properties of soil and the scores of PC1 and PC2 are summarized in Table 4-2. The closer the absolute value of the coefficient is to 1.00, the stronger the linear relationship between the two variables; the positive and negative values indicate whether the two are positively or negatively correlated. The analysis (Table 4-2) shows strong relationships between TC and TN, sand and silt, as well as sand and clay, with correlation coefficients (r^2) of 0.86, -0.72, and -0.81 respectively. In addition, a moderate relationship exists between N-uptake and NH_4^+, N-uptake and yield, as well as NO_3^- and yield, with r^2 values of 0.64, 0.63 and 0.42, respectively. The correlation between N-uptake and yield in the fine-texture set dramatically increases to an r^2 of 0.91. In addition, in the coarse-texture set, a similar increased correlation is found between sand and silt, with an r^2 value of -0.91. Other correlations among the rest of the properties are weak for the total sample set as well as for the two texture subsets.

In the total sample set, the scores of PC1 are mainly correlated to sand (r^2 0.45), clay (r^2 -0.35), and C/N (r^2 0.32). However, no correlation between scores and properties are found for PC2. This result is consistent with the loadings plot for PC2 in Figure 4-3, which shows that this PC mainly accounts for the variation of the baseline. Similar results are found for the coarse-texture

101

subset, where the scores for PC1 have stronger correlations with the properties, mainly the minerals and organic matter, such as TC, than the scores for PC2. In contrast, for the fine-texture subset, the scores for PC2 show stronger correlations with sand and silt than the scores for PC1.

Table 4-2. Correlation matrix between 10 properties of soils and the first two PC scores obtained by principal component analysis of the DRIFT-NIR spectra of the total sample set, the fine-texture subset, and the coarse-texture subset

	TC	TN	C/N	NH_4^+	NO_3^-	Sand	Silt	Clay	N uptake	Yield
					Total set					
TC	1.00									
TN	**0.86**	1.00								
C/N	0.36	-0.16	1.00							
NH_4^+	0.16	0.34	-0.29	1.00						
NO_3^-	0.06	0.10	-0.10	-0.02	1.00					
Sand	-0.15	-0.29	0.25	-0.05	0.06	1.00				
Silt	-0.02	0.11	-0.22	0.10	0.12	**-0.72**	1.00			
Clay	0.23	0.33	-0.17	-0.01	-0.19	**-0.81**	0.18	1.00		
N uptake	-0.02	0.17	-0.33	**0.64**	0.43	0.07	0.17	-0.24	1.00	
Yield	0.05	0.12	-0.12	0.16	0.42	0.04	-0.02	-0.05	**0.63**	1.00
PC1 (NIR)	**0.28**	0.11	**0.32**	-0.27	0.24	**0.42**	-0.28	-0.35	0.09	0.03
PC2 (NIR)	0.11	0.04	0.12	-0.09	-0.07	-0.04	0.07	0.00	-0.05	0.10

Table 4-2. Cont.

	TC	TN	C/N	NH$_4^+$	NO$_3^-$	Sand	Silt	Clay	N uptake	Yield
					Fine-texture subset					
TC	1.00									
TN	**0.89**	1.00								
C/N	0.46	0.02	1.00							
NH$_4^+$	0.09	0.32	-0.33	1.00						
NO$_3^-$	-0.05	-0.10	0.07	-0.21	1.00					
Sand	-0.37	-0.27	-0.27	0.18	0.01	1.00				
Silt	0.15	0.09	0.13	-0.10	0.17	-0.49	1.00			
Clay	0.25	0.19	0.17	-0.10	-0.17	-0.61	-0.40	1.00		
N uptake	0.05	0.08	-0.02	0.36	0.24	0.00	0.09	-0.09	1.00	
Yield	-0.02	0.01	-0.06	-0.01	0.37	0.03	0.15	-0.17	**0.91**	1.00
PC1 (NIR)	**0.35**	0.24	0.26	**-0.38**	0.06	-0.14	-0.23	**0.36**	0.08	-0.07
PC2 (NIR)	**0.37**	0.26	0.29	-0.05	-0.15	**-0.50**	**0.53**	0.04	-0.29	-0.23
					Coarse-texture subset					
TC	1.00									
TN	**0.81**	1.00								
C/N	0.37	-0.22	1.00							
NH$_4^+$	0.21	0.38	-0.27	1.00						
NO$_3^-$	0.18	0.30	-0.20	0.07	1.00					
Sand	0.17	-0.09	0.39	-0.12	-0.03	1.00				
Silt	-0.17	0.04	-0.31	0.15	0.14	**-0.91**	1.00			
Clay	-0.09	0.12	-0.35	0.00	-0.17	-0.68	0.31	1.00		
N uptake	-0.01	**0.30**	-0.44	0.65	0.52	0.00	0.21	**-0.39**	1.00	
Yield	0.06	0.16	-0.14	0.17	0.46	0.17	-0.11	-0.20	0.54	1.00
PC1 (NIR)	**0.44**	0.25	0.32	-0.26	0.28	**0.36**	**-0.25**	**-0.39**	0.06	0.11
PC2 (NIR)	-0.03	-0.08	0.05	-0.11	-0.03	0.05	-0.10	0.06	0.06	0.34

4.3.2.4. PLSR Calibration Models for DRIFT-NIR Spectra

Tables 4-3, 4-4, and 4-5 summarize the calibration and cross-validation statistics of the PLSR models developed for the 10 soil properties with the pre-processed DRIFT-NIR spectra of the total sample set and the fine-texture and coarse-texture subsets. For the total sample set (Table 4-3), the PLSR models for TC, TN, C/N, sand, and clay produced excellent prediction accuracy, with R_c^2 values of $0.85 - 0.93$, R_{cv}^2 values of $0.72 - 0.83$, and RPD values of $1.45 - 1.80$. The correlations between the measured and predicted values as well as the PRESS plots for these five properties are shown in Figure 4-5. PRESS plots indicate how the predicted residual error sum of squares decreases with the number of latent variables used. The number of latent variables used in each calibration corresponded to the minimum PRESS value.

Table 4-3. Calibration (C) and cross-validation (CV) of PLSR models developed with pre-processed DRIFT-NIR spectra: Total sample set ($n = 278$)

Model information			Evaluation parameters					
Property	Spectral pre-treatment	Calibration region (cm^{-1})	$R_c^2\|R_{cv}^2$	RMSEC	RMSECV	LVs	RPD	RPIQ
TC		7506 - 4050	0.93|0.80	1.93	3.22	6	1.65	2.28
TN		8009 - 4157	0.89|0.72	0.22	0.33	6	1.45	1.95
C/N		8009 - 4157	0.85|0.75	0.75	0.93	4	1.51	1.73
NH$_4^+$	Savitzky-Golay	7766 - 4157	0.79|0.61	1.06	1.38	3	1.26	0.90
NO$_3^-$	smoothing with 1st	7515 - 4112	0.69|0.45	3.60	4.55	5	1.09	1.37
Sand	derivative in	9986 - 4182	0.85|0.76	107	135	7	1.60	2.15
Silt	calibration region	9986 - 4182	0.66|0.48	96	112	3	1.14	1.59
Clay		9986 - 4182	0.93|0.83	55	81	6	1.80	2.23
N-uptake		8009 - 4157	0.66|0.46	24	28	4	1.11	0.99
Yield		9987 - 4050	0.35|0.20	1510	1600	1	1.01	1.85

For the properties NH$_4^+$, NO$_3^-$, silt, and N-uptake, the correlations between the predicted and reference values are lower, with R_c^2 values of $0.66 - 0.79$ and R_{cv}^2 values of $0.46 - 0.61$. Based

on their RPD values between 1.09 and 1.26, the models are classified as less reliable. For the property yield, the correlation between the predicted and reference values is poor with a R_c^2 of 0.35 and an R_{cv}^2 of 0.20. As well, the model for yield is classified as less reliable, with an RPD of 1.01.
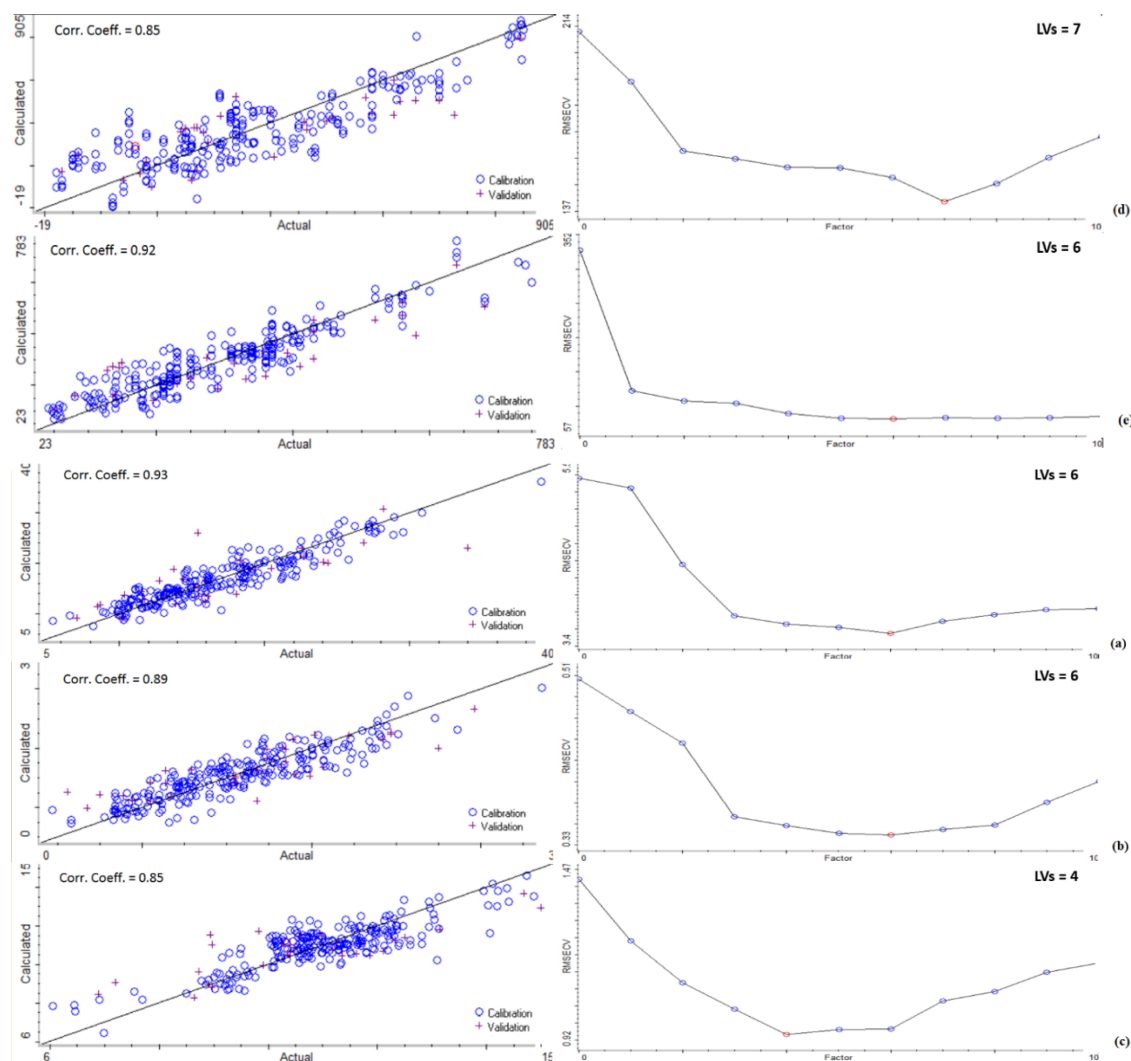
Fig. 4-5. Calibration (left) and PRESS plots (right) of PLSR calibrations based on the DRIFT-NIR spectra of the total sample set for the properties TC (a), TN (b), C/N (c), sand (d), and clay (e).

For the fine-texture subset (Table 4-4), similar results to those for the total sample set were found, where the PLSR models for TC, TN, CN, and clay showed excellent prediction performances. The correlation coefficients and model performances for these properties improved for the fine-texture subset, with R_c^2 values of $0.86 - 0.96$, R_{cv}^2 values of $0.73 - 0.91$, and RPD values of $1.44 - 2.43$. However, the performance of the model for sand deteriorated, with an RPD value of <1.40. The correlations between the predicted and reference values for the other properties generally improved for the fine-texture subset, with R_c^2 values of $0.62 - 0.87$. Nevertheless, based on RPD values, the models for these properties were still classified as less reliable.

Table 4-4. Calibration (C) and cross-validation (CV) of PLSR models developed with pre-processed DRIFT-NIR spectra: Fine-texture subset ($n = 100$)

	Model information		Evaluation parameters					
Property	Spectral pre-treatment	Calibration region (cm^{-1})	$R_c^2 \| R_{cv}^2$	RMSEC	RMSECV	LVs	RPD	RPIQ
TC		7506 - 4050	0.96|0.91	1.49	2.28	7	2.43	3.10
TN		8009 - 4157	0.96|0.88	0.14	0.22	7	2.20	3.19
C/N		8009 - 4157	0.86|0.73	0.49	0.67	5	1.44	1.81
NH$_4^+$	Savitzky-Golay smoothing with 1st derivative in calibration region	7766 - 4157	0.71|0.61	0.61	0.69	3	1.28	1.30
NO$_3^-$		7515 - 4112	0.62|0.21	3.07	3.99	1	0.98	1.08
Sand		9986 - 4182	0.82|0.64	53	72	3	1.29	2.01
Silt		9986 - 4182	0.76|0.57	57	73	2	1.19	1.09
Clay		9986 - 4182	0.90|0.74	44	69	6	1.47	2.18
N-uptake		8009 - 4157	0.87|0.44	13	25	5	1.10	1.07
Yield		9987 - 4050	0.86|0.51	954	1630	4	0.95	0.95

For the coarse-texture subset (Table 4-5), excellent PLSR prediction performances were found for the properties TC, TN, C/N, sand, clay, and N-uptake, with R_c^2 values of $0.79 - 0.97$, R_{cv}^2

values of 0.71 – 0.88, and RPD values of 1.42 – 2.08. Among them, the calibration for N-uptake showed great improvement, where the performance of the model for the coarse-texture subset is considered to be very reliable. This may be due to the stronger correlations between N-uptake and TN and between N-uptake and clay in the coarse-texture subset, where the correlation coefficients increase from 0.08 to 0.33 and from -0.09 to -0.39, respectively, between the total sample set and the coarse-texture subset (Table 4-2). For the other properties, the correlation coefficients and the prediction performance of the models are improved for the coarse-texture subset but the RPD values still remain less than 1.40. Hence, PLSR cannot quantitatively model these properties.

Table 4-5. Calibration (C) and cross-validation (CV) of PLSR models developed with pre-processed DRIFT-NIR spectra: Coarse-texture subset ($n = 178$)

	Model information			Evaluation parameters				
Property	Spectral pre-treatment	Calibration region (cm^{-1})	$R_c^2 \mid R_{cv}^2$	RMSEC	RMSECV	LVs	RPD	RPIQ
TC		7506 - 4050	0.97|0.88	1.19	2.47	7	2.08	2.85
TN		8009 - 4157	0.91|0.76	0.18	0.29	5	1.54	2.31
C/N		8009 - 4157	0.94|0.85	0.55	0.85	4	1.88	2.05
NH_4^+	Savitzky-Golay smoothing with 1st derivative in calibration region	7766 - 4157	0.81|0.62	0.97	1.29	3	1.28	0.82
NO_3^-		7515 - 4112	0.72|0.60	3.73	4.37	2	1.24	1.78
Sand		9986 - 4182	0.79|0.73	106	119	3	1.46	2.24
Silt		9986 - 4182	0.77|0.64	90	109	4	1.29	1.97
Clay		9986 - 4182	0.80|0.71	49	57	5	1.42	2.29
N-uptake		8009 - 4157	0.88|0.78	17	23	4	1.59	1.30
Yield		9987 - 4050	0.71|0.45	1250	1620	2	1.10	1.26

The RPD values of each property for the total, fine-texture, and coarse-texture sample sets are compared in Figure 4-6. The two horizontal lines divide the plot into three zones corresponding

to RPD values above 2.00, between 1.40 and 2.00, and below 1.40. These three zones indicated the reliability of the PLSR model to be very reliable, reliable or less reliable, respectively. According to this criterion, the models for TC, TN, C/N, sand, and clay are all considered reliable. Moreover, the prediction performances for TC and TN improved for the fine-texture subset and hence these models are considered very reliable. However, for the properties NH_4^+, NO_3^-, silt, N-uptake and yield, the quantification performance of the PLSR models was considered less reliable. Among these five properties, N-uptake showed improved prediction accuracy in the coarse-texture subset and the quantification is considered reliable.
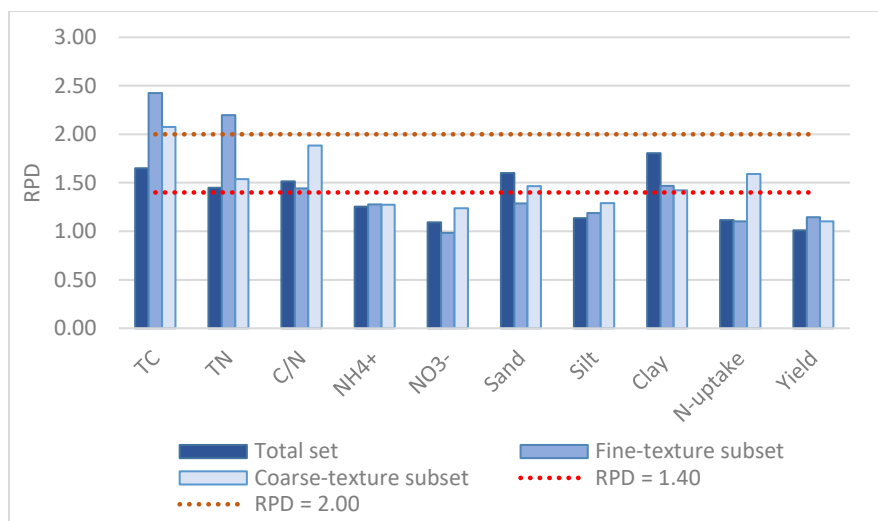
Fig. 4-6. Comparison of RPD values of the models for 10 properties developed with the total sample set and the fine-texture and coarse-texture subsets.

4.3.2.5. Pure Component Spectra Derived from PLSR Analysis of DRIFT-NIR Spectra

The 1st derivative pure component spectra for the 10 properties, which are extracted from the spectra of the total sample set by PLS analysis, are stacked in Figure 4-7. Compared to the 1st derivative soil spectrum (first spectrum in Fig. 4-7), the 1st derivative pure component spectra for TC, TN, NH_4^+, and clay show a similar absorption pattern, containing the absorption band in the region between 5400 and 5150 cm^{-1} characteristic of O-H, C-H, and N-H functional groups. Absorption bands in this region are also found in the pure component spectra for other

properties; however, the bands are either inverted (in the case of C/N, NO_3^+, silt, N-uptake, and yield) or shifted (in the case of sand). Since there is no direct relationship between these properties and absorption in this region, the inverted and shifted bands may result from the negative correlation between these properties and TC, TN, or clay minerals, all of which have absorptions in this region.
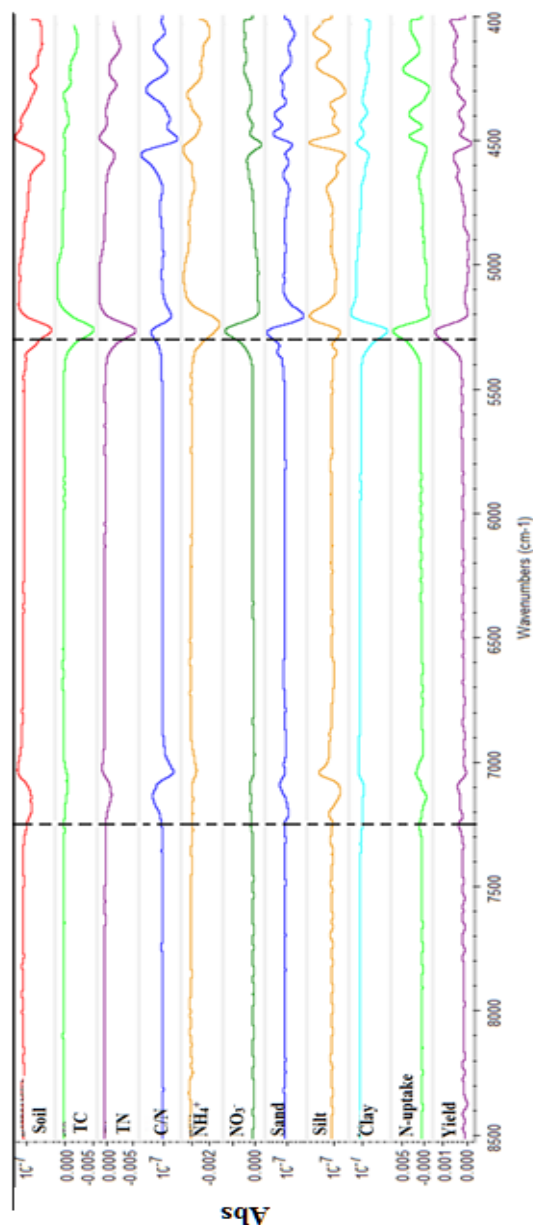
Fig. 4-7. 1st derivative pure component spectra for 10 soil properties obtained from PLSR modelling of the 1st derivative DRIFT-NIR spectra of the total sample set against the reference values for each property

Absorptions in the region between 7260 and 6860 cm^{-1}, which are due to O-H bending in the mineral lattice, are also observed in the 1st derivative pure component spectra for TC, TN, sand, silt, clay, and N-uptake. It is not surprising to observe these bands in the case of silt and clay, since absorption in this region is characteristic of minerals. However, the band found in the pure component spectrum is not due to absorption by sand since it is NIR inactive, but rather is due to its close correlation to clay, which has strong NIR absorption in this region. This explanation also applies to the pure component spectra for TC, TN, and N-uptake, in which the same absorption in the region 7260 – 6860 cm^{-1} specific to minerals is observed, but with much weaker intensity. In the case of the pure component spectra for NH$_4^+$, NO$_3^-$, and yield, no band in this region is observed.

The 1st derivative pure component spectra for all 10 properties show absorptions below 4630 cm^{-1}. The region below 4630 cm^{-1} is the combination region of the fundamental vibrations of various functional groups, such as aliphatic C-H, phenolic O-H, amine N-H, and amide N-H, as well as the mineral lattice. It is impossible to assign the bands in this region to a specific functional group since the bands due to the various functional groups are highly overlapped. Furthermore, the pattern of absorptions in this region varies among the properties. This may be due to different correlations and interactions between these functional groups.

4.3.2.6. Evaluation of Performances of DRIFT-NIR-PLSR Models Based on RPD and RPIQ
RPD and RPIQ values as model performance indicators are summarized and compared in Figure 4-8. In general, models with high RPD values have high RPIQ values. For example, for all three sample sets, the RPIQ values of the models for TC, TN, sand, and clay are all greater than their RPD values, and they are all above the upper threshold value of 2.00, which is the criterion for very reliable performance. Therefore, by basing the evaluation of model performances on RPIQ values, the models for TC, TN, sand, and clay are all classified as very reliable. Similar improvements are found in the case of the models for C/N and silt, where their RPIQ values are greater than 1.40, indicating reliable performance. However, in the case of other properties such as NH$_4^+$, NO$_3^-$, N-uptake, and yield, in general, the RPIQ values are similar to the RPD values. In addition, some RPIQ values are lower than the corresponding RPD values, such as the values

for the NH_4^+ model in the case of both the total sample set and the coarse-texture subset. Overall, the models for the properties, NH_4^+, NO_3^-, N-uptake, and yield are classified as less reliable, no matter which indicator is used. Exceptions are the model of NO_3^- in the case of the coarse-texture subset and the model for yield in the case of the total set, for which the RPIQ values are much higher than the RPD values, making the models reliable based on the RPIQ criterion.
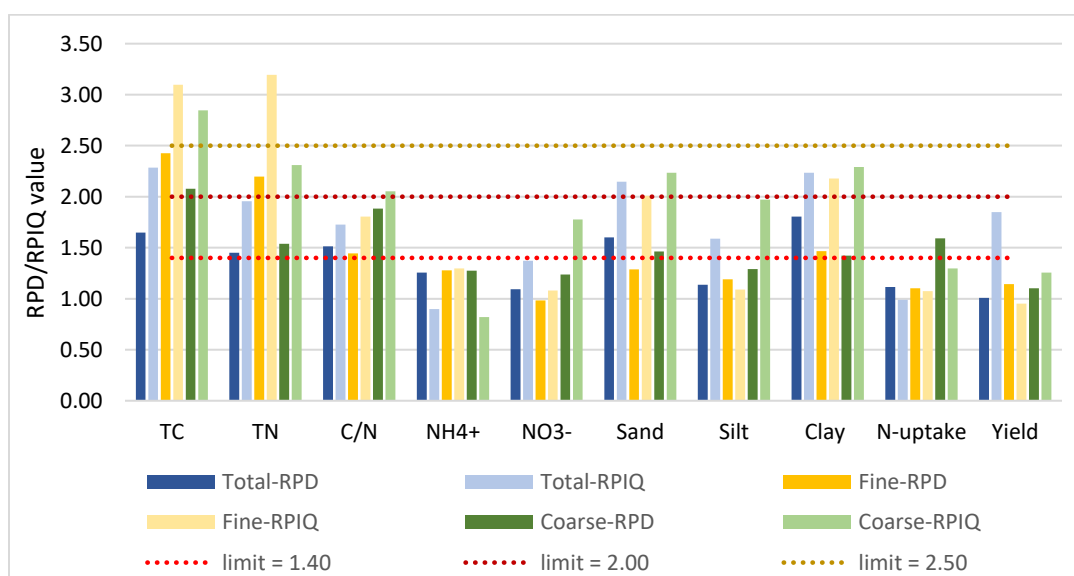
Fig. 4-8. RPD and RPIQ values of DRIFT-NIR calibration models for 10 soil properties built using the total, fine-texture, and coarse-texture sets.

4.4. Discussion

4.4.1. Quality of DRIFT-NIR-PLSR Models of 10 Soil Properties

According to the performance evaluation criteria, the DRIFT-NIR models for TC, TN, C/N, sand, and clay developed using the total sample set are considered reliable. This result meets our expectations, since soil organic matter and clay minerals are the fundamental constituents of the soil and have well-recognized absorption features in NIR spectra. For these reasons, TC is the constituent that has most frequently modeled by NIR spectroscopy over the past few decades, followed by clay content and TN (Rossel, Walvoort *et al*. 2006; Stenberg, Rossel *et al*. 2010).

Although sand is NIR-inactive and C/N does not have a primary NIR signal, these two components show significant correlation to components that have primary NIR signals, such as clay and TC, resulting in the successful modelling of these two components by the PLSR calibrations.

4.4.1.1. SOM

The performances of calibration models for TC, OC, and SOM reported in the literature are variable (Table 4-6), with some models being considered very reliable. In our study, variability in the performance of the TC calibration models was also found among the three datasets (total, fine-texture, and coarse-texture). A possible explanation for this is the low percentage (6%) of TC in soil and the weak TC signal in NIR spectra. In addition, the model performance is very sensitive to the large values of TC in a dataset, since TC in agricultural soils is expected to exhibit natural skewness of the data toward low values. Stenberg, Rossel *et al*. (2010) summarized the relationship between r^2 of OC calibrations and the standard deviation of the reference values from the published data (Martin, Malley *et al*. 2002; Udelhoven, Emmerling *et al*. 2003; McCarty and Reeves 2006; Rossel, Walvoort *et al*. 2006; Wetterlind, Stenberg *et al*. 2008), where r^2 increased from 0.6 to 0.9 when the SD increased from 2.5 to 10 mg/g. However, this effect of the SD of the reference values is not pronounced in our TC models since the SD values and skewness of the three datasets are similar, with SD values between 5.13 and 5.32 g/kg and skewness between 0.75 and 0.87.

Another factor influencing the performance of the TC calibration models is the highly variable mineral matrix among soil samples. Because the TC signal in the NIR spectra is much weaker than signals due to the mineral matrix, it may be masked by mineral variations, especially in the situation when the soil dataset examined includes many different soil types and soils from different geological conditions. For this reason, it is often reported that field- or farm-scale calibrations would have better performance than larger-scale calibrations based on soils collected over larger geographic areas. Stenberg, Jonsson *et al*. (2002) found that OC calibrations were improved if the sandiest soils were removed. Stenberg, Rossel *et al*. (2010) later reported that SOC was overestimated and caused larger errors if the sample population contained large

amounts of sand. Udelhoven, Emmerling *et al*. (2003) suggested that stratification of the samples according to their geological condition can produce better results. In our results, the TC calibrations for the two texture subsets have better performance than the calibration for the total set. Therefore, in our study, variation in soil type had a pronounced effect on the performance of TC calibrations.

Similar results were found for our TN calibrations, where the performances ranged from reliable to very reliable. These performances are similar to those reported in the literature (Table 4-6). Moreover, as in the case of the TC calibrations, the TN calibrations for the fine-texture and coarse-texture subsets again performed better than the calibration for the total set. This may again be attributed to the larger variation of the mineral matrix which masks the variation of TN, which is general below 1% and only comprises 1/10 of the SOM (Stenberg, Rossel *et al*. 2010). The mechanism behind TN prediction is debatable. Some authors argue that TN is predicted on the basis of specific absorption since it is associated with specific overtone and combination absorptions in the NIR region (Chang and Laird 2002). However, N-specific absorptions in NIR spectra are very weak, and therefore some authors argue that TN is predicted through its correlation to TC. Consequently, TN calibrations rarely perform better than the calibrations for TC or SOM (Rossel, Walvoort *et al*. 2006). Martin, Malley *et al*. (2002) reported that the calibration of TN failed when the correlation between C and N was only 0.67, while the calibration of TN became successful when the correlation was as high as 0.96. This may suggest that when the correlation between C and N is strong, the good performance of the TN calibration is based on its correlation to TC. When such correlation is absence, the TN calibration is based on N-specific absorption in NIR spectra (Stenberg, Rossel *et al*. 2010). In our study, the correlation between TC and TN is strong in all three datasets, with an r^2 of 0.86 for the total sample set, and the performances of the TN calibrations are good but not as good as those of the TC calibrations. It may be noted that the largest performance discrepancy between the TC and TN calibration was that for the coarse-texture subset, which also has the least strong correlation between TC and TN, with an r^2 of 0.81.

4.4.1.2. Minerals

For the three datasets, the calibration models for clay were all very reliable and the models for sand ranged between very reliable and reliable, while the models for silt were less reliable. Our findings are in accordance with the literature, where models for clay have been reported to perform well (Chang, Laird *et al*. 2001; Islam, Singh *et al*. 2003; Stenberg, Rossel *et al*. 2010). This is because clay minerals have strong and specific NIR absorption. On the other hand, sand is NIR-inactive; and therefore calibration must be based on correlations between sand content and other components that have NIR signals. For this reason as well as due to the important properties that clay minerals provide, such as formation of soil aggregates, nutrient adsorption and release, and water dynamics, modeling of clay content has received more focus in NIR studies (Stenberg, Rossel *et al*. 2010).

The performances of calibrations for sand, silt, and clay reported in the literature are variable. A possible explanation for this variability may be the differences in the calibration ranges among the different studies published in the literature. For example, in the case of calibration models for sand, Chang, Laird *et al*. (2001) reported a 2.32 RPD, Islam, Singh *et al*. (2003) reported a 1.50 RPD, and Veum, Sudduth *et al*. (2015) reported a 1.00 RPD. The RPD values are related to the SD of the reference values for the population, where the SD values in these three studies were 278 g/kg, 231 g/kg, and 49 g/kg, respectively. In addition, the higher the geological heterogeneity, the less robust the model performance will be. For example, in the case of calibration models for clay, Wetterlind, Stenberg *et al*. (2007) reported a 2.80 RPD with samples collected from a single field in South Sweden, while Islam, Singh *et al*. (2003) published a 1.90 RPD with samples representing 11 types of soil in Australia. Although the SD of the population in the latter study (187 g/kg) was larger than that in the former study (108 g/kg), the performance of the model was poorer since the samples were much more geologically heterogeneous.

4.4.1.3. Other Properties

Other properties including two chemical properties, the mineralized N (NH_4^+ and NO_3^-), and two comprehensive properties, N-uptake and yield, were not reliably estimated, where the RPD and RPIQ values fell below the lowest boundary. There are several possible explanations to these unsuccessful calibrations. In the case of mineralized N, the first is the low content in soil, less than 50 mg/kg in our dataset. Therefore, not much information on mineralized N is captured in the NIR spectra. Furthermore, all four properties are uncorrelated with TC and clay content ($r^2 <$ 0.24). Furthermore, N-uptake and yield may be affected due to the anthropogenic inputs of fertilizers, whereby the relationship between N-uptake or yield and the primary soil properties producing spectral features, such as TC, TN, and clay, is disrupted. Hence, calibrations cannot be achieved via correlation to other properties with primary NIR absorptions. These results emphasize the importance of primary or secondary associations between soil properties and NIR spectral features for reliable calibration. The inability to model comprehensive properties is not limited to yield and N-uptake, as other researchers reported that comprehensive properties such as aggregate stability, bulk density, and water-filled pore space were not successfully estimated by NIR spectroscopy (Veum, Sudduth *et al*. 2015).

Table 4-6. Summary of literature on modeling of soil properties using NIR spectroscopy with multivariate calibration

Attribute	Range	$n_{cali}|n_{vali}$ [b]	r_c^{2} [c]	RPD [d]	RPIQ [e]	LVs [f]	Authors
Total Carbon (g/kg)	1.3-285.8	743	0.87	2.79	NA	7	(Chang, Laird et al. 2001)
Total Nitrogen (g/kg)	2.3-16.5	744	0.85	2.52	NA	7	(Chang, Laird et al. 2001)
	1.0-3.4	125|104	0.84	2.4	4.1	8	(Veum, Sudduth et al. 2015)
Mineralizable Nitrogen (mg/kg)	0.4-555.1	764	0.72	1.84	NA	8	(Chang, Laird et al. 2001)
	0-133	125|104	0.57	1.5	2.1	8	(Veum, Sudduth et al. 2015)
Sand (g/kg)	12-952	743	0.82	2.32	NA	8	(Chang, Laird et al. 2001)
	83-983	121|40	0.53	1.5	NA	NA	(Islam, Singh et al. 2003)
	0-250	125|104	0.11	1.0	1.0	10	(Veum, Sudduth et al. 2015)
Silt (g/kg)	31-853	743	0.84	2.52	NA	8	(Chang, Laird et al. 2001)
	0-400	121|40	0.05	0.9	NA	NA	(Islam, Singh et al. 2003)
	58-86	125|104	0.30	1.1	1.6	7	(Veum, Sudduth et al. 2015)
Clay (g/kg)	7-352	743	0.67	1.71	NA	12	(Chang, Laird et al. 2001)
	17-717	121|40	0.72	1.9	NA	NA	(Islam, Singh et al. 2003)
	120-620	52	0.86	2.8	NA	3	(Wetterlind, Stenberg et al. 2007)
	84-167	125|104	0.67	1.7	1.9	5	(Veum, Sudduth et al. 2015)
	0.2-543	70|32	0.82	2.34	3.4	2	(Nawar, Buddenbaum et al. 2016)

4.4.2. Effect of Soil Texture on Model Performance

Based on comparison of both the RPD and RPIQ values for each property's model among the total sample set and the two texture subsets, only the models for TC and TN show significant improvement in the two texture subsets. For example, in the case of models for TC, the performance of the model for the fine-texture subset is the best, followed by that for the coarse-texture subset, with increases in the RPIQ value of 36% and 25%, respectively, compared to that for the total sample set; the corresponding increases in RPD value are 47% and 26%, respectively. However, in the case of the models for the other properties, the performances did not vary substantially among the three sample sets, with < 20% difference in RPD or PRIQ values.

There are several possible explanations for the variations in the performance of the TC and TN models. (Stenberg, Rossel *et al*. 2010) indicated that the variation in SOM itself is the key factor causing the variation of the model performance. However, in our case, the variation of TC and TN is similar in the three sample sets; the SD of TC in the total, fine-texture, and coarse-texture sample sets is 5.32, 5.53, and 5.13 g/kg, respectively; while the SD of TN in three sets is 0.48, 0.48, and 0.45 g/kg respectively. Hence, in our case, the extent of variation of the properties is not the key factor causing variation in the model performance.

Another possible explanation is the physical variation caused by differences in particle size. The distribution of particle sizes affects the extent of light scattering, where the coarser particles scatter light more and thereby increase the interactions of the light with the sample, effectively increasing the path length and, consequently, increasing the absorbance. However, in our results, both the models for the fine-texture and coarse-texture subsets performed similarly in terms of accuracy. In addition, compared to the contributions of chemical variations to the NIR spectra, the contributions of the physical variation are minor, as shown by the PCA analysis: the loading plot for PC1 indicates that the most significant variations in the spectra are associated with SOM and clay minerals while the physical variation (leading to baseline shift and tilt) is accounted for by PC2, which only explains 7% of the total variance (Fig. 4-3). These effects of physical variation are eliminated or minimized after the spectral pre-processing steps (Savitzky-Golay smoothing and transformation to 1st derivative spectra) performed prior to calibration.

Our results indicate that less variability in soil texture within the calibration set of samples results in a better calibration. Stenberg, Jonsson *et al*. (2002) divided soils into different soil classes according to clay content, and the results showed that SOM could be better predicted if the models were restricted to soils with a fairly high clay content or with a limited texture variability (Fig. 4-9). Our results agree to those of Stenberg, Jonsson *et al*. (2002), where the best-performing TC model was that for the fine-texture subset, in which the clay content of the soils is >350 g/kg. In addition, the TC model for the coarse-texture subset had better predictive accuracy than the TC model for the total sample set, which may be attributed to the higher textural variability in the latter set. The same trends were observed for the performance of the TN models developed for the three sample sets. This is to be expected owing to the significant correlation between TN and TC.

Class	Sand/Silt	Loam	Clay Loam	Clay
SOC	4-70	9.3-70	8.1-70	11.6-70
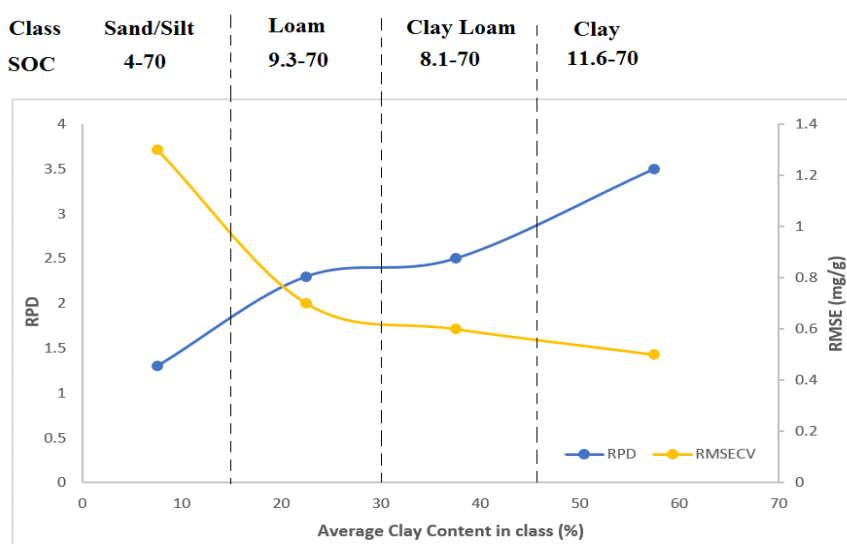
Fig. 4-9. Differences in calibration performance for soil organic carbon (SOC) between different texture classes

4.4.3. Comparison of the Performance Indicators RPD and RPIQ

Traditionally, the evaluation of NIR model performance is based on the parameters of coefficient of determination (r^2) and RMSE. Rossel, Walvoort *et al*. (2006) summarized literature results

published between 1986 and 2003 by tabulating the r^2 and RMSE parameters, in order to compare the quantitative predictions of various soil attributes using multivariate statistical analysis techniques applied to spectral responses in the ultraviolet (UV), visible (VIS), NIR, and MIR regions. However, these parameters are related to the population range; and therefore, they cannot be used for comparison of results obtained with different sets of soils,

To address this issue, RMSE is standardized to remove the effect of the population range, which is done by taking a ratio of RMSE and any statistical index representing the population, such as standard deviation (SD). Consequently, the RPD value, which is the ratio of the SD to RMSE, has become the most commonly used indicator for evaluation of calibration performance (Chang, Laird *et al.* 2001; Bellon-Maurel, Fernandez-Ahumada *et al.* 2010). RPIQ is another standardized RMSE value, where the RMSE value is standardized against the interquartile distance (IQ). The adoption of RPIQ has gradually increased since it was first proposed by Bellon-Maurel, Fernandez-Ahumada *et al.* (2010).

According to Figure 4-8, where the RPD and RPIQ values of all models for the total sample set are plotted, the models of TC, TN, C/N, NO_3^-, sand, silt, clay, and yield have RPIQ values that are increased relative to RPD values. These increases are due to the larger range of the population spanned by the IQ as compared to the SD. In general, when the distribution is normal or approximately normal, the interquartile range is about 1.3 times the SD. This relationship changes depending on how normal the distribution is. However, when the distribution is highly skewed, this relationship is no longer valid, and it may become the case that the SD is much greater than the IQ, especially if the dataset contains outliers. For the properties listed above, the skewness of their distribution is less than 1.00, which is not considered highly skewed. In contrast, in the case of the models for NH_4^+ and N-uptake, the RPIQ values are lower than the RPD values. This is due to the high skewness in the distributions of these two properties, with skewness values for the calibration set of 2.74 and 1.96 for NH_4^+ and N-uptake, respectively. These two properties follow a log-normal distribution, where after logarithmic transformation ($\log_{10}$) of the data, the skewness is notably reduced to 0.91 and 0.33 for NH_4^+ and N-uptake, respectively. In the case of RPD, the SD of the sample set is used to normalize RMSE but can only suitably describe the distribution of the population if it follows a normal or approximately

normal distribution. In a normal population, a 2SD interval (±1 SD) around the mean includes 66% of the population; whereas it represents 93% of the population spread in the log-normal population (Bellon-Maurel, Fernandez-Ahumada et al. 2010). This accounts for a much larger range of values and leads to a larger RPD value. Therefore, the RPD value of a dataset having a log-normal distribution gives an artificially good performance. On the other hand, the IQ value accounts for 50% of the population around the median, which better represents the spread of the populations, especially for those in a log-normal distribution. Therefore, RPIQ is a better performance indicator since IQ accounts much better for the spread of the population. In our results, based on the RPD values, the models for NH_4^+ and N-uptake have an artificially better performance, especially in the case of N-uptake for the coarse-texture subset, which has reliable performance. However, the performance decreases and the models become less reliable when evaluated on the basis of the RPIQ values. A similar trend is also found in the literature, where the RPD value for a log-normal population distribution is higher than the RPD value for a normal population distribution of the same RPIQ (Bellon-Maurel, Fernandez-Ahumada *et al*. 2010; Veum, Sudduth *et al*. 2015).

Overall, the RPD values correlate weakly with the RPIQ values across all 10 models, with a r^2 of 0.49 (Fig. 4-10). This indicates that RPD and RPIQ values cannot be predicted from one another. Furthermore, this shows that the distributions of the properties are non-normal; therefore, the population spreads described by SD and IQ are not correlated. However, after the removal of the points representing NH_4^+ and N-uptake, the r^2 value increases to 0.64. Therefore, whether RPD or RPIQ better describes the performance of a model depends on the distribution of the population. For many soil properties, which do not follow a normal distribution but follow more closely a log-normal distribution, the use of RPD values to evaluate models may be inappropriate. Therefore, in our study, both RPD and RPIQ are adopted to better evaluate the performance of the models. However, there is no statistical basis for the evaluation criteria. The criteria based on RPD values used in our study follow those proposed by Chang, Laird *et al*. (2001), In the case of RPIQ, it has been suggested in the literature that similar criteria to those based on RPD values be used (Nduwamungu, Ziadi *et al*. 2009). However, some properties follow an approximate-normal distribution, where the IQ is around 1.3 times the SD, so that a value of 2.50 instead of 2.00 should be used as the upper threshold of RPIQ-based criteria. In

general terms, only models that fall in the upper range of both RPD and RPIQ can be considered very reliable.
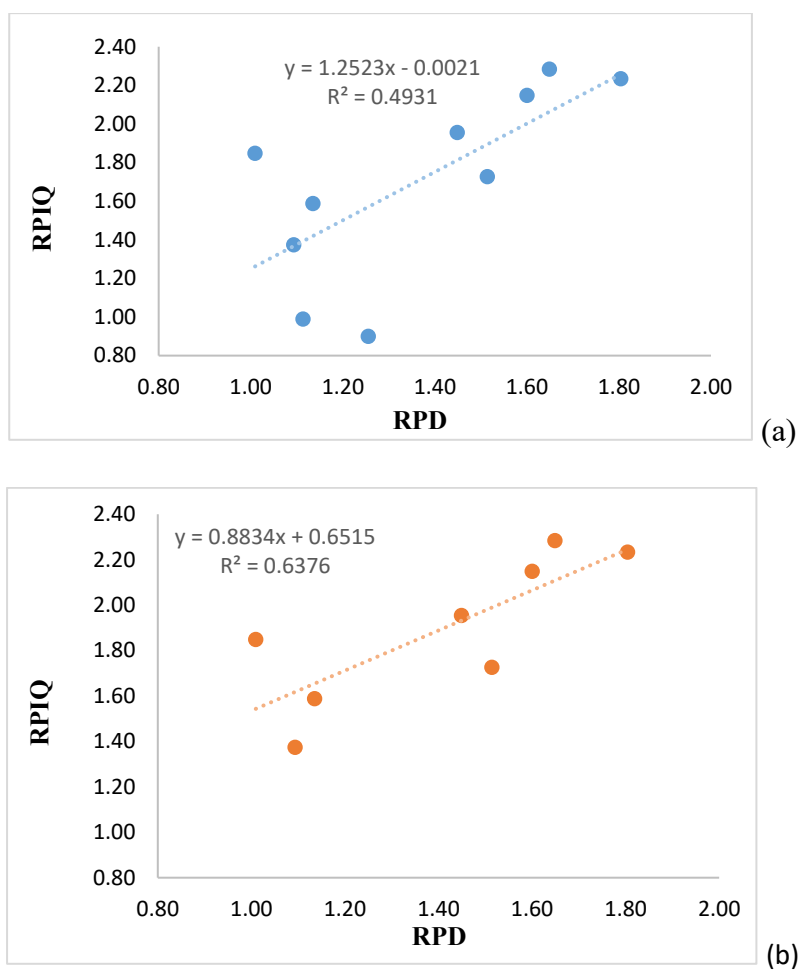
Fig. 4-10. Correlation between RPD and RPIQ for the models developed using the total sample set. (a) correlation for all 10 models; (b) correlation after removal of the models for NH4+ and N-uptake

4.4.4. Comparison between ATR-FTIR and DRIFT-NIR Calibration Models of Soil Properties based on RPIQ

The RPIQ indicators of each of the calibration models based on ATR-FTIR or DRIFT-NIR spectra are presented in a bar chart in Figure 4-11. In general, both techniques, ATR-FTIR and DRIFT-NIR spectroscopy, coupled with PLSR, display promising capability to model the properties TC, TN, sand, and clay, in terms of prediction performance. All the models for these properties, for either the total set of samples or the two texture subsets, are classified as very reliable, with RPIQ values greater than 2.00. This result is not surprising since all these components have specific signals in both MIR and NIR regions, except for sand, which does not have an NIR signal but had significant correlation to clay.

ATR-FTIR spectroscopy displays better modeling capability than DRIFT-NIR spectroscopy for the properties TN, sand, and clay, with average RPIQ increments of 11.68%, 36.25%, and 11.61%, respectively. The improved modeling of these properties may be due to their more intense and more characteristic signals in ATR-FTIR soil spectra as compared to DRIFT-NIR soil spectra. In addition, the RPIQ increment is much more significant in the case of sand, which has strong MIR absorption; consequently, the ATR-FTIR calibration for sand is directly based on spectral signals due to sand. However, because sand is NIR-inactive; the DRIFT-NIR calibration for sand is based on the correlation to other soil components, such as clay, which is NIR-active. In the case of the TC calibrations, the DRIFT-NIR models perform slightly better than the ATR-FTIR models for the two texture subsets; however, for the total set of samples, which includes various soil types, the ATR-FTIR model performs better than the DRIFT-NIR model. This is because the TC signal in the NIR region is weak and is masked by the signals from clay minerals, which have much higher variations. In contrast, in the MIR region, TC has distinct and characteristic absorption bands that are not be masked by absorptions by minerals. Overall, our results agree to the literature, where it was reported that MIR spectroscopy predicted soil organic matter and sand as well as clay minerals better than NIR spectroscopy (Rossel, Walvoort *et al*. 2006).

In the case of the properties C/N, and silt, both ATR-FTIR and DRIFT-NIR models were classified as reliable. The two spectroscopic techniques had similar prediction performances

except in the case of silt, where ATR-FTIR spectroscopy performed better than DRIFT-NIR spectroscopy. However, in the case of the properties NH_4^+, NO_3^-, N-uptake, and yield, both spectroscopic techniques failed to provide reliable calibrations, yielding RPIQ values below 1.40.

Overall, our results show that both ATR-FTIR and DRIFT-NIR spectroscopy can be used for the simultaneous assessment of various soil properties. The choice of which technique is to be used will depend on the accuracy of the predictions. For example, ATR-FTIR spectroscopy is recommended if soil texture is to be assessed. In addition, the cost of the technology and the required amount of sample preparation are other considerations when making the decision. For example, if TC is property to be evaluated, the 11% improvement in prediction accuracy (11% reduction in RMSECV) achieved by using ATR-FTIR spectroscopy instead of DRIFT-NIR spectroscopy may not be significant, considering that more sampling preparation is required and that the cost of the ATR-FTIR instrumentation is higher. For in-field implementation, cost and efficiency are important, and therefore these trade-offs are more pronounced for in-field soil analysis. As time progresses and technologies develop, portable MIR spectrometers of lower cost and requiring less sample preparation may become available for in-field soil analysis (Janik, Merry *et al*. 1998; Rossel, Walvoort *et al*. 2006).
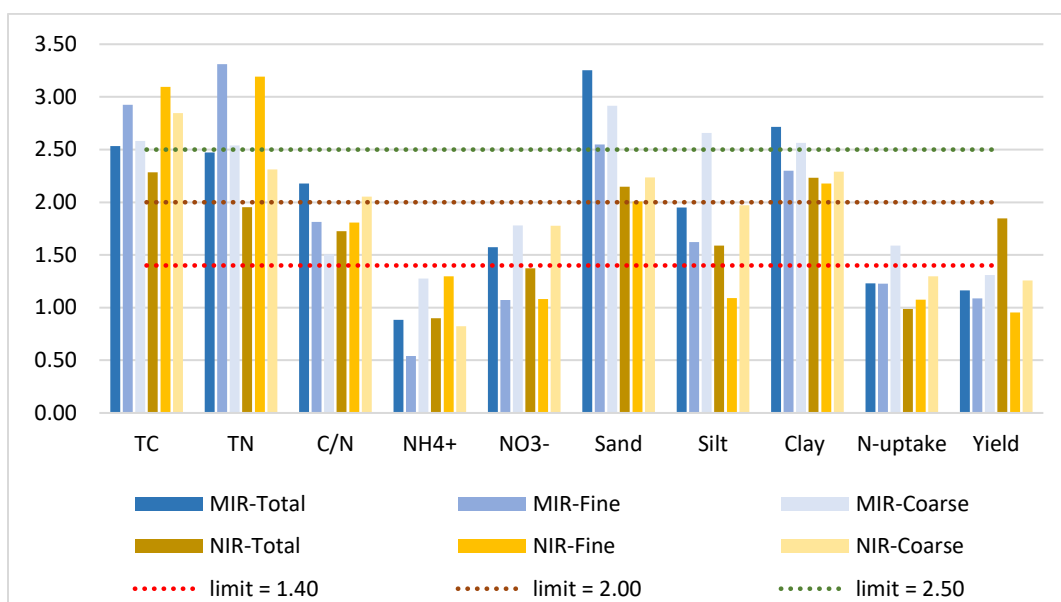
Fig. 4-11. Comparison of RPIQ values of ATR-FTIR and DRIFT-NIR calibration models for 10 soil properties built using the total set of samples as well as the fine-texture and coarse-texture subsets

4.5. Conclusion

DRIFT-NIR spectroscopy coupled with PCA and PLSR was applied for soil classification and prediction of 10 properties closely related to soil quality, including TC, TN, C/N, NH_4^+, NO_3^-, sand, silt, clay, N uptake, and yield. The results of PCA indicated that the information captured in DRIFT-NIR spectra was adequate to classify soils according to their texture based on the specific NIR signals of clay minerals. A total of 278 soils collected from four Canadian provinces were successfully clustered into fine-texture and coarse-texture groups by DRIFT-NIR spectroscopy with the use of PCA.

Calibrations for 10 properties were built using PLSR. Six out of 10 models, including TC, TN, C/N, sand, silt, and clay, were considered successful with reliable to very reliable prediction performances according to evaluation criteria widely adopted by other researchers. However, in the case of other properties, such as NH_4^+, NO_3^-, N uptake, and yield, the calibrations were less reliable and therefore DRIFT-NIR spectroscopy is not recommended to be used in quantitative

124

analysis of these properties. In agreement with the literature, this study suggests that DRIFT-NIR spectroscopy, coupled with proper spectral pre-processing, has the potential for successful prediction of soil TC, TN, C/N, sand, silt, and clay.

Both ATR-FTIR and DRIFT-NIR spectroscopy yielded very reliable models for TC and TN. However, in the case of properties related to soil texture, ATR-FTIR spectroscopy exhibited better performance than DRIFT-NIR spectroscopy, where the ATR-FTIR calibration models for sand, silt, and clay are very reliable to reliable, while the DRIFT-NIR calibration models are reliable to less reliable. For other properties, including NH_4^+, NO_3^-, N uptake, and yield, neither technique provided reliable calibrations. When choosing the proper technique to evaluate soil quality, prediction accuracy, cost, and sample preparation should all be considered. Although ATR-FTIR spectroscopy provides more accurate predictions for many soil properties, DRIFT-NIR spectroscopy is more economical and requires less sample preparation and so is more suitable for in-field soil analysis.

CHAPTER 5

CONNECTING STATEMENT

In the previous two chapters, the quality of agricultural soils was successfully modeled by both ATR-FTIR and DRIFT-NIR spectroscopy, and it was demonstrated that IR spectroscopy is able to capture both chemical and physical variations in soil. In Chapter 5, the research target shifted to bituminous-contaminated soil, where the bitumen residues in Alberta tailing soils were quantified by using ATR-FTIR and DRIFT-NIR spectroscopy

CHAPTER 5

DIRECT DETERMINATION OF BITUMEN RESIDUES IN OIL SAND TAILINGS BY FTIR SPECTROSCOPY BEFORE AND AFTER A REMEDIATION PROCESS

Abstract

The FTIR spectroscopic determination of bitumen residues in oil sand tailings as a technique for monitoring remediation processes was investigated. The application of both mid- and near-infrared (MIR and NIR) spectroscopy as rapid tools for determination of bitumen residues in tailings and remediated tailings was examined. In both cases, bitumen residues were directly determined from the neat samples without any chemical separations or extractions. Attenuated total reflectance mid- infrared (ATR-FTIR) spectroscopy coupled with partial-least-squares regression (PLSR) yielded the best calibration for bitumen determination, where an r^2 of 0.99 and a 1.76 wt% RMSEC were obtained for a calibration model built using artificial tailing soils with bitumen content ranging between 0.70 and 40.70 wt%, and an r^2 of 0.90 and a 1.55 wt% RMSEC were obtained for a model built using natural Athabasca tailing soils with bitumen content ranging between 9.70 and 26.59 wt%. These methods were reproducible with an average 0.91 wt% difference among triplicate analyses. The classification of unremediated and remediated tailing soils by principal component analysis (PCA) of their ATR-FTIR spectra was investigated. Soils were successfully classified according to their level of bitumen content, but classification based on discrimination between unremediated and remediated soils was not successful. This result implied the lack of a direct relationship between bitumen content and the remediation process, which was attributed to the variable bitumen content of the feedstocks and the use of an un-optimized remediation process. Therefore, the on-line MIR-PCA classification as well as the MIR-PLSR quantification is necessary for feedstock categorization based on bitumen level in order to optimize the remediation process and for subsequent evaluation of the remediation process to ensure the remediation goal has been met.

Keywords bitumen residues FTIR quantification remediation process

5.1. Introduction

Canada has the third-largest oil reserves in the world, after Saudi Arabia and Venezuela. According to the latest government report (Alberta Oil Sands Industry 2016), it is estimated that the total oil Canada's oil reserves is about 1.8 trillion barrels. The Canadian oil is very viscous and is bound to the soil minerals surrounded by a thin layer of water, which makes the oil resources in Canada called "oil sands". A special technique called the "Hot Water Extraction Process HWEP" is required to extract the bitumen from oil sands, whereby hot steam water is added into the oil sands to strip bitumen from the individual sand grains by a strong shearing force (Clark and Pasternack 1932). Since bitumen has similar density to water, it floats to the top attached to the injected air bubbles and is later skimmed off to achieve the recovery. The "tailings", which is the by-product from the extraction process, is stored in ponds constructed near the mining site.

The tailings are mostly composed of water (70.8%) and soil minerals (27.4%) and contain a small amount of bitumen residues, which is about 1.8% (Kessick 1977). When deposited in a tailing pond, the sand settles out quickly to form dykes and beaches. However, in the case of the fine materials, such as clays, their destiny in the tailing pond varies. Depending on the makeup of the tailings stream and the method of deposition, only 1/3 to 1/2 of the fine materials is retained in the tailings sand deposits. The majority of the fines separates during tailings sand deposition and is suspended in the water to form fluid fine tailings. It is reported that about 33% of the solids content in fluid tailings is almost all fines (Scott and Ozum 2010).

The HWEP technique and the accompanying tailings are the subject of much concern due to their large environmental impact. Firstly, to produce one barrel of bitumen, seven to nine barrels of water are required. Although only 1/3 of the water is the fresh water from the Athabasca River and most of the water is recycled from the tailing ponds, large amounts of non-recycled tailing waters are still generated as a result of the large daily bitumen production, which reaches 1.7 million barrels per day and is projected to double to 3.7 million barrels per day by 2019. Currently, the volume of Alberta's tailing ponds is about 720 million cm^3, covering an area of about 130 km^2 (Steward and Williams 2013). The tailing waters are found to contain various types of compounds that are believed to be toxic to aquatic organisms, such as organic acids,

phenolic compounds, sulfur compounds, nitrogen compounds, and hydrocarbons (Strosher and Peake 1978). Another concern is the disrupted mining area and the bitumen-contaminated tailing soils. It was reported that as of 2015, over 895 km^2 of land had been disturbed by oil sands mining activities (Natural Resources Canada 2015).

These hazards of oil sands tailings were documented as early as 1973, but they did not receive much attention and did not become a high priority for government, industry, academia, and the news media until 2000. In 2008, tailings became an intense focus of discussion after the "1,600 ducks died" issue occurred in Syncrude tailings (Steward and Williams 2013). In 2009, the *Directive 074* was announced by Alberta's Energy Resources Conservation Board (ERCB) to regulate the management of tailings and to ensure the environmentally sustainable development of Alberta's oil sands (Alberta Oil Sands Industry 2009). It requires that the amount of fluid tailings be reduced; that the size of the storage ponds be minimized and eventually eliminated; and that the fine tailings be converted to reclaimable landscapes (Alberta Energy Regulator 2009). In March 2015, the *Directive 074* was suspended with the release of new requirements for tailings management, the *Tailings Management Framework for Mineable Athabasca Oil Sands* (*TMF*) by the Government of Alberta. In addition to the requirements addressed in *Directive 074*, the *TMF* emphasizes the requirement of performance-monitoring to keep industry on track, where the monitoring should assess air and water quality as well as the quality and quantity of tailings (Alberta Energy Regulator 2015).

Currently, there are 33 approved oil sands exploitation projects and about 130 primary recovery projects (Energy Resources Conservation Board 2011). They all have a specific focus on minimizing the release of contaminants to the surrounding environment. The bitumen residues in tailings are one of the main contaminants that are considered toxic to wildlife; for example, chronic health effects on marine birds include triggering tumors and higher mortality rates, causing hypothermia when the bitumen becomes coated onto the feathers. In addition, bitumen is very resistant to microbial degradation; therefore, it can persist in the environment for years if it is not removed (Peterson, Rice *et al*. 2003). Therefore, prior to being released back to the environment, tailings must be remediated to remove bitumen residues to prevent or minimize any adverse effects on the environment.

The *TMF* requirement that monitoring should be in place to ensure that remediation is on-track relies heavily on the availability of analytical techniques for performance monitoring to evaluate the remediation progress. Therefore, to help the industry meet the monitoring requirement, to evaluate the reclamation quality, and to determine the reclamation performance in a timely manner, a fast, reliable and economical analytical technique that is amenable to on-line use is in demand.

Fourier transform infrared (FTIR) spectroscopy is a rapid and sensitive technique that enables the analysis of complex mixtures with minimum, or even without the need for any, sample pre-treatment. This technique can be used to detect all organic compounds that undergo dipole moment changes when irradiated by infrared light. Each type of IR-active functional group has its own characteristic absorption frequency, which can be used to identify as well as quantify different functional groups simultaneously from a single IR spectrum without any chemical separations or extractions. Compounds prevalently found in oil sand tailings, such as bitumen, can be determined by FTIR spectroscopy.

In this study, a fast and on-line method for bitumen quantification based on FTIR spectroscopy was established, designed for use in the tailings remediation plant for initial bitumen content evaluation at the feedstock reception point, evaluation of remediation progress, and final assessment to ensure that the clean-up goal has been met. By using this method, bitumen content can be directly evaluated from the neat soil sample without any bitumen extraction processes. Both ATR-FTIR and DRIFT-NIR spectroscopies, as well as two different quantification methods, namely, a simple Beer's law linear regression and partial-least-squares (PLS) regression, were used and compared to determine the approach best suited to on-line bitumen quantification in the remediation plant. Furthermore, an FTIR-based classification method was also established to assist the remediation plant in classifying and categorizing the initial feedstocks based on its bitumen content, which eventually benefits optimization of the remediation process.

5.2. Materials and Methods

5.2.1. Materials

5.2.1.1. Natural Athabasca Tailing Soils

The natural Athabasca tailing soils were received directly from different processing batches of the pilot plant (Gradek Energy Inc.), where the soils were undergoing a remediation process. A total of 32 tailing soil samples were received, where half ($n=16$) were unremediated and the other half ($n=16$) had undergone a remediation process. All the samples were first dried in the open air at room temperature overnight and then were ground and passed through a 2-mm sieve. The sieved soils were stored for later chemical and spectroscopic analysis.

5.2.1.2. Artificial Tailing Soils

The artificial tailing soils were prepared in the laboratory by spiking clean Athabasca tailing soils with bitumen. To obtain clean bitumen-free tailing soils, the Athabasca tailing soils were mixed with 2-methyltetrahydrofuran (2-MeTHF) in a 1:9 (wt/wt) soil-to-solvent ratio and the resulting solution was vortexed for 5 min and then centrifuged at 8000 rpm for 15-min. The supernatant containing the extracted bitumen and the solvent was collected and the sediment was mixed with 2-MeTHF again to perform the second extraction. This procedure was repeated three times until the supernatant was clear and colorless. All the supernatants were combined and were dried in a fume hood overnight to obtain the bitumen. The bitumen was measured gravimetrically to estimate the bitumen content in the tailing soils, and this bitumen was later used for the preparation of artificial tailing soil. The sediment fraction was dried in a fume hood overnight to obtain the clean Athabasca tailing soils.

To prepare artificial tailing soils with bitumen contents ranging between 0 and 40 wt%, a 50-mL stock solution of bitumen in 2-MeTHF solvent (bitumen/2-MeTHF = 1 g/5 mL) was prepared. The solution was considered homogeneous such that each unit volume (1 mL) of the solution contained 0.2 g of bitumen. To prepare each artificial tailing soil, the required volume of this solution was added to 5 g of clean Athabasca tailing soils, and the soils were suspended into the bitumen solution by vigorously stirring using a mechanical stirrer at 300 rpm for 20 min. After 20 min, the mixture was removed from the stirrer and was dried in a fume hood overnight. After

solvent evaporation, the samples were ground and passed through a 2-mm sieve. The samples prepared in this manner were stored for later IR spectroscopic measurement.

5.2.2. Methods

5.2.2.1. Determination of Tailing Soil Type by Hydrometer Method

Soil type was analyzed using the hydrometer method, which is based on the different sinking rates exhibited by mineral particles of different sizes. The density at a specific time point was measured by a hydrometer and was later used to calculate the proportion of different soil components.

Since the adsorbed bitumen in tailing soils affects the density of the mineral components; bitumen was removed from the tailing soils by washing with 2-MeTHF solvent at a 1:9 (wt/wt) soil-to-solvent ratio until the final extract was clear. The washed tailing soils were dried at room temperature in a fume hood overnight and stored for analysis by the hydrometer method.

For the analysis, 40 g of dried cleaned tailing soil was soaked in the Calgon solution (50 g/L, sodium hexametaphosphate) overnight to completely disperse soil minerals. The samples were then well mixed using an electric blender and transferred into a 1-L cylinder. After mixing of the sample several times using the plunger, the hydrometer was placed down once the mixing had stopped. The reading on hydrometer was recorded at 40 s and at 7 h. At every reading, the temperature was measured to correct for the buoyancy variation caused by the temperature (Sheldrick and Wang 1993). The same procedures were applied for the blank measurement.

The percentages of clay, sand, and silt in the tailing soils were calculated using the following equations:

$$Clay\ \% = \frac{R_{7h} - R_{blank}}{40} \times 100\% \dots\dots\dots\dots\dots\dots\dots\dots\dots\dots\dots\dots\dots. (5\text{-}1)$$

$$Sand\ \% = 100 - \frac{R_{40s} - R_{blank}}{40} \times 100\% \dots\dots\dots\dots\dots\dots\dots\dots\dots. (5\text{-}2)$$

$$Silt\ \% = 100 - (Clay\ \% + Sand\ \%) \ \dots\dots\dots\dots\dots\dots\dots\dots\dots\dots\dots\dots\dots \text{(5-3)}$$

where, R_{7h}, R_{40s}, and R_{blank} represent the hydrometer readings at 7 h and 40 s and the reading of the blank. The corrected hydrometer reading at 40 s represents the percentage of material still in suspension at the end of 40 seconds. Subtraction of the corrected hydrometer reading at 40 s from 100 yields the percentage of material that settled out at the end of 40 seconds, which represents all the sand in the soil (particle size of 2.00 – 0.05 mm). The corrected hydrometer reading at 7 h represents the material still in suspension at the end of 7 hours, which is the clay (particle size< 0.002 mm). The percentage of silt, with particle size between 0.05 and 0.002 mm, is obtained by difference (Bouyoucos 1962). The soil type was determined according to the relative proportions of the three fractions based on the reference values from the United States Department of Agriculture (USDA) triangular diagram.

5.2.2.2. Bitumen Content Determination by Total Combustion

Bitumen content of the natural Athabasca tailing soils was determined as elemental carbon percentage in the soil (C %) by using total combustion (FlashEA® 1112 Organic Elemental Analyzer, Thermo Scientific). A precise amount of sample (0.1 g) was weighed into a tin capsule and introduced into the combustion reactor, where a special furnace is heated at 900 – 1000 °C. A small volume of pure oxygen was added to the system to help burn the samples and convert them into elemental gases, which were quantified by gas chromatography with a thermal conductivity detector (GC-TCD). Standards of known carbon content were analyzed along with the unknowns to calibrate the instrument.

5.2.2.3. Background Bitumen Content Determination

To prepare the artificial tailing soil samples, bitumen was removed prior to spiking. After bitumen was removed, the "clean" tailing soil was sent to determine the amount of bitumen residues by using the total combustion method (FlashEA® 1112 Organic Elemental Analyzer, Thermo Scientific). The amount of bitumen residues determined was regarded as the background

bitumen content of the "clean" tailing soil and was added to each of the spiked amounts to obtain the total bitumen contents of the spiked samples.

5.2.2.4. FTIR Measurements

5.2.2.4.1. ATR-FTIR Spectroscopy

ATR-FTIR spectra were collected by an ALPHA FTIR spectrometer equipped with a ZnSe ATR crystal sampling accessory (Bruker Optics, Billerica, MA, USA) over the spectral range of 4000 – 400 cm^{-1} at 4 cm^{-1} resolution by co-addition of 128 scans. Spectra were scanned using OPUS software (Bruker) and were saved in .spc format. An initial background spectrum was collected to test the spectrometer performance and as a reference for calculating the sample spectra in absorbance units. Spectral acquisition time was about 1 minute per sample. Before further analyzing the spectra, vector normalization and baseline correction were applied to each spectrum using OMNIC™ Series Software (version 7.3; Thermo Scientific).

5.2.2.4.2. DRIFT-NIR Spectroscopy

DRIFT-NIR spectra were collected by a TANGO FTIR spectrometer (Bruker Optics, Billerica, MA, USA). Approximately 5 g of sample contained in a clean glass vial was placed into a measurement window with a diameter of 10 mm. All spectra were recorded in diffuse reflectance mode over the range of 4000 – 12,500 cm^{-1} (2500 – 800 nm) at 4 cm^{-1} resolution by co-addition of 128 scans. Each spectral acquisition took about 1 minute per sample.

Diffuse-reflectance spectra were transformed into absorbance spectra using log(1/R), as absorbance is directly proportional to the concentration of the absorber according to the Beer-Lambert law. The absorbance spectra were generated using OPUS software (Bruker) and were saved in .spc format.

Each soil sample was scanned in duplicate and the duplicate spectra were averaged. Before sample spectral acquisition, an initial background spectrum was collected to test the spectrometer performance and as a reference for calculating the sample spectra in absorbance units.

5.2.2.5. Spectroscopic Characterization Methods

5.2.2.5.1. Cluster Analysis (CA)

CA was applied to cluster the natural Athabasca tailing soils into groups based on spectral similarity. The samples were labeled as either "Before" or "After" based on whether they had undergone the remediation process prior to spectral acquisition. In addition, the samples were also labeled as either "High" or "Low" based on their bitumen content. Those labeled as "High" had bitumen content higher than the median value, while those labeled as "Low" had bitumen content below the median.

In cluster analysis, samples with similar spectral features will cluster together. In theory, samples having the same label should cluster together if their similarity is reflected by the spectral information.

5.2.2.5.2. Principal Component Analysis (PCA)

In order to examine whether the information contained in ATR-FTIR spectra is sufficient to distinguish between the remediated and the unremediated natural Athabasca tailing soils, PCA was conducted to extract and analyze the most variations from the spectra. By interpreting the scores and loadings of the extracted principal components (PCs) and variables, the components causing the most spectral differences between the remediated and unremediated soils were revealed.

5.2.2.6. Quantification of Bitumen in Tailing Soils

5.2.2.6.1. Simple Beer's Law Linear Regression

Since the intensity of an IR signal is linearly related to the concentration of the absorbing component, and given that bitumen has a strong, distinct, and characteristic IR absorption band between 2768 and 2989 cm^{-1}, a simple Beer's law linear regression for the quantification of bitumen in soil was examined. Since Beer's law is valid only when the path length is constant, it was necessary to compensate for the path length variation caused by light scattering before the regression was performed. To correct for the path length variation, the integrated area under the bitumen band was divided by the integrated area under the clay band between 3577 and 3746 cm^{-}

[1], and this bitumen/clay area ratio was regressed against the bitumen content determined by chemical analysis.

5.2.2.6.2. Partial-Least-Squares Regression (PLSR)

In addition to the simple linear regression, multivariate regression, in the form of PLSR, was used to build a bitumen calibration model based on the bilinear regression between the principal components, which are extracted from the original X-matrix, and the Y-matrix.

Before the regression, all the spectra underwent baseline correction, path length correction, and smoothing using the Savitzky-Golay algorithm (using a 7-point averaging interval and a second-order polynomial). The spectra pre-treatments and the PLSR were conducted using TQ Analyst™ software (version 7.2; Thermo Scientific).

5.2.2.6.3. Model Validation

To more thoroughly validate the established model, a set of validation samples completely independent of the calibration set may be used. In this work, two sets of calibration samples were used to build two PLSR calibration models; one set was composed of natural Athabasca tailing soils, and the second set was composed of artificial tailing soils. Each of these two calibration models was validating by employing the other model's calibration samples as a validation set; given the unreliability of model extrapolation, only the samples in the validation set having a bitumen content within the bitumen calibration range of the model being tested were chosen as validation samples. The validation error, accuracy, and precision were chosen as the parameters for evaluation of the models.

5.3. Results

5.3.1. Characterization of Tailing Soils

5.3.1.1. ATR-FTIR Spectral Characterization

The ATR-FTIR spectrum of bitumen is presented in Figure 5-1. Bitumen is mainly composed of hydrocarbons with aliphatic and aromatic carbons, as well a small quantity of heteroatoms, such

as O, N, and S. As observed in the pure bitumen spectrum, bitumen has strong MIR absorption in two main regions, 2768 – 2989 cm^{-1} and 1350 – 1487 cm^{-1}, where the absorption in the former region is due to the C-H stretching vibrations of methyl (–CH$_3$) and methylene (–CH$_2$) group and the absorption in the latter region is due to their bending vibrations. In more detail, the peaks in the stretching region represent the asymmetric C-H stretching vibration of –CH$_3$ (2951 cm^{-1}), the asymmetric C-H stretching vibration of –CH$_2$ (2921 cm^{-1}), and the symmetric C-H stretching vibration of –CH$_2$ (2853 cm^{-1}). In the bending region, the peaks at 1455 cm^{-1} and 1376 cm^{-1} are due to the asymmetric bending of –CH$_3$ and –CH$_2$ and the symmetric bending of –CH$_2$, respectively.
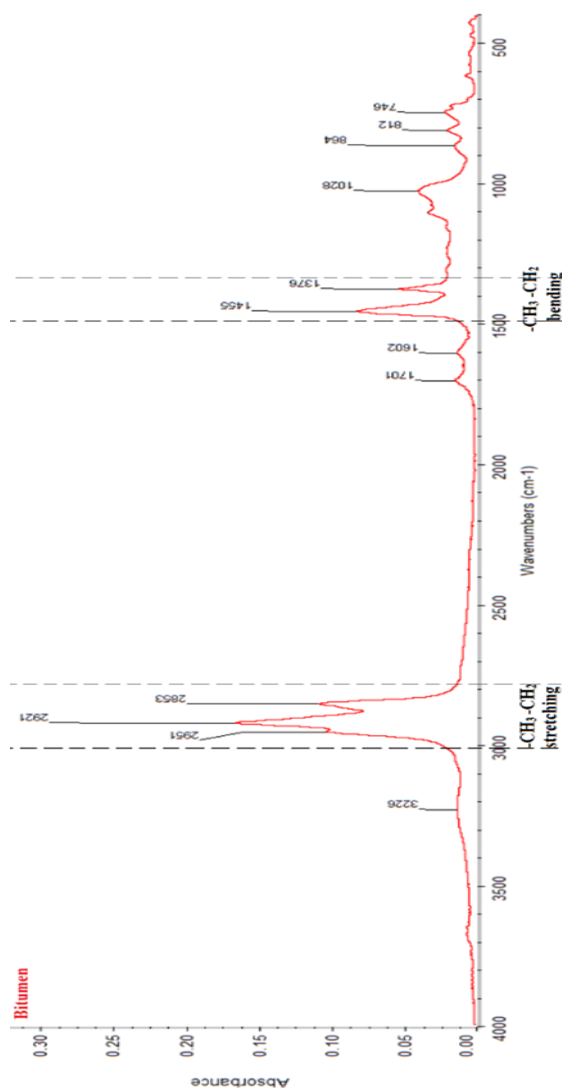
Fig. 5-1. ATR-FTIR spectrum of bitumen

In addition to the aliphatic carbons, the unsaturated carbons are also revealed by the spectrum, where a small band at 1602 cm^{-1} and a series of weak bands between 864 and 746 cm^{-1} are due to vibrations of carbon-carbon double bonds. Furthermore, the carbonyl moiety (C=O) and sulfoxide moiety (S=O) are also reflected in the spectrum by a small broad band at 1701 cm^{-1} and a band at 1028 cm^{-1}, respectively. However, the bands characteristic of C-H stretching vibrations of aromatic rings in the region between 3100 – 3000 cm^{-1} are not observed in the spectrum. This may be attributable to the relatively low absorptivity of these bands by comparison with aliphatic C-H stretching absorptions but may also indicate a low percentage of aromatic hydrocarbons in the bitumen as well as their polycyclic nature, resulting in a reduced number of C-H bonds per molecule by comparison with mono-aromatics.

The ATR-FTIR spectra of 3 tailing soil samples with low (0.70%), medium (12.70%), and high (25.70%) bitumen content are presented in Figure 5-2. The tailing soil spectrum contains the absorptions of bitumen (2768 – 2989 cm^{-1}) and clay (3578 – 3745 cm^{-1}), as well as the absorptions of sand and clay (below 1200 cm^{-1}). The broad band between 1300 and 1500 cm^{-1} may be the combination of the bitumen C-H bending vibration between 1330 and 1487 cm^{-1} and the Al-O bending vibration of soil minerals between 1347 and 1360 cm^{-1} (Saikia and Parthasarathy 2010).

Apart from the changes in the intensity of the bitumen band among the three samples, the intensity of the spectra in other regions shows slight variations, which might be caused by path length variation among the samples.
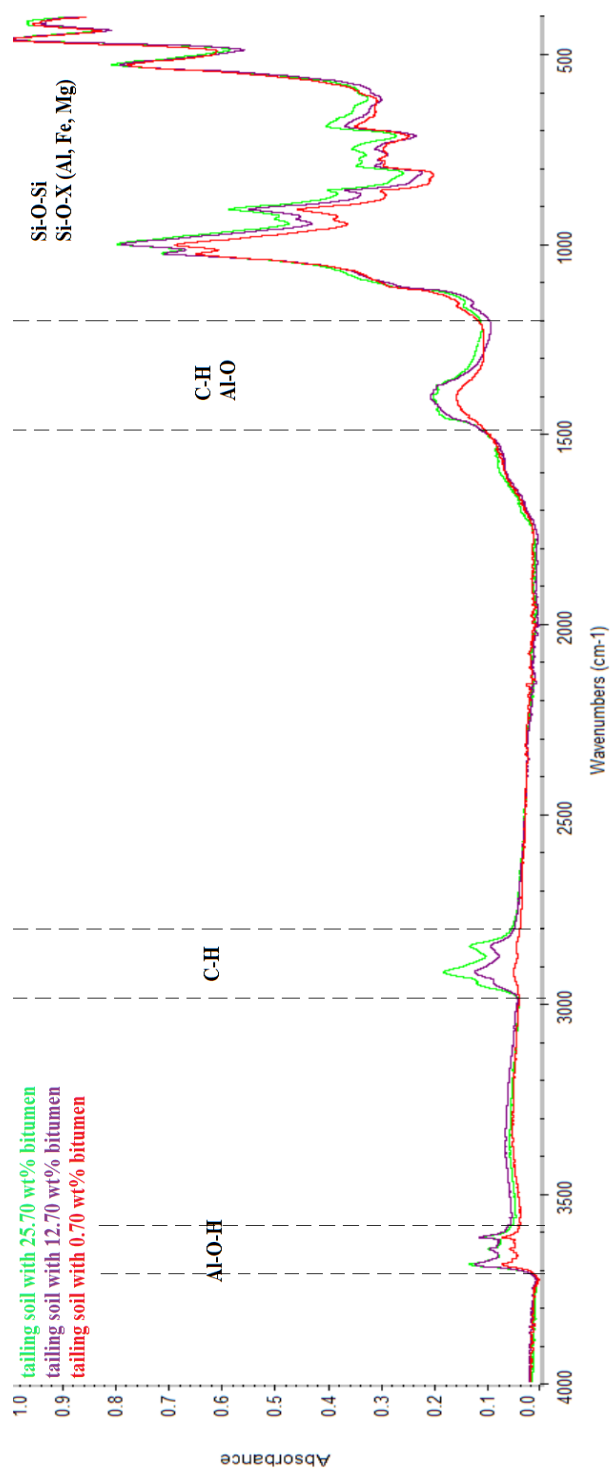
Fig. 5-2. ATR-FTIR spectra of 3 tailing soils with different bitumen content

5.3.1.2. DRIFT-NIR Spectral Characterization

The DRIFT-NIR spectrum of bitumen is presented in Figure 5-3. Since most of the useful information occurs in the combination and 1st overtone regions, only the spectral range between 9000 and 4000 cm^{-1} is presented.
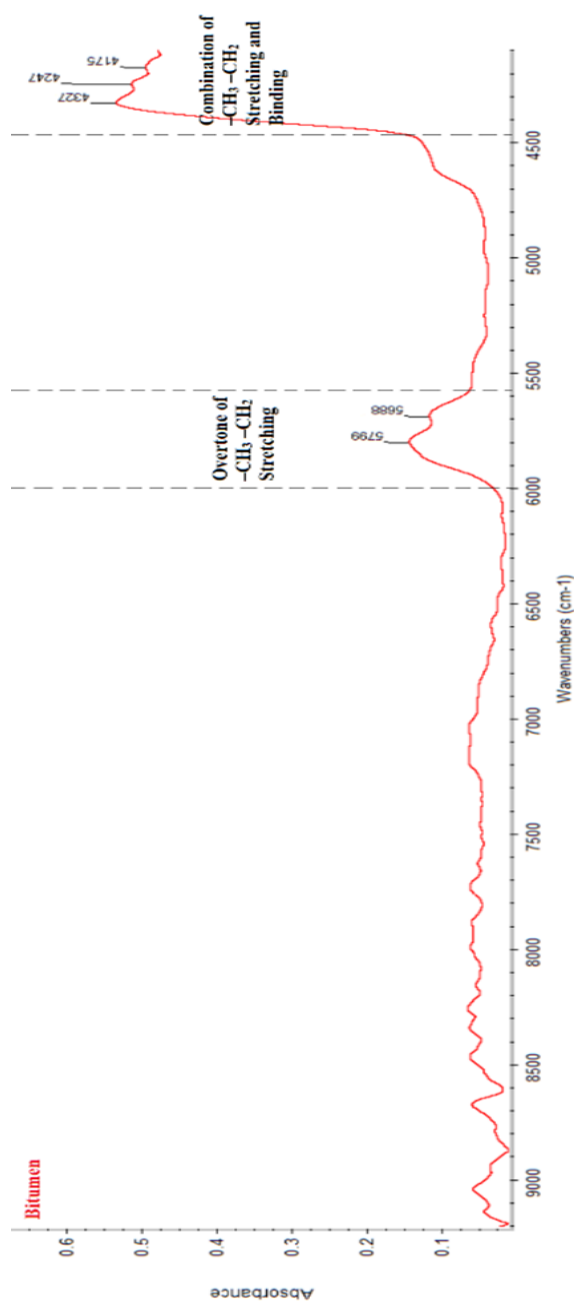
Fig. 5-3. DRIFT-NIR spectrum of bitumen

As seen in Figure 5-3, the NIR absorption of bitumen mainly occurs in the region between 6000 and 5600 cm^{-1} (1666 – 1785 nm) and the region between 4327 and 4175 cm^{-1} (2311 – 2395 nm). The absorption in the higher wavenumber region is caused by the overtone of methyl and methylene stretching vibrations, while the absorption in the lower wavenumber region is due to the combination of these groups' stretching and bending vibrations. Since most absorptions in the NIR region are caused by X-H (X = C, O, N) functional groups, only the C-H groups of bitumen are reflected in the NIR spectrum, making it less informative and less useful for bitumen characterization than the MIR spectrum.
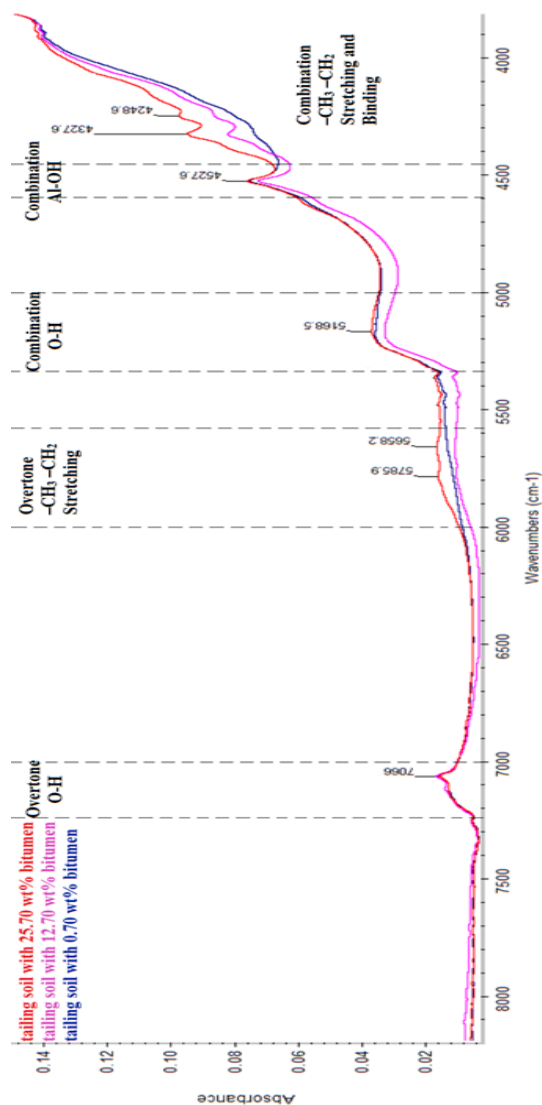
Fig. 5-4. DRIFT-NIR spectra of 3 tailing soils with different bitumen content

The DRIFT-NIR spectra of 3 tailing soils with low (0.70 wt%), medium (12.70 wt%), and high (25.70 wt%) bitumen contents are presented in Figure 5-4. Dried tailing soil is mostly composed of soil minerals, bitumen, and a small amount of intermolecular water, where the compounds containing X-H (X = C, O, N) may generate NIR absorption signals. In Figure 5-4, the spectra are divided into several regions, where the bands in the region between 7250 and 7000 cm^{-1} (1379 – 1429 nm) and the region between 5325 and 5000 cm^{-1} (1878 – 2000 nm) are due to the O-H bonds of water; a broad band in the region between 6000 and 5600 cm^{-1} (1666 – 1785 nm) and two small peaks between 4327 and 4175 cm^{-1} (2311 – 2395 nm) are due to the C-H bonds in bitumen; and a sharp band in the region between 4550 and 4475 cm^{-1} (2198 – 2235 nm) is due to the Al-OH bonds in clay minerals (Rivard, Lyder et al. 2010).

NIR absorption intensity is proportional to the constituent's concentration. However, due to the overlapping of some peaks, as well as the sloping baseline, it is difficult to correlate the peak intensity to the concentration of the constituent by using the original NIR spectrum. By further processing the spectrum, such as taking the 2nd derivative, the bands are better resolved and the sloping baseline can be eliminated (Fig. 5-5). After taking the 2nd derivative, the bands in the region between 4575 and 4200 cm^{-1} representing the clay mineral and bitumen constituents are well resolved. The intensity of three resolved bands between 4450 and 4200 cm^{-1} is proportional to the bitumen content in soil; therefore, the integrated area of these bands can be regressed against the bitumen content to obtain a calibration equation.
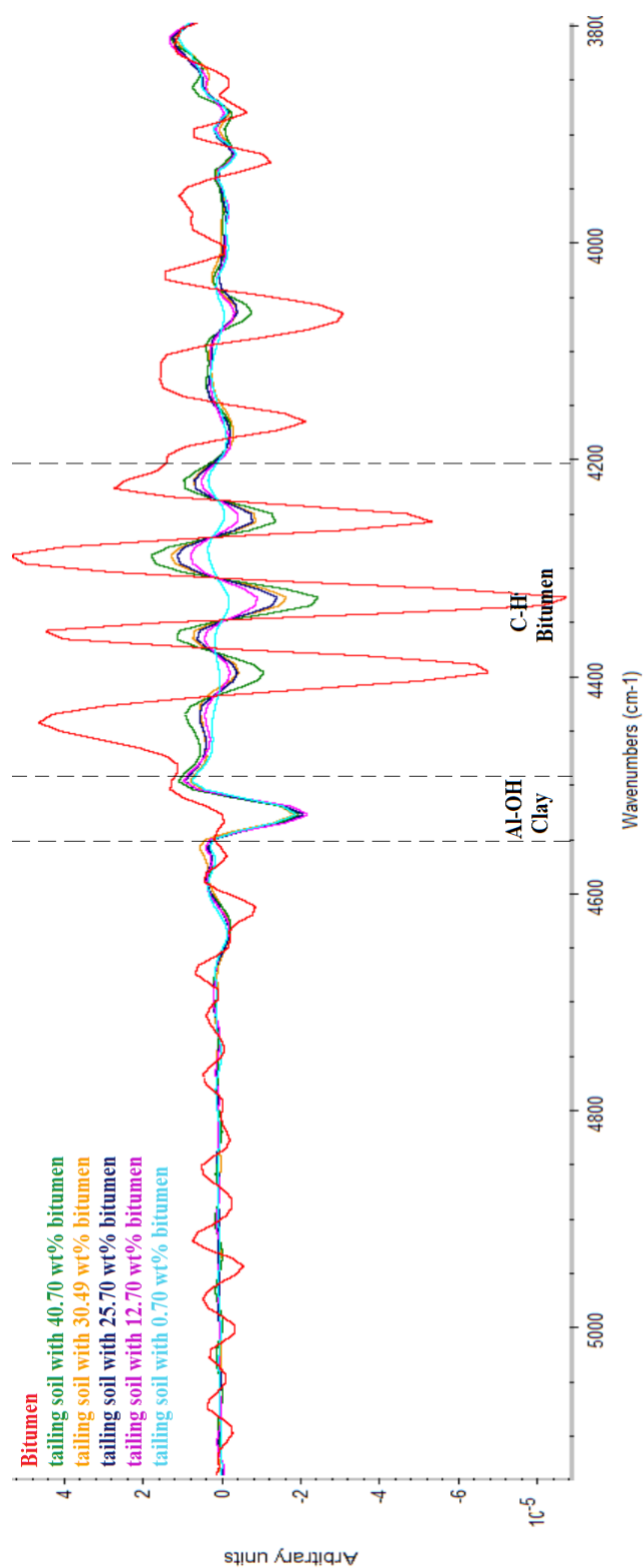
Fig. 5-5. Second derivative of DRIFT-NIR spectra of bitumen and tailing soils with different bitumen content

143

5.3.2. Bitumen Quantification in Tailing Soils

5.3.2.1. Calibration with Artificial Tailing Soils

5.3.2.1.1. Description of Samples

After washing of Athabasca tailing soils with 2-MeTHF, the clean tailing soil was obtained. Part of the soil was sent for determination of the soil texture by the hydrometer method. According to the United States Department of Agriculture (USDA) triangular diagram of soil texture classification, the clean tailing soil is classified as loam soil. Another part of the soil was sent for determination of the bitumen residue in the clean soil by the total combustion method. A bitumen concentration of 0.70 wt% was determined and this value was incorporated into the calculation of the concentrations of the spiked samples as background bitumen content. The range of the bitumen content in the artificial tailing soil samples was between 0.70 wt% and 40.70 wt%, with an average of 19.64 wt% (Table 5-1).

Table 5-1. Statistics of artificial tailing soil samples

Background bitumen wt%	Bitumen range in soil wt%	Average bitumen wt%	Sand wt%	Silt wt%	Clay wt%	Soil type
0.70	0.70 – 40.70	19.64	42.5	41.2	16.3	Loam

5.3.2.1.2. Path Length Correction

The ATR-FTIR spectra acquired in triplicate from two soil samples with high and low bitumen content are presented in Fig. 5-6. Among the triplicates, the intensity of both the bitumen and clay bands varies. This phenomenon can be explained by two reasons. Firstly, the composition of different portions of the sample may be different, due to the heterogeneity of tailing soil. In addition, the optical variation caused by differences in the optical path length is another possible cause for the intensity variation.

To eliminate the optical variation, the bitumen band area was ratioed against the clay band area, as the effect of the optical variation can be considered constant over a limited wavenumber range. After the correction, the coefficient of variation (CV) of the bitumen band among triplicate spectra decreased from 9.00% to 2.91% for the soil with the higher bitumen content and from 5.13% to 3.71% for the soil with the lower bitumen content (Table 5-2). The corrected bitumen spectral intensity instead of the original bitumen band intensity was used for the calibration.
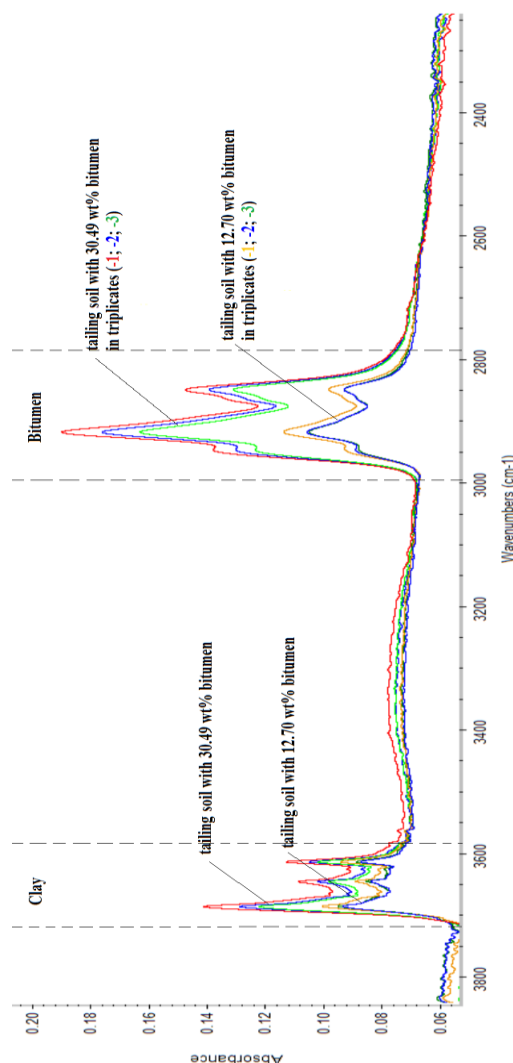
Fig. 5-6. Triplicate ATR-FTIR spectra of two tailing soils with high (30.49 wt%) and low (12.70 wt%) bitumen content.

Table 5-2. Variance of integrated area of bitumen band among triplicates

Sample	Replicate	Bitumen area	CV (%)	Bitumen/clay band area	CV (%)
Tailing soil with 30.49 wt% bitumen	1	8.28		2.52	
	2	9.29	9.00	2.625	2.91
	3	10.33		2.44	
Tailing soil with 12.70 wt% bitumen	1	1.96		1.01	
	2	1.96	5.13	0.93	3.71
	3	1.75		0.94	

5.3.2.1.3. ATR-FTIR Beer's Law Calibration

The calibration information and performance of the ATR-FTIR Beer's law calibration are presented in Table 5-3 and Figure 5-7. The calibration built using the ATR-FTIR spectra of the artificial tailing soils and a simple Beer's law regression shows excellent linearity between the actual and predicted bitumen content, with a r_c^2 of 0.98. The model performs with high accuracy with a 2.12 wt% RMSEC in the range of bitumen content between 0.70 and 40.70 wt%.

Table 5-3. Statistical information of ATR-FTIR Beer's law calibration for bitumen in artificial tailing soils

Bitumen range (wt%)	Calibration region (cm^{-1})	$n_{cali}|n_{vali}$ [a]	r_c^2 [b]	RMSEC (%)	RMSECV (%)
0.70 – 40.70	3000 - 2795	28|6	0.98	2.12	NA

[a] n_{cali}: number of calibration samples; n_{vali}: number of validation sample

[b] r_c^2: correlation coefficient of calibration;

y = 0.245x
Corr. Coeff. = 0.98
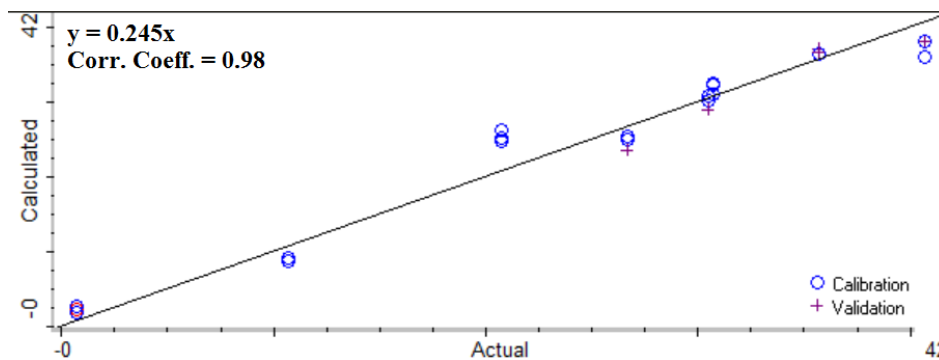
Fig. 5-7. ATR-FTIR Beer's law calibration plot for bitumen in artificial tailing soils

5.3.2.1.4. ATR-FTIR PLSR Calibration

The calibration information and performance of the PLSR calibration are presented in Table 5-4 and Figure 5-8. The calibration built using the ATR-FTIR spectra of the artificial tailing soils and multivariate PLS regression shows excellent linearity between the actual and predicted bitumen content, with a r_c^2 of 0.99. The model performs with high accuracy with a 1.76 wt% RMSEC and a 2.34 wt% RMSECV in the range of bitumen content between 0.70 and 40.70 wt%.

Table 5-4. Statistical information of ATR-FTIR PLSR calibration for bitumen in artificial tailing soils

Bitumen range (wt%)	Calibration region (cm^{-1})	$n_{cali}|n_{vali}$ [a]	$r_c^2|r_{cv-1}^2$ [b]	RMSEC (%)	RMSECV (%)	LVs
0.70 – 40.70	3745 - 2795	26|6	0.99|0.98	1.76	2.34	1

[a] n_{cali}: number of calibration samples; n_{vali}: number of validation samples.

[b] r_c^2: correlation coefficient of calibration; r_{cv-1}^2: correlation coefficient of leave-one-out cross-validation.

147

The graph of the predicted residual error sum of squares (PRESS) is shown in Fig. 5-9, showing the RMSECV as a function of the number of latent variables (LVs) included in the calibration model. In this calibration, the RMSECV value reaches a minimum with the use of the 1st LV. This means that the information contained in the 1st LV is sufficient to describe most of the variation of bitumen in the soil samples, making the calibration successful. The incorporation of other LVs into the model will not decrease the RMSECV and, consequently, will not improve the quantification performance.
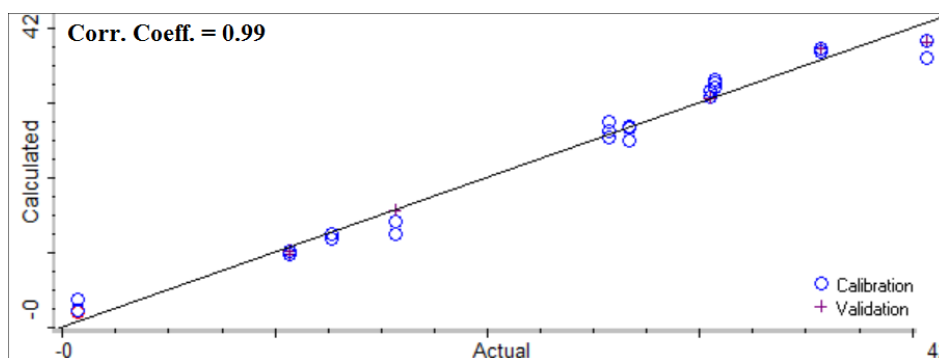
Fig. 5-8. ATR-FTIR PLSR calibration plot for bitumen in artificial tailing soils
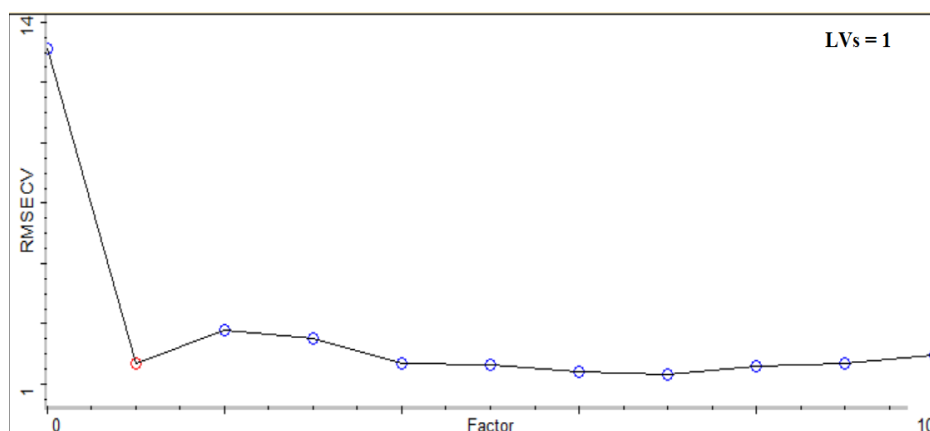
Fig. 5- 9. PRESS plot of ATR-FTIR PLSR calibration for bitumen in artificial tailing soils

5.3.2.1.5. DRIFT-NIR Beer's Law Calibration

The calibration information and performance of the DRIFT-NIR Beer's law calibration are presented in Table 5-5 and Figure 5-10. The calibration built using 2nd derivative DRIFT-NIR spectra of the artificial tailing soils and simple Beer's law regression shows excellent linearity between the actual and predicted bitumen content, with a r_c^2 of 0.99. The model performs with high accuracy with a 1.23 wt% RMSEC in the range of bitumen content between 0.70 and 40.70 wt%.

Table 5-5. Statistical information of DRIFT-NIR Beer's law calibration for bitumen in artificial tailing soils

Bitumen range (wt%)	Calibration region (cm^{-1})	$n_{cali}\|n_{vali}$ [a]	r_c^2 [b]	RMSEC (%)	RMSECV (%)
0.70 – 40.70	4350 – 4312	31|6	0.99	1.23	NA

[a] n_{cali}: number of calibration samples; n_{vali}: number of validation samples.

[b] r_c^2: correlation coefficient of calibration

149
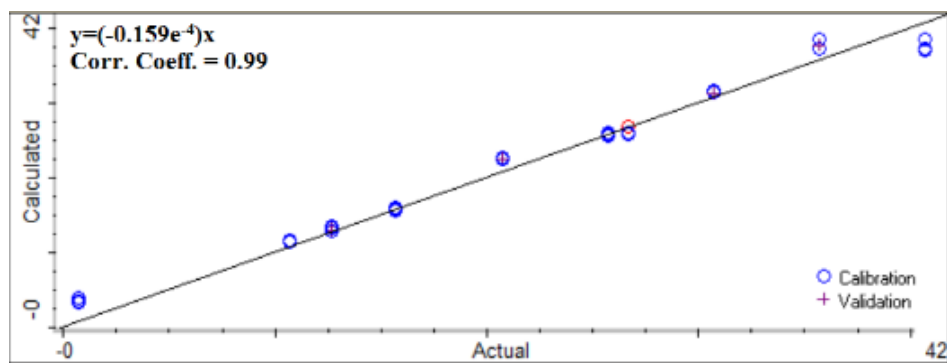
Fig. 5-10. DRIFT-NIR Beer's law calibration plot for bitumen in
artificial tailing soils

5.3.2.1.6. DRIFT-NIR PLSR Calibration

The calibration information and performance of the DRIFT-NIR PLSR calibration are presented
in Table 5-6 and Figure 5-11. The calibration built using 2nd derivative DRIFT-NIR spectra of
artificial tailing soils and multivariate PLS regression shows excellent linearity between the
actual and predicted bitumen content, with a r_c^2 of 0.99. The model performs with high accuracy
with a 0.77 wt% RMSEC and a 2.51 wt% RMSECV in the range of bitumen content between
0.70 and 40.70 wt%.

Table 5-6. Statistical information of DRIFT-NIR PLSR calibration for bitumen in artificial
tailing soils

Bitumen range (wt%)	Calibration region (cm⁻¹)	n_{cali}|n_{vali} [a]	r_c^2|r_{cv-1}^2 [b]	RMSEC (%)	RMSECV (%)	LVs
0.70 – 40.70	4698 - 3996	31|5	0.99|0.98	0.78	2.51	4

[a] n_{cali}: number of calibration samples; n_{vali}: number of validation samples.

[b] r_c^2: correlation coefficient of calibration; r_{cv-1}^2: correlation coefficient of leave-one-out cross-validation
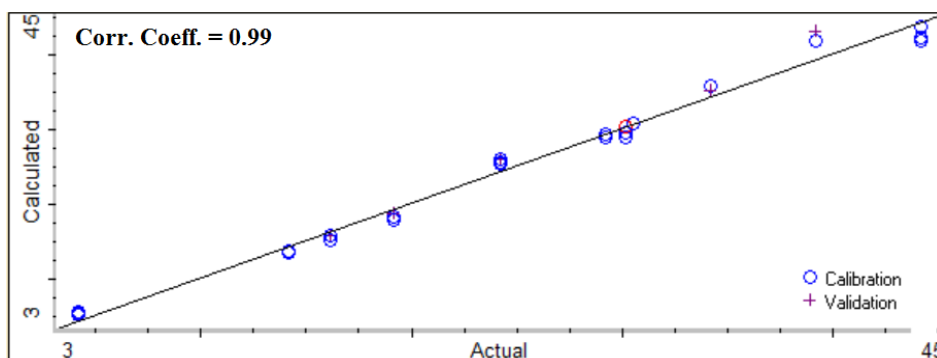
The PRESS plot for this calibration is shown in Fig. 5-12. In this calibration, the RMSECV

Fig. 5- 11. DRIFT-NIR PLSR calibration plot for bitumen in artificial tailing soils

value reaches a minimum with the use of the first 4 LVs, where the RMSECV drops most sharply with the use of the 1ˢᵗ LV. The 1ˢᵗ LV carries the most useful information required by the bitumen calibration model. The other 3 LVs also contain extra information which benefits the model performance. However, their contribution is not considered significant.
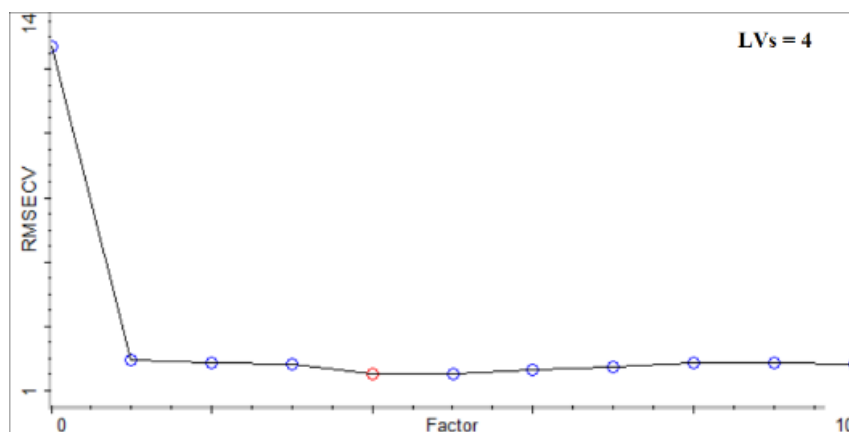
Fig. 5-12. PRESS plot of DRIFT-NIR calibration for bitumen in artificial tailing soils

151

5.3.2.2. Calibration with Natural Athabasca Tailing Soils

5.3.2.2.1. Description of Samples

The statistical information about the 32 natural Athabasca tailing soil samples employed in this study is listed in Table 5-7. Bitumen content was measured as total carbon and ranges between 9.70 and 26.59 wt%. The distribution of the population is slightly right-skewed, with a -0.58 skewness, indicating the distribution is concentrated on the left side, corresponding to the high values of total carbon content (Fig. 5-13).

Table 5-7. Statistical information of natural Athabasca tailing soil samples ($n = 32$)

Constituent	Range (wt%)	Median (wt%)	Skewness
Total carbon	9.70 – 26.59	19.98	-0.58
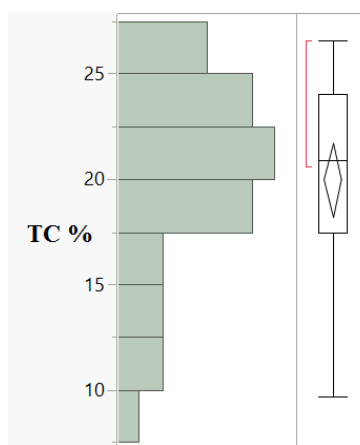
Fig. 5-13. Distribution of natural Athabasca tailing soil samples according to total carbon (TC) content ($n = 32$)

5.3.2.2.2. ATR-FTIR PLSR Calibration

The calibration information and performance of the ATR-FTIR PLSR calibration are presented in Table 5-8 and Fig. 5-14. The calibration built using the path length-corrected ATR-FTIR spectral information and multivariate PLS regression shows excellent linearity between the actual and predicted total carbon content, with a r_c^2 of 0.90. The model performs with high accuracy with a 1.55 wt% RMSEC and a 1.87 wt% RMSECV in the range of bitumen content between 9.70 and 26.59 wt%. The RPD value is another model performance indicator and is not influenced by the sample population. A 2.55 RPD is obtained from the model, indicating the prediction performance of the model is excellent.

Table 5-8. Statistical information of ATR-FTIR PLSR calibration for bitumen in natural Athabasca tailing soils

Bitumen range (wt%)	Calibration region (cm⁻¹)	$n_{cali}|n_{vali}$ [a]	$r_c^2|r_{cv-1}^2$ [b]	RMSEC (wt%)	RMSECV (wt%)	LVs	RPD [c]
9.70 – 26.59	3748 – 2714 1885 – 1208	70|10	0.90|0.86	1.55	1.87	4	2.55

[a] n_{cali}: number of calibration samples; n_{vali}: number of validation samples.

[b] r_c^2: correlation coefficient of calibration; r_{cv-1}^2: correlation coefficient of cross-validation.

[c] RPD: ratio of performance to deviation = SD/RMSECV
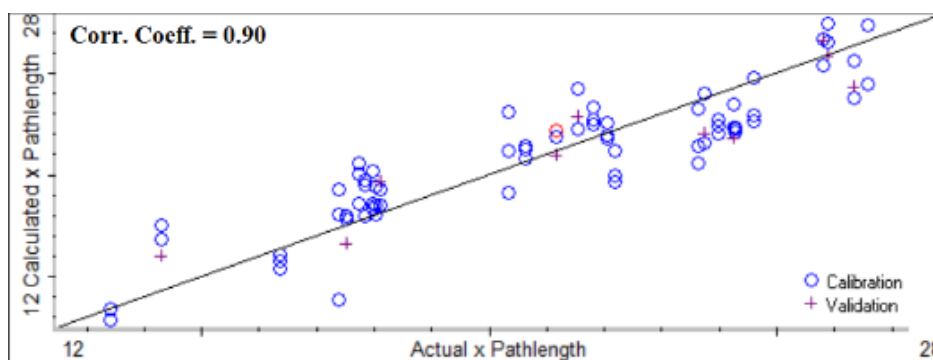
Fig. 5- 14. ATR-FTIR PLSR calibration plot for bitumen in natural
Athabasca tailing soils

The PRESS plot for this calibration is shown in Figure 5-15. In this calibration, the RMSECV value reaches a minimum with the use of the first 4 LVs, where the RMSECV drops most with the 1st LV, followed by the 2nd LV. These 2 LVs carry the most useful information required by the bitumen calibration model. The remaining two LVs contain extra information that benefits the model performance. However, this contribution is not considered significant.
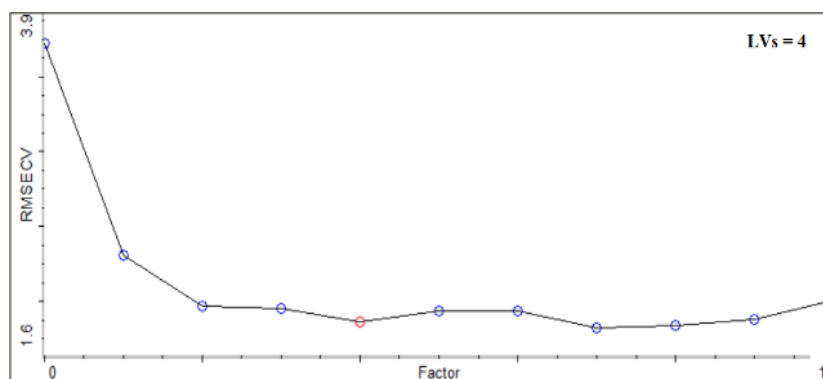
Fig. 5- 15. PRESS plot of ATR-FTIR PLSR calibration for bitumen
in natural Athabasca tailing soils

5.3.2.3. Validation of Bitumen Calibrations

The prediction performances of the three ATR-FTIR calibrations described above were evaluated with an independent validation set. The results are presented in Table 5-9 in terms of the prediction error, the prediction accuracy and the prediction precision. The first two parameters measure the closeness of the prediction to the true value, while the third parameter evaluates the repeatability of the predictions. The smaller the error, as well as the closer the accuracy is to 1.00, the more accurate the calibration is. In addition, the smaller the precision value, the more reproducible and reliable the calibration is. A totally independent validation set is used to avoid the calibration's "memorizing effect", which may be manifested when the validation samples are similar to the calibration samples. In addition, to reduce the uncertainty of the prediction and to reduce the risk of producing meaningless results, only the validation samples containing bitumen content within the range of the calibration set are predicted.

For the validation of the calibrations developed with a calibration set consisting of artificial tailing soils, the natural Athabasca tailing soils were employed as the validation set, and vice versa. The range of bitumen content in these two sets of soils is similar, 13.42 - 26.34 wt% as compared to 15.70 - 25.70 wt%. Regarding the accuracy of the models, they all provide a similar percentage of error, ranging between 9.89 and 12.99 %, and similar accuracy, ranging between 0.98 and 1.08. These results indicate the high accuracy of these three models when predicting a completely independent set of tailing soil samples. Furthermore, considering the repeatability of the models, the models built using artificial tailing soils show higher precision, where the predictions among three replicates vary within ±0.51 to ±0.69 wt% difference. However, in the case of the model built using natural Athabasca tailing soils, the variation of the predictions among triplicates doubles, where the predictions vary within ±1.30 wt%.

Table 5-9. Model prediction performances using an independent validation set

Calibration set	Independent validation set	Prediction range (wt%)	Calibration method	Error [d] ± SD (wt%)	Accuracy [d] ± SD	Precision [e] ± SD (wt%)
Artificial [a] (n=36)	Natural [b] (n=48)	13.42 – 26.34	Beer's law	3.89 ± 3.30	1.04 ± 0.12	0.69 ± 0.34
			PLSR	4.55 ± 2.50	0.98 ± 0.14	0.51 ± 0.28
Natural [b] (n=70)	Artificial [a] (n=21)	15.70 – 25.70	PLSR	2.85 ± 1.40	1.08 ± 0.10	1.30 ± 0.81

[a] Artificial: artificial tailing soils; [b] Natural: natural Athabasca tailing soils

[c] $Error \% = \frac{|predicted-actual|}{actual} \times 100\%$

[d] $Accuracy = \frac{predicted}{actual}$

[e] $Precision = \frac{\sum_{i=3}|predict(i)-mean|}{3}$

5.3.3. Characterization of Tailing Soils Remediated by the Re-usable Hydrocarbon Sorbent (RHS) Technology

5.3.3.1. ATR-FTIR Analysis of RHS Beads before and after Tailing Soils Remediation Process

The RHS technology for tailing soil remediation developed by Gradek Energy Inc. (http://www.gradekenergy.com/) is based on the use of beads that have the ability to retain hydrocarbons and repel water. The RHS beads have an oval form and are light blue in color when clean. After the tailing soil remediation process, the bead surface is coated with bitumen and the color turns black (Fig. 5-16). The ATR-FTIR spectra of RHS beads before and after the remediation process are presented in Figure 5-17. In the spectrum of the coated RHS beads, characteristic bands of bitumen corresponding to methyl and methylene stretching (2768 – 2989 cm^{-1}) and bending (1350 – 1487 cm^{-1}) vibrations are observed. In addition, clay bands are also observed in the region of 3578 – 3745 cm^{-1} and the region below 1150 cm^{-1}. The clean beads also exhibit a C-H signal in the region between 2768 and 2989 cm^{-1}. This background C-H signal does not interfere with the ATR-FTIR analysis of the bitumen coating, since the depth of penetration of the evanescent wave generated at the surface of the ATR crystal is only 0.5 to 2 µm (depending on the wavelength) and thus does not extend into the interior of the bead. This is

proved by the absence of the characteristic bands of the clean beads in the region between 1760 and 1150 cm^{-1} from the coated bead spectrum.

Fig. 5-16. Clean RHS beads (left) and RHS beads after remediation of tailing soils (right)
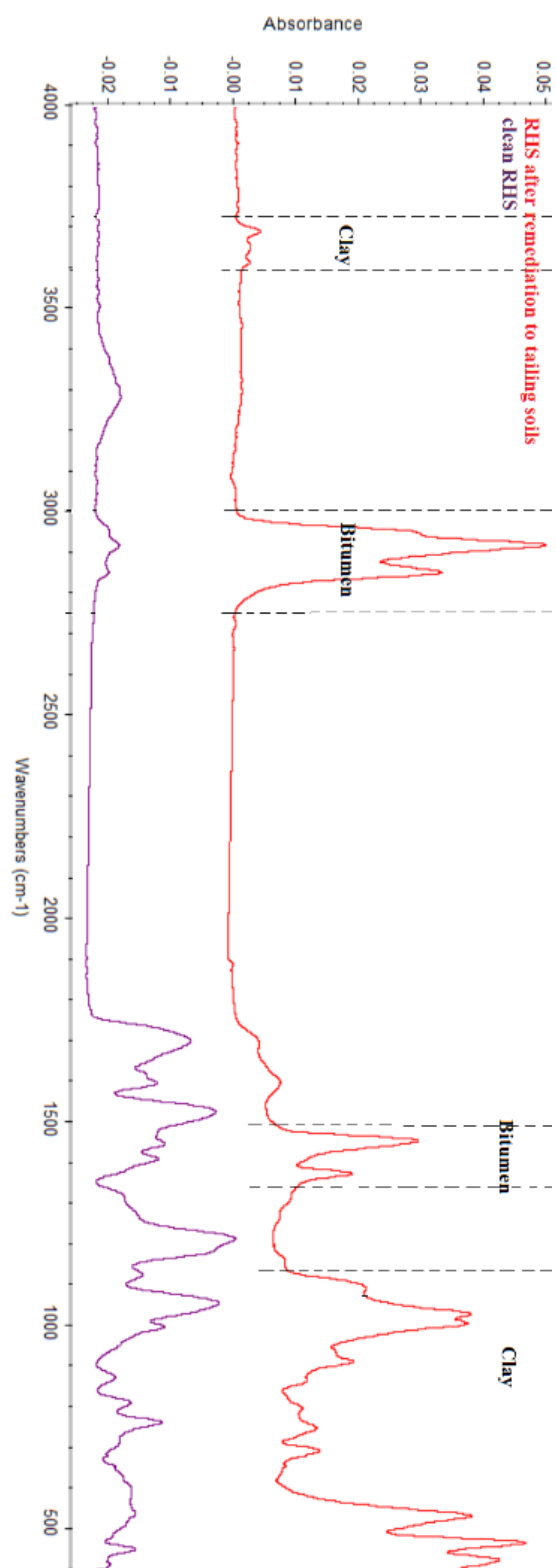
Fig. 5- 17. ATR-FTIR spectra of RHS beads before and after remediation of tailing soils

5.3.3.2. ATR-FTIR Analysis of Natural Athabasca Tailing Soils Remediated by RHS Beads

Since bitumen has distinct and characteristic MIR absorption and the absorption intensity is linearly related to the bitumen content in soil, ATR-FTIR spectra can be analyzed to quickly determine the drop in bitumen content resulting from the RHS remediation process and therefore quickly assess the performance of the process. Spectra of tailing soils before and after RHS remediation are shown in Figure 5-18. The unremediated and remediated soils have a similar spectral profile but with differences in relative intensity. The most pronounced difference is in the region between 2768 and 2989 cm^{-1} (Fig. 5-18), where the intensity of the bitumen bands drops to half after one pass of the remediation process.

In order to eliminate the effect of path length variation, the bitumen band area ($area_{2768\text{-}2989}$) and the clay band area ($area_{3578-3745}$) were normalized to the integrated area under the full spectrum ($\sum area$). The corresponding indices, the clay index ($I_{CLAY} = area_{3578-3745}/\sum area$) and the bitumen index ($I_{BITUMEN} = area_{2768-2989}/\sum area$), were used to evaluate the performance of RHS remediation of tailing soils (Fig. 5-19). The bitumen index value drops to half after one pass of the remediation process. However, after the 2nd pass, the value does not continue to decrease but slightly increases. In general, after 1 or 2 passes of the remediation process, the bitumen index value decreases 50% compared to its value prior to remediation. The clay index value remains consistent during the remediation. Although the value increases slightly after one pass of the remediation process, this increase is not considered significant and is attributed to the sample heterogeneity.
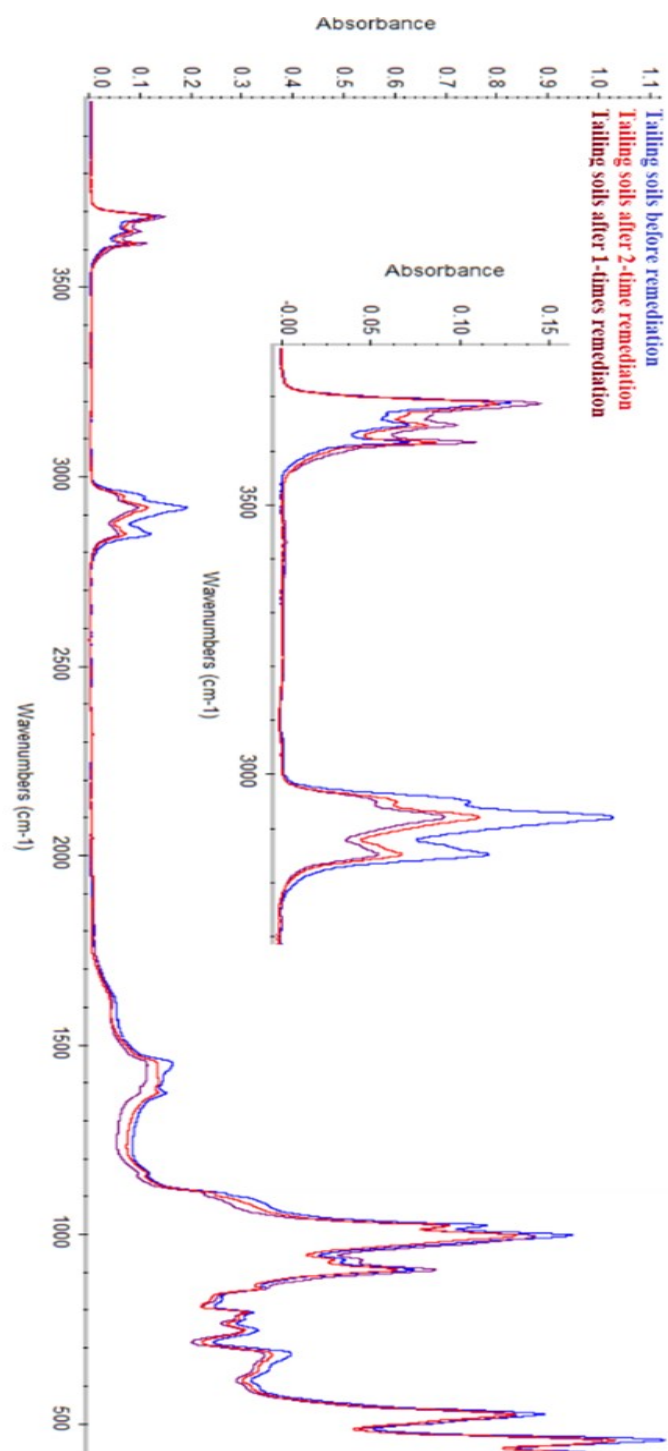
Fig. 5-18. ATR-FTIR spectra of tailing soils before and after 1 and 2 passes of the RHS remediation process. The inset is a magnification of the 4000 – 2700 cm^{-1} spectral region
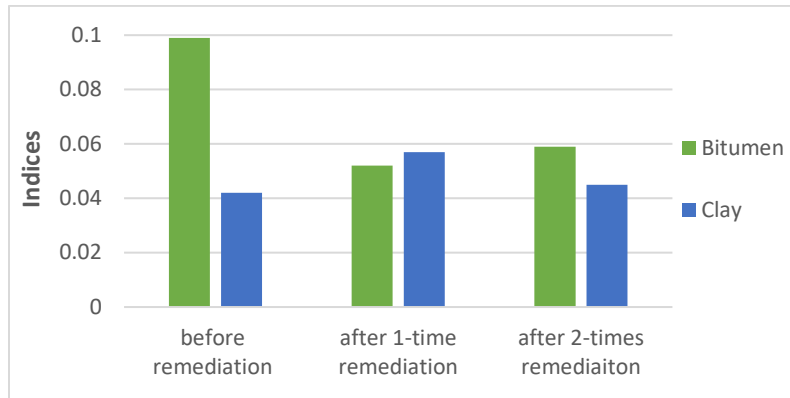
Fig. 5-19. Bitumen and clay indices before and after 1 and 2 passes of the RHS remediation process

5.3.3.3. Remediated Tailing Soils Cluster Analysis (CA)

The cluster analysis results are shown in constellation graphs, where the longer the stem, the less similar the spectra. There is no clear clustering reflecting the RHS remediation process; instead, the green spots representing "After remediation" are intermingled with the orange spots, which represent "Before remediation" samples (Fig. 5-20). This indicates that the chemical and physical changes caused by the remediation process are not reflected in the spectra, or that the spectral differences are not large enough to be distinguished in cluster analysis.
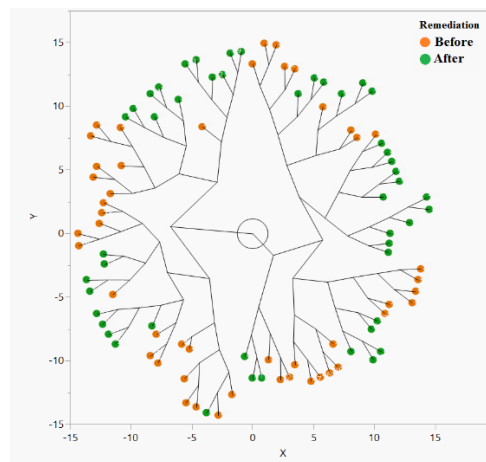
Fig. 5-20. Constellation graph obtained by cluster analysis of 96 spectra of tailing soils labeled based on RHS remediation

Cluster analysis successfully clusters samples based on bitumen content, as shown in Figure 5-21. Most of the red and blue spots representing soils with high and low bitumen content are nicely separated into two groups and are located on opposite sides of the constellation graph (Fig. 5-21). This indicates that the bitumen content of the soils is reflected in their ATR-FTIR spectra and can be distinguished in cluster analysis.
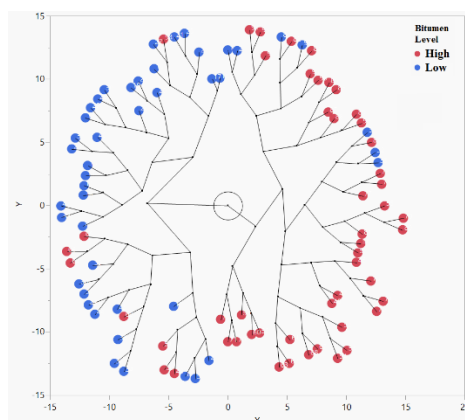
Fig. 5-21. Constellation graph obtained by cluster analysis of 96 spectra of tailing soils labeled based on bitumen content

However, a few samples are grouped in the wrong category and are considered as outliers. The ATR-FTIR spectra of the outliers and the sample with median bitumen content are presented in Figure 5-22. The outliers, which are labeled as "Low" bitumen content but are grouped into the "High" bitumen content category, indeed have higher bitumen absorbance than the median; meanwhile, those outliers labeled as "High" bitumen content but grouped into the "Low" bitumen content category have weaker bitumen absorbance than the median. This indicates that ATR-FTIR spectroscopy is capable of capturing the information truly reflecting the bitumen level. These outlier samples may be associated with the issue of representative sampling, which is particularly significant when samples are naturally heterogeneous, such as tailing soils. The portion of the sample sent for chemical analysis, which was used to label the sample as being of

"High" or "Low" bitumen content, is different from the portion of the sample employed for spectroscopic analysis, which is used in the cluster analysis. However, this representative sampling problem is not prevalent in our study, since only 7 out of 96 spectra are incorrectly grouped.
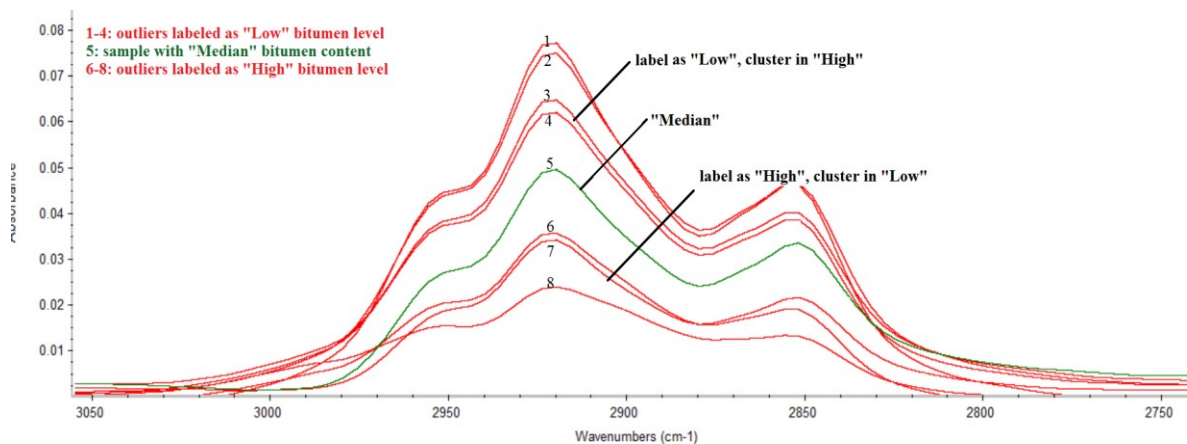
Fig. 5- 22. ATR-FTIR spectra in the bitumen absorption region of samples with median bitumen content and outliers labeled as "low" and "high" bitumen level

5.3.3.4. PCA of ATR-FTIR Spectra of Remediated Tailing Soils

The cluster analysis described above is mainly based on spectral similarity. In order to study further the remediated tailing soil classification by ATR-FTIR spectroscopy, PCA was used to extract the most significant information from the data matrix. By studying this extracted information, we can understand what the key information is for determining the remediated soil classification.

5.3.3.4.1. PCA Loadings of RHS Remediated Tailing Soil

The complete data matrix including all the spectra (*n*=96) and the wavenumbers in the selected region of 4000 – 2500 cm^{-1} was modeled by PCA. The first two PCs accounted for 95.6% (PC1) and 2.0% (PC2) of the total variance of the data, cumulatively accounting for 97.6% of the variance, and therefore only the first two PCs are considered here.

Loadings are the correlations between the components (PCs) and the original variables (wavenumbers). In addition, a loadings plot for a given PC indicates how much of the variations in a variable (wavenumber) is explained by that PC. The higher the loadings value, the more variation is explained. Therefore, by examining the loadings plot, it is clear at which wavenumbers the most variations explained by that PC occur. The loadings plot for PC1 is presented in Figure 5-23-a and resembles an inverse ATR-FTIR spectrum of tailing soils. In PC1, the loadings values are high in the regions between 2768 and 2989 cm^{-1} and between 3578 and 3745 cm^{-1}, which are the absorption regions specific to bitumen and clay, respectively. Therefore, PC1 mainly carries the variations of soil minerals and bitumen. Figure 5-23-b is the loadings plot for PC2, which is also similar to the ATR-FTIR spectrum of tailing soils. In the loadings of PC2, a similar profile to the loadings of PC1 is observed, where two peaks in the clay and bitumen absorption regions are found. However, compared to the intensity of the PC1 loadings, the intensity of PC2 loadings is much weaker. This illustrates that the variations explained by PC2 are small, which is true since only 2.0% of the total variance is extracted by this PC. In general, the most variations among the 96 spectra representing the raw tailing soils and RHS remediated tailing soils lie in the bitumen and clay absorptions, which are mainly captured in PC1.
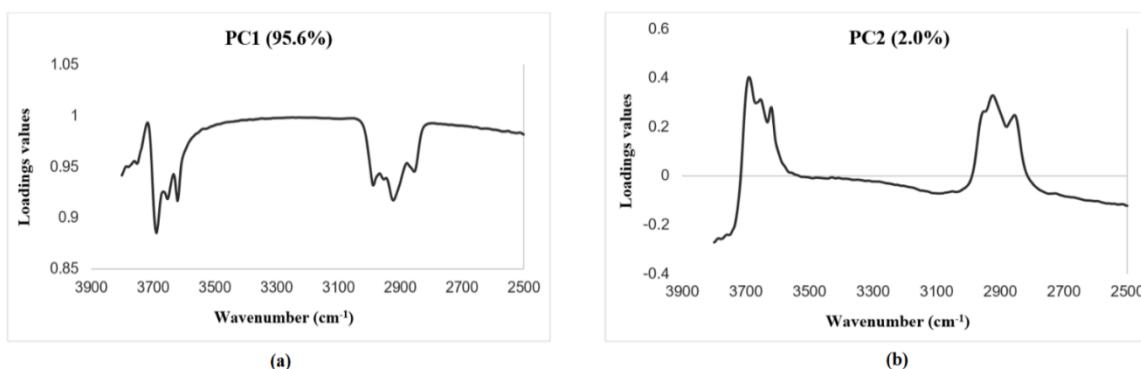
Fig. 5-23. PCA loadings plots: (a) PC1; (b) PC2

5.3.3.4.2. PC Scores of RHS Remediated Tailing Soils

By plotting the PC1 and PC2 scores of each spectrum, the relationship among the spectra and the PCs is revealed. In order to examine the relationship among the properties of the tailing soils and PC1 and PC2, the 96 spectra are labeled as "Before" or "After" RHS remediation and as "High" or "Low" bitumen content. Each category is assigned a specific color and symbol. By examining the distribution of the colored symbols in the scores plot, the relationship among the properties and PCs is shown.

Similar to the result of cluster analysis, PCA does not produce any separation between unremediated and remediated tailing soils (Fig. 5-24-a). Most of the points are centered in the scores plot, and neither PC1 nor PC2 separates the "Before" spectra from the "After" spectra. This indicates that the most significant spectral variations caused by the chemical or physical differences among the samples are not related to the remediation process.

However, in the case of the property of bitumen content, there is a clear separation of the two classes by PCA (Fig. 5-24-b). The colored points are nicely separated by PC1, where the blue spots representing "Low" bitumen content are located on the negative side of PC1, while the red spots representing "High" bitumen content are grouped on the positive side of PC1. However, when looking at the PC2 dimension, all the points are intermingled and located in the center of PC2. This indicates that the information on bitumen content is overwhelmingly contained in

165

PC1, which is proved by the loadings of PC1, where the most spectral information extracted into PC1 is assigned to bitumen.
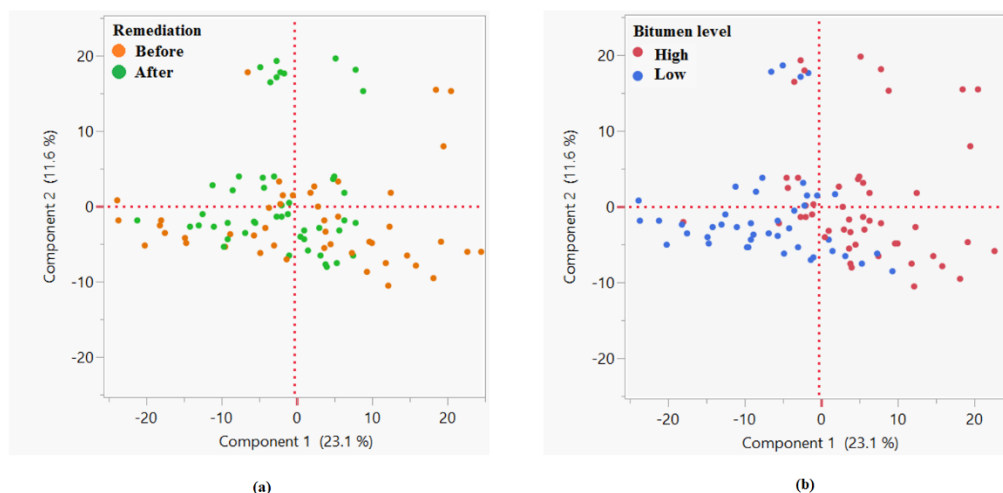
Fig. 5-25. Examination of clustering of spectra on PC scores plots based on two properties: (a) before and after RHS remediation; (b) bitumen content

5.4. Discussion

5.4.1. Performance of Bitumen Quantification Models

Bitumen quantification in both artificial tailing soils and natural Athabasca tailing soils using either ATR-FTIR or DRIFT-NIR spectroscopy coupled with simple linear regression (Beer's law) or multivariate regression (PLS) was successfully achieved, with low RMSE values being obtained for all the models (Table 5-10). The performances of our models are comparable to those published in the literature; for example, Forrester *et al*. (Forrester, Janik et al. 2010) reported a r_{cali}^2 of 0.81 and a 4.5 wt% RMSECV for their MIR PLS model based on natural petroleum-contaminated soil with bitumen content ranging between 0 and 60 wt%. They also reported that a similar result was obtained using NIR spectroscopy but with a higher RMSECV (6.3 wt%).

166

Table 5-10. Comparison of bitumen calibrations based on MIR or NIR spectra with Beer's law or PLS

Samples	Bitumen range (wt%)	IR range	Calibration method	Region(s) (cm^{-1})	$r_{cali}^2|r_{vali}^2$	RMSEC (wt%)	RMSECV (wt%)
Artificial tailing soils	0.70 – 40.70	MIR	Beer's law	3000 – 2795	0.98|0.97	2.12	NA
			PLSR	3745 – 2795	0.99|0.98	1.76	2.34
		NIR	Beer's law	4350 – 4312	0.99|0.99	1.23	NA
			PLSR	4698 – 3996	0.99|0.98	0.78	2.51
Natural Athabasca tailing soils	9.70 – 26.59	MIR	PLSR	3745 – 2795 1885 – 1208	0.90|0.86	1.55	1.87

Both simple linear regression (Beer's law) and PLSR yielded accurate calibrations for bitumen in tailing soils, with the PLSR models performing better than the Beer's law calibrations, in terms of higher r^2 and lower RMSEC (Table 5-10). In Beer's law regression, a standard curve is generated to correlate the absorbance of a single characteristic band to concentration (Smith 2011), (Qiu, Song et al. 2013), while a multivariate method such as PLS regression extracts much more spectral information from complex spectra to build up a calibration model for the prediction of concentration or other physicochemical properties (Chu 2011). In the tailing soils studied in this work, bitumen intermingles with clay minerals to form a complex mixture. Therefore, the inclusion of the spectral signal of clay minerals (3745 – 3578 cm^{-1}) in the PLS regression provides additional information that improves the prediction accuracy of the model.

Comparison among the four calibrations based on artificial tailing soils in terms of accuracy led to the selection of MIR spectroscopy coupled with PLSR as the best suited method to establish a calibration with natural Athabasca tailing soils. The performance of the latter model is acceptable and comparable to that based on artificial tailing soils. The slightly lower accuracy of the natural

Athabasca tailing soils model is probably due to the inherent heterogeneity of the natural soils in terms of bitumen chemistry and distribution, as well as the bitumen-soil interactions (Schwartz, Ben-Dor et al. 2012). This inherent heterogeneity reduces the modeling accuracy; relative to the models based on the artificial tailing soils, which were all prepared by spiking "cleaned" reference soils with bitumen from the same source. In addition, the interactions between bitumen and soil in the artificial tailing soils should be identical, since all the artificial soils were spiked under identical condition. It is suspected that the bitumen-soil interactions occurring in the spiked samples, which are mainly via surface adsorption, are different from the interactions occurring gradually over time in the Athabasca tailing soils under the natural environmental conditions. Under the latter conditions, water, salinity, and various types of ions all impact the formation of the bitumen-soil matrix, where bitumen-soil interactions may occur via surface adsorption, physical retention, or binding of bitumen in the intermolecular layers of the minerals (Lagaly, Ogawa et al. 2013). Furthermore, Forrester *et al.* (Forrester, Janik et al. 2010) indicated that the porosity of the minerals shields the bitumen trapped within the internal structures of soils from the IR beam, which would adversely affect the performance of the calibration model.

The effect of sample heterogeneity on the accuracy of the PLS calibration model developed with the natural Athabasca tailing soils can be estimated by the parameter of precision, where the average deviation of the replicate predictions from their mean is calculated (Table 5-9). The calibrations based on artificial tailing soils exhibited higher precision, with an average ± 0.60 wt% difference. In the case of the PLS calibration model based on natural Athabasca tailing soils, the variation of the replicate predictions doubles, with an average difference among triplicates of ±1.30 wt%.

5.4.2. Remediation by RHS Beads

According to the results presented in Sections 5.3.3.1 and 5.3.3.2, showing that bitumen is held on the surface of RHS beads and that the bitumen content of tailing soils is reduced in half after a single pass of the RHS remediation process, the RHS beads are effective in removing bitumen from tailing soils. Furthermore, a reduction in clay minerals after the remediation process is also observed, indicating that clay minerals are recovered by the beads along with bitumen. The RHS

beads have strong affinity for all hydrophobic hydrocarbons. When the polymeric beads are mixed with the tailing soils, the high interfacial tension at the surface of the beads causes them to strongly attract and hold the hydrocarbons. However, clay is an ultra-fine particle less than 2 μm in diameter, which provides an enormous amount of active surface with high charge density. Clay interacts with and adsorbs the bitumen, forming clay-bitumen complexes. Apparently, the RHS beads are unable to compete with the fine clays for bitumen. The clay minerals have a much larger active surface area per unit mass compared to the RHS beads. Therefore, clay minerals are strongly attached to the bitumen that is stripped out of the tailing soil by the RHS beads.

5.4.3. Relationship between RHS Remediation and Bitumen Content Explained by PCA

From the FTIR analysis of bitumen content in tailing soils and on the RHS bead surface after the soil remediation process, bitumen is successfully removed from tailing soils and ends up on the RHS bead surface (Sections 5.3.3.1 & 5.3.3.2). Therefore, a relationship between RHS bead remediation and bitumen content would be expected. However, according to the results of PCA of 96 spectra obtained from the before- and after-remediation samples, the relationship between the remediation process and bitumen content does not exist, as there is no clear separation of these 96 spectra based on RHS remediation while there is a good separation based on bitumen content. (Section 5.3.3.4.2).

There are several possible explanations for this finding. First of all, the heterogeneity of the feedstocks may be a factor. Athabasca oil sands deposits are extremely heterogeneous with respect to geometry, mineralogy and mineral chemistry, aqueous fluid distribution and chemistry such as the salinity, and the distribution and chemistry of bitumen. These interrelated properties reflect the origin and quality of the ore and determine the bitumen stripping and extraction techniques, the quantity and quality of the extracted bitumen, as well as the quality of the tailings (Larter, Adams et al. 2008). For example, the high-quality ore has a higher amount of bitumen with an average bitumen content of 13.7 wt%, lower water content with an average of 1.0 wt%, and much less mineral fines (< 44 μm) with an average content of 7.5 wt% in the total solids. On the other hand, the low-quality ore has lower bitumen content with an average content of 7.6

wt%, a higher amount of water with an average water content of 6.3 wt%, and a much higher amount of fines with an average content of 34.6 wt%. After the extraction process, which is tailored and optimized according to the ore quality, 98 wt% of the total bitumen is recovered from the high-quality ore, leaving a small amount of bitumen residue in the tailing soils; while in the case of the low-quality ore, only 76 wt% of the total bitumen is recovered, leaving 24 wt% of bitumen in the tailings (Romanova, Valinasab et al. 2006).

Therefore, the feedstocks sent to the remediation pilot plant, which were the tailing slurries containing most of the processing water, soil minerals and bitumen residues, varied from batch to batch in the content of bitumen and fines in the soils. In addition, the fines, which are mainly the clay minerals, play an important role in the formation of bitumen-water emulsions and therefore determine the recovery of bitumen from the tailing slurries. These clay minerals are ultra-fine and biwettable, strongly adsorb bitumen, and become suspended in the middle layer of the tailing slurries. When the RHS beads are added to the tailing slurries, the part of the bitumen that is mechanically entrained in the coarse sand grains is easily removed by the RHS beads. However, the fine clay minerals, which also adsorb part of the bitumen, adversely affect the separation of bitumen. The biwettable fines attach at the bitumen-water interface and stabilize the bitumen-water emulsions by forming a rigid barrier between water droplets and the continuous bitumen phase. Moreover, the fines are porous and may internally trap bitumen and thereby adversely affect the extraction of bitumen by the RHS beads (Sparks, Kotlyar et al. 2003). Therefore, the variation of the bitumen content and fine clay content in the feedstocks, as well as the different degrees to which the fines inhibit the bitumen separation, make the remediation process inconsistent and consequently lead to the unsuccessful clustering of IR spectra of samples from different remediation batches.

5.5. Conclusion

In this study, IR spectroscopy coupled with Beer's law or with the PLS algorithm has been successfully employed for quantitation of bitumen directly from neat tailing soils without any chemical extractions. The spectral information provided by both near-IR and mid-IR spectroscopy allowed the development of calibrations of high accuracy and precision. The

inclusion of clay spectral information in the PLS modeling is beneficial to the accuracy of the bitumen calibration. The robustness, accuracy, and reliability of the models are proved by examination of the prediction performance using a set of completely independent validation samples.

The application of IR spectroscopy coupled with the PCA algorithm for the classification of tailing soils and the evaluation of a remediation process has also been investigated in this study. This method successfully clusters the tailing soils according to the bitumen content level. However, the bitumen content level fails to serve as an indicator of the RHS-bead remediation process, as the bitumen content in some "After-remediation" samples is higher than that in some "Before-remediation" samples. To avoid this inconsistent remediation outcome, an IR-PCA spectroscopic method could be implemented at the material reception point to characterize and categorize the feedstocks based on the initial bitumen content level to ensure the remediation process is optimized according to the initial bitumen content. Furthermore, the same IR-PCA technique can also be applied during the remediation process as well as at the end of the process, where it could play a screening role to ensure the clean-up goal has been met.

CHAPTER 6

CONNECTING STATEMENT

In Chapter 6, bitumen recovery from Alberta tailing soils was studied by using green solvent extraction. The recovery performance was evaluated in terms of the product quality, as well as quantify of the recovered bitumen and the non-recovered bitumen. The bitumen fractions were quantitated by using an ATR-FTIR-PLSR model, which was developed in Chapter 5. In addition, the chemical structures of the recovered and non-recovered bitumen were investigated by using ATR-FTIR spectroscopy.

USE OF ATR-FTIR SPECTROSCOPY FOR QUANTITATIVE AND QUALITATIVE ANALYSIS OF BITUMEN

EXTRACTED BY THE GREEN SOLVENT 2-MeTHF FROM ALBERTA OIL SANDS

Abstract

2-MeTHF is a green solvent that is widely used as a substitute for organic solvents such as toluene and dichloromethane (DCM). Toluene and DCM have been widely used in the bitumen extraction process as the extracting solvents. In this study, 2-MeTHF was examined as an alternative extraction solvent for bitumen. In a room-temperature 2-min vortex extraction, 2-MeTHF was able to recover 89% of the total bitumen in Alberta tailing soils, which was 9% and 14% higher than the recovery obtained with toluene and DCM, respectively. In addition, the extraction was optimized when the solvent-to-soil ratio was 2:1 wt/wt, beyond which there was no increase in the extraction efficiency; when toluene or DCM was used, a larger solvent-to-soil ratio was required to reach a similar extraction efficiency to that obtained with 2-MeTHF. Moreover, the bitumen obtained from 2-MeTHF extraction had higher quality as less clay migration was found in the final products by DRIFT-NIR analysis.

The bitumen residues after the single-stage extraction were further separated into less-soluble and insoluble fractions, where those resistant to room-temperature extraction were regarded as the less-soluble fraction and those resistant to Soxhlet extraction were regarded as the insoluble fraction. An MIR-PLSR calibration was used to quantify these two fractions. The less-soluble fraction accounted for 14.36% of the total bitumen and the insoluble fraction accounted for 8.77% of the total bitumen. The less-soluble fraction was further characterized by using ATR-FTIR spectroscopy, and it was found that it contained longer aliphatic chains and less branched structure with higher amounts of aromatic carbons and carbonyl groups than the easily soluble fraction.

2-MeTHF is a promising bitumen extraction solvent, considering its higher extraction efficiency, higher product quality, and lower environmental impact. However, 2-MeTHF is unstable when heat and Lewis acids are present, which trigger 2-MeTHF protonation, ring-opening and consequent polymerization reactions. The polymerized 2-MeTHF is in oil form, which mixes

with and ends up in the final bitumen product and cannot be removed during solvent recovery. The presence of the polymerized 2-MeTHF by-products in the bitumen extracted by boiling 2-MeTHF was evidenced by the results obtained from ATR-FTIR, MS-PACI, and elemental analysis.

Key words   green solvent   2-MeTHF   bitumen   extraction performance   IR spectroscopy

6.1. Introduction

Alberta's oil sands resources are the third largest crude oil reservoir in the world, after Saudi Arabia and Venezuela. As the conventional oil reserves of the Middle East decrease, the demand for unconventional oil sources, which usually refers to the oil sands of Canada, dramatically increases (Attanasi and Meyer 2010). It is estimated that crude oil production in Alberta will increase from 1.3 million barrels/day in 2008 to 3 million barrels/day in 2018 (Burrowes, Teare *et al*. 2011). The traditional recovery of crude oil, which is commonly referred to as bitumen, from the oil sands employs the water-based extraction process, which was first introduced by Karl Clark in the 1920s and was first commercially applied in 1967 (Masliyah, Zhou *et al*. 2004). The characteristic feature of oil sands, which is that a thin layer of water separates the hydrophobic bitumen and the hydrophilic sand grains, makes the simple water-based extraction feasible. However, this method has several disadvantages, which are mainly related to the environmental impact, such as large water consumption, the tailing ponds formed by the accumulation of the wastewater, which are a risk to wildlife (Board 2006), and the high energy consumption and high greenhouse gas emission (Wu and Dabros 2012). Therefore, new technologies need to be developed to overcome the environmental shortcomings of the water-based extraction.

Solvent-based extraction is a good alternative to the water-based process, as it greatly decreases fresh water demand and eliminates the tailing ponds. A wide range of solvents that can dissolve bitumen have been investigated. For example, (Graham, Helstrom *et al*. 1987) patented the use of heptane to recover bitumen with centrifugation, filtration and steam stripping. (Farcasiu and Whitehurst 1977) used the combination of light naphtha and methanol as the solvent system to

extract bitumen, where the most desirable and non-polar fractions were recovered from the light naphtha phase while the more polar fractions were recovered from the methanol phase and the less desirable asphaltenes precipitated. used hot toluene and centrifugation to recover bitumen from tar sand. (Wu and Dabros 2012) suggested using cyclopentane to extract bitumen from oil sands as it provided comparable extraction to the water-based extraction and it was easily recovered.

The selection of extracting solvent for use in bitumen extraction has been focused on naphtha, benzene, toluene, chloroform, methanol, alkanes, and cycloalkanes (Wang, Robbins *et al*. 2004). However, various factors need to be considered in solvent selection, such as the source, cost, recovery, volatility, and toxicity as well as the solubility of bitumen. For example, naphtha is considered a good solvent as it is cheap and has low toxicity but it fails to extract the heavy components in bitumen. Bitumen has high solubility in toluene, but this solvent is difficult to recover owing to its high boiling point.

Solvents is the most consumed material where more than 80% of the material consumption comes from solvent (Constable, Jimenez-Gonzalez *et al*. 2007). In addition, solvent use also consumes about 60% of the overall energy and accounts for 50% of the post-treatment greenhouse gas emissions (Jiménez-González, Curzons *et al*. 2004). Therefore, considering the large quantities of solvent to be consumed in the bitumen extraction process, a proper solvent selection significantly affects the energy savings as well as the environmental impact. Recently, the concept of "green solvents" has emerged, which expresses the goal of minimizing the environmental impact resulting from the use of solvents in chemical production (Capello, Fischer *et al*. 2007). In general, the concept of green solvents has developed in four directions; substitution of hazardous solvents with ones that show better EHS (environmental, health, and safety) properties (Gani, Jiménez-González *et al*. 2006); substitution of organic solvents with either supercritical fluids that are environmentally harmless or with ionic liquids that show low vapour pressure and thus less emission into air (Nalawade, Picchioni et al. 2006) and use of "bio-solvents" that are produced from renewable resources (Capello, Fischer *et al*. 2007).

2-Methyltetrahydrofuran (2-MeTHF) is a green solvent, as it can be derived from renewable resources, such as furfural or levulinic acid; therefore, it can reduce the use of petrochemically

fabricated solvents, which leads to an avoidance of fossil resource use and fossil fuel CO_2 emissions to the environment (Capello, Fischer *et al.* 2007). In addition, it has low miscibility in water, a low boiling point, and a higher production yield, which makes it a popular substitute for tetrahydrofuran (THF), toluene, and dichlromethane (DCM) in many applications, such as organocatalysis, biomass processing, and biocatalysis (Pace, Hoyos *et al.* 2012).

The use of 2-MeTHF in bitumen extraction as a substitute for the traditionally used organic solvents, such as toluene and DCM, is seldom reported. Similar to toluene and DCM, 2-MeTHF is able to dissolve both light and heavy components in bitumen, but 2-MeTHF is more easily recovered than toluene as it has a lower boiling point. In addition, unlike DCM, 2-MeTHF is immiscible in water, making it easier to separate and recover from water and thereby reducing the waste stream. Therefore, 2-MeTHF shows great potential as a green extraction solvent for use in solvent-based bitumen extraction processes.

In this study, 2-MeTHF was examined as the solvent for the extraction of bitumen from Alberta tailing soils. The extraction performances of 2-MeTHF as well as the traditional solvents toluene and DCM were studied and compared based on a comprehensive analysis, including extraction efficiency, bitumen recovery, extraction rate, and the extraction loss. Optimization of solvent usage was also studied to minimize the solvent input. However, the optimization of the extraction and drying process, such as the extraction time, extraction technique, number of extraction stages, and drying temperature, was not the purpose of the present study. In addition, the quality of the final bitumen products was evaluated in terms of the fine clay migration, since from a bitumen production viewpoint; it is desirable if the fine solids coagulate less with bitumen.

6.2. Materials and Methods
6.2.1. Materials
6.2.1.1. Soil Samples
The soil samples used in this study come from the Athabasca tailing soils provided by Gradek Energy Inc., as described in Chapter 5. In order to minimize the sample variability, the soil
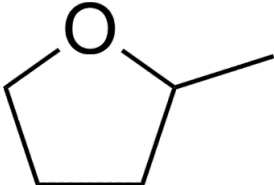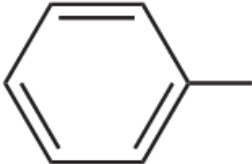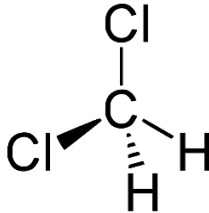
samples were taken from the same batch. The soils were air-dried in a fume hood for a week, then were finely ground and passed through a 2-mm sieve and stored in a sealed 1-L glass bottle.

6.2.1.2. Solvents

Three organic solvents were used independently in this study: 2-methyltetrahydrofuran (2-MeTHF), toluene, and dichloromethane (DCM). They were anhydrous grade with ≥99.0% purity purchased from Sigma-Aldrich. The physical and chemical properties of the three solvents are listed in Table 6-1.

Table 6-1. Physical and chemical properties of 2-MeTHF, toluene, and DCM solvents

Solvent	2-MeTHF	Toluene	DCM
Chemical formula	$C_5H_{10}O$	C_7H_8	CH_2Cl_2
Chemical structure			
Molar mass (g/mol)	86.13	92.14	84.93
Density (g/mL)	0.85	0.87	1.33
Boiling point (℃)	80.2	111.0	39.6
Water solubility (g/L at 25 ℃)	0.14	0.52	22.81
Hildebrand solubility parameter($MPa^{1/2}$)	16.9	18.2	20.2
Dynamic viscosity (mPa.s at 25℃)	0.51	0.56	0.41
Kinematic viscosity (cSt at 25℃)	0.60	0.65	0.31

6.2.2. Methods

6.2.2.1. Room-Temperature Bitumen Extraction

Exactly 6.00 ± 0.05 g of dried tailing soils was weighed and added into a 50-mL screw-cap centrifugation tube. A controlled amount of organic solvent was added into the tube. In order to compare the extraction efficiency among the solvents, each solvent was independently added. The soil-solvent mixture was vortexed at room temperature for 2 min to complete the extraction. The extracts were separated from the soil by centrifugation at 8000 rpm for 15 min. The supernatant was collected and dried in a fume hood at room temperature (25 °C) for 3 days to obtain the recovered bitumen. The precipitate, which was the solvent-extracted soil, was dried in the fume hood at room temperature overnight to obtain the solvent-free extracted soil.

6.2.2.2. Optimization of Solvent Extraction

As mentioned in Section 6.2.2.1, the amount of solvent added into the samples was controlled at seven different solvent-to-soil ratios (wt/wt), 1:1, 1.25:1, 1.5:1, 1.75:1, 2:1, 2.5:1, and 3.24:1. The recovered bitumen and the washed and dried soil were measured gravimetrically to calculate the extraction recovery (%), extraction loss (%), and extraction efficiency (%) by using the following equations (Alenyorege, Hussein et al. 2015):

$$Extraction\ recovery\ (\%) = \frac{B_1}{S_1} \times 100\% \dots\dots\dots\dots\dots\dots\dots\dots\dots\dots\dots\dots\ (6\text{-}1)$$

$$Extraction\ loss\ (\%) = \frac{S_1-(B_1+S_2)}{S_1} \times 100\% \dots\dots\dots\dots\dots\dots\dots\dots\dots\dots\ (6\text{-}2)$$

$$Extraction\ efficiency\ (\%) = \frac{B_1}{B_T \times S_1} \times 100\% \dots\dots\dots\dots\dots\dots\dots\dots\dots\ (6\text{-}3)$$

where B_1 is the weight of recovered bitumen; B_T is the percentage of bitumen in the soil; S_1 is the weight of soil before extraction; and S_2 is the weight of soil after extraction and solvent evaporation.

6.2.2.3. Calculation of Viscosities of Tailing Soils Solutions

The viscosities of the extraction systems were calculated using the double-logarithmic Refutas equation in a three-step procedure, which is commonly used in the petroleum industry for petroleum blending purpose (Tat and Van Gerpen 1999):

$$Viscosity\ Blending\ Index\ (VBI) = 14.534{\times}In[In(v_X + 0.8)] + 10.975 \ldots\ldots (6\text{-}4)$$

$$VBI(blend) = (W_A{\times}VBI_A) + (W_B{\times}VBI_B) + \cdots + (W_X{\times}VBI_X) \ldots\ldots\ldots (6\text{-}5)$$

$$Kinematic\ Viscosity\ of\ the\ blend\ system\ (v) = e^{e^{(VBI-10.975)\div14.534}} - 0.8 \ldots\ldots\ldots (6\text{-}6)$$

where, v_X is the kinematic viscosity of the Xth component in the system and W_X is the weight fraction of the Xth component in the system.

In this study, the extraction system is the binary system obtained by blending the tailing soil with controlled amount of organic solvent. The kinematic viscosities of the three selected solvents are listed in Table 6-1, whereas the kinematic viscosity of tailing soil is 0 cSt. According to the literature, the kinematic viscosity of tailings relates to the solids content and remains 0 cSt until the solid contents is greater than 68% (Johnson, Moghaddam et al. 2013). In this study, the tailing soil contents in all the extraction systems were below 60%. The kinematic viscosity of each extraction system is presented in Table 6-2.

Table 6-2. Kinematic viscosities of the extraction systems

Solvent	Solvent-to-soil ratio (wt/wt)	Solvent (wt%)	Tailing soil (wt%)	Blend viscosity (cSt)
2-MeTHF	1:1	50	50	0.99
	1.25:1	56	44	0.93
	1.5:1	60	40	0.88
	1.75:1	63	37	0.85
	2:1	67	33	0.82
	2.5:1	71	29	0.78
	3.24:1	76	24	0.75
Toluene	1:1	50	50	1.04
	1.25:1	56	44	0.98
	1.5:1	60	40	0.94
	1.75:1	63	37	0.90
	2:1	67	33	0.88
	2.5:1	71	29	0.84
	3.24:1	76	24	0.80
DCM	1:1	50	50	0.58
	1.25:1	56	44	0.53
	1.5:1	60	40	0.49
	1.75:1	63	37	0.47
	2:1	67	33	0.45
	2.5:1	71	29	0.42
	3.24:1	76	24	0.39

6.2.2.4. Soxhlet Extraction of Bitumen

Soxhlet extractions were conducted using 2-MeTHF, toluene, and DCM to determine the content of bitumen in tailing soil. The Soxhlet apparatus consisted of a 250-mL round-bottomed flask, fitted with a condenser and extractor tube, seated in a temperature-controlled heating mantle. The tailing soil (5 g) was added carefully into the thimble, while the solvent (150 mL) with several glass beads was added into the flask. The heating temperature was set according to the boiling point of the solvent, where 80℃, 110℃, and 40℃ were set for 2-MeTHF, toluene, and DCM, respectively. The extraction was carried out for 4 h. After the extraction, the solvent was evaporated on a rotary evaporator. The residue, which is the extracted bitumen, was measured by gravimetric method. Duplicate extractions with each solvent were carried out.

6.2.2.5. Examination of Bitumen Extracted by ATR-FTIR Spectroscopy

The bitumen extracts and the soils obtained from both the room-temperature extraction and Soxhlet extraction were scanned by ATR-FTIR spectroscopy over the full MIR range (4000 – 400 cm^{-1}) at 4 cm^{-1} resolution with co-addition of 128 scans. The quality of the bitumen extracts was evaluated by the characterization of the bitumen fractions as well as the fine minerals. The quantification of bitumen residues after extraction was conducted by using the MIR-PLSR bitumen calibration model presented in Chapter 5.

6.2.2.6. Characterization of Bitumen Extracts by APCI-MS

The bitumen extracts obtained from different organic solvents were characterized by using a mass spectrometer equipped with an atmospheric-pressure chemical ionization (APCI) source (MaXis Impact, Bruker) with the capillary voltage set at 4000 V and heated to 450 ℃. Spectra were acquired in the positive ion mode over the range of 100 to 1000 *m/z* with a scan time of 1.5 min.

6.3. Results

6.3.1. Bitumen Room-Temperature Extraction Efficiency Comparison among 3 Solvents

6.3.1.1. Mass Balance of the Extraction

The mass balance of the solvent extraction is presented in Table 6-3. Under this scenario, no chemical reactions occurred during the solid-liquid extraction but simply the mass transfer between phases. Therefore, the mass balance equation is simplified as "*input = output*", where "*input*" refers to the soil samples before extraction, while "*output*" refers to the sum of the extracted bitumen and the soil after extraction. The difference between the input and output is the loss during the extraction process.

Table 6-3. Mass balance of bitumen room-temperature extraction by three different solvents

Solvent	Raw data (average of duplicates)				Result		
	Solvent-to-soil ratio (wt/wt)	Soil sample (g)	Recovered bitumen (g)	Extracted soil (g)	Extraction recovery (%)	Extraction loss (%)	Extraction efficiency (%)
2-MeTHF	1:1	6.011	0.253	5.668	4.210	1.507	59.301
	1.25:1	6.003	0.310	5.635	5.157	0.974	72.635
	1.5:1	6.063	0.328	5.686	5.417	0.800	76.289
	1.75:1	6.084	0.373	5.651	6.122	1.024	86.232
	2:1	6.017	0.378	5.539	6.289	1.650	88.574
	2.5:1	6.064	0.377	5.570	6.222	1.562	87.635
	3.24:1	6.039	0.368	5.616	6.098	0.908	85.881
Toluene	1:1	6.025	0.263	5.730	4.360	0.530	60.389
	1.25:1	6.019	0.276	5.690	4.582	0.887	63.465
	1.5:1	6.006	0.291	5.672	4.837	0.722	66.995
	1.75:1	6.012	0.308	5.561	5.127	2.373	71.008
	2:1	6.020	0.305	5.600	5.059	1.911	70.063
	2.5:1	6.007	0.337	5.556	5.612	1.893	77.724
	3.24:1	6.002	0.346	5.501	5.758	2.587	79.749
DCM	1:1	6.018	0.248	5.594	4.126	2.926	58.112
	1.25:1	6.004	0.255	5.605	4.247	2.403	59.818
	1.5:1	6.001	0.266	5.630	4.426	1.756	62.337
	1.75:1	6.002	0.278	5.632	4.633	1.546	65.256
	2:1	6.022	0.309	5.523	5.133	3.142	72.300
	2.5:1	6.001	0.330	5.531	5.492	2.408	77.347
	3.24:1	6.005	0.326	5.577	5.422	1.695	76.372

The extraction recovery and the loss for each treatment are presented in Figure. 6-1. In general, the bitumen recovery increases with increasing solvent-to-soil ratio. In particular, the recovery obtained with the solvent 2-MeTHF is the highest at 6.3%, which accounts for 88.7% of the total bitumen. The bitumen recoveries obtained with toluene and DCM are similar, with the highest recoveries being 5.76% and 5.49%, respectively. However, both toluene and DCM reach their highest recoveries at a higher solvent-to-soil ratio (about 1.5 times higher) than 2-MeTHF (Fig. 6-1-a).
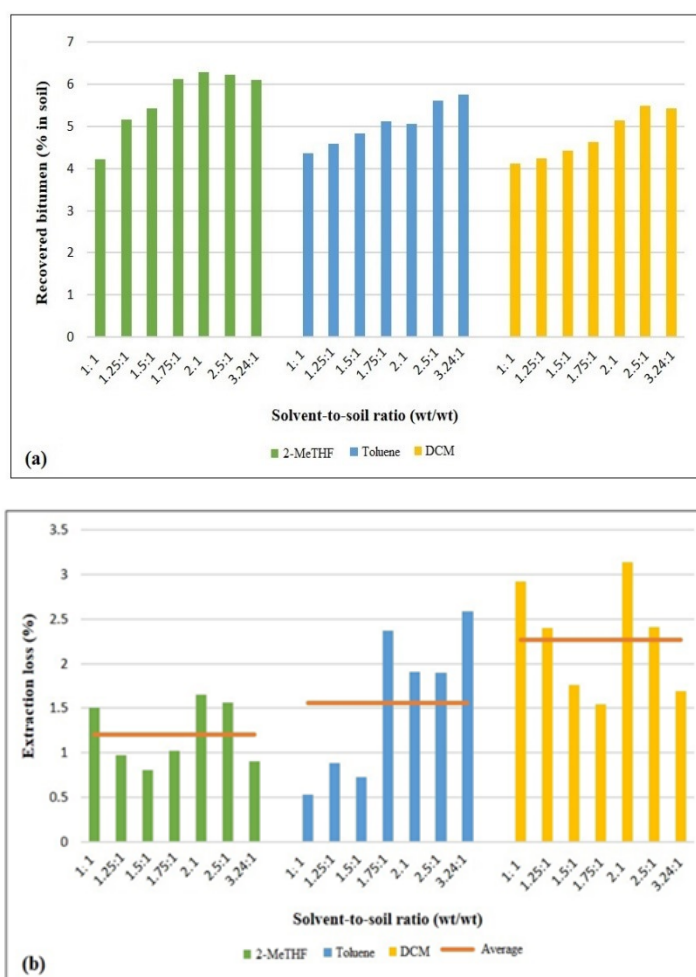
Fig. 6-1. Bitumen room-temperature extraction by 2-MeTHF, toluene, and DCM; (a) extraction recovery; (b) extraction loss

183

In terms of loss, the extractions conducted with 2-MeTHF generated the lowest loss, with an average of 1.20 % ± 0.33 %. The losses occurring in the toluene and DCM extractions were about 1.3 and 1.8 times greater, with an average loss of 1.58 % ± 0.77% and 2.27% ± 0.58 %, respectively. Nevertheless, the recovery loss is randomly distributed among the extractions; therefore, there is a lack of a relationship between the degree of loss and the amount of solvent used in the extraction (Fig. 6-1-b).

6.3.1.2. Bitumen Extraction Efficiency

The extraction efficiency among the three solvents is compared in Figure 6-2. 2-MeTHF shows stronger bitumen extraction power than the other two solvents. As can be seen, the extraction efficiency increases with increasing solvent-to-soil ratio until it reaches 2:1; the efficiency then levels off. At the solvent-to-soil ratio of 2:1, the 2-MeTHF bitumen extraction efficiency of a single-stage extraction can reach around 90%. The extraction efficiency of toluene and DCM are similar but lower than that of 2-MeTHF, with the maximum extraction efficiency around 80% (Fig. 6-2-a).

In addition, the extraction rate is revealed by plotting the recovered bitumen content against the solvent volume (Fig. 6-2-b). The changes of the extraction rates by the three solvents are in a similar pattern, where the extraction increases at a constant rate until reaching the maximum point, and then the extraction levels off. Among these three solvents, the extraction rate of 2-MeTHF is the highest, followed by DCM and toluene. The extraction rate of 2-MeTHF is 0.0214 g/mL, which is 1.6 times higher than that of DCM (0.013 g/mL), and 3.1 times higher than that of toluene (0.0069 g/mL).

As well, the volume of the solvent required to reach the extraction plateau is the smallest for DCM (11.28 mL), followed by 2-MeTHF (12.35 mL) and toluene (17.24 mL). However, at the extraction plateau, the amount of bitumen recovered is the highest for 2-MeTHF extraction (0.38 g), followed by toluene (0.35 g) and DCM extraction (0.33 g). This indicates that the solubility of bitumen is the highest in 2-MeTHF, followed by DCM and toluene. In addition, under these extraction conditions, where single-stage extraction at room temperature for 2 min is applied, the

diffusion efficiency of bitumen into 2-MeTHF is the highest, resulting in the highest extraction performance, in terms of the extraction efficiency and the extraction rate.
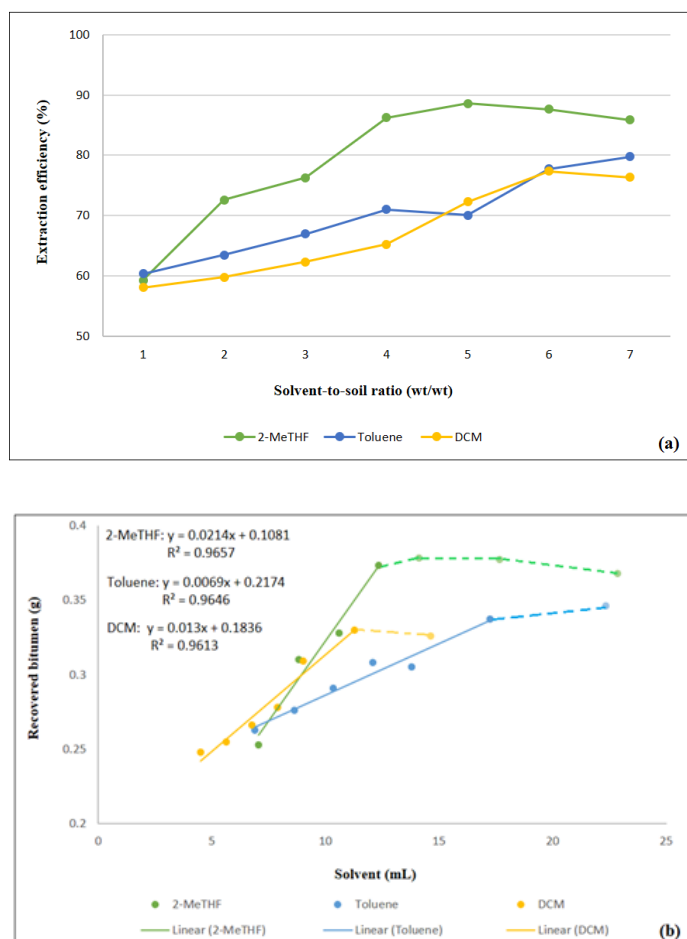
Fig. 6- 2. Bitumen room-temperature extraction by 2-MeTHF, toluene, and DCM; (a) extraction efficiency; (b) extraction rate

Furthermore, the viscosities of all the extraction systems formed by the different solvents and the various solvent amounts are compared in Figure 6-3. In general, the viscosity decreases with increasing solvent-to-soil ratio. Among the three solvents, the viscosity of the system formed by DCM is the lowest, followed by 2-MeTHF and toluene. The viscosity of the system can have an impact on the extraction performance, where lower viscosity is more beneficial to the process. When the bitumen content of the tailing soil is low (i.e. ≤ 0.3 g, $\leq 5\%$ in soil, Fig. 6-2-b), the extraction performance by DCM is the best, where the amount of recovered bitumen is the

highest. However, when the bitumen content increases (i.e. > 0.3 g, > 5% in soil), the extraction performance by 2-MeTHF is superior.
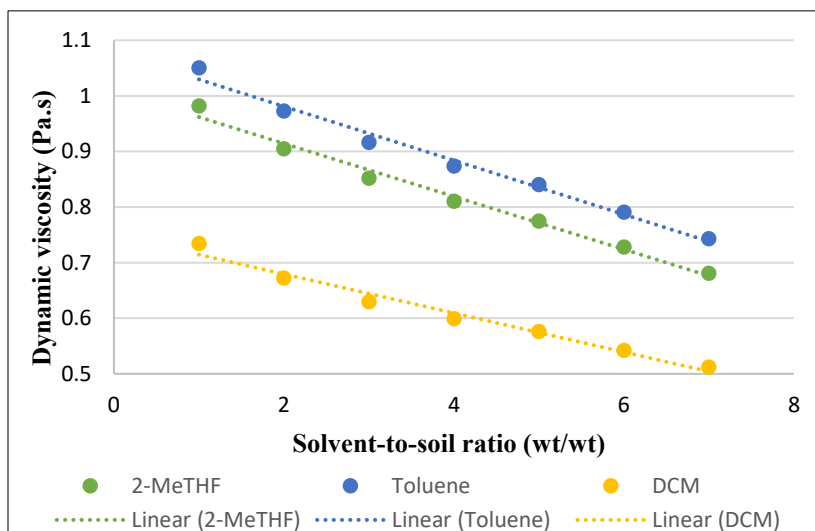
Fig. 6-3. Change of system viscosities (Pa.s) with solvent type and solvent-to-soil ratio

6.3.1.3. Characterization of Recovered Bitumen

6.3.1.3.1. ATR-FTIR Spectroscopy

The bitumen extracted by the 3 different solvents at the lowest (1:1) and the highest (3.24:1) solvent-to-soil ratio was characterized by ATR-FTIR spectroscopy. The distributions and abundances of the functional groups are illustrated in Figure 6-4.
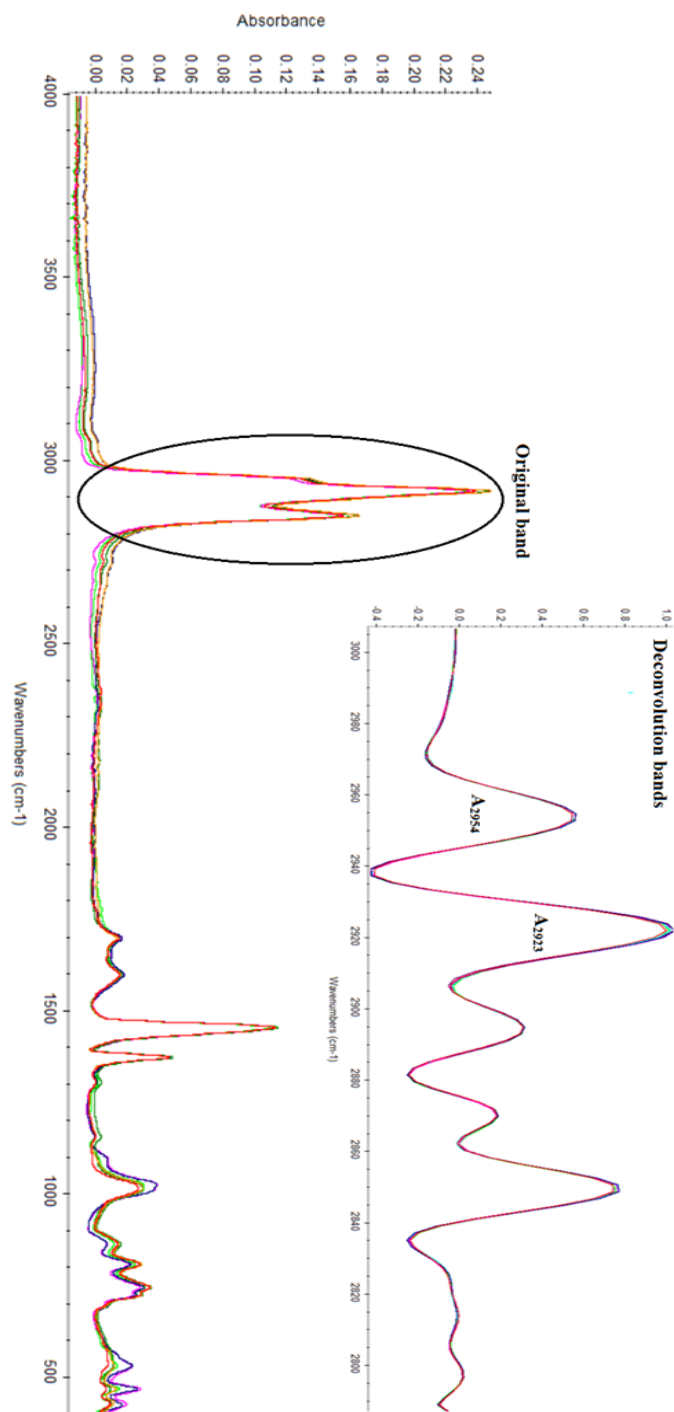
Fig. 6-4. Original spectra of extracted bitumen and the deconvolved spectra in the aliphatic region between 3000 and 2800 cm^{-1}

The particular interest is the aliphatic stretching region (3000 – 2800 cm^{-1}). The aliphatic stretching region, which is better resolved after band deconvolution, is used to calculate a -CH$_3$/-CH$_2$ ratio that provides information about the chain length and the degree of branching of aliphatic compounds (Table 6-4). The -CH$_3$/-CH$_2$ ratios are identical (0.70) for the extracts obtained by the 3 different solvents at a 1:1 solvent-to-soil ratio. This indicates that the three bitumen extracts are structurally identical, in terms of the degree of branching and the length of the aliphatic chains.

Table 6-4. A$_{2954}$/A$_{2923}$ index of bitumen extracted by different solvents at room temperature with the lowest and highest solvent-to-soil ratio

Extraction condition	Solvent	Solvent-to-soil ratio (wt/wt)	A$_{2954}$ (-CH$_3$)	A$_{2923}$ (-CH$_2$)	A$_{2954}$/A$_{2923}$ (-CH$_3$/-CH$_2$)
Room temperature	2-MeTHF	1:1	13.381	19.180	0.70
		3.24:1	13.495	19.587	0.69
	Toluene	1:1	13.671	19.390	0.71
		3.24:1	13.500	19.537	0.69
	DCM	1:1	13.835	19.837	0.70
		3.24:1	13.858	19.853	0.70

Nevertheless, among all the extracts, the -CH$_3$/-CH$_2$ ratios obtained at the highest solvent-to-soil ratio (3.24:1) are slightly lower than those obtained at the lowest ratio (1:1). This suggests that bitumen extracted by a larger amount of solvent (higher solvent-to-soil ratio) contains more long-chain and unbranched aliphatic groups. This is due to the lower solubility of the larger size molecules with longer carbon chains, which are outcompeted by the shorter carbon chain molecules when only a small amount of extracting solvent is employed (ratio 1:1). Therefore, when the bitumen is extracted at a solvent-to-soil ratio of 1:1, the solvents are saturated by the fractions with shorter carbon chains, which are dissolved first. When the amount of the solvent increases (ratio 3.24:1), the non-saturated portions of the solvents start to dissolve the bitumen

fractions with longer carbon chains. Consequently, the bitumen extracted at a solvent-to-soil ratio of 3.24:1 is composed mostly of the short carbon chain fractions together with part of the long carbon chain fractions. The inclusion of the longer carbon chain fractions decreases the -CH_3/-CH_2 ratios, which is reflected by the ATR-FTIR spectra.

6.3.1.3.2. DRIFT-NIR Spectroscopy

The DRIFT-NIR spectra of the bitumen recovered by solvent extraction with the three different solvents are presented in Figure 6-5. All the bitumen extracted by the different solvents shows a similar NIR spectral pattern, with absorption bands representing the presence of water, hydrocarbons, and clay minerals. However, the spectral signal is very weak and noisy throughout the whole spectrum. This is because only a small fraction of light is reflected back to the detector, as most of the light is absorbed by the bitumen due to its naturally dark color.

The DRIFT-NIR spectra were mathematically processed by taking the 2nd derivative to resolve the broad bands, and the resulting spectra in the range between 5000 and 4000 cm^{-1} are presented in Figure 6-6. The three bands between 4450 and 4280 cm^{-1} are due to the combination of methyl and methylene stretching and bending vibrations. In the region between 4550 and 4500 cm^{-1}, there is a sharp band representing the presence of clay minerals. In the spectrum of the clean soil, there is no absorption in the hydrocarbon region but strong absorption in the clay region, as there is no bitumen in the clean soil sample. In turn, in the spectrum of the recovered bitumen, there should be only hydrocarbon absorptions. However, a small clay band is observed in the spectra of the toluene- and DCM-recovered bitumen. This suggests that a small portion of the clay is recovered along with bitumen when toluene and DCM are used as extraction solvents. The presence of clay in the bitumen aids light reflection, causing the relatively stronger and less noisy signals in the spectra of toluene- and DCM-recovered bitumen as compared to the signals in the spectrum of 2-MeTHF-recovered bitumen.
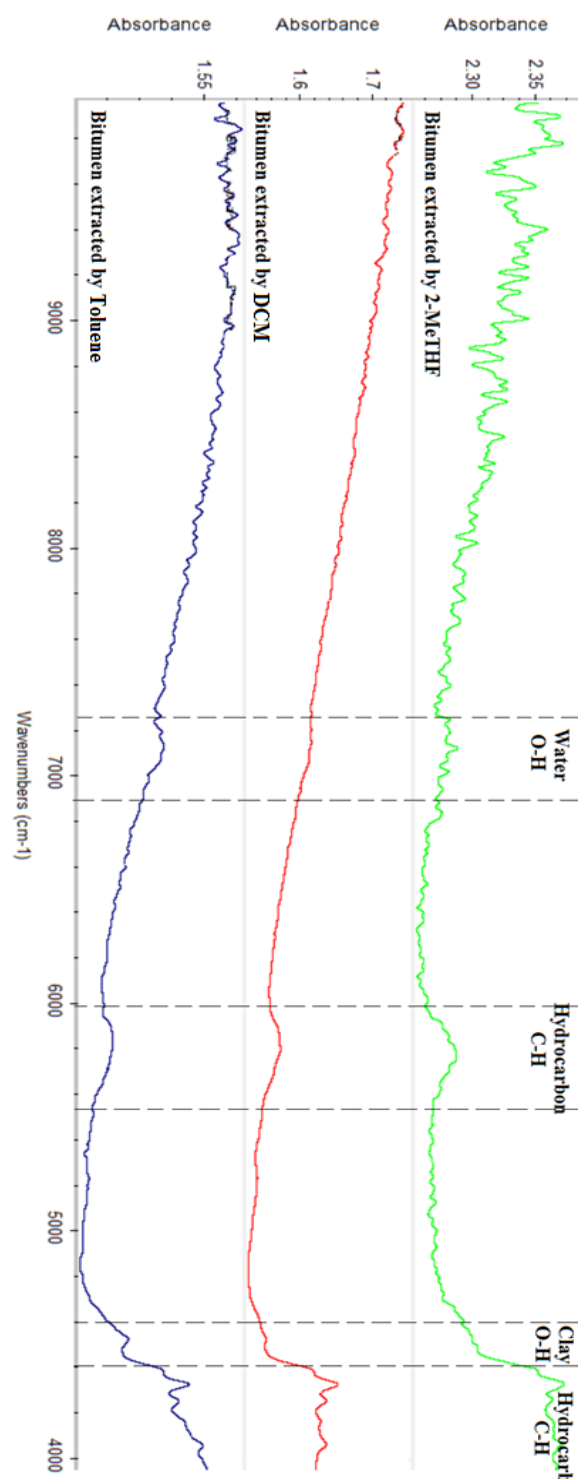
Fig. 6-5. Stacked DRIFT-NIR spectra of bitumen recovered from tailing soil by 2-MeTHF, toluene, or DCM extraction
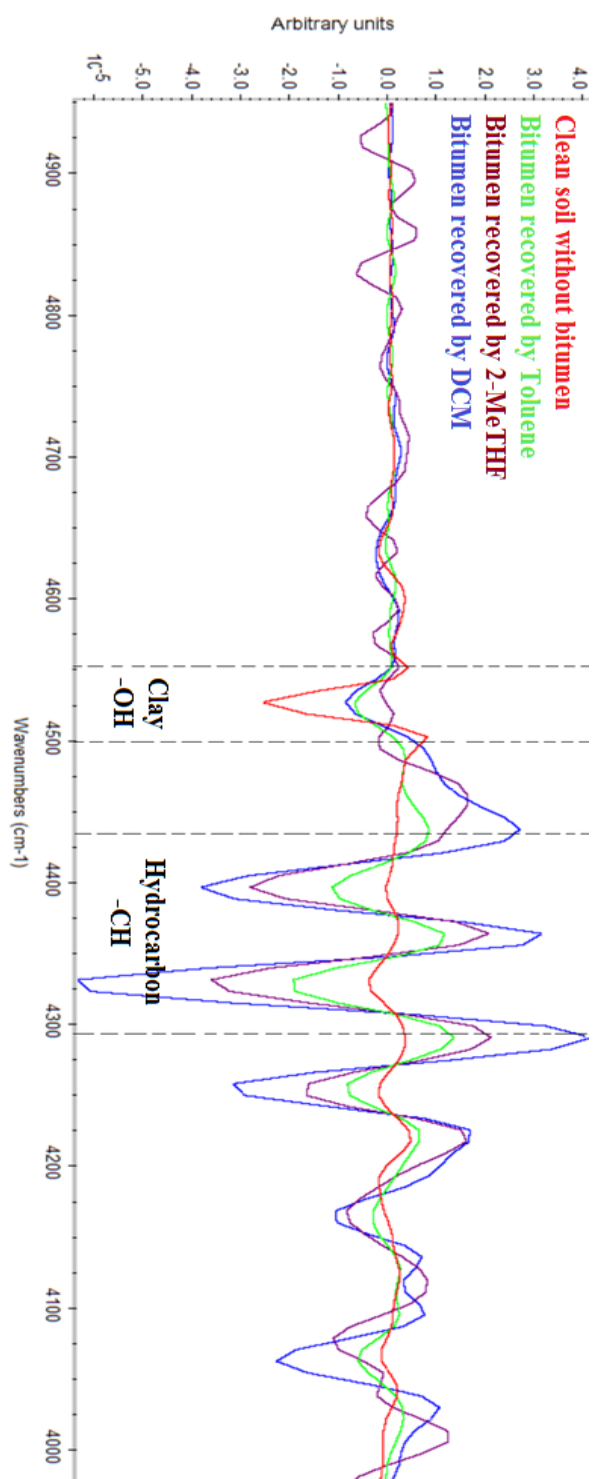
Fig. 6-6. Second derivative DRIFT-NIR spectra of clean soil and bitumen recovered from tailing soil by 2-MeTHF, toluene, or DCM extraction

6.3.2. Determination of Bitumen Residues by ATR-FTIR Spectroscopy

6.3.2.1. ATR-FTIR Spectra of Bitumen Residues from Room-Temperature Extraction and Soxhlet Extraction

6.3.2.1.1. Determination of Less-Soluble Bitumen by Room-Temperature Extraction

To evaluate the extraction performance under different extraction conditions, the tailing soil samples obtained after different extraction treatments were examined by ATR-FTIR spectroscopy. The extraction performance was evaluated based on the bitumen content left in the tailing soil samples after the different extraction treatments.

Based on the hydrocarbon band intensity in the ATR-FTIR spectra, the content of bitumen residues decreases with increased amount of organic solvent (Fig. 6-7). After the extraction at the lowest solvent-to-soil ratio (1:1), the bitumen band intensity is more than 50% reduced relative to the band intensity in the spectrum of the raw tailing soil. In the case of extraction by 2-MeTHF, the amount of bitumen extracted gradually increases with increasing amount of 2-MeTHF used, which is reflected by the ATR-FTIR spectra, where the band intensity drops gradually and smoothly as a function of the amount of solvent used. However, in the case of the other two solvents, toluene and DCM, the removal of bitumen is not in proportion to the amount of solvent used. For example, the bitumen residues after toluene extraction at solvent-to-soil ratios of 1:1 and 1.5:1, as well as after DCM extraction at solvent-to-soil ratios of 1:1 and 1.75:1, are almost identical, as revealed by the ATR-FTIR spectra, where the spectra representing different solvent usages are nearly overlaid with similar bitumen band intensity. This indicates that under the same extraction conditions, the extraction efficiency of toluene and DCM is not as good as that of 2-MeTHF, since increasing the amount of the former two solvents used in bitumen extraction did not reduce the bitumen residues content of the treated soil as much as 2-MeTHF did.

In addition, the decrease in the bitumen residues content of the treated soil ceases when the solvent-to-soil ratio reaches a certain point. In the case of 2-MeTHF, beyond a solvent-to-soil ratio of 2.5:1, the bitumen band intensity no longer decreases. In the case of toluene, the bitumen band becomes stable beyond a solvent-to-soil ratio of 1.75:1. This fraction of bitumen, which cannot be further extracted by the solvent under the room-temperature 2-min vortex extraction

conditions, is assumed to be the less-soluble bitumen. Under such extraction conditions, additional amounts of organic solvent cannot remove the rest of the bitumen.
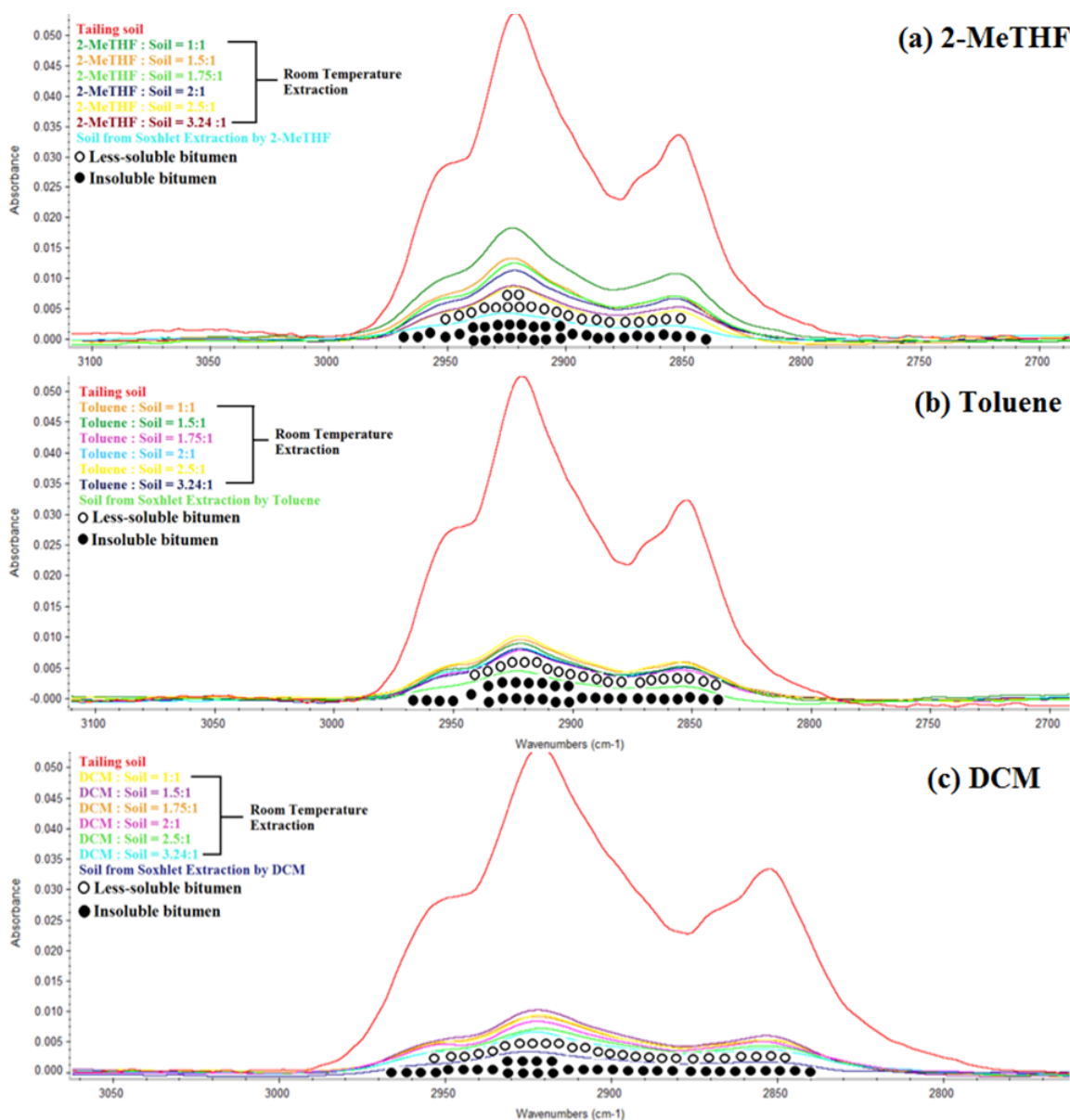
Fig. 6-7. ATR-FITR spectra of tailing soils after room-temperature extraction at different solvent-to-soil ratios and after Soxhlet extraction by (a) 2-MeTHF, (b) toluene, and (c) DCM

6.3.2.1.2. Determination of Insoluble Bitumen by Soxhlet Extraction

In order to verify whether the less-soluble bitumen can be extracted by the organic solvents, Soxhlet extraction, which provides much harsher extraction conditions involving heating in the boiling solvent for 4 h, was used to extract the tailing soil sample. The spectrum of the extracted tailing soil was scanned by ATR-FTIR spectroscopy and the bitumen region between 2975 and 2750 cm^{-1} was examined (Fig. 6-7). By comparing the band intensities among the spectra from room-temperature extraction and from Soxhlet extraction, it is observed that the bitumen band in the spectra of the Soxhlet extraction samples has the lowest intensity. This indicates that the Soxhlet method extracts more bitumen than the room-temperature method with the highest solvent-to-soil ratio. Thus, the Soxhlet method is able to extract part of the less-soluble bitumen fraction. However, the Soxhlet method is unable to extract all of the bitumen, as the bitumen band is still observed in the ATR-FTIR spectrum of the extracted tailing soil sample. That bitumen fraction resistant to Soxhlet extraction is therefore considered to be the insoluble bitumen. The ATR-FTIR spectra of the less-soluble and insoluble fractions obtained with each extraction solvent are presented in Figure 6-8. The hydrocarbon band in the spectra of the insoluble fractions is about 50% less intense than in the spectra of the less-soluble fractions. This indicates that about half of the less-soluble bitumen can be extracted under the vigorous conditions of Soxhlet extraction.
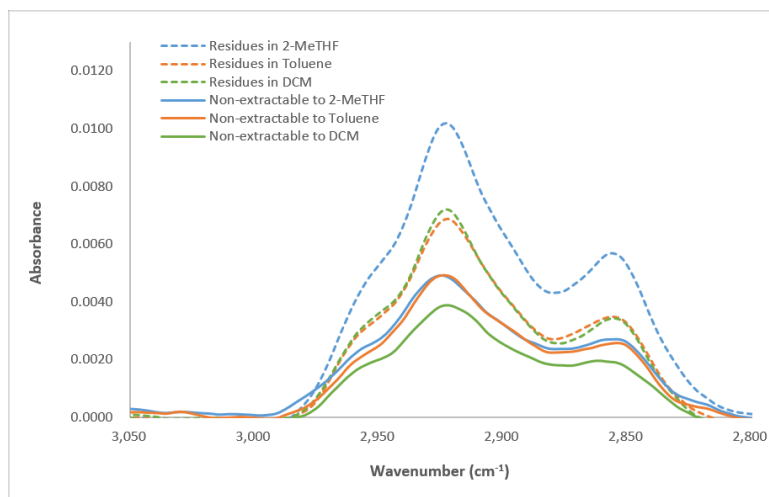
Fig. 6-8. Bitumen absorption region in the ATR-FTIR spectra of tailing soils after room- temperature extraction (dashed line) and after 3.5-h reflux extraction (solid line) by 2-MeTHF, toluene, and DCM

6.3.2.2. Quantification of Bitumen Residues by ATR-FTIR-PLSR

To determine the bitumen residues in soil after different extractions, the MIR-PLSR calibration model based on the ATR-FTIR spectra of artificial tailing soils presented in Chapter 5 was used to quantify bitumen residues. This calibration model is valid within the bitumen content range between 0.70 and 40.70 wt%. As shown in Chapter 5, this model has a 2.34 wt% RMSECV and 12.99% error within that range.

6.3.2.2.1. Quantification of Less-Soluble Bitumen

The MIR-PLSR calibration model was used to determine the less-soluble bitumen from the tailings after room-temperature extraction at different solvent-to-soil ratios. The recovered bitumen and the less-soluble bitumen (resides) of each treatment are presented in Table 6-5 and Figure 6-9. It is estimated that after the extraction at the highest solvent-to-soil ratio, the less-soluble fraction in 2-MeTHF extracts is the least (1.64 wt%) followed by the residues from toluene (1.86 wt%) and that from DCM (2.21 wt%).
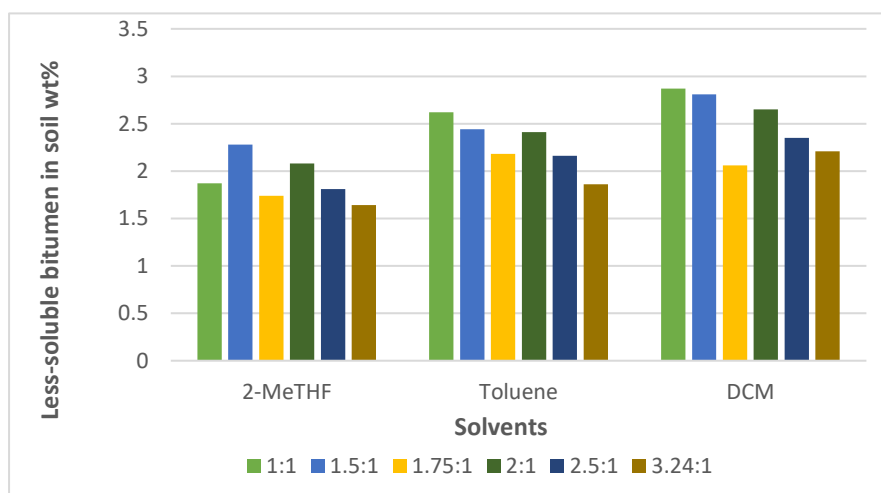
Fig. 6- 9. PLSR-predicted bitumen residues following room-temperature extraction with different solvent-to-soil ratios

Table 6-5. Determination of less-soluble bitumen following
room-temperature extractions by using MIR-PLSR calibration model

Solvent	Solvent-to-soil ratio (wt/wt)	Bitumen extracted [a] (wt%)	Less-soluble bitumen [b] (wt%)
2-MeTHF	1:1	4.21	1.87
	1.5:1	5.42	2.28
	1.75:1	6.12	1.74
	2:1	6.29	2.08
	2.5:1	6.22	1.81
	3.24:1	6.10	1.64
Toluene	1:1	4.36	2.62
	1.5:1	4.84	2.44
	1.75:1	5.13	2.18
	2:1	5.06	2.41
	2.5:1	5.61	2.16
	3.24:1	5.76	1.86
DCM	1:1	4.13	2.87
	1.5:1	4.43	2.81
	1.75:1	4.63	2.06
	2:1	5.13	2.65
	2.5:1	5.49	2.35
	3.24:1	5.42	2.21

[a] Bitumen extracted: determined gravimetrically (weight difference).

[b] Less-soluble bitumen: determined by ATR-FTIR spectroscopy coupled with PLS calibration.

6.3.2.2.2. Quantification of Insoluble Bitumen

The same MIR-PLSR calibration was also applied to quantify the insoluble fraction and the results are presented in Table 6-6. In the room-temperature extraction with the highest solvent-to-soil ratio (3.24:1), the residues are 54%, 43%, and 42% removed by 2-MeTHF, toluene, and DCM by comparison with the 3.5-h reflux extraction condition, respectively. The rest, which cannot be further removed under these reflux conditions, is the non-extractable fraction. The non-extractable bitumen content in tailing soil following Soxhlet extraction with 2-MeTHF, toluene, and DCM is 0.60, 0.59, and 0.45 wt%, which corresponds to 9.55 %, 9.29%, and 7.48% of the total bitumen, respectively.

Table 6-6. Soxhlet extraction of tailing soil sample after
room-temperature extraction at 3.24:1 solvent-to-soil ratio

Soxhlet extraction		Insoluble fraction			
Solvent	Solvent-to-soil ratio (wt/wt)	Less soluble (wt%)	Insoluble (wt%)	Insoluble / Less soluble (%)	Insoluble / Total bitumen (%)
2-MeTHF	40:1	1.64	0.60	36.59	8.45
Toluene	40:1	1.86	0.59	31.72	8.17
DCM	40:1	2.21	0.45	20.36	6.34

6.3.2.2.3. Total Bitumen Content Determination without Compensation for Insoluble Bitumen

Total bitumen in dried tailing soils was first predicted from the MIR-PLSR calibration model and then compared to the Soxhlet extraction results (Table 6-7; Fig. 6-10). In general, the MIR-PLSR predictions for replicate soil samples are consistent, giving a range of bitumen content between 6.90 and 7.24 wt% among 9 replicates, with an average of 7.14 ± 0.13 wt%. In the case of the Soxhlet extraction, the bitumen content obtained varies among the three organic solvents employed, where the bitumen content extracted by 2-MeTHF is the highest with an average 6.42

wt%, followed by toluene and DCM, with an average of 5.93 wt% and 5.53 wt% bitumen, respectively. The average bitumen content determined by Soxhlet extraction is 6.07 ± 0.34 wt%. The bitumen content determined by Soxhlet extraction varies more, with a 0.34 wt% standard deviation (SD), than the MIR-PLSR predictions, which have a 0.13 wt% SD.

Table 6-7. Total bitumen content determination by using MIR-PLSR prediction compared to Soxhlet extraction without compensation for insoluble bitumen

Raw tailing soil	Bitumen content by Soxhlet extraction (wt%)	Bitumen content by MIR-PLSR (wt%)	Prediction difference (wt%)	Prediction error (%)
2-MeTHF				
Replicate-1	6.40	7.18	0.78	12.19
Replicate-2	6.38	6.90	0.52	8.15
Replicate-3	6.47	7.22	0.75	11.59
Average ± SD	6.42 ± 0.04	7.10 ± 0.14	0.68 ± 0.12	10.64 ± 1.78
Toluene				
Replicate-1	5.94	7.35	1.41	23.74
Replicate-2	5.87	7.06	1.19	20.27
Replicate-3	5.98	7.24	1.26	21.07
Average ± SD	5.93 ± 0.05	7.22 ± 0.12	1.29 ± 0.09	21.69 ± 1.48
DCM				
Replicate-1	5.52	7.12	1.60	28.42
Replicate-2	5.43	7.02	1.59	29.28
Replicate-3	5.63	7.15	1.52	27.00
Average ± SD	5.53 ± 0.08	7.10 ± 0.06	1.57 ± 0.04	28.42 ± 1.01
Average among 9 extracts	6.07 ± 0.34	7.14 ± 0.13	1.07 ± 0.39	18.02 ± 7.45

Comparing the MIR-PLSR bitumen predictions with results of the Soxhlet extraction, which is the reference method for bitumen quantification, the MIR-PLSR calibration model overestimates the bitumen content. The MIR-PLSR method estimates 0.68 wt% more bitumen content when compared to 2-MeTHF Soxhlet extraction, 1.29 wt% more compared to toluene Soxhlet extraction, and 1.57 wt% more compared to DCM Soxhlet extraction. These overestimations represent 10.64 to 28.42 % prediction error relative to the reference method. The extent of the error is related to the type of extraction solvent used in the reference method, where the prediction error is the largest when DCM is used (Fig. 6-10).
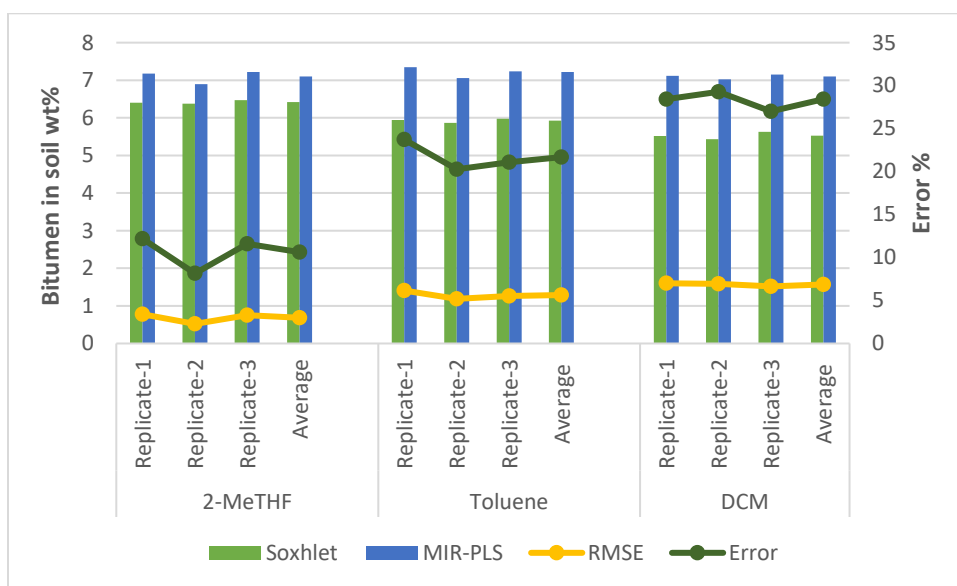
Fig. 6-10. Bitumen determination by Soxhlet extraction (without compensation for residues) and by MIR-PLSR prediction

6.3.2.2.4. Total Bitumen Content Determination with Compensation for Insoluble Bitumen
The prediction error from the MIR-PLSR calibration is exaggerated when the results are compared to those provided by Soxhlet extraction as the reference method because in the latter case only the fraction of bitumen that is soluble in the extraction solvent is determined as the bitumen content. Therefore, the Soxhlet extraction underestimates the total bitumen content in tailing soil since the insoluble fraction is still trapped in the tailing soil and is not accounted for.

In contrast, the MIR-PLSR prediction includes all the bitumen that gives rise to C-H absorption in the MIR spectrum of the sample.

Table 6-8. Total bitumen content determination by using MIR-PLSR prediction compared to Soxhlet extraction with compensation for insoluble bitumen

Raw tailing soil	Bitumen content by Soxhlet extraction with compensation for bitumen residues (wt%)	Bitumen content by MIR-PLSR (wt%)	Prediction difference (wt%)	Prediction error %
2-MeTHF with 0.60 % residues				
Replicate-1	7.02	7.18	0.16	2.28
Replicate-2	7.00	6.90	0.10	1.43
Replicate-3	7.09	7.22	0.13	1.83
Average ± SD	7.04 ± 0.04	7.10 ± 0.14	0.13 ± 0.02	1.85 ± 0.35
Toluene with 0.59 % residues				
Replicate-1	6.53	7.35	0.82	12.56
Replicate-2	6.46	7.06	0.60	9.29
Replicate-3	6.57	7.24	0.67	10.20
Average ± SD	6.52 ± 0.05	7.22 ± 0.12	0.70 ± 0.09	10.68 ± 1.37
DCM with 0.45% residues				
Replicate-1	5.97	7.12	1.15	19.26
Replicate-2	5.88	7.02	1.14	19.39
Replicate-3	6.08	7.15	1.07	17.51
Average	5.98 ± 0.08	7.10 ± 0.06	1.12 ± 0.04	18.75 ± 0.82
Average among 9 extracts	6.44 ± 0.46	7.14 ± 0.13	0.65 ± 0.41	10.42 ± 6.97

This situation is made evident by the ATR-FTIR spectra of tailing soils after 3.5-h Soxhlet extraction in Figure 6-7, where a small hydrocarbon band in the region between 2990 and 2750 cm^{-1} is observed. Therefore, this small fraction of non-extractable bitumen should be added to the total bitumen content determined by Soxhlet extraction. According to the results of Section 6.3.2.2.2, the non-extractable bitumen fraction is predicted using the MIR-PLSR calibration as 0.60, 0.59, and 0.45 wt% for 2-MeTHF, toluene and DCM extraction respectively.

After the insoluble fraction is incorporated into the total bitumen content obtained by Soxhlet extraction, the MIR-PLSR prediction error relative to the Soxhlet results decreases. The difference and error of the MIR-PLSR prediction decrease to 0.13 wt% and 1.85 % relative to 2-MeTHF Soxhlet extraction; the corresponding values relative to toluene Soxhlet extraction are 0.88 wt% difference and 10.68 % error and those relative to DCM Soxhlet extraction are 1.16 wt% difference and 18.75 % error (Table 6-8; Fig. 6-11). Although the MIR-PLSR predictions are still higher by an average of 0.65 wt% than the values obtained by the Soxhlet reference method, the accuracy of the MIR-PLSR method for fast and direct bitumen determination is acceptable, and this method provides a high degree of reproducibility.
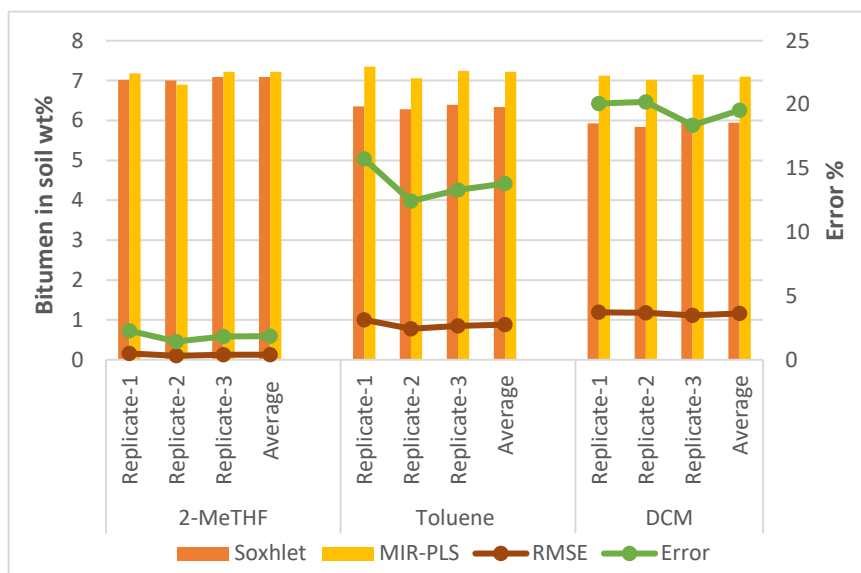
Fig. 6-11. Bitumen determination by Soxhlet extraction (after compensation for residues) and by MIR-PLSR prediction

6.3.3. Characterization of Bitumen Recovered from Room-Temperature and Soxhlet Extraction by ATR-FTIR Spectroscopy

6.3.3.1. General Analysis of the Soluble Fraction

6.3.3.1.1. Bitumen Recovered from Room-Temperature Extraction

The ATR-FTIR spectra of room-temperature-extracted and Soxhlet-extracted bitumen obtained by extraction with the three solvents examined in this study are presented in Figure 6-12. The bands are identified and assigned based on the functional group assignment table (Table 6-9).

Table 6-9. Bitumen band assignments
(Yut and Zofka 2011; Odebunmi and Olaremu 2015)

Wavenumber (cm^{-1})	Peaks observed in the spectra (cm^{-1})	Assignment
3700 – 3580	Sharp band	Hydroxyl -OH (free) stretching
3550 – 3220	Broad band	Hydroxyl -OH (intermolecular H-bonded) stretching
3080 – 3000	3060	Aromatic C-H stretching
2953 – 2850	2953, 2920, 2854	Methyl -CH_3 and methylene -CH_2 stretching
1705 – 1680	1702	Carbonyl C=O stretching
1650 – 1580	1602	C=C bonds and aromatic ring stretching; Hydroxyl -OH bending
1455 – 1450	1455	-CH_3 and -CH_2 bending
1380 – 1370	1375	-CH_3 and cyclic -CH_2 vibrations
1250 – 1230	1230	Phenolic C-O bond
1030	1030	Sulfoxide S=O stretching; Aromatic amines
980 – 890		C=C bonds
900 – 700	866, 811, 748	Aromatic out-of-plane deformation
725 – 650		Aliphatic chains longer than C4; Aliphatic halogen compounds

The MIR spectra show a combination of aliphatic and aromatic structures. In the room-temperature-extracted bitumen spectra (Fig. 6-12-a), the spectral profiles of the bitumen extracted by the three solvents are similar, where the absorption bands are observed in the same location to within ± 1 cm^{-1}. In addition to the bands due to aliphatic and aromatic moieties, bands due to C=C, C=O, and S=O bonds are also found in the spectra, but their relative intensity is low. The region below 900 cm^{-1} is considered the fingerprint region and it provides detailed information related to the aromatic structures and the aliphatic chain length. Apart from the hydrocarbon fraction, the presence of clay minerals is also observed from the spectra, with a small band located at 3670 cm^{-1}, representing the O-H bond in the clay structure. The presence of clay in bitumen is due to their strong attachment to each other; therefore, clay enters into the solvent extracts along with bitumen. However, since clay is hydrophilic but the solvent is hydrophobic, not much clay is able to transit to the organic layer, only clay strongly adsorbed to bitumen can.

6.3.3.1.2. Bitumen Recovered by Soxhlet Extraction

In the case of the Soxhlet-extracted bitumen, aliphatic chains are the main structural component, as indicated by the strong aliphatic C-H band in the region 2953 – 2850 cm^{-1} (Fig. 6-12-b). Carbonyl and aromatic bonds are also observed in the spectra. In general, the toluene or DCM Soxhlet-extracted bitumen has a similar spectral profile to the bitumen extracted by these solvents at room temperature. However, in the case of the bitumen extracted by 2-MeTHF, the spectral profile following Soxhlet extraction differs from that following room-temperature extraction.

In the spectrum of the 2-MeTHF Soxhlet-extracted bitumen, a set of new bands (highlighted by the yellow box) is observed in the region below 1300 cm^{-1}, which is the fingerprint region of the MIR spectrum. In this region between 1300 and 1000 cm^{-1}, the bands in the spectrum are mainly due to S=O, C-N, O-H, and C-O bonds. The new bands indicate that the structure and the composition of the bitumen extract after extraction in boiling 2-MeTHF is changed.

(a)

204
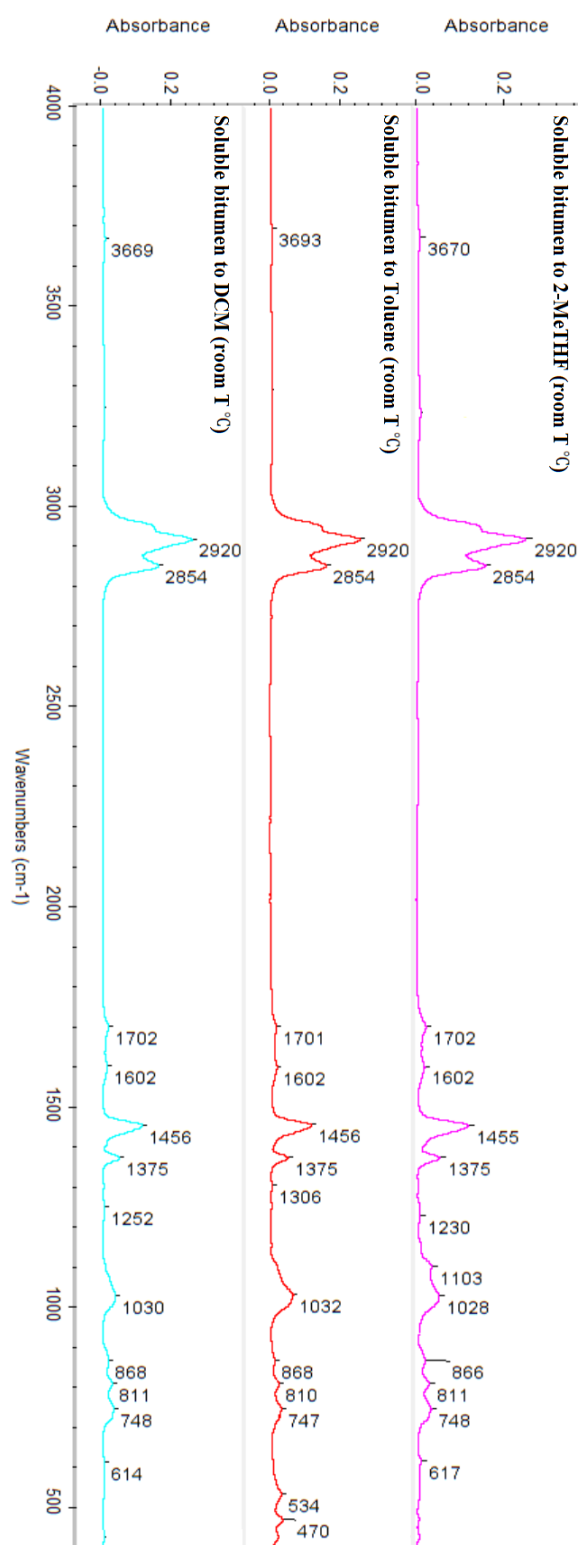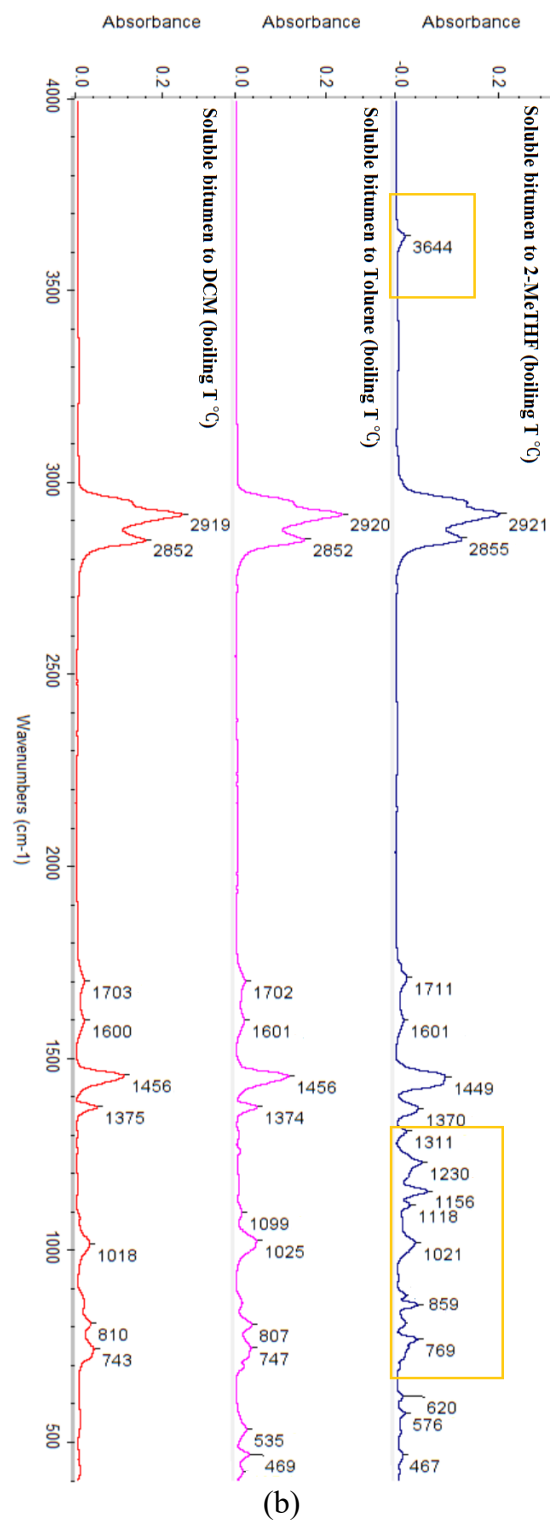
Fig. 6- 12. ATR-FTIR spectra of bitumen soluble in 2-MeTHF, toluene or DCM under (a) room-temperature and (b) Soxhlet extraction conditions

205

In general, the changes may be attributed to the formation of C-O single bonds, which have characteristic stretching bands located at 1320 – 1210 cm^{-1}, 1300 – 1000 cm^{-1}, and 1100 – 1040 cm^{-1} (Table 6-10). In addition, a sharp band at 3644 cm^{-1} is observed, which is due to the free O-H bond stretching. However, in the case of the bitumen extracted by 2-MeTHF under room-temperature conditions, no such changes in composition of the extract are indicated by the spectrum.

Table 6-10. Band positions for C-O stretching vibrations

Wavenumber (cm^{-1})	Peaks observed in the spectra (cm^{-1})	Assignment
1320 – 1210 (two peaks)	1311, 1230	C-O stretching
1100 – 1040	1021	

6.3.3.2. Analysis of Aliphatic Bands in the 300 – 2800 cm^{-1} Region

6.3.3.2.1. General Observations

As mentioned in the previous chapter, the region between 3000 and 2800 cm^{-1} is characteristic of bitumen, which is mainly composed of hydrocarbons. Deconvolution was performed to enhance the resolution of the bands in this region. This assists in the determination of the positions, widths and areas of the aliphatic bands, which helps in elucidation of the structure of the bitumen based on the relationship between the intensities of the absorptions due to methyl (-CH$_3$) and methylene (-CH$_2$) groups.

The deconvolved bands of bitumen from different extractions are presented in Figure 6-13. These spectra show no differences in band positions, but only in their intensities. In the case of the room-temperature extraction, the composition of the aliphatic moiety of the bitumen extracted by different solvents is almost the same, as indicated by the identical position, shape and intensity of the deconvolved bands of bitumen (Fig. 6-13-a). In contrast, in the case of the Soxhlet extraction, the deconvolved bands change in intensity among the three solvents, where

the change is greatest in the case of the bitumen extracted by 2-MeTHF (Fig. 6-134-b). This indicates that the composition of the aliphatic moiety in 2-MeTHF Soxhlet extracts is dramatically different from that in toluene and DCM Soxhlet extracts.
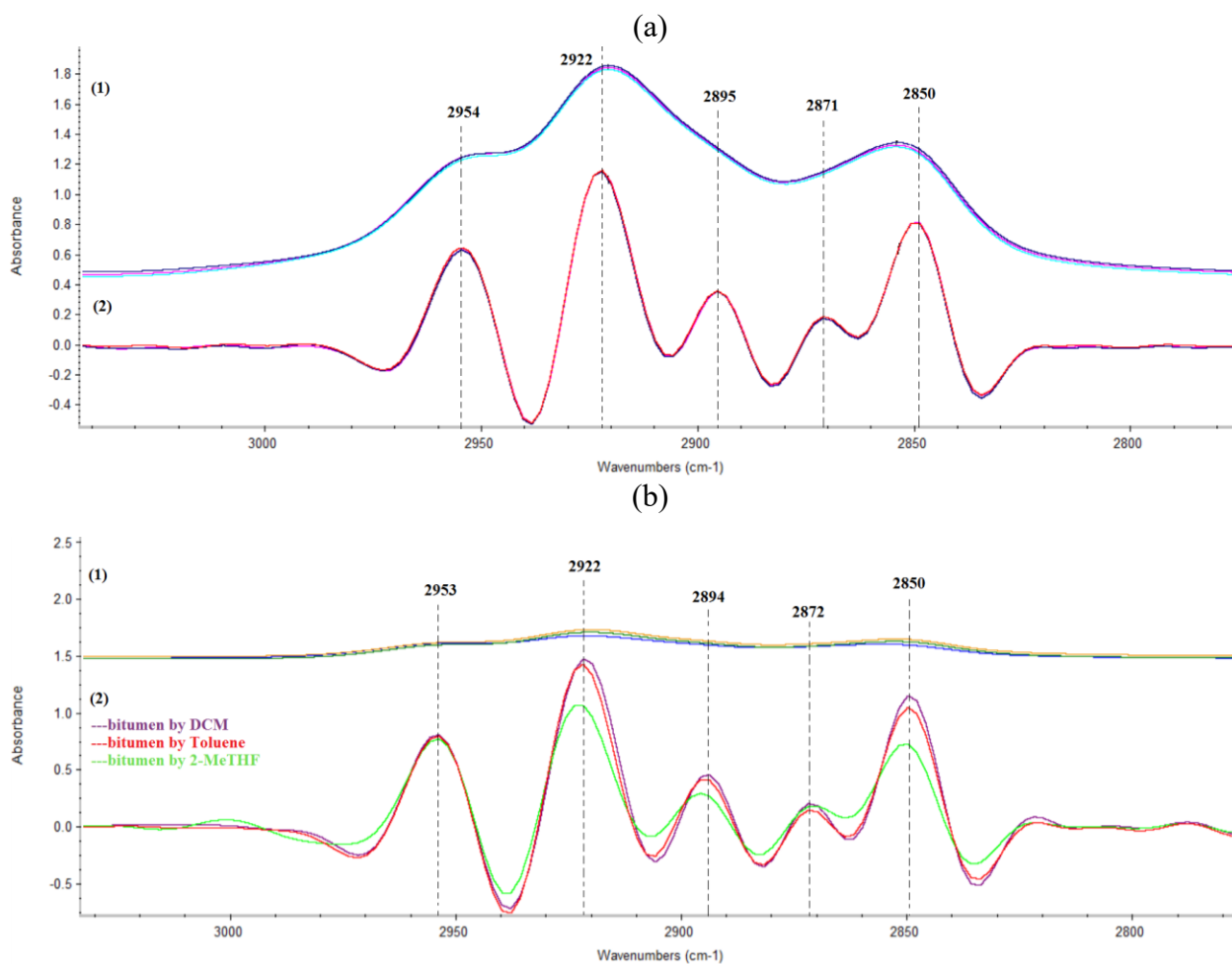
Fig. 6- 13. Deconvolution of the region from 3000 to 2800 cm^{-1}; (1) original spectra; (2) deconvolved bands of bitumen extracted by (a) room temperature extraction; (b) Soxhlet extraction

6.3.3.2.2. Methyl-to-Methylene Index

To further study the structure of the aliphatic moiety, the ratio of the bands at 2954 cm^{-1} and 2922 cm^{-1} was calculated. These two bands are assigned to the methyl and methylene groups (Table 6-11) and are selected due to their strong intensity. The ratio of these two bands provides information on the aliphatic-chain length and the degree of branching of the bitumen. If the ratio has low values, the structure is dominated by long and straight aliphatic chains. On the other hand, higher values of the ratio indicate shorter and more branched aliphatic chains.

Table 6-11. Mid-infrared band assignment in the region between 3000 and 2800 cm^{-1} after band convolution (Socrates 2004)

Wavenumber (cm^{-1})	Assignment
2953	Asymmetric stretching of -CH$_3$
2922	Asymmetric stretching of -CH$_2$
2894	Stretching of -CH
2872	Symmetric stretching of -CH$_3$
2850	Symmetric stretching of -CH$_2$

The values of this ratio for the bitumen extracted by the three solvents under room-temperature and Soxhlet extraction conditions are presented in Table 6-12. In the case of the bitumen extracted at room temperature by the three solvents, the ratio values are almost identical, which indicates that the structure of the hydrocarbon soluble in these three solvents is identical. However, the ratio values for the bitumen from the Soxhlet extraction differ among the three extraction solvents and are also all different from the values for the bitumen extracted at room temperature, the 2-MeTHF-Soxhlet extracted bitumen has the highest A$_{2954}$/A$_{2923}$ value, which indicates that it is composed of shorter and more branched aliphatic chains. The DCM-Soxhlet extracted bitumen has the lowest ratio value, indicating that it has fewer -CH$_3$ terminals. The toluene-Soxhlet extracted bitumen has a slightly lower ratio value than the bitumen from the toluene room-temperature extraction.

Table 6-12. A_{2954}/A_{2923} index of bitumen extracted by different solvents under different extraction conditions

Extraction solvent	A_{2954} (-CH$_3$)	A_{2923} (-CH$_2$)	A_{2954}/A_{2923} (-CH$_3$/-CH$_2$)
Room-Temperature Extraction			
2-MeTHF	16.97	22.80	0.75
Toluene	16.79	22.85	0.74
DCM	16.96	23.21	0.73
Soxhlet Extraction			
2-MeTHF	18.44	22.57	0.82
Toluene	21.57	30.73	0.70
DCM	21.16	32.01	0.66

6.3.3.3. Structural Comparison between Soluble and Less-Soluble Fractions by ATR-FTIR Spectroscopy

As mentioned in Sections 6.3.2.1 and 6.3.2.2, bitumen cannot be totally extracted under room-temperature conditions; about 80 – 90% of total bitumen was extracted depending on the type of extraction solvent employed. This fraction is considered the soluble fraction. When the bitumen residues were further extracted by Soxhlet extraction, an additional 6 – 11% of bitumen was extracted, which is considered the less-soluble fraction, and the remaining bitumen trapped in the soil is considered the insoluble fraction. To study how the chemical structure affects the solubility, ATR-FTIR spectroscopy was used to study the structural differences between the less-soluble and insoluble fractions. The ATR-FTIR spectra and the variance between the two fractions are presented in Figures 6-14, 6-15, and 6-16.

6.3.3.3.1. Soluble and Less-Soluble Fractions of Toluene Extracts

The soluble and less-soluble fractions extracted by toluene have the identical spectral profile in terms of the band positions of the aliphatic hydrocarbon bands in the regions 2953 – 2850 cm^{-1}

and 1455 – 1370 cm^{-1} (Fig. 6-14). However, they vary in intensity, where the soluble fraction contains a higher amount of aliphatic groups compared to the less-soluble fraction. To better understand the difference in branching of the aliphatic structure, the A_{2954}/A_{2923} index was calculated from the band area measurements after the band deconvolution process (Table 6-13). The two fractions show very similar A_{2954}/A_{2923} index values, indicating a similar extent of branching. On the other hand, the spectra show higher variance in the band at 1706 cm^{-1} and in the fingerprint region below 1350 cm^{-1}. The higher absorption intensity of the less-soluble fraction in these regions suggests a higher content of carbonyl and aromatic C=C bonds, which increases the polarity and consequently decreases solubility in the non-polar toluene solvent.

Table 6-13. A_{2954}/A_{2923} index of soluble and less-soluble
bitumen extracted by different solvents

Solvent	Bitumen fraction	A_{2954}	A_{2923}	A_{2954}/A_{2923}
2-MeTHF	Soluble	12.22	15.25	0.80
	Less-soluble	14.84	9.63	1.54
Toluene	Soluble	14.69	19.85	0.74
	Less-soluble	12.79	18.04	0.71
DCM	Soluble	14.12	20.23	0.70
	Less-soluble	13.18	20.66	0.64

Fig. 6- 14. ATR-FTIR spectra of soluble and less-soluble bitumen extracted by toluene room-temperature and Soxhlet extraction, respectively, and their variance

6.3.3.3.2. Soluble and Less-Soluble Fractions of DCM Extracts

In the case of the fractions obtained by DCM, similar results to those described above for toluene extraction were found, where the soluble fraction has a higher amount of aliphatic groups than the less-soluble fraction (Fig. 6-15). In addition, the less-soluble fraction contains a higher amount of C=O groups and also contains more hydrocarbon with longer carbon chains, as indicated by the bands below 535 cm^{-1} in the spectrum of the less-soluble fraction. Regarding the structure of the aliphatic moiety, the less soluble fraction has a lower value of the A_{2954}/A_{2923} index, indicating longer aliphatic chains and less branched structure. However, this structural difference between the two fractions is not considered significant.

6.3.3.3.3. Soluble and Less-Soluble Fractions of 2-MeTHF Extracts

As mentioned in Section 6.3.3.1, the structure of the bitumen obtained by 2-MeTHF Soxhlet extraction was different from that of the bitumen from the room-temperature extraction. Therefore, it is not comparable between the soluble bitumen extracted under room temperature condition and the structurally changed less-soluble bitumen obtained from Soxhlet extraction. Hence, both the soluble and the less-soluble fractions of bitumen used for comparison are from Soxhlet extraction (Fig. 6-16). The less-soluble fractions were Soxhlet extracted from the samples pre-treated by room temperature extraction, where the soluble fractions were removed.

In general, these two fractions show similar spectral profiles apart from the band intensity. The less-soluble fraction has higher C=O, C-O, and C=C band intensities. Furthermore, the profile of the aliphatic hydrocarbon band is very different between the two fractions. In terms of the values of the A_{2954}/A_{2923} index, the value for the less-soluble fraction is almost double the value for the soluble fraction (Table 6-13). This suggests that the less-soluble fraction is composed of a much higher amount of branched aliphatic chains. To further understand in what manner, the aliphatic structure has changed in the boiling 2-MeTHF environment, the soluble fractions obtained from the Soxhlet extraction are compared to those obtained from room-temperature extraction. The value of the A_{2954}/A_{2923} index for the Soxhlet-extracted bitumen, which is 0.80, is higher than the value for the room-temperature extracted bitumen, which is 0.75 (Table 6-12). This suggests that the boiling condition favours branching, or possibly the breaking of a long aliphatic chain into smaller segments, causing the higher amount of -CH$_3$ groups. Similar reactions occurred more

extensively in the less-soluble fraction during the Soxhlet extraction, resulting in a high A_{2954}/A_{2923} index value (1.54).
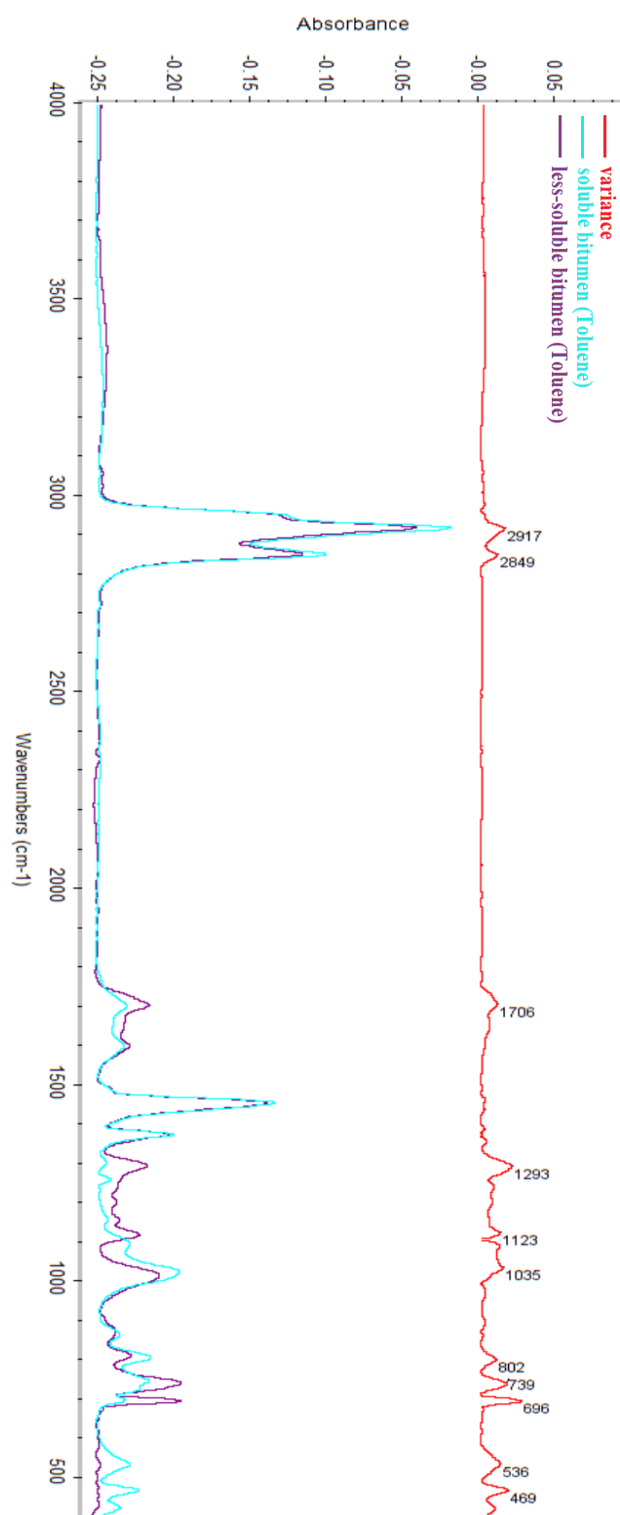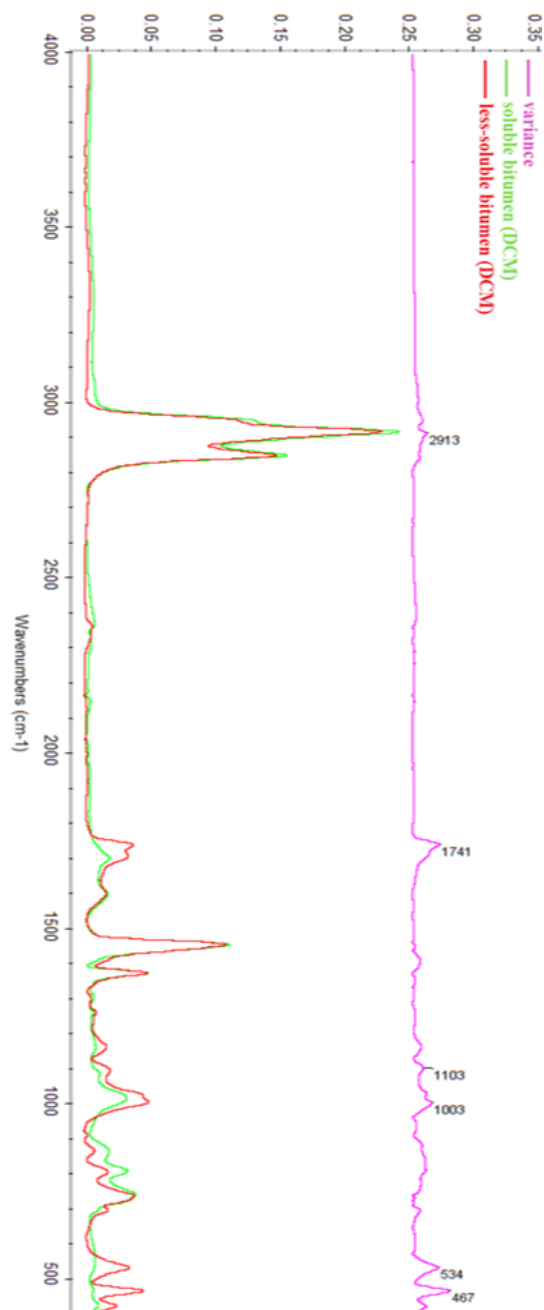

Fig. 6- 15. ATR-FTIR spectra of soluble and less-soluble bitumen extracted by DCM room-temperature and Soxhlet extraction, respectively, and their variance
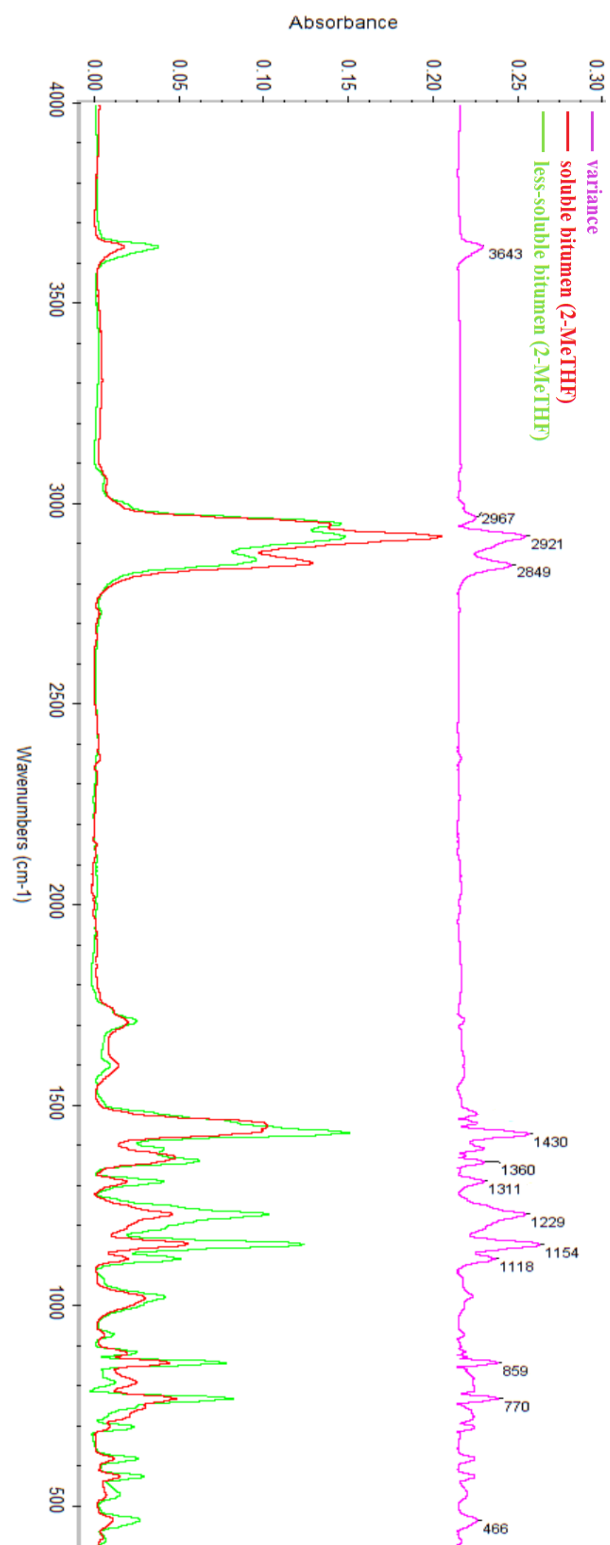
Fig. 6- 16. ATR-FTIR spectra of soluble and less-soluble bitumen
extracted by 2-MeTHF Soxhlet extraction and their variance

6.3.4. Characterization of Bitumen from Soxhlet Extraction by APCI-MS

6.3.4.1. APCI-MS Spectral Information of 2-Me-SEB and T-SEB

The DIP-APCI mass spectra of two bitumen samples are presented in Figure 6-17. The average resolution is 10176 and 9324 in the case of 2-MeTHF- and toluene-Soxhlet extracted bitumen between m/z 100 and 3000. The 2-Me-SEB and T-SEB MS spectra are presented on the identical intensity scale. The mass range for the 2-MeTHF-Soxhlet extracted bitumen (2-Me-SEB) is from $100 < m/z < 1050$, centered at m/z 615. Similarly, the mass range for the toluene-Soxhlet extracted bitumen (T-SEB) is from $105 < m/z < 1522$, centered at m/z 680. The average masses of 2-Me-SEB and T-SEB are 482 and 607 Da, respectively. The average mass is calculated using the following equation (Kim et al., 2011),

$$Average\ Mass = \frac{\sum_i M_i I_i}{\sum_i I_i} \dots\dots\dots\dots\dots\dots\dots\dots\dots\dots\dots\dots\dots\dots\dots\dots (6\text{-}7)$$

where M_i is the mass of peak i, and I_i is the relative intensity of peak i.

To reduce the amount of information, those ion fractions with intensity greater than 6000, which account for 2% of the total ion fractions, were selected and studied. In particular, the ion fractions with m/z 411.39 or 411.40 in both spectra were removed, as they originated with the glass capillary which was used as the sample introduction accessory. The potential formula of each ion fraction with the lowest mass error is presented in Table 6-14.
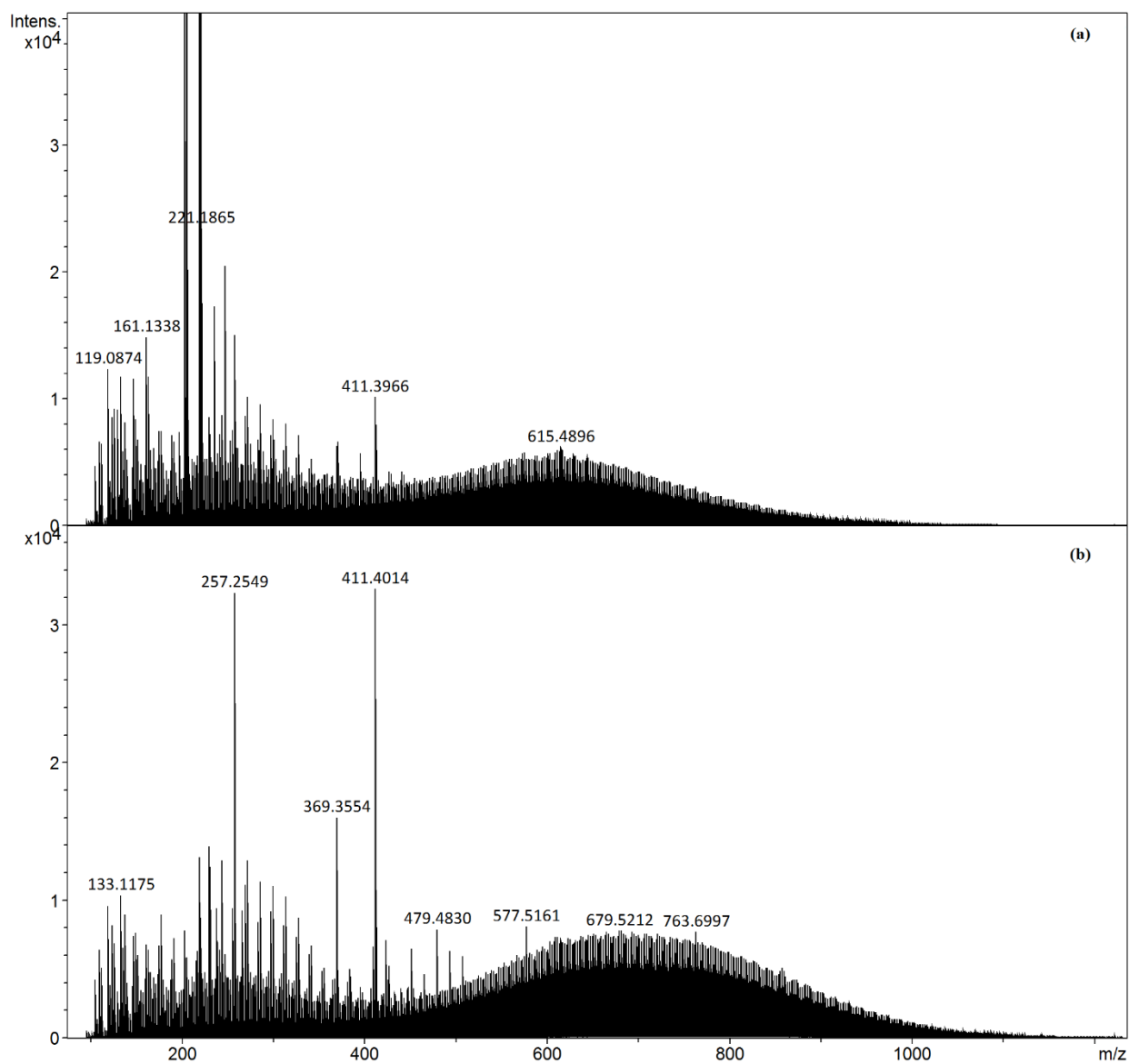
Fig. 6- 17. DIP-APIC mass spectra of bitumen: (a) 2-Me-SEB and (b) T-SEB

Table 6-14. Chemical information on the ion fractions obtained from two bitumen samples, 2-Me-SEB and T-SEB

2-Me-SEB				T-SEB			
Measured m/z	Ion formula	Error (ppm)	Intensity (%)	Measured m/z	Ion formula	Error (ppm)	Intensity (%)
119.0878	C_9H_{11}	14.482	11.1	215.1563	$C_{14}H_{19}N_2$	6.862	17.2
129.0556	$C_6H_9O_3$	3.338	8.2	219.1831	$C_{11}H_{25}NO_3$	1.568	40.3
133.1024	$C_{10}H_{13}$	5.068	10.5	231.2198	$C_{13}H_{29}NO_2$	0.126	38.3
147.0658	$C_6H_{11}O_4$	0.45	7.2	243.1868	$C_{16}H_{23}N_2$	2.781	35.2
147.118	$C_{11}H_{15}$	4.245	10.4	255.1862	$C_{17}H_{23}N_2$	0.299	28.5
149.0237	$C_8H_5O_3$	1.134	7.5	257.2018	$C_{17}H_{25}N_2$	0.102	41.5
161.1339	$C_{12}H_{17}$	5.427	13.3	257.2544	$C_{13}H_{31}N_5$	13.789	99.1
163.1133	$C_{11}H_{15}O$	6.191	10.6	269.2013	$C_{18}H_{25}N_2$	1.76	34.3
197.1202	$C_{14}H_{15}N$	6.243	6.6	271.2169	$C_{18}H_{27}N_2$	1.932	39.6
203.1807	$C_{15}H_{23}$	3.565	46	283.2164	$C_{19}H_{27}N_2$	3.615	25.8
204.184	$C_{10}H_{24}N_2O_2$	1.087	5.9	285.2321	$C_{19}H_{29}N_2$	3.415	34.8
205.1602	$C_{14}H_{21}O$	4.678	74.8	297.2316	$C_{17}H_{31}NO_3$	4.058	28.3
206.1633	$C_9H_{22}N_2O_3$	1.249	10	299.2472	$C_{17}H_{33}NO_3$	3.863	34
219.1754	$C_{15}H_{23}O$	2.325	100	313.2625	$C_{18}H_{35}NO_3$	2.573	31.5
220.183	$C_{15}H_{24}O$	1.293	93	325.2616	$C_{19}H_{35}NO_3$	0.289	22.6
221.1865	$C_8H_{23}N_5O_2$	5.99	21	327.2777	$C_{19}H_{37}NO_3$	1.088	26.8
229.1621	$C_{13}H_{25}OS$	2.23	7.7	339.2773	$C_{20}H_{37}NO_3$	0.13	18.7
235.1683	$C_{13}H_{21}N_3O$	0.69	15.5	341.2929	$C_{20}H_{39}NO_3$	0.276	20.7
241.1801	$C_{14}H_{25}O_3$	1.118	6.5	353.2926	$C_{21}H_{39}NO_3$	1.116	14.9
243.1781	$C_{14}H_{27}OS$	0.663	7.9	355.3083	$C_{21}H_{41}NO_3$	0.969	15.7
246.9696	$C_3H_7N_2O_7S_2$	0.539	18.3	359.367	$C_{29}H_{47}$	1.964	11.4
255.1777	$C_{15}H_{27}OS$	2.199	6.8	361.261	$C_{13}H_{33}N_{10}S$	0.102	7.4

Table 6-14. Cont.

2-Me-SEB				T-SEB			
Measured m/z	Ion formula	Error (ppm)	Intensity (%)	Measured m/z	Ion formula	Error (ppm)	Intensity (%)
257.1934	$C_{15}H_{29}OS$	1.988	8.8	363.2763	$C_{20}H_{35}N_4O_2$	0.822	9.1
257.2468	$C_{14}H_{31}N_3O$	0.34	13.5	365.2912	$C_{20}H_{37}N_4O_2$	1.236	13.2
259.1922	$C_{14}H_{27}O_4$	0.277	6.9	367.3081	$C_{22}H_{41}NO_3$	1.482	13.3
269.193	$C_{14}H_{27}N_3S$	1.603	7.8	369.3554	$C_{24}H_{49}S$	0.263	49.1
271.209	$C_{16}H_{31}OS$	2.07	9.1	381.3238	$C_{23}H_{43}NO_3$	1.296	12.6
283.2087	$C_{15}H_{29}N_3S$	1.7	6.1	409.3839	$C_{30}H_{49}$	1.156	20.5
285.2242	$C_{15}H_{31}N_3S$	1.162	8.6	419.3372	$C_{22}H_{41}N_7O$	0.141	9.8
297.2244	$C_{16}H_{31}N_3S$	1.788	6.4	433.3538	$C_{25}H_{45}N_4O_2$	1.042	10.1
299.2409	$C_{18}H_{35}OS$	0.129	7.5	447.3678	$C_{24}H_{53}N_3S_2$	0.648	11.2
301.0405	$C_7H_7N_7O_7$	0.65	6.1	461.3831	$C_{24}H_{51}N_3O_5$	0.495	10.3
311.2404	$C_{19}H_{35}OS$	1.483	5.4	545.4104	$C_{36}H_{53}N_2O_2$	0.557	14.3
325.2556	$C_{18}H_{35}N_3S$	1.326	4.8	547.4241	$C_{26}H_{57}N_7O_3S$	0.474	13.8
327.2714	$C_{18}H_{37}N_3S$	1.776	6.4	559.3379	$C_{30}H_{49}N_5OS_2$	0.085	16.1
353.2873	$C_{22}H_{41}OS$	1.448	3.4	561.3525	$C_{29}H_{47}N_5O_6$	0.239	17.3
355.3027	$C_{20}H_{41}N_3S$	1.635	3.6	563.3667	$C_{27}H_{55}N_4O_4S_2$	0.404	16.9
371.3158	$C_{22}H_{43}O_4$	0.902	6	565.4696	$C_{32}H_{61}N_4O_4$	0.563	13
413.3771	$C_{27}H_{47}N_3$	0.245	7.2	573.4403	$C_{36}H_{63}NS_2$	0.188	17.6
459.3905	$C_{24}H_{51}N_4O_4$	1.156	2.5	574.3554	$C_{31}H_{50}N_4O_4S$	0.214	12.1
461.3168	$C_{30}H_{41}N_2O_2$	0.008	3.3	575.368	$C_{30}H_{57}NO_5S_2$	0.321	18.3
461.379	$C_{33}H_{49}O$	1.428	2.8	575.4574	$C_{38}H_{59}N_2O_2$	0.442	17.1
463.3328	$C_{23}H_{43}N_8S$	0.732	3.2	577.3822	$C_{28}H_{57}N_4O_4S_2$	0.091	17.9
465.3467	$C_{28}H_{43}N_5O$	0.131	3	577.5161	$C_{31}H_{63}N_9O$	0.939	24.9

Table 6-14. Cont.

2-Me-SEB				T-SEB			
Measured m/z	Ion formula	Error (ppm)	Intensity (%)	Measured m/z	Ion formula	Error (ppm)	Intensity (%)
497.4096	$C_{30}H_{51}N_5O$	0.48	3.4	579.397	$C_{34}H_{53}N_5OS$	0.142	18.1
505.3786	$C_{25}H_{53}N_4O_4S$	0.301	3.7	581.4122	$C_{34}H_{63}NS_3$	0.109	19.1
509.4088	$C_{23}H_{55}N_7O_3S$	0.178	3.5	589.4705	$C_{35}H_{57}N_8$	0.202	17.8
511.4254	$C_{31}H_{53}N_5O$	0.76	3.8	591.4869	$C_{29}H_{65}N_7O_3S$	0.101	17.3
519.3945	$C_{26}H_{55}N_4O_4S$	0.189	4	593.5002	$C_{34}H_{65}N_4O_4$	0.643	15.6
523.4243	$C_{24}H_{57}N_7O_3S$	0.114	3.6	595.4281	$C_{28}H_{59}N_4O_9$	0.176	20.4
525.3505	$C_{24}H_{53}N_4O_4S_2$	0.614	4.1	601.4723	$C_{38}H_{59}N_5O$	0.563	19.3
525.4405	$C_{32}H_{55}N_5O$	0.307	3.7	607.4292	$C_{30}H_{63}N_4O_4S_2$	0.209	21.6
537.4396	$C_{32}H_{59}NO_5$	0.514	3.9	609.4439	$C_{29}H_{61}N_4O_9$	0.075	22.6
539.3661	$C_{31}H_{49}N_5OS$	0.59	4.3	611.4585	$C_{35}H_{65}NO_5S_1$	0.254	22.6
553.3819	$C_{26}H_{57}N_4O_4S_2$	0.402	4.6	613.4724	$C_{25}H_{61}N_{10}O_7$	0.113	21.2
567.4866	$C_{34}H_{65}NO_5$	0.574	4.2	615.4881	$C_{33}H_{67}N_4O_4S$	0.329	21.9
573.4412	$C_{30}H_{61}N_4O_4S$	0.265	5.1	617.504	$C_{33}H_{69}N_4O_4S$	0.077	21.5
575.4573	$C_{30}H_{63}N_4O_4S$	0.517	5.2	627.4866	$C_{39}H_{65}NO_5$	0.519	21
579.4877	$C_{36}H_{61}N_5O$	0.153	4.7	629.5016	$C_{38}H_{61}N_8$	0.507	21.2
581.5028	$C_{36}H_{71}NS_2$	0.013	4.7	631.5158	$C_{37}H_{75}O_3S_2$	0.059	20.1
587.4572	$C_{31}H_{63}N_4O_4S$	0.344	5	639.4886	$C_{35}H_{67}N_4O_4S$	0.465	22.5
603.488	$C_{32}H_{67}N_4O_4S$	0.501	5.1	643.5176	$C_{40}H_{69}NO_5$	0.04	21.9
611.4596	$C_{36}H_{61}N_5OS$	0.135	5.4	645.4466	$C_{35}H_{59}N_5O_6$	0.101	23.1
613.4742	$C_{35}H_{67}NO_5S$	0.334	5.5	647.4605	$C_{33}H_{67}N_4O_4S_2$	0.196	22.7
615.4896	$C_{34}H_{63}N_8S$	0.065	5.6	659.5482	$C_{32}H_{71}N_{10}O_2S$	0.026	21
617.5046	$C_{41}H_{65}N_2O_2$	0.007	5.4	681.5356	$C_{46}H_{69}N_2O_2$	0.447	23.9

Table 6-14. Cont.

2-Me-SEB				T-SEB			
Measured m/z	Ion formula	Error (ppm)	Intensity (%)	Measured m/z	Ion formula	Error (ppm)	Intensity (%)
621.5336	$C_{31}H_{71}N_7O_3S$	0.499	4.6	695.5512	$C_{39}H_{75}N_4O_4S$	0.428	23.3
623.46	$C_{37}H_{61}N_5OS$	0.51	4.7	707.5525	$C_{42}H_{77}NO_5S$	0.36	23.4
623.5492	$C_{38}H_{73}NO_5$	0.552	4.5	709.5668	$C_{40}H_{77}N_4O_4S$	0.074	23.2
627.4029	$C_{31}H_{57}N_5O_6S$	0.088	3.3	713.5959	$C_{45}H_{79}NO_5$	0.106	22.8
627.4884	$C_{34}H_{67}N_4O_4S$	0.156	4.8	721.5682	$C_{43}H_{79}NO_5S$	0.422	23.2
627.5789	$C_{36}H_{75}N_4O_4$	0.108	3.3	727.6117	$C_{48}H_{81}NO_5$	0.31	22.6
629.4172	$C_{29}H_{57}N_8O_5S$	0.1	3.6	763.6997	$C_{55}H_{89}N$	0.259	23.7
629.5033	$C_{40}H_{63}N_5O$	0.061	5				

6.3.4.2. Distribution of Oxygen Atoms in 2-Me-SEB and T-SEB

The content of the main elements composing bitumen is presented in Table 6-15. Both 2-Me-SEB and T-SEB are mainly composed of C (80%) and H (10%) atoms in a similar percentage. However, the O content in 2-Me-SEB is almost doubled (6.0%) compared to the O content in T-SEB (3.7%). Both bitumen samples are low in N and S content, which is less than 1%.

Table 6-15. Elemental analysis of 2-Me-SEB and T-SEB

Sample	C %	H %	C/H	O %	N %	S %
2-Me-SEB	80.06	9.95	0.67	6.03	< 1	< 1
T-SEB	83.34	9.88	0.70	3.74	< 1	< 1

The distribution of oxygen atoms in 2-Me-SEB and T-SEB is clearly indicated by plotting the number of oxygen atoms against the number of carbon atoms (Fig. 6-18). The numbers of

oxygen and carbon atoms were obtained from the ion formulas listed in Table 6-14. By observing the distribution of the points representing each ion fraction, it can be seen that the portion of the plot corresponding to 0 – 20 carbon atoms (Fig. 6-18, upper left) is dominated by the orange points, which indicates that 2-Me-SEB is rich in small-size fractions composed of a small number of carbon atoms (< 15) with 1 to 7 oxygen atoms. The blue points representing fractions from T-SEB are not found in this portion of the plot but start to show up when the number of carbon atoms is greater than 15. In the case of the medium-size fractions containing between 21 and 35 carbon atoms, both 2-Me-SEB and T-SEB show similar oxygen distributions. These fractions mainly contain 0 – 4 oxygen atoms, while there is a small group of fractions containing up to 10 oxygen atoms (Fig. 6-18, upper right). In the case of the large-size fractions composed of up to 50 carbon atoms, T-SEB contains more such fractions than 2-Me-SEB. These fractions also contain 1 to 5 oxygen atoms (Fig. 6-18, lower left).
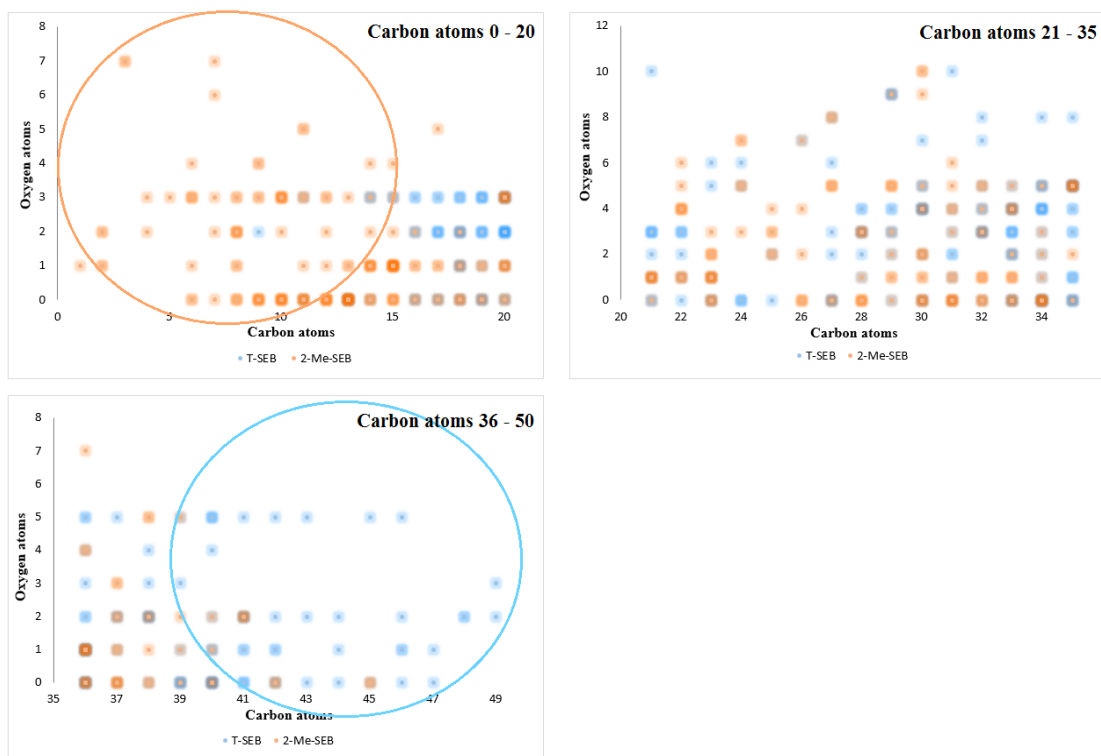
Fig. 6-18. Plots of number of oxygen atoms as a function of number of carbon atoms for ion fractions from APIC-MS spectra of 2-Me-SEB (orange) and T-SEB (blue)

6.3.4.3. Alkylation and Aromaticity Distribution in 2-Me-SEB and T-SEB

According to the number of atoms provided in the potential chemical formula, the double bond equivalents (DBEs), carbon numbers, and the extent of alkylation were determined. DBE is the sum of the number of rings and double bonds calculated from the molecular formula using the following equation (Wang, Robbins et al. 2004),

$$DBE = c - \frac{1}{2}h + \frac{1}{2}n + 1 \; (for \; C_cH_hN_nO_oS_s) \; \dots\dots\dots\dots\dots\dots\dots\dots\dots \; (6\text{-}8)$$

The average carbon numbers of 2-Me-SEB and T-SEB are 17.2 and 26.8, respectively. The average DBEs of 2-Me-SEB and T-SEB are 3.9 and 4.7, respectively. The average carbon numbers and average DBEs are calculated using equations similar to equation (6-7), where the masses of the peaks in the equation are replaced by the carbon numbers and DEB values, respectively. The compositional differences between 2-Me-SEB and T-SEB can be visualized by color-coded iso-abundance plots of DBE value versus carbon number (Fig. 6-19). The x-axis is the carbon number, which indicates the extent of alkylation, the y-axis indicates the aromaticity and the third dimension is the relative intensity (I%) represented by color.

According to equation (6-8), the simplest aromatic compound, benzene (C_6H_6), has a DBE value of 4. Therefore, the non-aromatic compounds have DBE values between 0 and 3. The relative intensity of compounds with DBE values between 0 and 3 is relatively high in T-SEB, which is shown by the purple to red area in Fig. 6-19-b. In addition, almost half of the contour graph with 20 – 40% relative intensity denoted by yellow to orange color has DEB values between 6 and 14. For 2-Me-SEB, the most concentrated compounds denoted by purple to red color are located primarily in the DEB 4-6 range. Moreover, about 1/3 of the graph in yellow color representing low intensity (< 10%) locates in the DEB 6 – 12 range, whereas the rest of the graph has DBE below 6 (Fig. 6-19-a). The DBEs of the simplest polycyclic aromatics, naphthalene ($C_{10}H_8$) and anthracene ($C_{14}H_{10}$), are 7 and 10, respectively. This suggests that the aromatic hydrocarbons in 2-Me-SEB are primarily mono-aromatics, while in T-MEB, the hydrocarbons are mainly composed of non-aromatics and polyaromatics with more than two benzene rings.

In addition, the length of the alkyl chains attached to the aromatic group can be estimated from the carbon number distributions. A higher carbon number with the same DBE value indicates that longer alkyl chains are attached to the aromatic group. The carbon number distribution at each DBE value for T-SEB is wider and higher than that for 2-Me-SEB, which suggests that T-SEB contains more alkyl side chains than 2-Me-SEB. In general, T-SEB contains primarily aliphatics with lower carbon numbers and polyaromatic hydrocarbons with longer, or a greater number of, alkyl side chains; while 2-Me-SEB contains mainly small aliphatic (< 10 carbons) and mono-aromatic hydrocarbons with shorter, or a lower number of, alkyl side chains.
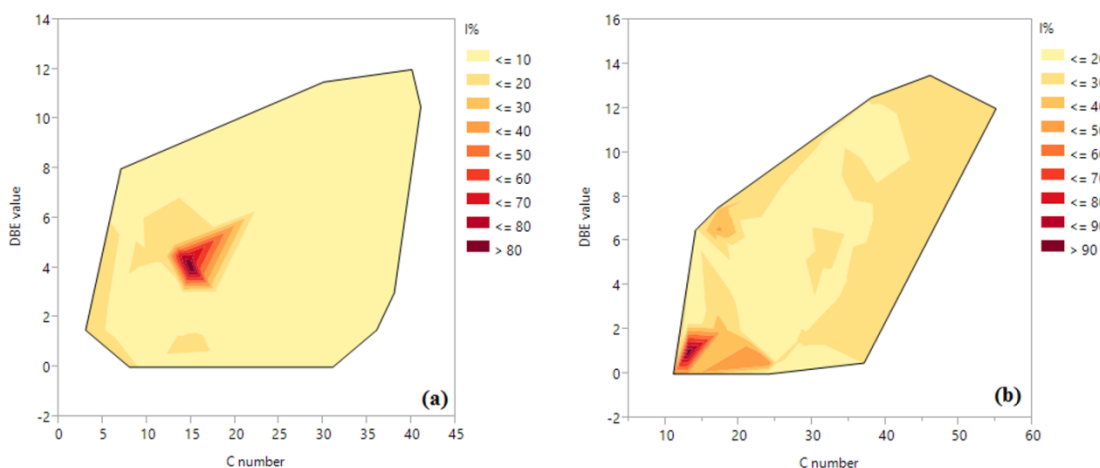
Fig. 6-19. Color-coded iso-abundance contour plot of DBE values versus carbon number of bitumen Soxhlet-extracted by (a) 2-MeTHF and (b) toluene

6.4. Discussion

6.4.1. Factors Affecting Bitumen Extraction by Organic Solvents

6.4.1.1. Water Content

Bitumen extraction from tailing soil matrices by organic solvents is affected by several factors. Water content is one of the most significant factors, as water can produce oil-in-water emulsions that reduce the extraction efficiency (McGill and Rowell 1980). Yeung, Johnson et al. (1994) showed that the Soxhlet extraction efficiency decreased with increasing water content, where the bitumen recovery was reduced from 97% to 58% when the moisture content increased from 0%

223

to 70%. Air- or oven-drying can improve bitumen recovery by reducing the moisture content. However, about 4% and 6% of crude oil was lost by air-drying at room temperature and oven drying at 40 ℃ for 7 hours, respectively. In this study, air-drying of tailing soil at room temperature was used to avoid the effect of water on extraction efficiency.

6.4.1.2. Extraction Methods

The extraction methods determine the quantity and quality of the extracted bitumen. In Soxhlet extraction, bitumen recovery increases significantly with longer extraction times and sample stirring. It was reported that bitumen recovery increased from 85% to 95% when the extraction time was increased from 3 hours to 7 hours (Yeung, Johnson *et al*. 1994). The result from the present study is consistent with the reported finding, as Soxhlet extraction for 4 hours resulted in around 82 to 93% recovery of bitumen.

When comparing the bitumen recovery among different methods, the methods of extraction do not have a significant influence, but they have significant influences on other factors such as solvent consumption, energy input, length of extraction time, efficiency, and so on. For example, sonication is another commonly used method for bitumen recovery from soil as it is relatively low-cost, consumes small volumes of solvent, and eliminates the need for elaborate glassware. (Guerin 1999) reported similar bitumen recovery by using Soxhlet extraction (86% recovery after 4 h) and rigorous sonication (95% recovery after 15 h) with dichloromethane and acetone mixtures. However, the recovery by Soxhlet extraction was lower, which was explained by the losses of the volatile bitumen components after 1-4 hours of extraction. Therefore, sonication may be a better method if the lower molecular weight and more volatile components are the analysis targets of interest.

Accelerated solvent extraction (ASE), which combines elevated temperatures and pressures with organic solvents, has been reported as a method for bitumen recovery from soil. Richter, Jones *et al*. (1996) reported a similar bitumen recovery to Soxhlet extraction when the extraction conditions were set to 15 min, a solvent volume 1.5 times the sample volume, elevated temperature between 50 and 200 ℃, and elevated pressure between 500 and 3000 psi.

6.4.1.3. Extraction Temperature

The use of liquid solvents at elevated temperature and pressure provides enhanced extraction performance compared to extraction at room temperature and atmospheric pressure. The higher temperatures increase the capacity of solvents to solubilize analytes, such as bitumen in this study. It was reported that the solubility of hydrocarbons such as *n*-eicosane can increase several hundred-fold as the temperature increases from 50 to 150 ℃ (Pitzer and Brewer 1961). In addition, faster diffusion rates occur as a result of increasing the temperature of the extraction, where the diffusion rates increase roughly 2 to 10-fold upon increasing the temperature from 25 to 150 ℃ (Perry and Green 1999). Moreover, the fresh solvent introduced in Soxhlet extraction increases the concentration gradient between the solution and the sample matrix, resulting in an improved mass transfer and hence an enhanced extraction performance. Furthermore, the strong solute-soil matrix interactions caused by van der Waals forces, hydrogen bonding, and dipole attractions can be disrupted by the increased temperatures (Richter, Jones *et al*. 1996). As well, a better penetration of matrix particles and, therefore, an enhanced extraction is provided by the decreased viscosity of the solvents at higher temperature (Perry and Green 1999). Therefore, in this study, the bitumen recovery obtained from Soxhlet extraction is higher than that obtained from room-temperature extraction by around 5 wt%.

6.4.2. Bitumen Room-Temperature Extraction Performance Comparison among 3 Solvents

6.4.2.1. Quantitative Comparison

Bitumen recovery by single-stage short-time room-temperature extraction reached 90%, which is similar to recoveries under similar extraction conditions reported in other publications, where 86 – 95% recoveries were reported (Nikakhtari, Vagi et al. 2013). In this study, the ranking of bitumen recovery among the three solvents is 2-MeTHF (88.57%) > toluene (79.75%) > DCM (77.35%) at their optimized solvent-to-soil ratios. When compared to the recovery obtained from Soxhlet extraction, the order of the ranking is the same, where 2-MeTHF is the highest with 93.22% recovery, followed by toluene with 90.70% recovery and DCM with 92.48% recovery.

6.4.2.2. Solvent Viscosity

In the early stage of the solvent extraction, convective mass transfer dominates the extraction speed. It is reported that up to 85% of the extraction is mainly due to the convective mass transfer (Nikakhtari, Vagi *et al*. 2013). The viscosity of the solvent may have an impact on the mass transfer rate, where lower viscosity is more beneficial to mass transfer. Among the three solvents, DCM has the lowest viscosity (0.41 mPa.s), followed by 2-MeTHF (0.51 mPa.s) and toluene (0.56 mPa.s). Therefore, at the very beginning of the extraction, the amount extracted would be the highest in DCM extraction, as the solvent viscosity is the predominant factors determining the mass transfer. When the bitumen concentration increased in the extracting solvent, the amount extracted by 2-MeTHF became the greatest as other factors, such as solute concentration, temperature, and diffusive effect started contributing to the mass transfer.

6.4.2.3. Solvent Diffusion Rate

Mass transfer can only occur by convection and diffusion. In solvent extraction, convective mass transfer is dominant up to about 85% extraction, beyond which the solvent diffusion into aggregates becomes rate-limiting (Nikakhtari, Vagi *et al*. 2013). Before calculating the diffusion rate, the diffusion coefficients of the molecules must be obtained, preferably via experiments. However, there is a lack of information about the diffusion coefficients of hydrocarbon solvents in bitumen and therefore, the solvent diffusion rate into bitumen substrates cannot be compared among the three solvents. (Fu and Phillips 1979) initiated experiments to determine the diffusivities of several light hydrocarbons in semi-solid bitumen. They indicated that the diffusivities of hydrocarbons in bitumen depend on the molecular structures of the hydrocarbons, where the diffusivities decrease with increasing molecular weight, increasing branching, and the presence of ring structures. In particular, non-planar cyclic molecules, such as cyclohexane, show lower diffusivity than aromatics, such as benzene and toluene.

6.4.3. Qualitative Comparison of Extracts

The presence of fine solids in the extracted bitumen is one of the most important parameters in evaluation of the quality of the extraction method, as the fine solids content determines the

acceptability of the extracts to downstream refineries and upgraders. In this study, fine solids were found in the extracts, where the ranking of extracting solvents was DCM > toluene > 2-MeTHF.

6.4.3.1. Solvent Solubility Parameter

There are several reasons explaining the migration of fine solids into the product bitumen during solvent extraction. Properties of the solvent in terms of the solubility parameter and density are among the factors affecting the migration of fine solids. Solvents with higher solubility parameters are more effective in dispersing fine solids (Nikakhtari, Vagi *et al.* 2013). Therefore, the behavior of the fine solids in the solution is dominated by dispersion, resulting in the decrease of the sedimentation rate. In this study, the solubility parameter ranking (Barton 1991) of the selected solvents is DCM (20.2 MPa$^{1/2}$) > toluene (18.2 MPa$^{1/2}$) > 2-MeTHF (16.9 MPa$^{1/2}$), which explains the observation in this study that the content of the fine solids is the highest in the product bitumen extracted by DCM, followed by the toluene extracts and 2-MeTHF extracts, as the fine solids are more dispersed in the DCM-bitumen supernatant after the centrifugation and hence, more fines are left in the product bitumen after solvent evaporation.

6.4.3.2. Relative Density

In addition, the relative density between the solvent and the fine solids is another factor affecting the migration of the fine solids. In this study, centrifugation was used to separate the supernatant, which is the solvent with dissolved bitumen, from the precipitate, which is composed of the soil minerals.

In the centrifugation, the force applied to the particles is called centrifugal force (F_c) and is calculated from the Newton equation:

$$F_c = m \times a = m \times v^2 \times r \dots\dots\dots\dots\dots\dots\dots\dots\dots\dots\dots\dots\dots\dots (6\text{-}9)$$

where m is the mass of the particle, a is the acceleration, v is the angular velocity, and r is the radius of the particle. This equation is applicable to vacuum conditions. However, when the solution system is centrifuged, the particles are not in a vacuum but in a solvent and therefore the centrifugal force acts on both the particles and the solvent medium. Hence, a buoyancy factor $(1 - \frac{\rho}{\rho_r})$ is incorporated to describe the relationship between the surrounding medium and the particles in the centrifugation system:

$$F_c = m \times (1 - \frac{\rho}{\rho_r}) \times v^2 \times r \dots\dots\dots\dots\dots\dots\dots\dots\dots\dots\dots\dots\dots\dots \text{(6-10)}$$

where ρ is the density of the solvent and ρ_r is the density of the particle. Consequently, the particle sediments if the density of the particle exceeds that of the solvent; while the particle floats if the density of the particle is lower than that of the solvent. When the density of the particle equals the density of the solvent, the particle will not move relative to the solvent and no separation occurs. Therefore, the larger the difference in density between the solvent and the fine solids, the better is the separation that can be obtained. The fine solids, which are mainly clay minerals, have a bulk density around 1.10 g/cm^3, which is closest to the density of DCM (1.33 g/cm^3), followed by the density of toluene (0.87 g/cm^3) and 2-MeTHF (0.85 g/cm^3).

6.4.3.3. Water Content

The fine solids show a range of surface properties, from hydrophobic to hydrophilic (Kotlyar, Ripmeester *et al*. 1988; Sparks, Kotlyar *et al*. 2003). Kotlyar, Ripmeester *et al*. (1988) and Nikakhtari, Wolf *et al*. (2014) reported that the hydrophobic solids tend to appear in the bitumen product in both the solvent extraction and the water-based process. In the presence of water, migration of the hydrophilic solids into the bitumen product is prevented by hydrogen bonding to water. Nikakhtari, Wolf *et al*. (2014) reported an optimum range of water content between 3.4 and 14% to bind the fine solids to the sands. Furthermore, when the water was removed by drying or when too much water was added, more fine solids were carried into the bitumen product. As well, they indicated that within this water range, bitumen recovery was

insignificantly affected. In the present study, the water was removed by air-drying before the solvent extraction, which favors the migration of fines into the bitumen product.

In addition to water removal by drying, water extraction by organic solvents can also increase the amount of fine solids in the final product. Among the three solvents, DCM is the only solvent that is fully miscible in water, while 2-MeTHF and toluene are immiscible with water. Hence, DCM can extract both water and bitumen at the same time by solubilizing both phases, giving a miscible mixture and having more fine solids in the mixture. This result agrees to the finding of Nikakhtari, Wolf *et al*. (2014), who reported that the content of fine solids in bitumen significantly increased from less than 0.2% to 3.7% when ethanol was used as the extracting agent.

6.4.4. Potential Reactions in 2-MeTHF Soxhlet Bitumen Extraction System

6.4.4.1. Information from ATR-FTIR Spectroscopy

According to the bitumen characterization based on the ATR-FTIR spectra, the bitumen extracted by the three solvents in either room-temperature extraction or Soxhlet extraction shows a similar spectral profile, except in the case of the bitumen extracted by 2-MeTHF Soxhlet extraction, where boiling temperature was applied. The ATR-FTIR spectra of the bitumen extracted by 2-MeTHF under Soxhlet and room-temperature extraction conditions are presented in Figure 6-20. The main differences between these spectra are in the aliphatic region (3000 – 2800 cm^{-1}), where the -CH$_3$/-CH$_2$ ratio of 2-Me-SEB is high, which indicates that there is a higher amount of shorter or more branched aliphatic chains in 2-Me-SEB. In addition, there is a group of new bands in the region below 1300 cm^{-1}, which indicates the presence of C-O, S=O, and H-O groups. In particular, the new bands centered at 1311, 1230, 1155, and 1117 cm^{-1} are assigned to the C-O bonds of ether or ester compounds (Table 6-16). As well, a new sharp band is observed at 3644 cm^{-1}, which represents the free O-H group of alcohols.
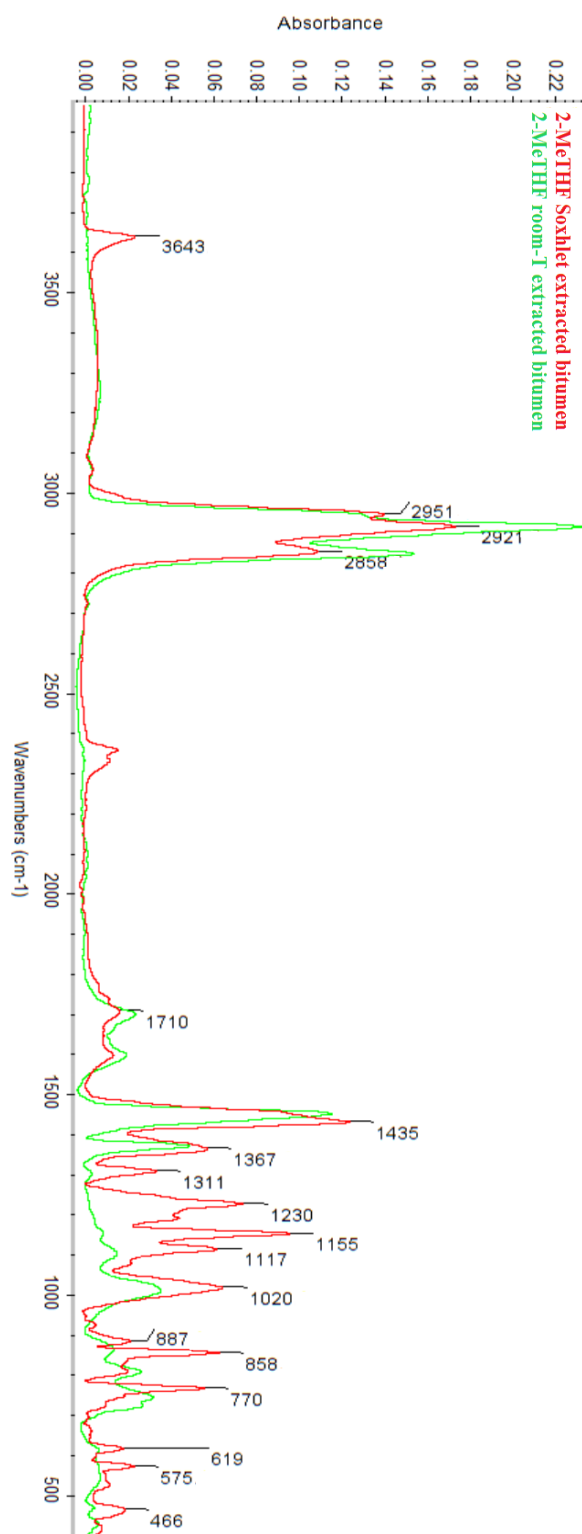
Fig. 6-20. ATR-FTIR spectra of bitumen extracted by Soxhlet
extraction (red) and by room- temperature extraction using 2-MeTHF

Table 6-16. Postulated infrared band assignments for the new bands observed following 2-MeTHF Soxhlet extraction (Socrates 2004)

Peak (cm^{-1})	Range (cm^{-1})	Vibrational mode	Functional group
3643	3660 – 3593	Stretching	Hydroxyl from alcohol (free)
1311	1338 – 1287	Stretching	Aromatic ester
1230	1287 – 1199	Stretching	Alkyl aryl ether
1155	1177 – 1136	Stretching	Ester
1117	1136 – 1095	Stretching	Aliphatic ether

6.4.4.2. Information from APCI-MS and Elemental Analysis

2-Me-SEB and T-SEB, which is regarded as the reference bitumen, were sent for elemental analysis and MS-APCI analysis in order to obtain additional information in order to understand the chemical differences between the two bitumen samples. From the elemental analysis, it was found that the oxygen content was doubled in 2-Me-SEB compared to that of the reference bitumen. The results from MS analysis further prove that there is a group of ion fragments from 2-Me-SEB in the lower molecular weight range, between *m/z* 119 and 219, which are not observed in the case of T-SEB. This group of ion fragments contains between 5 and 10 carbon atoms. In addition, it is found that the oxygen atoms in 2-Me-SEB are mainly distributed in the ion fragments with shorter carbon chains and lower molecular weight. Furthermore, the amount of oxygen atoms in this shorter carbon chain group is relatively high, between 3 and 6. In contrast, the oxygen atoms in the ion fragments of T-SEB are mainly found in the higher molecular weight range (Fig. 6-18).

6.4.4.3. Potential Reaction and Mechanism

All the information above suggests that chemical reaction(s) occurred in the system in which bitumen and 2-MeTHF solvent were mixed together at the boiling temperature of around 90 °C. After the reaction(s), a series of low-molecular-weight compounds with short carbon chains and oxygen atoms was produced. There are many potential reactions that could have occurred in the

system; but it is very important to note that there are no such findings when toluene or DCM is present instead of 2-MeTHF. Therefore, the reaction(s) that occurred /may be attributed to the properties of 2-MeTHF, such as its cyclic ether structure.

One possible reaction is the ring-opening reaction and polymerization of 2-MeTHF when exposed to Lewis acids and high temperature. It is known that cyclic ethers having 3-, 4-, and 5-membered rings (e.g., epoxides, oxetanes, THF) can undergo ring-opening polymerization and yield polymeric ethers. Polymerization can be initiated by Lewis acids, such as metal cations, which can accept an electron pair provided by a Lewis base such as THF, in which the oxygen atom has two lone electron pairs that it can donate (Braun, Cherdron *et al*. 2012). Delaney, Johnstone *et al*. (1986) reported a simple ring-opening with simultaneous dimerization by reacting a variety of cyclic ethers with $TiCl_4$ under refluxing conditions. The reaction of $TiCl_4$ with excess THF produces 1,9-dichloro-5-oxanonane. The generation of this product gives rise to mid-infrared absorption bands at 3420 and 1055 cm^{-1}, which represent the presence of O-H and C-O-C groups, respectively. They also reported that 2-MeTHF can also undergo ring-opening and dimerization reactions with Lewis acids, which required longer reaction time. There are also other studies showing that 2-MeTHF undergoes ring-opening under acidic conditions (Pace, Hoyos *et al*. 2012).

The reaction scheme of 2-MeTHF with Lewis acids is presented in Figure 6-21. In general, the reaction can be described as consisting of three steps. In the initial step, 2-MeTHF is protonated by the Lewis acids and forms the cyclic ether ion (Fig. 6-21-a). The less substituted carbon atom in the ether group is activated and is attacked by a 2-MeTHF molecule in an S_N2-reaction, resulting in the opening of the ring (Fig. 6-21-b). Chain growth proceeds via the same mechanism (Fig. 6-21-c). The reaction products are black and oil-like, which makes them more soluble in bitumen. After the Soxhlet extraction is finished and the excess 2-MeTHF solvent is removed by evaporation, the end product containing the recovered bitumen mixed with the polymers is obtained, which gives rise to the new ATR-FTIR bands related to the free-OH and C-O bonds of the polymers.

In bitumen recovered from the Athabasca oil sands, there are many potential Lewis acids that can initiate the reaction, such as naphthenic acids, N-containing cations, and other trace amounts of cations. The decrease of the carboxyl absorption in the carbonyl region of the ATR-FTIR spectrum of bitumen after Soxhlet extraction suggests the participation of Lewis acids containing carboxylic groups in the ring-opening reactions (Fig. 6-22).
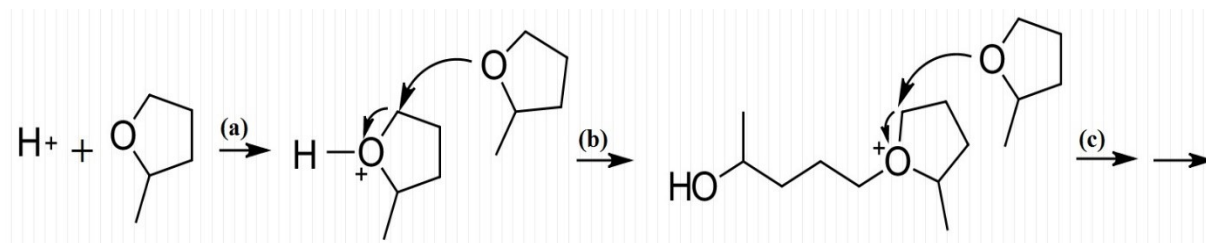
Fig. 6-21. Ring opening and polymerization reaction of 2-MeTHF with Lewis acids
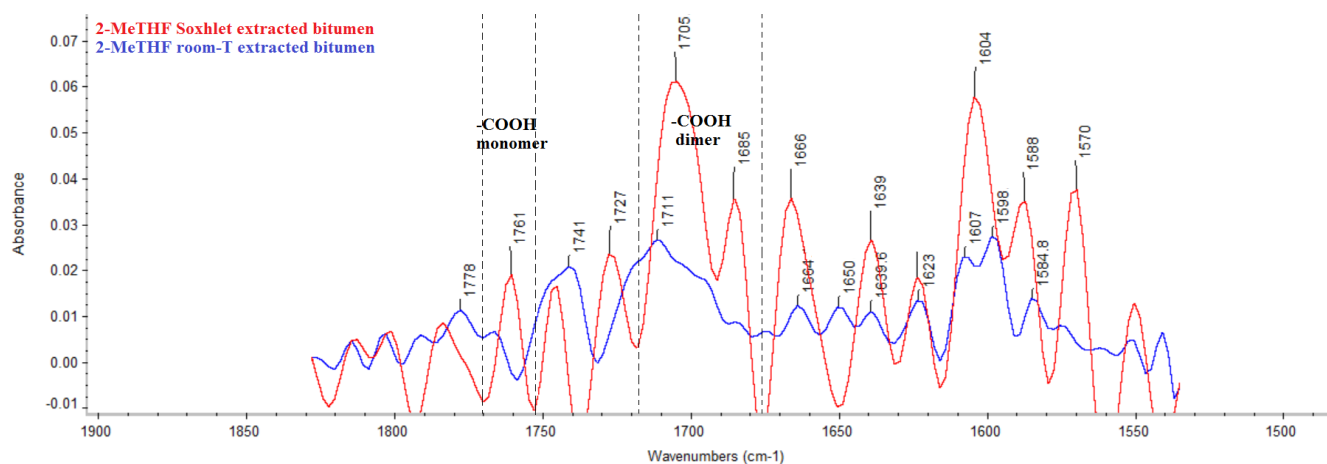
Fig. 6-22. Deconvolution of ATR-FTIR spectra of Soxhlet extracted and room-temperature extracted bitumen in the region between 1850 and 1500 cm^{-1}. The extraction solvent was 2-MeTHF

6.5. Conclusion

The bitumen extraction performance of the green solvent 2-MeTHF was evaluated in terms of extraction efficiency and product quality. The extraction was performed under mild conditions, where room-temperature 2-min vortex was applied. 2-MeTHF showed powerful bitumen

extraction ability whereby half of the bitumen in tailing soil samples was recovered in a single-stage extraction at the lowest solvent-to-soil ratio examined. In addition, 2-MeTHF provided higher bitumen extraction efficiency than the traditionally used organic solvents, toluene and DCM. Furthermore, according to ATR-FTIR and DRIFT-NIR analysis, the bitumen recovered by 2-MeTHF had higher quality as less clay migration was found in the final bitumen products.

The solvent usage in the room-temperature extraction was optimized by measuring the yield in relation to the solvent usage. The extraction yield was maximized when the amount of the solvent 2-MeTHF was double the amount of soil sample used. Beyond that ratio, the yield did not increase with increasing solvent usage. When toluene or DCM was used, larger amounts of solvent were required to reach a bitumen yield similar to that obtained by extraction with2-MeTHF. Therefore, considering the higher extraction yield, less clay migration, and less environmental impact, 2-MeTHF can be used as an alternative to the traditional organic solvents, such as toluene and DCM, in the bitumen room-temperature solvent extraction process.

The non-extractable bitumen under the mild extraction condition was further studied by using ATR-FTIR spectroscopy. According to the $-CH_3/-CH_2$ index, the less-extractable fraction contains longer aliphatic chains and less branched structure. In addition, it contains a higher content of carbonyl and aromatic groups, making this fraction more polar and therefore decreasing its solubility in the non-polar organic solvent.

2-MeTHF is a good substitute for the traditionally used extracting solvents. However, when heat is applied during the extraction process, such as in Soxhlet extraction, 2-MeTHF is unstable and may undergo ring-opening and polymerization reactions, which are triggered by the Lewis acids present in the bitumen samples. The polymerized 2-MeTHF products are oil-like and thus mix with the recovered bitumen and end up in the final product. Therefore, the use of 2-MeTHF is not recommended when heat is to be applied during the extraction process. In addition, distillation cannot be employed to recover 2-MeTHF from the final product.

Soil quality is one of the main focuses in agricultural practice as it determines crop quality and yield. Improper farm management practices have resulted in a loss of soil quality and soil degradation (Forge 1998), leading to an urgent need for new farm management techniques. Precision agriculture (PA) is an innovative farm management strategy, which focuses on effective resource utilization and ultimately improves production and reduces the environmental impact of farming (Reichardt and Jürgens 2009). The success of PA requires the implementation of many techniques, among which is data collection on and analysis of soil quality across the whole field. Soil quality is traditionally analyzed by wet-chemical techniques, which are not suited for application in PA due to various limitations, such as the amount of time and labour required to perform them and high cost. Fourier transform infrared (FTIR) spectroscopy is considered as a potential alternative method considering its significant advantages, particularly the speed of the analysis and amenability to automation (Ismail, van de Voort *et al*. 1997).

Soil contamination is also related o soil quality from the environmental point of view. Contamination of soil by bitumen residues is severe in Alberta due to the large-scale exploitation of oil sands and improper handling of tailings. The reclamation of the contaminated tailings prior its release is enforced by *Directive 074*. In addition, the reclamation performance, particularly the quantity and quality of the remediated tailings, must be monitored to meet the requirements of the *Tailings Management Framework for Mineable Athabasca Oil Sands (TMF)* issued by the Government of Alberta (Alberta Energy Regulator 2015). The advantages of FTIR spectroscopy, such as direct analysis of soils and on-line monitoring capability, make it a promising technique for this monitoring application.

In this context, two forms of FTIR spectroscopy were investigated and compared in this thesis. The first involves the use of the mid-infrared (MIR) region and employs a single-bounce attenuated total reflectance (ATR) sample-handling accessory. In the MIR region, absorptions due to the fundamental vibrations of molecules occur, giving rise to intense and distinct absorption bands in MIR spectra. The ATR technique allows MIR spectra to be acquired from

semi-solid and solid samples with minimal sample preparation. The second form of FTIR spectroscopy investigated in this thesis involves the use of the near-infrared (NIR) region, in which absorptions are due to the overtones and combinations of the fundamental vibrations measured in the MIR region. Although the signals associated with NIR absorption are less intense than those observed in the MIR region, the less expensive optics and the amenability to *in situ* and on-site applications make NIR spectroscopy a widely used technique.

The contributions to knowledge stemming from this research on the potential application of these techniques in agricultural soil quality modeling and in monitoring of remediation of bitumen-contaminated tailings are summarized in the following paragraphs.

The feasibility of employing ATR-FTIR spectroscopy to monitor 10 selected soil properties, including chemical properties such as total carbon (TC), total nitrogen (TN), carbon-to-nitrogen ratio (C/N), ammonium (NH_4^+), and nitrate (NO_3^-), physical properties such as the percentages of sand, silt, and clay making up the soil, and comprehensive properties such as N-uptake and yield was demonstrated in Chapter 3. Ten partial-least-squares (PLS) calibration models were developed to model these properties using the ATR-FTIR spectra of 278 agricultural soil samples collected across four Canadian provinces. The properties TC, TN, C/N, sand, silt, and clay were successfully modeled, as evidenced by r^2 values of >0.90 and RPD values of >2.00. In addition, the effect of dataset normalization by logarithmic transformation was studied but the performance of the models was not significantly improved, ATR-FTIR spectroscopy was shown to be convenient for the analysis of dry soil samples, with only a small amount of sample being required. Based on these results, it was concluded that ATR-FTIR spectroscopy coupled with PLS provides a rapid, reliable, and simple means of soil quality monitoring for PA.

The utility of DRIFT-NIR spectroscopy for the assessment of soil quality and comparison of its performance with that of ATR-FTIR spectroscopy were explored in Chapter 4. To better evaluate the performance of calibration models, the RPIQ index was used instead of RPD, as it takes into account the spread of the dataset distribution. According to the criteria of r^2 >0.90 and RPIQ > 2.50, the calibration models for the prediction of the properties TC, TN, C/N, sand and clay were considered reliable. The ATR-FTIR calibration models for the same properties had better prediction accuracy with 12% to 36% RPIQ increment. However, when cost and feasibility for

in-field use are considered, DRIFT-NIR spectroscopy is a more suitable technique for PA practice.

Chapter 5 addressed the possibility of using ATR-FTIR and DRIFT-NIR spectroscopy to directly quantify bitumen residues in Alberta tailing soils. Calibrations were developed by both PLSR and simple linear regression using artificial bitumen-spiked samples as the calibration set. The combination of ATR-FTIR spectroscopy and PLSR yielded the best calibration, with an r^2 of 0.99 r^2 and a 1.76 wt% RMSEC over the bitumen content range between 0.70 and 40.70 wt%, and was selected for the development of a calibration using natural tailing soil samples, which provided an r^2 of 0.90 and a 1.55 wt% RMSEC over the bitumen content range between 9.70 and 26.59 wt%. In addition, the classification of tailing soils by principal component analysis (PCA) of their ATR-FTIR spectra was studied. Classification based on the bitumen residue content was successfully achieved, but classification based on discrimination between unremediated and remediated soils did not succeed, as the remediatiom process had not been optimized and consequently there was a lack of a direct relation between bitumen residue content and the remediation process. Based on the results of this study, ATR-FTIR spectroscopy coupled with PLS and PCA techniques showed potential as a technique for on-line remediation monitoring to determine the remediation performance and aid in optimization of the remediation process.

Chapter 6, as an extension of the study presented in Chapter 5, evaluated the use of the green solvent 2-methyltetrahydrofuran (2-MeTHF) for extraction of bitumen from tailing soils. The extraction was conducted under room-temperature/2-min vortex conditions and the solvent amount was optimized based on bitumen recovery. According to gravimetric measurements, 89% of the total bitumen was recovered by extraction into 2-MeTHF with an optimized solvent-to-soil ratio of 2:1 wt/wt. The bitumen recovery obtained using 2-MeTHF was shown to be higher than that obtained with the traditionally used solvents toluene and dichloromethane (DCM), where these two solvents recovered 9% and 14% less bitumen, respectively. The less-extractable and non-extractable bitumen fractions were quantified using the calibration models described in Chapter 5. It was estimated that these two fractions accounted for 5.59 and 8.77% of the total bitumen. The quality of the recovered bitumen was studied by using ATR-FTIR spectroscopy and it was found that less clay migration into bitumen occurred when 2-MeTHF

was used as the extraction solvent. However, under the elevated-temperature condition of Soxhlet extraction, 2-MeTHF was postulated to form oil-like products via protonation, ring-opening, and polymerization reactions. Evidence for the presence of such products in the extracted bitumen was obtained by ATR-FTIR spectroscopy and atmospheric-pressure chemical ionization mass spectroscopy (APCI-MS). Thus, if 2-MeTHF is to be applied in solvent extraction of bitumen, high-temperature condition should be avoided in the extraction and solvent recovery processes.

The research summarized above has laid the foundation for the application of ATR-FTIR and DRIFT-NIR spectroscopy in soil analysis. Especially, this research was undertaken in the Canadian context, entailing the creation of a spectral library of Canadian agricultural soils and the development of calibrations modeling soil quality condition across four Canadian provinces. In addition, the bitumen-contaminated soils studied in this research were from the province of Alberta. The rapid, accurate, and reagent/solvent-free FTIR spectroscopic methods for soil analysis established in this research can find application in the agricultural sector and in the tailings remediation industry, which will consequently benefit from the reductions in time, labor costs and solvent use associated with the replacement of the traditionally used wet-chemical methods by these instrumental methods.

REFERENCES

Acton, D. and Gregorich, L. (1995). Understanding soil health. *The health of our soils: toward sustainable agriculture in Canada.*: 5-10.

Afshar, S., Mirmontazeri, L.and Yeung, A. (2014). Potential use of naphthenic acids in soil remediation: Examination of pore-scale interfacial properties. *Fuel* **116**, 395-398.

Alberta Energy Regulator (2009). Directive 074: Tailings Performance Criteria and Requirements for Oil Sands Mining Schemes. A. E. Regulator. Alberta, Canada.

Alberta Energy Regulator (2015). Lower Athabasca Region - Tailings Management Framework for the Mineable Athabasca Oil Sands. Government of Alberta.

Alberta Oil Sands Industry. (2009). Quarterly Update Winter 2009, Government of Alberta.

Alberta Oil Sands Industry. (2016). Quarterly Update Spring 2016, Government of Alberta.

Alenyorege, E. A., Hussein, Y. A. and Adongo, T. A. (2015). Extraction yield, efficiency, and loss of the traditional hot water floatation (HWF) method of oil extraction from the seeds of Allanblackia floribunda. *Int. J. Sci. Technol. Res.* **4**, 92-95.

Ali, M. F., Bukhari A.and Misbah-ul-Hasan (1989). Structural characterization of Arabian heavy crude oil residue. *Fuel Science & Technology International* **7**, 1179-1208.

Aske, N., Kallevik, H. and Sjöblom, J. (2001). Determination of saturate, aromatic, resin, and asphaltenic (SARA) components in crude oils by means of infrared and near-infrared spectroscopy. *Energy & Fuels* **15**, 1304-1312.

Attanasi, E. D. and Meyer, R. F. (2010). Natural bitumen and extra-heavy oil. *Survey of Energy Resources* **22**, 123-140.

Baes, A. and Bloom, P. (1989). Diffuse reflectance and transmission Fourier transform infrared (DRIFT) spectroscopy of humic and fulvic acids. *Soil Science Society of America Journal* **53**, 695-700.

Barton, A. F. (1991). *CRC Handbook of Solubility Parameters and Other Cohesion Parameters*, Barton, A. F. (ed.), CRC Press, US.

Bautista-Cruz, A., Carrillo-González, R., Arnaud-Viñas, M., Robles, C. and León-González, F. (2007). Soil quality properties on Agave angustifolia Haw. plantations. *Soil and Tillage Research* **96**, 342-349.

Bellon-Maurel, V., Fernandez-Ahumada, E., Palagos, B., Roger, J. M.and McBratney, A. (2010). Critical review of chemometric indicators commonly used for assessing the quality of the prediction of soil attributes by NIR spectroscopy. *TrAC Trends in Analytical Chemistry* **29**, 1073-1081.

Bellon-Maurel, V. and McBratney A. (2011). Near-infrared (NIR) and mid-infrared (MIR) spectroscopic techniques for assessing the amount of carbon stock in soils–Critical review and research perspectives. *Soil Biology and Biochemistry* **43**, 1398-1410.

Blum, W. E. H. (1993). Soil protection concept of the Council of Europe and integrated soil research. In: *Integrated Soil and Sediment Research: A Basis for Proper Protection*, Eijsackers, H. and Hamers, T. (eds.), Springer**,** pp. 37-47.

Bouyoucos, G. J. (1962). Hydrometer method improved for making particle size analyses of soils. *Agronomy Journal* **54**, 464-465.

Bowers, S. and Hanks, R. (1965). Reflection of radiant energy from soils. *Soil Science* **100**, 130-138.

Bowman, K. (2008). Economic and environmental analysis of converting to controlled traffic farming. *6th Australian Controlled Traffic Farming Conference,* 61-68.

Brady, N. C. and Weil, R. R. (1996). Nitrogen and sulfur economy of soils. In: *The Nature and Properties of Soils*, Brady, N. C. and Weil, R. R. (eds.), Prentice-Hall Inc., New Jersey, **PP.** 400-444.

Brady, N. C. and R. R. Weil (1996). Soil mineral. In: *The Nature and Properties of Soils*, Brady, N. C. and Weil, R. R. (eds.), Prentice-Hall Inc., New Jersey, PP. 20-23.

Brady, N. C. and R. R. Weil (1996). Soil organic matter. In: *The Nature and Properties of Soils*, Brady, N. C. and Weil, R. R. (eds.), Prentice-Hall Inc., New Jersey, PP. 361-398.

Bramley, R. G. V. and Janik, L. J. (2005). Precision agriculture demands a new approach to soil and plant sampling and analysis—examples from Australia. *Communications in Soil Science and Plant Analysis* **36**, 9-22.

Braun, D., Cherdron, H., Rehahn, M., Ritter, H.and Voit, B. (2012). Synthesis of macromolecules by Chian growth polymerization. In: *Polymer Synthesis: Theory and Practice: Fundamentals, Methods, Experiments,* Springer Science & Business Media, Germany.

Brejda, J. J., Moorman, T. B., Smith, J. L., Karlen, D. L., Allan, D. L. and Dao, T. H. (2000). Distribution and variability of surface soil properties at a regional scale. *Soil Science Society of America Journal* **64**, 974-982.

Burrowes, A., Teare, M., Marsh, R., Gigantelli, P., Macgillivray, J., Evans, C., Hein, F., Parks, K., Rokosh, D.and Hurst, T. (2011). Alberta's energy reserves 2010 and supply/demand outlook 2011-2020. *Energy Resources Conservation Board (June 2011)*.

Cabaniss, S. E., Madey, G., Leff, L., Maurice, P. A. and Wetzel, R. (2005). A stochastic model for the synthesis and degradation of natural organic matter. Part I. Data structures and reaction kinetics. *Biogeochemistry* **76**, 319-347.

Canada National Energy Board (2006). Canada's Oil Sands: Opportunities and Challenges to 2015: an Update.

Capello, C., Fischer, U.and Hungerbühler, K. (2007). What is a green solvent? A comprehensive framework for the environmental assessment of solvents. *Green Chemistry* **9**, 927-934.

Cass, A., Hansen, D.and Dowley, A. (2002). Grape performance and soil conditions. In: *Sustainable Viticultural Production: Optimising Soil Resources*. Cass, A. (ed.), GWRDC Final Report: CRS.

Chang, C. W., and Laird, D. A. (2002). Near-infrared reflectance spectroscopic analysis of soil C and N. *Soil Science* **167**, 110-116.

Chang, C. W., Laird, D. A., Mausbach, M. J. and Hurburgh, C. R. (2001). Near-infrared reflectance spectroscopy–principal components regression analyses of soil properties. *Soil Science Society of America Journal* **65**, 480-490.

Chu, X. L. (2011). Chemometrics. In: *Molecular Spectroscopy Analytical Technology Combined with Chemometrics and Its Applications*, Chu, X. L. (ed.), Hua Xue Gong Ye Press, Beijing.

Clark, K. and Pasternack, D. (1932). Hot water seperation of bitumen from Alberta bituminous sand. *Industrial & Engineering Chemistry* **24**, 1410-1416.

Constable, D. J., Jimenez-Gonzalez, C.and Henderson, R. K. (2007). Perspective on solvent use in the pharmaceutical industry. *Organic Process Research & Development* **11**, 133-137.

Corwin, D. L. and Lesch, S. M. (2003). Application of soil electrical conductivity to precision agriculture. *Agronomy Journal* **95**, 455-471.

Cozzolino, D. and Moron, A. (2003). The potential of near-infrared reflectance spectroscopy to analyse soil chemical and physical characteristics. *The Journal of Agricultural Science* **140**, 65-71.

Daviesa, A. and Fearnb, T. (2006). Back to basics: calibration statistics. *Spectroscopy Europe* **18,** 31-32.

Delaney, P. A., Johnstone, R. A. and Entwistle, I. D. (1986). Metal-assisted reactions. Part 17. Ring-opening and dimerization of cyclic ethers by titanium halides. *Journal of the Chemical Society*, 1855-1860.

Desbiez, A., R. Matthews, B. T. and Ellis-Jones, J. (2004). Perceptions and assessment of soil quality by farmers in the mid-hills of Nepal. *Agriculture, Ecosystems & Environment* **103**, 191-206.

Dexter, A. R. (2004). Soil physical quality: Part I. Theory, effects of soil texture, density, and organic matter, and effects on root growth. *Geoderma* **120**, 201-214.

Dhanoa, M., Lister, S., Sanderson, R. and Barnes, R. (1994). The link between multiplicative scatter correction (MSC) and standard normal variate (SNV) transformations of NIR spectra. *J. Near Infrared Spectrosc.* **2**, 43-47.

Đorđević, D. M., Stanković, M. N., Đorđević, M. G., Krstić, N. S., Pavlović, M. A., Radivojević, A. R. and Filipović, I. M. (2012). FTIR Spectroscopic Characterization of Bituminous Limestone: Maganik Mountain (Montenegro). Studia Universitatis Babes-Bolyai, Chemia **57**, 39-54.

Draper, N. R., Smith, H. and Pownell, E. (1966). Fitting a straight line by least squares. In: *Applied Regression Analysis*, Draper, N. R. and Smith, H. (eds.), Wiley, New York.

Du, C., Ma, F., Lu, Y.and Zhou, J. (2015). Soil quality assessed by infrared spectroscopy. In: *Soil-specific Farming: Precision Agriculture*, Lal R. and Stewart B. A. (eds.), CRC Press, US, pp. 155-185.

Dunn, B., Batten, G., Beecher, H. and Ciavarella, S. (2002). The potential of near-infrared reflectance spectroscopy for soil analysis—a case study from the Riverine Plain of south-eastern Australia. *Animal Production Science* **42**, 607-614.

Energy Resources Conservation Board (2011). Alberta's Energy Reserves 2010 and Supply/Demand Outlook 2011-2020. Energy Resrouces Conservation Board, Calgary, Alberta.

Eriksson, L., Byrne, T., Johansson, E., Trygg, J.and Vikström, C. (2013). PCA. In: *Multi-and Megavariate Data Analysis Basic Principles and Applications,* Umetrics Academy, Sweden, pp. 33-53.

Eriksson, L., Byrne, T., Johansson, E., Trygg, J.and Vikström, C. (2013). Transformation and expansion. In: *Multi-and Megavariate Data Analysis Basic Principles and Applications*, Umetrics Academy, Sweden.

European Committee for Standardization (2000). *EN 12597: Bitumen and Bituminous Binders – Terminology*, Brussels.

FAO and ITPS (2015). Status of the World's Soil Resources (SWSR) - Main Report. Rome, Italy, Food and Agriculture Organization of the United Nations and Intergovernmental Technical Panel on Soils.

Farcasiu, M. and Whitehurst, D. D. (1977). Double solvent extraction of organic constituents from tar sands, Google Patents.

Farkish, A. and Fall, M. (2013). SAP based rapid dewatering of oil sands mature fine tailings. *Miner. Eng.* **50**, 38-47.

Foley, W. J., McIlwee, A., Lawler, I., Aragones, L., Woolnough, A. P. and Berding, N. (1998). Ecological applications of near infrared reflectance spectroscopy–a tool for rapid, cost-effective

prediction of the composition of plant and animal tissues and aspects of animal performance. *Oecologia* **116**, 293-305.

Forge, F. (1998). Agriculture soil conservation in Canada. P. R. Branch.

Forrester, S., Janik, L., McLaughlin, M.and Gilkes, R. (2010). An infrared spectroscopic test for total petroleum hydrocarbon (TPH) contamination in soils. In: *Proceedings of the 19th World Congress of Soil Science: Soil solutions for a changing world, Brisbane, Australia, 1-6 August 2010. Working Group 1.5 Soil sense: rapid soil measurements*, International Union of Soil Sciences (IUSS), c/o Institut für Bodenforschung, Universität für Bodenkultur, pp. 13-16.

Friesen, W. I. (1996). Qualitative analysis of oil sand slurries using on-line NIR spectroscopy. *Applied spectroscopy* **50**, 1535-1540.

Fu, B. C. and Phillips, C. R. (1979). New technique for determination of diffusivities of volatile hydrocarbons in semi-solid bitumen. *Fuel* **58**, 557-560.

Gani, R., Jiménez-González, C., Kate, A. T., Crafts, P. A., Jones, M., Powell, L., Atherton, J. H. and Cordiner, J. L. (2006). A modern approach to solvent selection. *Chemical Engineering* **113**, 30-43.

Ge, Y., Thomasson, J. A. and Morgan, C. L. S. (2014). Mid-infrared attenuated total reflectance spectroscopy for soil carbon and particle size determination. *Geoderma* **213**, 57-63.

Gebbers, R. and Adamchuk, V. I. (2010). Precision agriculture and food security. *Science* **327**, 828-831.

Gee, G. W., Bauder, J. W. and Klute, A. (1986). Particle-size analysis. In: *Methods of Soil Analysis. Part 1. Physical and Mineralogical Methods*, American Society of Agronomy, Winsconsin, US, pp. 383-411.

Graham, R., J. Helstrom and Mehlberg, R. (1987). A solvent extraction process for tar sand. *Eastern Oil Shale Symposium*, pp. 93-99.

Griffin, T., Lambert, D.and Lowenberg-DeBoer, J. (2005). Economics of lightbar and auto-guidance GPS navigation technologies. *Precision Agriculture* **5**, 581-587.

Guerin, T. (1999). The extraction of aged polycyclic aromatic hydrocarbon (PAH) residues from a clay soil using sonication and a Soxhlet procedure: a comparative study. *Journal of Environmental Monitoring* **1**, 63-67.

Haaland, D. M. and Thomas, E. V. (1988). Partial least-squares methods for spectral analyses. 1. Relation to other quantitative calibration methods and the extraction of qualitative information. *Analytical Chemistry* **60**, 1193-1202.

Hastie, T., Tibshirani R. and Friedman J. (2001). Model assessment and selection. In: *The Elements of Statistical Learning: Data Mining, Inference, and Prediction*, Hastie, T., Tibshirani R. and Friedman J. (eds.), Springer, New York, pp. 193-224.

Hesse, P. R. (1971). Carbon and organic matter. In: *A Textbook of Soil Chemical Analysis,* Hesse P. R. (ed.), John Murray Ltd, London, pp. 204-250.

Hesse, P. R. (1971). Nitrogen. In: *Textbook of Soil Chemical Analysis*, Hesse P. R. (ed.), John Murray Ltd, London, pp. 149-195.

Huber, G. W., Iborra, S. and Corma, A. (2006). Synthesis of transportation fuels from biomass: chemistry, catalysts, and engineering. *Chemical Reviews* **106**, 4044-4098.

Islam, K., Singh, B. and McBratney, A. (2003). Simultaneous estimation of several soil properties by ultra-violet, visible, and near-infrared reflectance spectroscopy. *Soil Research* **41**, 1101-1114.

Ismail, A. A., van de Voort, F. R. and Sedman, J. (1997). Fourier transform infrared spectroscopy: principles and applications. *Techniques and Instrumentation in Analytical Chemistry* **18**, 93-139.

Jahn, B., Linker, R., Upadhyaya, S., Shaviv, A., Slaughter, D. and Shmulevich, I. (2006). Mid-infrared spectroscopic determination of soil nitrate content. *Biosystems Engineering* **94**, 505-515.

Janik, L. and Skjemstad, J. (1995). Characterization and analysis of soils using mid-infrared partial least-squares .2. Correlations with some laboratory data. *Soil Research* **33**, 637-650.

Janik, L., Skjemstad, J. and Raven, M. (1995). Characterization and analysis of soils using mid-infrared partial least-squares .1. Correlations with XRF-determined major-element composition. *Soil Research* **33**, 621-636.

Janik, L. J., Merry, R. H. and Skjemstad, J. O. (1998). Can mid infrared diffuse reflectance analysis replace soil extractions? *Australian Journal of Experimental Agriculture* **38**, 681-696.

Ji, W., Li, S., Chen, S., Shi, Z., Rossel, R. A. V.and Mouazen, A. M. (2016). Prediction of soil attributes using the Chinese soil spectral library and standardized spectra recorded at field conditions. *Soil and Tillage Research* **155**, 492-500.

Jiménez-González, C., Curzons, A. D., Constable, D. J. and Cunningham, V. L. (2004). Expanding GSK's solvent selection guide—application of life cycle assessment to enhance solvent selections. *Clean Technologies and Environmental Policy* **7**, 42-50.

Johnson, D., Moghaddam, R., Ahmed I. B. and Laroche, C. (2013). Comparative evaluation of surface disposal of thickened versus slurry tailings. *Proceedings of the 16th International Seminar on Paste and Thickened Tailings*, Belo Horizonte, Brazil.

Kattner, J., Lilek, D., Edelmann, E., Loibner, A. P. and Herbinger, B. (2011). Linearization of MIR-DRIFT soil spectra using the 2518 cm^{-1} carbonate band as internal standard. *Geophydical Research Abstracts* **13**.

Kemsley, E. K., Tapp, H. S., Scarlett, A. J., Miles, S. J., Hammond, R.and Wilson, R. H. (2001). Comparison of spectroscopic techniques for the determination of Kjeldahl and ammoniacal nitrogen content of farmyard manure. *Journal of Agricultural and Food Chemistry* **49**, 603-609.

Kessick, M. A. (1977). Clay tailings from Alberta Oil Sands and other sources: A review. Edmonton, Alberta, Canada, Alberta Environment, Research Secretariat.

Kim, H. J., Sudduth, K. A. and Hummel, J. W. (2009). Soil macronutrient sensing for precision agriculture. *Journal of Environmental Monitoring* **11**, 1810-1824.

Kotlyar, L. S., Ripmeester, J. A., Sparks, B. D. and Montgomery, D. S. (1988). Characterization of organic-rich solids fractions isolated from Athabasca oil sand using a cold water agitation test. *Fuel* **67**, 221-226.

Ladd, J. N., Amato, M.and Oades, J. M. (1985). Decomposition of plant material in Australian soils. III. Residual organic and microbial biomass C and N from isotope-labelled legume material and soil organic matter, decomposing under field conditions. *Soil Research* **23**, 603-611.

Lagaly, G., Ogawa, M.and Dekany, I. (2013). Clay Mineral-Organic Interactions. In: *Handbook of Clay Science,* Bergaya, F. and Lagaly, G. (eds.), Elsevier, Oxford, UK, pp. 436-505.

Larter, S., Adams, J., Gates, I., Bennett, B. and Huang, H. (2008). The origin, prediction and impact of oil viscosity heterogeneity on the production characteristics of tar sand and heavy oil reservoirs. *Journal of Canadian Petroleum Technology* **47**, 1-16.

Lesueur, D. (2009). The colloidal structure of bitumen: Consequences on the rheology and on the mechanisms of bitumen modification. *Advances in colloid and interface science* **145**, 42-82.

Lévêque, J.-M. and Cravotto, G. (2006). Microwaves, power ultrasound, and ionic liquids. A new synergy in green organic synthesis. *Chimia International Journal for Chemistry* **60**, 313-320.

Li, X., Sun, W., Wu, G., He, L., Li, H.and Sui, H. (2011). Ionic liquid enhanced solvent extraction for bitumen recovery from oil sands. *Energy & Fuels* **25**, 5224-5231.

Linker, R., Kenny, A., Shaviv, A., Singher, L. and Shmulevich, I. (2004). Fourier transform infrared–attenuated total reflection nitrate determination of soil pastes using principal component regression, partial least squares, and cross-correlation. *Applied Spectroscopy* **58**, 516-520.

Linker, R., Shmulevich, I., Kenny, A.and Shaviv, A. (2005). Soil identification and chemometrics for direct determination of nitrate in soils using FTIR-ATR mid-infrared spectroscopy. *Chemosphere* **61**, 652-658.

Linker, R., Weiner, M., Shmulevich, I. and Shaviv, A. (2006). Nitrate determination in soil pastes using attenuated total reflectance mid-infrared spectroscopy: Improved accuracy via soil identification. *Biosystems Engineering* **94**, 111-118.

Long, Y., Dabros, T.and Hamza, H. (2004). Analysis of Solvent-Diluted Bitumen from Oil Sands Froth Treatment Using NIR Spectroscopy. *The Canadian Journal of Chemical Engineering* **82**, 776-781.

Lund, E. D., Colin, P. E., Christy, D. and Drummond, P. E. (1999). Applying soil electrical conductivity technology to precision agriculture. In: *Precision Agriculture*, Robert, P. C., Rust, R. H., and Larson, W. E. (eds.), American Society of Agronomy, Madison, US, pp. 1089-1100.

Madari, B. E., Reeves, J. B., Machado, P. L., Guimarães, C. M., Torres, E.and McCarty, G. W. (2006). Mid-and near-infrared spectroscopic assessment of soil compositional parameters and structural indices in two Ferralsols. *Geoderma* **136**, 245-259.

Martin, P., D. Malley, G. M. and Fuller, L. (2002). Determination of soil organic carbon and nitrogen at the field level using near-infrared spectroscopy. *Canadian Journal of Soil Science* **82**, 413-422.

Masliyah, J., Zhou, Z. J., Xu, Z., Czarnecki, J. and Hamza, H. (2004). Understanding water-based bitumen extraction from Athabasca oil sands. *The Canadian Journal of Chemical Engineering* **82**, 628-654.

McCarty, G., Reeves, J., Reeves, V., Follett, R. and Kimble, J. (2002). Mid-infrared and near-infrared diffuse reflectance spectroscopy for soil carbon measurement. *Soil Science Society of America Journal* **66**, 640-646.

McCarty, G. W. and Reeves, J. B. (2006). Comparison of near infrared and mid infrared diffuse reflectance spectroscopy for field-scale measurement of soil quality parameters. *Soil Science* **171**, 94-102.

McGill, W. B. and Rowell, M. J. (1980). Determination of oil content of oil contaminated soil. *Science of the Total Environment* **14**, 245-253.

Miller, F. A. and Wilkins, C. H. (1952). Infrared spectra and characteristic frequencies of inorganic ions. *Analytical Chemistry* **24**, 1253-1294.

Minasny, B., Tranter, G., McBratney, A. B., Brough, D. M. and Murphy, B. W. (2009). Regional transferability of mid-infrared diffuse reflectance spectroscopic prediction for soil chemical properties. *Geoderma* **153**, 155-162.

Mintert, J., Widmar, D., Langemeier, M., Boehlje, M.and Erickson, B. (2016). The Challenges of Precision Agriculture: Is Big Data the Answer? In: *2016 Annual Meeting, February 6-9, 2016, San Antonio, Texas*, Southern Agricultural Economics Association.

Nalawade, S. P., Picchioni, F. and Janssen, L. (2006). Supercritical carbon dioxide as a green solvent for processing polymer melts: processing aspects and applications. *Progress in Polymer Science* **31**, 19-43.

Natural Resources Canada (2015). Land Use and Reclamation.

Nawar, S., Buddenbaum, H., Hill, J., Kozak, J. and Mouazen, A. M. (2016). Estimating the soil clay content and organic matter by means of different calibration methods of vis-NIR diffuse reflectance spectroscopy. *Soil and Tillage Research* **155**, 510-522.

Nduwamungu, C., Ziadi, N., Parent, L. É., Tremblay, G. F. and Thuries, L. (2009). Opportunities for, and limitations of, near infrared reflectance spectroscopy applications in soil analysis: A review. *Canadian Journal of Soil Science* **89**, 531-541.

Nguyen, T., Janik, L. and Raupach, M. (1991). Diffuse reflectance infrared fourier transform (DRIFT) spectroscopy in soil studies. *Soil Research* **29**, 49-67.

Niemeyer, J., Chen, Y.and Bollag, J. M. (1992). Characterization of humic acids, composts, and peat by diffuse reflectance Fourier-transform infrared spectroscopy. *Soil Science Society of America Journal* **56**, 135-140.

Nieuwoudt, H. H., Prior, B. A., Pretorius, I. S., Manley, M.and Bauer, F. F. (2004). Principal Component Analysis Applied to Fourier Transform Infrared Spectroscopy for the Design of Calibration Sets for Glycerol Prediction Models in Wine and for the Detection and Classification of Outlier Samples. *Journal of Agricultural and Food Chemistry* **52**, 3726-3735.

Nikakhtari, H., Vagi, L., Choi, P., Liu, Q. and Gray, M. R. (2013). Solvent screening for non-aqueous extraction of Alberta oil sands. *The Canadian Journal of Chemical Engineering* **91**, 1153-1160.

Nikakhtari, H., Wolf, S., Choi, P., Q. Liu and Gray, M. R. (2014). Migration of fine solids into product bitumen from solvent extraction of alberta oilsands. *Energy & Fuels* **28**, 2925-2932.

Njoroge, J. B., Ninomiya, K., Kondo, N.and Toita, H. (2002). Automated fruit grading system using image processing. In: *SICE 2002. Proceedings of the 41st SICE Annual Conference*, IEEE.

Nyiraneza, J., N'Dayegamiye, A., Gasser, M. O., Giroux, M., Grenier, M., Landry, C. and Guertin, S. (2010). Soil and crop parameters related to corn nitrogen response in Eastern Canada. *Agronomy Journal* **102**, 1478-1490.

Odebunmi, E. O. and Olaremu, A. G. (2015). Extraction of Chemical Constituents of Bitumen Using a Mixed Solvent System. *Open Journal of Applied Sciences* **5**, 485.

Oliveira, J. S., Montalvão, R., Daher, L., Suarez, P. A. and Rubim, J. C. (2006). Determination of methyl ester contents in biodiesel blends by FTIR-ATR and FTNIR spectroscopies. *Talanta* **69**, 1278-1284.

Osborne, B. G., Fearn, T.and Hindle, P. H. (1993). *Practical NIR Spectroscopy with Applications in Food and Beverage Analysis*, Osborne, B. G., Fearn, T., and Hindle, P. H. (eds.), Longman Scientific and Technical, Harlow, UK.

Pace, V., Hoyos, P., Castoldi, L., Domínguez de María, P. and Alcántara, A. R. (2012). 2-Methyltetrahydrofuran (2-MeTHF): A Biomass-Derived Solvent with Broad Application in Organic Chemistry. *ChemSusChem.* **5**, 1369-1379.

Page, A. L. (1982). *Methods of Soil Analysis. Part 2. Chemical and Microbiological Properties*, American Society of Agronomy, Soil Science Society of America.

Painter, P., Williams, P.and Mannebach, E. (2009). Recovery of bitumen from oil or tar sands using ionic liquids. *Energy & Fuels* **24**, 1094-1098.

Pansu, M. and Gautheyrou, J. (2007). *Handbook of Soil Analysis: Mineralogical, Organic and Inorganic Methods*, Springer Science & Business Media.

Peramanu, S., Pruden, B. B. and Rahimi, P. (1999). Molecular weight and specific gravity distributions for Athabasca and Cold Lake bitumens and their saturate, aromatic, resin, and asphaltene fractions. *Industrial & Engineering Chemistry Research* **38**, 3121-3130.

Perry, R. H. and Green, D. W. (1999). *Perry's Chemical Engineers' Handbook*, McGraw-Hill, New York.

Peterson, C. H., Rice, S. D., Short, J. W., Esler, D., Bodkin, J. L., Ballachey, B. E. and Irons, D. B. (2003). Long-term ecosystem response to the Exxon Valdez oil spill. *Science* **302**, 2082-2086.

Pierce, F. J. and Nowak, P. (1999). Aspects of precision agriculture. *Advances in Agronomy* **67**, 1-85.

Pirie, A., Singh, B. and Islam, K. (2005). Ultra-violet, visible, near-infrared, and mid-infrared diffuse reflectance spectroscopic techniques to predict several soil properties. *Soil Research* **43**, 713-721.

Pitzer, K. S. and Brewer, L. (1961). *Thermodynamics*, McGraw-Hill, New York.

Pulati, N., Lupinsky, A., Miller, B. and Painter, P. (2015). Extraction of bitumen from oil sands using deep eutectic ionic liquid analogues. *Energy & Fuels* **29**, 4927-4935.

Qiu, K., Song, X., Lai, Y., Wu, L., Tang, G. and Min, S. (2013). Comparison of ATR/transmittance FTIR combined with Beer's law and PLS to determine fipronil in matrine formulation. *Analytical Methods* **5**, 4790-4797.

Rajendram, G. and Devey, K. (2011). *Comparison between Mid-infrared and Near-infrared for Soil Analysis,* H. L. Ltd. Hamilton, New Zealand.

Reichardt, M. and Jürgens, C. (2009). Adoption and future perspective of precision farming in Germany: results of several surveys among different agricultural target groups. *Precision Agriculture* **10**, 73-94.

Reimann, C. and Filzmoser, P. (1999). Normal and lognormal data distribution in geochemistry: death of a myth. Consequences for the statistical treatment of geochemical and environmental data. *Environmental Geology* **39**, 1001 - 1014.

Rezac, J. (2010). *Tailings, a Lasting Oil Sands Legacy*. UK, World Wide Fund for Nature.

Richter, B. E., Jones, B. A., Ezzell, J. L., Porter, N. L., Avdalovic, N.and Pohl, C. (1996). Accelerated solvent extraction: a technique for sample preparation. *Analytical Chemistry* **68**, 1033-1039.

Rivard, B., Lyder, D., Feng, J., Gallie, A., Cloutis, E., Dougan, P., Gonzalez, S., Cox, D. and Lipsett, M. (2010). Bitumen content estimation of Athabasca oil sand from broad band infrared reflectance spectra. *The Canadian Journal of Chemical Engineering* **88**, 830-838.

Robert, P. C. (2002). Precision agriculture: a challenge for crop nutrition management. *Plant and Soil* **247**, 143-149.

Romanova, U., Valinasab, M., Stasiuk, E., Yarranton, H., Schramm, L. and Shelfantook, W. (2006). The effect of oil sands bitumen extraction conditions on froth treatment performance. *Journal of Canadian Petroleum Technology* **45**, 1-10.

Rosa, F. and Casquilho, M. (2012). Effect of synthesis parameters and of temperature of swelling on water absorption by a superabsorbent polymer. *Fuel Processing Technology* **103**,174-177.

Rossel, R. A. V., Walvoort, D. J. J., McBratney, A. B., Janik, L. J. and Skjemstad, J. O. (2006). Visible, near infrared, mid infrared or combined diffuse reflectance spectroscopy for simultaneous assessment of various soil properties. *Geoderma* **131**, 59-75.

Rudzinski, W. E., Aminabhavi, T. M., Sassman, S.and Watkins, L. M. (2000). Isolation and characterization of the saturate and aromatic fractions of a Maya crude oil. *Energy & fuels* **14**, 839-844.

Saikia, B. J. and Parthasarathy, G. (2010). Fourier transform infrared spectroscopic characterization of kaolinite from Assam and Meghalaya, Northeastern India. *Journal of Modern Physics* **1**, 206.

Scammells, P. J., Scott, J. L. and Singer, R. D. (2005). Ionic liquids: the neglected issues. *Australian Journal of Chemistry* **58**, 155-169.

Schellberg, J., Hill, M. J., Gerhards, R., Rothmund, M.and Braun, M. (2008). Precision agriculture on grassland: Applications, perspectives and constraints. *European Journal of Agronomy* **29**, 59-71.

Schueller, J. K. (1992). A review and integrating analysis of spatially-variable control of crop production. *Fertilizer Research* **33**, 1-34.

Schwartz, G., Ben-Dor, E.and Eshel, G. (2012). Quantitative analysis of total petroleum hydrocarbons in soils: comparison between reflectance spectroscopy and solvent extraction by 3 certified laboratories. *Applied and Environmental Soil Science* **2012**, 1-11.

Scott, J. D. and B. Ozum. (2010). *Oil Sands Tailings: What Needs to be Done*. Retrived from http://www.mining.com/oil-sands-tailings-what-needs-to-be-done/

Shaviv, A., Kenny, A., Shmulevitch, I., Singher, L., Raichlin, Y.and Katzir, A. (2003). Direct monitoring of soil and water nitrate by FTIR based FEWS or membrane systems. *Environmental Science & Technology* **37**, 2807-2812.

Sheldrick, B. H. and Wang, C. (1993). Particle size distribution. In: *Soil Sampling and Methods of Analysis*. Carter, M. R. (ed.), CRC Press, US, pp. 499-513.

Shenk, J. and Westerhaus, M. (1991). Population definition, sample selection, and calibration procedures for near infrared reflectance spectroscopy. *Crop Science* **31**, 469-474.

Smith, B. C. (2011). *Fundamentals of Fourier Transform Infrared Spectroscopy*, CRC Press, Florida.

Socrates, G. (2004). *Infrared and Raman Characteristic Group Frequencies: Tables and Charts*, John Wiley & Sons, Chichester.

Solomon, D., Lehmann, J., Kinyangi, J., Liang, B.and Schäfer, T. (2005). Carbon K-edge NEXAFS and FTIR-ATR spectroscopic investigation of organic carbon speciation in soils. *Soil Science Society of America Journal* **69**, 107-119.

Sorensen, L. H. (1981). Carbon-nitrogen relationships during the humification of cellulose in soils containing different amounts of clay. *Soil Biology and Biochemistry* **13**, 313-321.

Sparks, B., Kotlyar, L., O'Carroll, J.and Chung, K. (2003). Athabasca oil sands: effect of organic coated solids on bitumen recovery and quality. *Journal of Petroleum Science and Engineering* **39**, 417-430.

Spiecker, P. M., Gawrys, K. L. and Kilpatrick, P. K. (2003). Aggregation and solubility behavior of asphaltenes and their subfractions. *Journal of Colloid and Interface Science* **267**, 178-193.

St Luce, M., Ziadi, N., Nyiraneza, J., Tremblay, G. F., Zebarth, B. J., Whalen, J. K. and Laterrière, M. (2012). Near infrared reflectance spectroscopy prediction of soil nitrogen supply in humid temperate regions of Canada. *Soil Science Society of America Journal* **76**, 1454-1461.

Stenberg, B., Jonsson, A. and Börjesson, T. (2002). Near infrared technology for soil analysis with implications for precision agriculture. *Near Infrared Spectroscopy: Proceedings of the 10th International Conference, Kyongju S. Korea*, NIR Publications, Chichester, UK.

Stenberg, B., Rossel, R. A. V., Mouazen, A. M. and Wetterlind, J. (2010). Visible and near infrared spectroscopy in soil science. *Advances in Agronomy* **107**, 163-215.

Steward, P. J. G. and Williams, A. (2013). *The Alberta Oil Sands Then and Now: An Investigation of the Economic, Environmental and Social Discourses Across Four Decades*. Edmonton, Alberta, Oil Sands Research and Information Network, University of Alberta**: **108.

Steyerberg, E. (2009). Evaluation of performance. In: *Clinical Prediction Models: a Practical Approach to Development, Validation and Updating*, Springer, New York, pp. 255-280.

Strosher, M. T. and Peake, E. (1978). *Characterization of Organic Constituents in Waters and Wastewaters of the Athabasca Oil Sands Mining Area*, Alberta Oil Sands Environmental Research Program, Alberta, Canada.
Sudduth, K. A. and Hummel, J. W. (1993). Near-infrared spectrophotometry for soil property sensing. In: *Applications in Optical Science and Engineering*, International Society for Optics and Photonics, pp. 14-25.

Sudduth, K. A., Hummel, J. W. and Birrell, S. J. (1997). Sensors for site-specific management. In: *The State of Site Specific Management for Agriculture*, Pierce, F. J. and Sadler, E. J. (eds.), American Society of Agronomy, Madison, PP. 183-210.

Suncor Energy Inc. (2009). *Application for Tailings Reduction Operations Experimental Facilities*, Alberta, Canada.

Suncor Energy Inc. (2010). *Suncor Response to the ERCB Supplemental Information Requests*, Alberta, Canada.

Syncrude Canada Ltd. (2008). *Application for Approval of the Southwest Sand Storage Conversion Project*, Alberta, Canada.

Tat, M. E. and Van Gerpen, J. H. (1999). The kinematic viscosity of biodiesel and its blends with diesel fuel. *Journal of the American Oil Chemists' Society* **76**, 1511-1513.

Terra, F. S., Demattê, J. A. M. and Rossel, R. A. V (2015). Spectral libraries for quantitative analyses of tropical Brazilian soils: Comparing vis–NIR and mid-IR reflectance data. *Geoderma*, **255–256**: 81-93.

Thomasson, J., Sui, R., Cox, M.and Al-Rajehy, A. (2001). Soil reflectance sensing for determining soil properties in precision agriculture. *Transactions of the ASAE* **44**, 1445.

Troeh, F. R. and Thompson, L. M. (2005). Nitrogen. In: *Soil and Soil Quality*, Troeh, F. R. and Thompson, L. M. (eds.), Blackwell Publishing, Iowa, USA, pp. 211-230.

Udelhoven, T., Emmerling, C.and Jarmer, T. (2003). Quantitative analysis of soil chemical properties with diffuse reflectance spectrometry and partial least-square regression: A feasibility study. *Plant and Soil* **251**, 319-329.

Ure, A. M. (1996). Single extraction schemes for soil analysis and related applications. *Science of the Total Environment* **178**, 3-10.

US Environmental Protection Agency (2007). *Guidelines Establishing Test Procedures for the Analysis of Pollutants Under the Clean Water Act; National Primary Drinking Water Regulations; and National Secondary Drinking Water Regulations; Analysis and Sampling Procedures*.

Veum, K. S., Sudduth, K. A., Kremer, R. J. and Kitchen, N. R. (2015). Estimating a soil quality index with VNIR reflectance spectroscopy. *Soil Science Society of America Journal* **79**, 637-649.

Vohland, M., Ludwig, M., Thiele-Bruhn, S.and Ludwig, B. (2014). Determination of soil properties with visible to near- and mid-infrared spectroscopy: Effects of spectral variable selection. *Geoderma* **223–225**, 88-96.

Wang, F., Robbins, W. K. and Greaney, M. A. (2004). Speciation of nitrogen-containing compounds in diesel fuel by comprehensive two-dimensional gas chromatography. *Journal of Separation Science* **27**, 468-472.

Wetterlind, J., Stenberg, B.and Jonsson, A. (2007). Near infrared reflectance spectroscopy compared with soil clay and organic matter content for estimating within-field variation in N uptake in cereals. *Plant and Soil* **302**, 317-327.

Wetterlind, J., Stenberg, B.and Jonsson, A. (2008). Near infrared reflectance spectroscopy compared with soil clay and organic matter content for estimating within-field variation in N uptake in cereals. *Plant and Soil* **302**, 317-327.

Whelan, B. and McBratney, A. (2000). The "null hypothesis" of precision agriculture management. *Precision Agriculture* **2**, 265-279.

Whelan, B. and Taylor, J. (2013). Introduction to Precision Agriculture. In: *Precision Agriculture for Grain Production Systems*, Kretser, A. D. (ed.), Csiro publishing, Australia, pp. 1-9.

Wu, J. and Dabros, T. (2012). Process for solvent extraction of bitumen from oil sand. *Energy & Fuels* **26**, 1002-1008.

Xie, H., Yang, X., Drury, C., Yang, J. and Zhang, X. (2011). Predicting soil organic carbon and total nitrogen using mid-and near-infrared spectra for Brookston clay loam soil in Southwestern Ontario, Canada. *Canadian Journal of Soil Science* **91**, 53-63.

Yang, H. and Mouazen, A. M. (2012). Vis/near and mid-infrared spectroscopy for predicting soil N and C at a farm scale. *Infrared Spectroscopy—Life and Biomedical Sciences*, pp. 185-210.

Yeung, P. Y., Johnson, R. L. and Acharya, S. N. (1994). An improved procedure for determining oil content in wet soil samples. In: *Analysis of Soils Contaminated With Petroleum Constituents*, ASTM International.

Yoon, S., Bhatt, S. D., Lee, W., Lee, H. Y., Jeong, S. Y., Baeg, J. O. and Lee, C. W. (2009). Separation and characterization of bitumen from Athabasca oil sand. *Korean Journal of Chemical Engineering* **26**, 64-71.

Yoon, S., Son, J., Lee, W., Lee, H.and Lee, C. W. (2009). Prediction of bitumen content in oil sand based on FT-IR measurement. *Journal of Industrial and Engineering Chemistry* **15**, 370-374.

Yuan, H., Chu, X., Li, H., and Xu, Y. (2006). Determination of multi-properties of residual oils using mid-infrared attenuated total reflection spectroscopy. *Fuel* **85**, 1720-1728.

Yut, I. and Zofka, A. (2011). Attenuated total reflection (ATR) fourier transform infrared (FT-IR) spectroscopy of oxidized polymer-modified bitumens. *Applied Spectroscopy* **65**, 765-770.

Zarco-Tejada, P., Hubbard, N. and Loudjani, P. (2014). Precision Agriculture: An Opportunity for EU Farmers—Potential Support with the CAP 2014-2020. *Joint Research Centre (JRC) of the European Commission*.